ESTABLISHING AND CHARACTERISING RODENT MODELS OF PULMONARY AND GASTROINTESTINAL INFLAMMATION FOR THE INVESTIGATION OF SENSORY-IMMUNE INTERACTIONS

Doctoral (PhD) Thesis

Kata Csekő MD

Pharmacology and Pharmaceutical Sciences Doctoral School

Neuropharmacology Program

Leader of Doctoral School: Erika Pintér MD, PhD, DSc

Supervisor: Zsuzsanna Helyes MD, PhD, DSc

Department of Pharmacology and Pharmacotherapy

University of Pécs, Medical School

Pécs

2022

Table of contents

List of abbreviations

BALF: bronchoalveolar lavage fluid

BLC: B-lymphocyte chemoattractant

CD: Crohn's disease

CGRP: calcitonin gene-related peptide

COPD: chronic obstructive pulmonary disease

CS: cigarette smoke

CSE: cigarette smoke exposure

CT: computed tomography

DNBS: dinitrobenzene sulfonic acid

DRG: dorsal root ganglia

DSS: dextrane sulfate sodium

EEP: end-expiratory pause

EEW: end-expiratory work

EF50: tidal mid-expiratory flow

f: frequency

GluCys: γ-glutamyl-cysteine

GSH: glutathione

HE: hematoxylin and eosin

HPLC: high power liquid chromatograpy

IAA: iodoacetamide

IBD: inflammatory bowel disease

IFN- γ: interferon- γ

IHC: immunohistochemistry

IL: interleukin

IP-10: interferon-gamma inducible protein-10

ISH: *in situ* hybridization

I-TAC: interferon-inducible T-cell chemoattractant

KC: keratinocyte chemoattractant

LAA: low attenuation area

L_m: mean linear intercept

LPS: lipopolysaccharide

MCP: monocyte chemoattractant protein

M-CSF: macrophage colony-stimulating factor

MIG: monokine induced by gamma interferon

MIP-1: macrophage inflammatory protein

MMP: matrix metalloproteinase

MPO: myeloperoxidase

MV: minute ventilation

NACET: *N*-acetylcysteine ester

NF-κB: nuclear factor-kappa B

NK cells: natural killer cells

NKA, NKB: neurokinin A, B

NSAID: non-steroidal anti-inflammatory drugs

NO: nitric oxide

NOS: nitric oxide synthase

OPA: *ortho*-phthaldehyde

PACAP: pituitary adenylate cyclase activating polypeptide

PBS: phosphate buffered saline

PEF: peak expiratory flow

Penh: enhanced pause

PIF: peak inspiratory flow

qPCR: quantitative polymerase chain reaction

RANTES: regulated on activation, normal T cell expressed and secreted

Rl: airway resistance

ROS: reactive oxygen species

RT: relaxation time

RTX: resiniferatoxin

SDF-1: stromal cell-derived factor-1

sICAM-1: soluble intercellular adhesion molecule-1

SP: substance P

Te: expiratory time

tGSH: total glutathione

Ti: inspiratory time

TIMP-1: tissue inhibitor of metalloproteinase-1

TLV: total lung volume

TNBS: trinitrobenzene sulfonic acid

TNFα: tumor necrosis factor α

TPM: total particulate matter

TREM-1: triggering receptor expressed on myeloid cells-1

TRP: Transient receptor potential

TRPA1: Transient receptor potential ankyrin 1

Trpa1$^{+/+}$: TRPA1 wildtype

Trpa1$^{-/-}$: TRPA1 gene-deficient

TRPV1: Transient receptor potential vanilloid 1

TV: tidal volume

UC: ulcerative colitis

WBP: whole body plethysmography

1 Introduction, background

1.1 Transient receptor potential Vanilloid 1 (TPV1) and Ankyrin 1 (TRPA1) and their role in neurogenic inflammation

Transient receptor potential (TRP) ion channels comprise more than 30 structurally related ion channels, divided into the TRPC (Canonical), the TRPV (Vanilloid), the TRPM (Melastatin), the TRPP (Polycystin), the TRPML (Mucolipin), the TRPA (Ankyrin) and the TRPN (NOMPC) subfamilies based on their sequence homology (1). Most of them are non-selective cation channels, however, they exhibit differences in permeability and selectivity (2). These ion channels are tetramers composed of six transmembrane domains, with a pore formed by the hydrophobic region between the fifth and sixth segments. They can assemble as homo- or heterotetramers to form functional units (3). The physiological role of TRP channels ranges from store-operated calcium channels to thermo-, mechano- and chemosensors.

The most investigated members of the family in relation to gastrointestinal and airway inflammation include vanilloid 1 (TRPV1), ankyrin 1 (TRPA1). They are located predominantly on the capsaicin-sensitive sensory neurons, and often co-expressed mainly on these sensory fibers, but several non-neural expressions have recently been described that drew great attention to this research area (4). In general, they are activated by a variety of exogenous chemicals and endogenous mediators making them important regulatory structures in inflammatory and pain processes.

TRPV1 and TRPA1 are polymodal nociceptors playing an important role in thermo- mechanical- and chemo-sensation and play a complex role in hyperalgesia and neurogenic inflammation (5,6). Upon their activation on the capsaicin-sensitive afferents pro-inflammatory sensory neuropeptides, e.g., substance P (SP) and calcitonin gene-related peptide (CGRP) are released leading to neurogenic inflammation (vasodilatation, plasma protein extravasation and inflammatory cell activation) (6–8). Simultaneously with these pro-inflammatory mediators, anti-inflammatory neuropeptides, most importantly somatostatin and pituitary adenylate cyclase activating polypeptide (PACAP) are also released from the same terminals, counteracting the inflammatory process and tissue damage both locally and systemically (9–11) (Figure 1).

The endogenous activators of TRPV1 and TRPA1 are often produced during inflammation, e.g., lipoxygenase products, reactive oxygen species (ROS), bradykinin, prostanoids and the acidified

pH of the inflamed tissue (12–15). The gastrointestinal mucosa is frequently exposed to the exogenous agonists of TRPV1, such as capsaicin and piperine (the pungent agent of chili pepper and black pepper, respectively), as well as activators of TRPA1, such as cinnamaldehyde, allyl isothiocyanate (mustard oil), allicin (garlic), menthol etc. ingested by food (2,8,14,15). The airways on the other hand can be exposed to various TRPA1 agonists, such as bacterial endotoxin and environmental irritants like acrolein, crotonaldehyde, isocyanates and nicotine found in cigarette smoke, wood smoke, diesel exhaust and tear gas (19–27) (Figure 1).

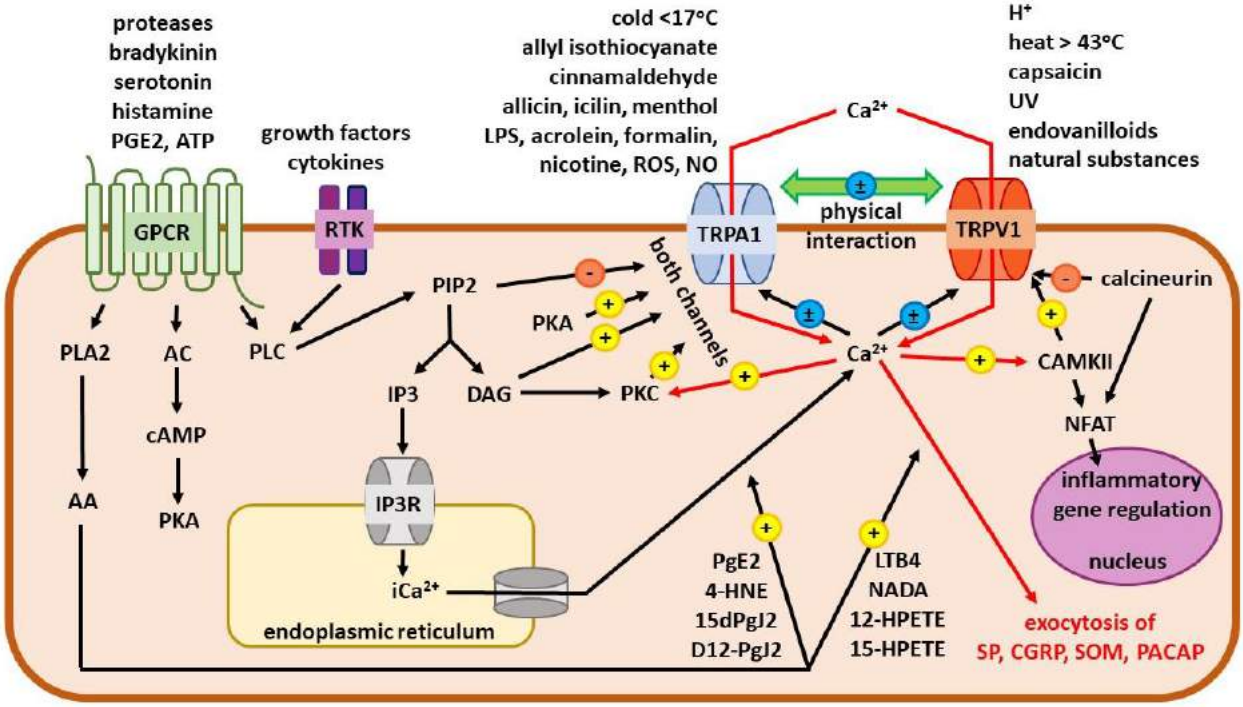

Figure 1. Activators, functional interaction, and signalization of TRPA1 and TRPV1 ion channels. Activation of the TRPA1 and TRPV1 channels leads to calcium influx resulting in the exocytosis of pro- and anti-inflammatory mediators, such as SP, CGRP, somatostatin (SOM) and PACAP. Besides, TRPA1 and TRPV1 are also able to functionally interact via the regulation of iCa^{2+} concentration, resulting in cross-sensitization/desensitization. (AA: arachidonic acid, CAMKII: Ca^{2+} /calmodulin-dependent kinase II, DAG: diacylglycerol, GPCR: G protein-coupled receptor, IP3: 1,4,5-trisphosphate, NFAT: nuclear factor of activated T-cell, PIP2: phosphatidylinositol 4,5-bisphosphate (PIP2), PLA2: phospholipase A2, PLC: phospholipase C, PKA: protein kinase A, PKC: protein kinase C RTK: receptor tyrosine kinase)(28)

TRPV1 and TRPA1 are capable of functional interaction, such as heterologous desensitization (29), since the majority of TRPA1 expressing nerve fibers co-express TRPV1 (30). Both ion channels can be sensitized by a variety of other mechanisms, such as prostaglandins, bradykinin and

proteases, e.g. cathepsin expressed by immune cells, via the protease-activated receptor 2 (PAR2) present on both capsaicin-sensitive nerve endings and the immune cells themselves (28,31,32) (Figure 1).

TRPV1 is also present on several non-neuronal structures in the gastrointestinal tract, such as the gastrin-secreting parietal and gastric epithelial cells, as well as the oesophageal, small intestinal and colonic epithelial cells (33,34). TRPA1 is less extensively studied in the gastrointestinal tract, but its expression was described in isolated crypts and epithelial cells of the colon, as well as small intestinal neuroendocrine cells (34,35). In the airways, TRPA1 is expressed on fibroblasts, tracheal, bronchial and alveolar epithelial cells, bronchial smooth muscle cells, as well as lymphocytes (36–39). Moreover, both receptors were reported on CD4+ T cells emphasizing their role in sensory-immune interactions (40,41).

Therefore, these ion channels were identified as novel anti-inflammatory, analgesic and gastroprotective targets (17,42).

1.2 The role of TRPA1 in the respiratory system

Due to its polymodal chemosensor function and its wide expression pattern, TRPA1 has been addressed as having a key role in physiological and pathophysiological processes, particularly in neuro-immune interactions (17,43,44). It is suggested to be a particularly important chemical sensor in the respiratory system, playing a role in physiological (protective reflexes, cough and sneeze) and pathophysiological responses (inflammation, bronchial hyperreactivity) (16,45,46). Although increasing evidence suggests TRPA1 involvement in the pathogenesis of chronic obstructive pulmonary disease (COPD), asthma, chronic cough, cystic fibrosis etc., pointing to the important therapeutic potential of TRPA1 in the pharmacological treatment of chronic pulmonary diseases (36,45,47–53), there are few *in vivo* data concerning its function in airway inflammation. Therefore, the results are far from being conclusive and more information is needed to determine the significance of TRPA1 as a possible pharmacological target in inflammatory lung disease, pneumonitis and COPD.

1.3 Chronic obstructive pulmonary disease (COPD)

COPD is a major global health problem worldwide in terms of economic and social burden of disease and in terms of mortality. According to the definition and description of the Global Initiative for Chronic Obstructive Lung Disease (GOLD 2017), from the Global Strategy for the Diagnosis, Management and Prevention of COPD, it is characterized by persistent respiratory symptoms and airflow limitation due to airway and/or alveolar abnormalities usually caused by significant exposure to noxious particles or gases. It is usually progressive and associated with an enhanced chronic inflammatory response in the airways and the lung. Exacerbations and comorbidities contribute to the overall severity (54). Functional respiratory disorders result from chronic obstructive bronchiolitis narrowing the small airways and emphysema due to lung parenchymal destruction. Cigarette smoking is the most common cause of COPD accounting for approximately 95% of cases in developed countries besides other predisposing factors, such as air pollutants and occupational exposure (55).

There is no curative treatment, the available therapy is restricted to corticosteroids, adrenergic β2 receptor agonists and acetylcholine muscarinic receptor antagonists that can only slow down the progression and alleviate the symptoms (54). However, these have limited effect in a relatively small patient population (56). Therefore, there is an urgent need to find novel therapeutic targets in COPD.

Due to the extensive interest in this area of research, our knowledge of the underlying mechanisms has remarkably expanded. Cigarette smoke and other airway irritants induce an abnormal inflammatory response involving CD8+ lymphocytes, neutrophils and macrophages. These immune cells release chemotactic factors, colony stimulating factors and proinflammatory cytokines, thus sustain and enhance inflammation and immune cell recruitment. Furthermore, proteases like neutrophil elastase, cathepsins and matrix metalloproteinases (MMPs) are responsible for elastin destruction resulting in emphysema formation (57,58). However, the complex pathophysiological mechanism, the inflammatory cascades and the role of the immune cells, sensory nerves and neuro-immune interactions, as well as the key mediators need to be determined to identify potential novel therapeutic targets (59).

1.4 Animal models of chronic airway inflammation

Besides human studies to analyse tissue samples, translational animal models are particularly important to define the pathophysiological processes underlying the molecular pathways. Many species like rodents, sheep, dogs, guinea pigs, and monkeys have been investigated for modelling COPD (60–62), but considering the possibilities of genetic engineering, easier handling and less compound requirement, mouse models seem to be most suitable and promising to elucidate the pathophysiological pathways and the complexity of the mechanisms (63–65).

Several studies focus on the protease-antiprotease imbalance and use only short-lasting models of various types of elastases, such as pancreatic elastase, neutrophil elastase, proteinase-3 (58,66–68), or lipopolysaccharides (LPS) and inorganic dusts to investigate their role in the development of emphysema. These models have been proved to be useful, however, they focus only on one factor that is an intermediate player of the pathophysiological cascade. Meanwhile, cigarette smoke (CS), which is the most common initial triggering stimulus in the human disease, switches on a variety of other pathways and mechanisms that are upstream mediators (67). To investigate the potential involvement of TRPA1 and the whole complexity of the chronic persistent inflammatory process, the only authentic translational model for COPD is the chronic cigarette smoke exposure (CSE) (69,70). This model has been used by several groups so far, but their broad conclusive potential is limited by the facts that they 1) applied different protocols, experimental paradigms, exposure durations and intensities, 2) did not have a longitudinal self-control follow-up design, 3) did not aim to use an integrative methodological approach to investigate the complexity of the disease, only focused on certain specific parameters and 4) used different strains. It is important to note that genetic variance and different cigarette types have a great influence on the outcome of chronic cigarette smoke exposure (71–74). Since C57Bl/6 mice are the most widely used one for genetic manipulations, and it is very sensitive to cigarette smoke (63) our goal was to set up, characterise and optimise a model in this strain. Therefore, we aimed to establish a translational mouse model for complex functional, morphological, immunological, and biochemical investigation of chronic pulmonary pathophysiological changes characteristic to COPD. This helps to analyse the mechanisms in different stages of the disease and provide a basis for further studies investigating the potential role of TRPA1 in COPD.

1.5 Expression of TRPV1 and TRPA1 in the gastrointestinal tract

In the gastrointestinal tract the expression and role of TRPV1 and TRPA1 were most extensively studied in animal models of colitis, such as 1%–5% dextran sulfate sodium (DSS)-, oxazolone-, acetic acid-, trinitrobenzene or dinitrobenzene sulfonic acid (TNBS/DNBS)- or *Il10*$^{-/-}$-induced spontaneous colitis models (75–77).

TRPV1 is often co-expressed with TRPA1 in capsaicin-sensitive extrinsic sensory nerves, especially in the primary sensory neurons of the dorsal root ganglia (DRG). The density of these TRPV1 positive fibers increase from proximal to distal regions of the colon in mice (78). Furthermore, during DSS colitis the proportion of DRG neurons expressing TRPV1, and their relative TRPV1 mRNA levels increase with a subsequently elevated release of sensory neuropeptides, such as CGRP and SP (79). Although the role of TRP-expressing afferents in inflammation is undisputable, there is growing evidence on the expression of TRPV1 and TRPA1 in intrinsic sensory neurons of the myenteric and submucosal plexuses (34,35,78,80), as well as on the surface epithelial cells of colonic mucosa (34,35,81). The importance of sensory-immune interactions in colonic inflammation is also supported by the expression of TRPV1 and TRPA1 on inflammatory cells like mucosal macrophages, as well as CD4+ T cells (34,40,41) (Tables 1-4).

Table 1. mRNA expression of *Trpv1* in the animal colon (qPCR: quantitative polymerase chain reaction) (82)

mRNA	Location	Method	Model, animal species/ strain	Ref
Trpv1	isolated crypts, submucosal and muscle layers of distal, middle and proximal colon	qPCR	intact male Wistar rats	(81)
	upregulated in colonic DRG to the distal colon in DSS-colitis		2.5% DSS-treated C57Bl/6 mice	(79)
	unaltered in distal colon, cell type not specified		DSS-colitis – male C57Bl/6 mice	(34)
	CD4+ T cells		primary cell culture from C57Bl/6 spleen	(41)

Table 2. mRNA expression of *Trpa1* in the animal colon (ISH: in situ hybridisation) (82)

mRNA	Location	Method	Model, animal species/ strain	Ref
Trpa1	muscularis externa and mucosa of duodenum, ileum and colon; cell type not specified	qPCR	intact C57Bl/6 mice	(35)
	surface epithelium of middle colon	ISH	intact male Wistar rats	(81)
	isolated crypts, submucosal and muscle layers of distal, middle and proximal colon	qPCR	intact male Wistar rats	(81)
	upreguated in distal colon, cell type not specified		DSS colitis – male C57Bl/6 mice	(34)

Table 3. Protein expression of TRPV1 in the animal colon (IHC: immunohistochemistry) (82)

Protein	Location	Method	Model, animal species/ strain	Ref
TRPV1	intrinsic sensory neurons of the myenteric plexus – longitudinal muscle of ileum and colon	IHC	intact Sprague-Dawley rats and Dunkun-Hartley guinea pigs of both sexes	(80)
	mucosa, submucosal layers, myenteric plexus and mucosal layer of rectum, distal, transverse and proximal colon		male ddY mice	(78)
	immunopositive neuron fiber density is higher in the distal than the proximal colon		intact and 2.5% DSS-treated C57Bl/6 mice colon	(79)
	enteric ganglia, epithelial cells of the distal colon, myenteric and submucosal plexuses, mucosal macrophages, leukocytes		male C57Bl/6 mice	(34)
	membrane of resting CD4+ T cells	immunoblotting, flow cytometry, confocal microscopy	primary cell culture from C57Bl/6 spleen	(41)

Table 4. Protein expression of TRPA1 in the animal colon (IHC: immunohistochemistry) (82)

Protein	Location	Method	Model, animal species/ strain	Ref
TRPA1	distal colonic epithelial cells, myenteric and submucosal plexuses, interstitial macrophages	IHC	male C57Bl/6 mice	(34)
	myenteric and submucosal ganglia; surface epithelial cells of small and large intestines		intact C57Bl/6 mice	(35)
	surface epithelium of middle colon		intact male Wistar rats	(81)
	membrane of resting CD4+ T cells	IHC, confocal microscopy	primary cell culture from C57Bl/6 spleen	(40)

In the stomach the gastroprotective effect of capsaicin-sensitive peptidergic sensory neurons innervating the gastric mucosa has long been investigated by our group (83). Low dose of the TRPV1 activator capsaicin is protective against the alcohol- and indomethacin-induced gastric mucosal injury (84), it reduces basal gastric acid secretion and enhances gastric emptying (85). However, in contrast to TRPV1, little is known about the expression changes and role of TRPA1 in the stomach (86), therefore, we aimed to elucidate the potential role of TRPA1 in an animal model of gastric injury.

1.6 Animal models of gastric ulceration

Gastric mucosal injury can be exhibited by various forms of macroscopic and histopathological alterations, such as diffuse hyperemia, inflammation, erosion, or even hemorrhagic ulcerations. Several attempts have been made to classify the different types of gastritis, but it is difficult due to the complexity of its pathophysiological mechanisms (87). There is often no correlation between the symptoms and the macroscopic lesions or histopathological changes (88). Based on its localization, the injury can be diffuse, antrum- or corpus-predominant, or even multifocal. Regarding the duration, we can differentiate between acute or chronic forms (89). However, the etiology of the condition is at least as important.

Several drugs may alleviate the gastric lesions induced by chemical factors such as the non-steroidal anti-inflammatory drugs (NSAID), alcohol or bile reflux, *Helicobacter pylori* infection or irradiation (90). The gold standard treatment is often limited to acid secretion inhibitors, such as

proton pump inhibitors or histamine H2 receptor antagonists, since enhancing cytoprotective mechanisms is challenging (91).

Animal models are important for the molecular investigation of gastric injury, since these models may reveal very early biochemical and molecular alterations, much before microscopic or macroscopic lesions can be seen. Good models should have translational relevance. However, in virtually all animal models of gastric injury (e.g., NSAID-, stress-induced) the lesions are well circumscribed (i.e., superficial erosions and/or deep ulcers). Gastritis in humans, on the other hand, is a diffuse inflammatory damage involving all or most parts of the stomach (87).

Iodoacetamide (IAA) is a water-soluble sulfhydryl alkylating chemical, which, by depleting sulfhydryl groups, including the protective antioxidant glutathione (GSH) in the gastric mucosa, allows ROS production and oxidative tissue damage (92). The reduced GSH plays an essential role in maintaining mucosal integrity (93). Nitric oxide synthase (NOS) also contributes to mucosal protection via the production of nitric oxide (NO), which increases mucosal blood flow like other gastroprotective compounds (94,95). IAA may interfere with NOS activity, thus also affecting gastric mucosal integrity. ROS react with various cell components including cell membrane, mitochondria and DNA, potentially leading to cell death/necrosis, which triggers neutrophil recruitment (96,97).

2 Primary Aims

The primary aims of my work was to establish and characterise rodent models of pulmonary and gastrointestinal inflammation for the investigation of sensory-immune interactions, as well as TRPA1 expressions and potential roles.

1) **Establishing and characterising mouse model of chronic airway inflammation**

There is no effective curative treatment for COPD, the complex pathophysiological mechanisms, inflammatory cascades and the role of the immune cells, therefore, sensory nerves and neuro-immune interactions, as well as the key mediators need to be determined to identify novel therapeutic interventions. Cigarette smoke-triggered inflammatory cascades and consequent tissue damage are the main causes of COPD, therefore, chronic CSE is the only translationally relevant animal model. We aimed to establish a translational mouse model for complex functional, morphological, immunological, and biochemical investigation of chronic pulmonary pathophysiological changes characteristic to COPD. This helps to analyse the mechanisms in different stages of the disease and identify key targets for pharmacological research.

2) **Investigating the role of TRPA1 in CSE-induced COPD mouse model**

Although increasing evidence suggests TRPA1 involvement in the pathogenesis of COPD, asthma, chronic cough, cystic fibrosis pointing to the important therapeutic potential of TRPA1 in the pharmacological treatment of chronic pulmonary diseases, there are few and conflicting *in vivo* data concerning its function in airway inflammation. We investigated the potential role of TRPA1 *in vivo* in a CSE-induced COPD mouse model using *Trpa1* gene-deficient mice in comparison with their wildtypes.

3) **Investigating the expression of TRPA1 and TRPV1 in iodoacetamide (IAA)-induced diffuse gastric injury model**

Although the gastroprotective effect of capsaicin-sensitive peptidergic sensory neurons innervating the gastric mucosa has long been investigated, in contrast to TRPV1, little is known about the expression changes and role of TRPA1 in the stomach. Therefore, our aim was to characterise a translationally relevant gastritis model using the irreversible sulfhydryl-group blocker IAA and to investigate the expression changes with special focus on TRPA1.

3 Experimental models and investigational methods

3.1 Cigarette smoke-induced chronic airway inflammation model

3.1.1 Animals and research ethics

Experiments were performed on 8-10-week-old C57Bl/6 mice, as well as on TRPA1 wildtype (*Trpa1*$^{+/+}$) and gene-deficient (*Trpa1*$^{-/-}$) counterparts weighing 20-25 g at the beginning of the study; each group consisted of 6 mice. The original heterozygote *Trpa1*$^{+/-}$ breeding pairs were a generous gift of Pierangelo Geppetti (Firenze, Italy)(98). Background strain of the gene-deleted animals was C57Bl/6, and the germline transmission of the mutated allele and excision of the selection cassette were verified by PCR analysis. Animals were bred and kept in the Laboratory Animal House of the Department of Pharmacology and Pharmacotherapy, University of Pécs, Pécs, Hungary at 24-25 °C, provided with standard chow and water *ad libitum*, maintained under 12h light-dark cycle. All procedures were carried out according to the 40/2013 (II.14.) Government Regulation on Animal Protection and Consideration Decree of Scientific Procedures of Animal Experiments (243/1988) and Directive 2010/63/EU of the European Parliament. Studies were approved and a license was given by the Ethics Committee on Animal Research of University of Pécs, Pécs, Hungary according to the Ethical Codex of Animal Experiments (licence No.: BA02/2000-5/2011, BA02/2000-35/2016). We addressed the ARRIVE guidelines for designing, performing and reporting the experiments wherever possible.

3.1.2. Experimental design for the integrative characterisation of cigarette smoke-induced COPD mouse model

Male C57Bl/6 mice were exposed to cigarette smoke in a whole-body smoke exposure chamber twice daily, 10 times/week for 6 months. Age-matched non-smoking mice kept under the same circumstances served as controls. Airway responsiveness was determined by unrestrained whole-body plethysmography (WBP), while pulmonary structural changes were imaged by a microtomograph at the end of each month (Figure 2). Before the treatment period and at the end of each month 6 smoking and 6 intact animals were sacrificed after ketamine and xylazine anesthesia. Total cell count and the ratio of lymphocytes, monocytes and granulocytes of the bronchoalveolar lavage fluids (BALF) were analysed with flow cytometer. Lungs were excised and rinsed with cold phosphate-buffered saline (PBS). MMP-2/-9 activity measurement was performed by gelatin zymography at the end of the 1st and 6th months, while cytokine concentrations were analysed with

the Mouse Cytokine Array Panel A from lung homogenates at the end of each month. One part of the lung tissue was placed in 6% formaldehyde solution for quantitative histological evaluation of emphysema and semiquantitative assessment of pulmonary inflammation. At the end of the 6th month restrained WBP was performed by invasive methodology in anaesthetised, tracheotomised and ventilated mice and blood samples were collected.

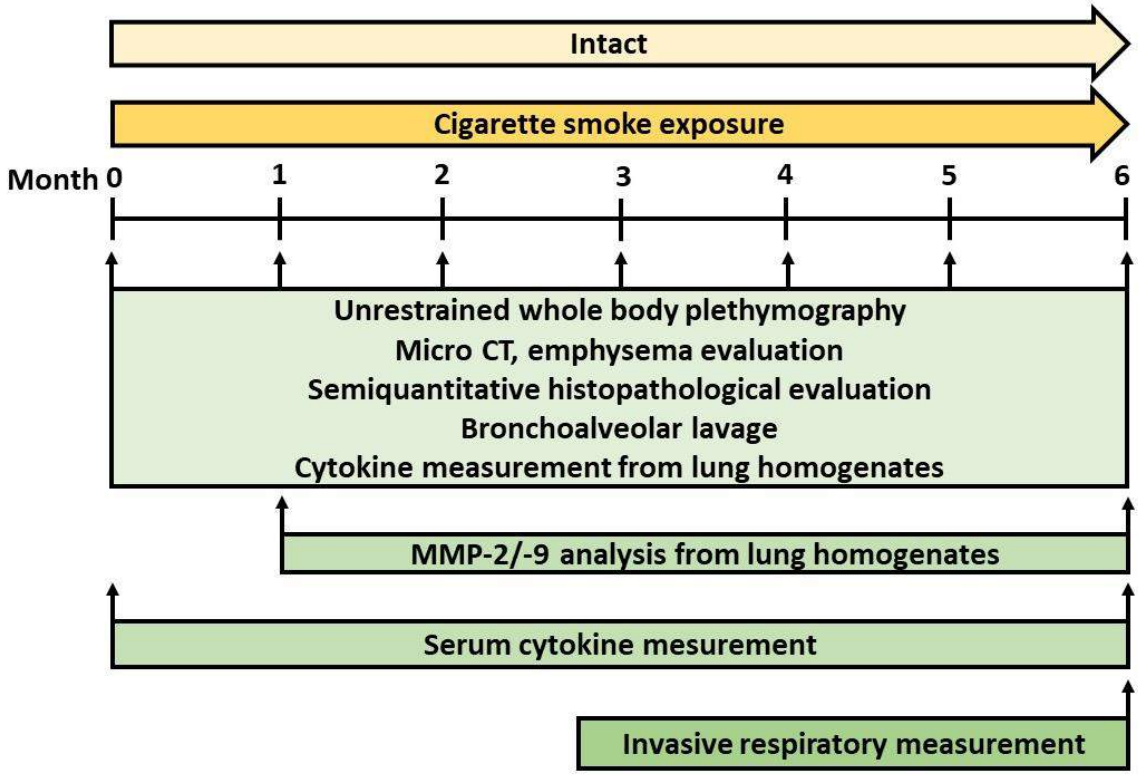

Figure 2. Experimental design for the characterisation of the chronic cigarette smoke exposure-induced COPD mouse model

3.1.3 Experimental design for investigating the involvement of TRPA1 in the cigarette smoke-induced COPD mouse model

Based on the results of the 6-month-long CSE mouse model we investigated the potential involvement of TRPA1 in chronic airway inflammation in a 4-month-long experimental design focusing on the peak of airway inflammation. *Trpa1*$^{-/-}$ and their *Trpa1*$^{+/+}$ counterparts were exposed to CSE twice daily, 10 times/week for 4 months. Age-matched non-smoking mice kept under the same circumstances served as controls. Airway function was determined by unrestrained WBP at the end of each month, while pulmonary structural and morphological changes were

imaged by a microtomograph and histopathological assessment after 2 and 4 months (Figure 3). BALF was analysed by flow cytometry at the end of the 2nd and 3rd months.

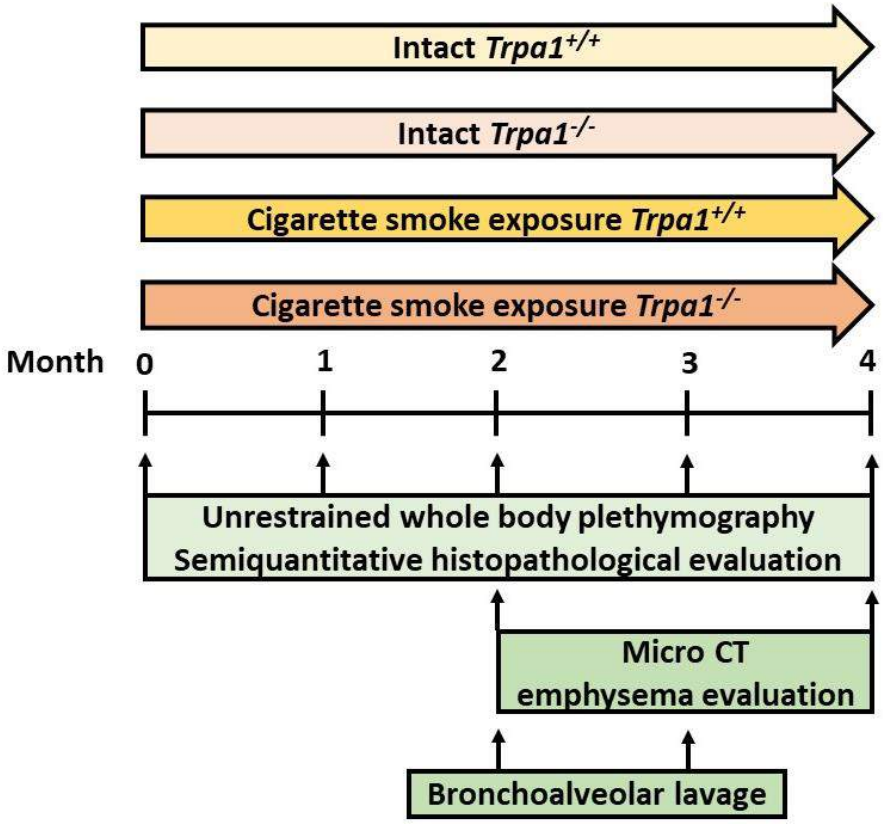

Figure 3. Experimental design for investigating the involvement of TRPA1 in the cigarette smoke-induced COPD mouse model.

3.1.4 Cigarette smoke (CS)-induced chronic airway inflammation

Chronic bronchitis was elicited by whole body CS (3R4F Kentucky Research Cigarette; University of Kentucky, USA) in a two-port TE-2 whole body smoke exposure chamber (Teague Enterprise, USA) twice daily, 10 times/week for 6 or 4 months depending on the experimental paradigm. Two cigarettes were smoked at a time for 10 minutes with a puff duration of 2 sec and a puff frequency of 1/min/cigarette, mice were exposed to smoke for 30 min followed by a ventilation period of 30 min during which smoke was driven from the chamber. The total particulate matter (TPM 154.97±5.18 mg/m3,), nicotine (9.86±0.33 mg/m3) and carbon-monoxide (147.57±4.93 ppm) concentrations were determined every week. Age-matched non-smoking mice kept under the same circumstances served as controls. The precise composition of the mainstream smoke is well established and described in detail (99).

3.1.5 Respiratory function measurement with unrestrained whole body plethysmography

Airway responsiveness was determined by unrestrained WBP with Buxco instrument (PLY3211, Buxco Europe Ltd., Winchester, UK) in conscious, spontaneously breathing animals before the treatment period serving as self-control values and at the end of each months during the 6 or 4 months CSE period. All measurements were performed on the same animals in a self-controlled manner. We determined the relaxation time (RT), breathing frequency (f), tidal volume (TV), minute ventilation (MV), inspiratory time (Ti), expiratory time (Te), peak inspiratory flow (PIF) and peak expiratory flow (PEF). Penh (enhanced pause) value correlating with airway reactivity was assessed by nebulising increasing concentrations (5.5, 11 and 22 mM) of the muscarinic receptor agonist carbachol (50 μL/mouse). Penh is a complex calculated parameter ((Te/RT)−1)/(PEF/PIF), well correlating with bronchoconstriction and airway resistance measured in ventilated animals using invasive techniques (5). These parameters were measured every 10 seconds during a 2-minute acquisition period and were averaged by the BioSystem XA Software for Windows (Buxco Research Systems) (100).

3.1.6 Invasive respiratory function measurement with restrained WBP

At the end of the 6-month protocol C57Bl/6 mice were anaesthetised with intraperitoneal administration of ketamine and xylazine and restrained WBP was performed by invasive methodology. Mice were tracheotomised and placed in a whole body plethysmograph (PLY4111, Buxco Europe Ltd., Winchester, UK) for measuring invasive resistance and compliance. The tracheal tube was connected to a mouse ventilator (MiniVent Type 845, Hugo Sach Elektronik - Harvard apparatus GmbH, March-Hugstetten, Germany) with a frequency of 120 strokes/min, and a stroke volume of 200 μL. After loading the animal, a water-coupled tube was inserted to the oesophagus to isolate the airway in the resistance calculations. The flow and pressure transducers (TRD5700 and TRD4515 Buxco Europe Ltd., Winchester, UK) were connected to the preamplifier module, which digitised the signals via an analogue-to-digital converter (MAX2270 Buxco Europe Ltd., Winchester, UK). All respiratory parameters, such as airway resistance (Rl), end-expiratory work (EEW), tidal mid-expiratory flow (EF50), end-expiratory pause (EEP), Te and Ti characteristic of COPD/emphysema and possible to determine with the BioSystem XA Software

for Windows were measured every 10 seconds and averaged during a 10-minute baseline reading period.

3.1.7 *In vivo* micro-computed tomography (micro-CT) analysis for emphysema quantification

Structural changes of the lungs were imaged by breath-gated tomography on a Skyscan 1176 high resolution microtomograph (Skyscan, Kontich, Belgium) at the end of each month in the 6-month-long protocol and and at the beginning and after the 2nd and 4th months in TRPA1 gene-deleted and wildtype mice in a self-controlled manner. Mice were anaesthetised with i.p. pentobarbital (70 mg/kg) and placed in supine position on the bed of the scanner, a piece of paper was placed onto the chest with a high-contrast sign to enable the video gating of the breathing movements to eliminate motion artefacts. Scanning parameters were the following: 50kV tube voltage, 500 μA tube current, 0.5 mm Al filter, 180 degree scan, 0.7 degree rotation angle between each camera angle and 10 acquired images per step. Pixel size was kept on 35 μm. One field of view covered the whole lung. With these settings one scan took about 12-15 minutes and provided a good combination of sufficient resolution, short scan time and low radiation. After sorting the images into 5 bins (stacks) of images, each bin contained at least 2 images, based on the video gating signal. The bins represent a certain phase of breathing cycle. One of the bins was chosen for reconstruction with following settings: ring artefact correction was set at 20, 35% beam hardening correction, smoothing was set at 5. Reconstruction and morphometric analysis were performed with a software package provided by the manufacturer. Image analysis was performed according to literature data (101). Briefly, air-filled pixels outside the animals were excluded from reconstructed images using a previously reconstructed image of a phantom with air-containing Eppendorf tube and using a "despeckle" command. The resulting images were reloaded and thresholding was repeated to determine the air-filled areas within the lung (with an additional "despeckle" command). Emphysema was calculated by the ratio of low attenuation area (LAA, from -750 to -1000 Hounsfield unit, representing the air-filled regions) and total lung volume (TLV) and was expressed in percentage (102).

3.1.8 Bronchoalveolar lavage fluid (BALF)

At the end of each month of the 6-month-long smoke exposure protocol mice were anaesthetised with ketamine and xylazine (100 mg/kg and 5 mg/kg, s.c., respectively), lungs were flushed with

cold PBS (5x1 mL) with the help of a trachea cannula and BALFs were collected. They were centrifuged at 1000 rpm for 5 minutes at room temperature, then stained and fixed for flow cytometry as follows: cells were resuspended in 500 μL staining solution (PBS with 0.1% bovine serum albumin (BSA) and 0.1% NaN_3) and incubated with 1 μL fluorescein isothiocyanate (FITC)-CD45 (mouse IgG1, Becton Dickinson, San Jose, CA) as a panleukocyte marker and 1 μL propidium iodine (Sigma-Aldrich, Budapest, Hungary) to exclude cellular debris for 30 min at room temperature in the dark. After the incubation, samples were centrifuged and washed, then resuspended in PBS with 2% neutral-buffered formalin. Cell preparations were immediately analysed with CyFlow Space flow cytometer (Sysmex Partec, Münster, Germany). Total cell count and the ratio of lymphocytes, monocytes and granulocytes were calculated regarding their forward/side scatter (FSC/SSC) feature. Gating was determined from mouse peripheral blood sample as control (103,104).

Based on the results in the 6-month-long CSE model perivascular/peribronchial oedema developed in the 1st month, while in the 2nd and 3rd months inflammatory cell infiltration dominated the histopathological picture, which decreased by the 4th month and was accompanied by tissue destruction (105). Based on these data, we investigated the number of inflammatory cells in the BALF of *Trpa1*$^{-/-}$ and *Trpa1*$^{+/+}$ mice after the 2nd and 3rd months.

3.1.9 Histopathological evaluation of pulmonary inflammation and emphysema

The mean linear intercept (chord) length (L_m), a widely used parameter to quantify distal air space enlargement, was measured to evaluate the size of the acinar air space complex related to emphysema (106). Slides were scanned by a Pannoramic DESK scanner (3DHISTECH Ltd., Budapest, Hungary) and the alveolar space or alveolar and ductal air space together were measured along parallel test lines by using the Case Viewer software (3DHISTECH Ltd., Budapest, Hungary). At least 3 sections were evaluated from each mouse from different depths on approximately 400,000 μm^2 representative areas to obtain reliable results (n=80-100 measurements per mouse). Tissue shrinkage or integrity damage were not observed.

Histopathological analysis of lung sections was performed by a pathologist in a blind manner in order to evaluate perivascular/peribronchial oedema, acute and chronic inflammation, interstitial acute and chronic inflammation, epithelial damage and goblet cells. Scores were assessed by observing several representative microscopic fields on a semiquantitative scale ranging from scores

0-3 (0 - normal, 1 – mild, 2 – moderate and 3 – severe histopathological alterations in the examined parameters).

3.1.10. Detection of MMP-2 and MMP-9 activities by gelatin zymography in the lung

To measure pulmonary MMP-2 and MMP-9 activities, gelatin zymography was performed from mouse lung samples. MMP-2 has 2 major isoforms, 72 kDa and 64 kDa (107). Basically, the 64 kDa MMP-2 activated by limited proteolysis is the active form of the enzyme, but 72 kDa MMP-2 can also be activated via an alternative way. The same can be observed in case of MMP-9: 86 kDa MMP-9 is the cleaved active form, but 92 kDa MMP-9 can also gain activity. Gelatinolytic activities of these MMP isoforms were examined as previously described (108). Briefly, 8% polyacrylamide gels were copolymerized with gelatin (2 mg/mL, type A from porcine skin, Sigma-Aldrich), and 50 μg of protein per lane was loaded. An internal standard (American Type Culture Collection, Manassas, VA) was loaded into each gel to normalize activities between gels. After electrophoresis (90 V, 90 min), gels were washed with zymogram renaturation buffer (Bio-Rad Laboratories, Hercules, CA) for 40 min. Lung samples were incubated for 20 h and at 37°C in zymogram development buffer (Bio-Rad Laboratories, Hercules, CA). Gels were then stained with 0.05% Coomassie brilliant blue (G-250, Sigma-Aldrich) in a mixture of methanol-acetic acid-water [2.5:1:6.5 (vol/vol)] and destained in aqueous 4% methanol-8% acetic acid (vol/vol). For positive controls, gelatinase zymography standard containing human MMP-2 and -9 (Chemicon Europe Ltd., Southampton, UK) were used. For negative control, lanes containing tissue samples were cut off after renaturation of the gel and were separately incubated for 20 h at 37°C in development buffer in the presence of the calcium chelator ethylene glycol-bis(2-aminoethylether)-N,N,N′,N′-tetraacetic acid (EGTA; 10 mM). Gelatinolytic activities were detected as transparent bands against the dark-blue background. Gels were scanned in a transilluminator, and band intensities were quantified, expressed as the ratio to the internal standard, and presented in arbitrary units.

3.1.11 Cytokine profile analysis

Excised lung tissues were thawed, weighed, and immediately homogenised in PBS containing 1% protease inhibitor phenylmethylsulfonyl fluoride (PMSF, Sigma-Aldrich, Budapest, Hungary), and centrifuged at 10,000 g for 5 min to remove cell debris. Triton X-100 was added to a final concentration of 1%. Blood samples from 6 months smoking and intact animals were left to clot in room temperature for 30 min, then centrifuged for 20 min at 2000g. Serum was removed and

processed as follows. Total protein content of the homogenates and serum samples were determined prior to cytokine measurement with BioRad DC protein assay kit. Samples were diluted regarding their total protein content in 1 g wet tissue or in 1 mL serum. Forty different inflammatory cytokines were determined simultaneously with Mouse Cytokine Array Panel A (R&D Systems) according to the manufacturer's instruction. Briefly, capture antibodies of forty pre-selected cytokines were spotted in duplicate on nitrocellulose membrane. Diluted samples and biotinylated detection antibody mixtures were incubated on the membranes overnight. Chemiluminescent detection was performed on the 2nd day and semiquantitative analysis based on densitometry was done with ImageJ freeware. To eliminate the interassay variability all data were re-calculated with the same control-spot densities (109). Cytokine heat map was generated by Matrix2png 1.2.1 online freeware (110).

3.1.12 Statistical analysis

Values for all measurements were expressed as the mean ±SEM of n=6 mice in each group except for restrained WBP (n=5 per group) and cytokine determination of lung homogenates (n=3 per group). Evaluation of the unrestrained WBP, and micro-CT results have been performed by repeated measures ANOVA followed by Bonferroni's modified t-test to see statistical differences between different data sets and then between the respective data points. Data collected from BALF flow cytometry and mean linear intercept length (80-100 measurements/slides) were analysed with two-way ANOVA followed by Sidak's multiple comparison test. Expression level of forty different cytokines was statistically compared to intact values with two-way ANOVA followed by Bonferroni's post-test. Restrained WBP results were analysed by Student's t-test for unpaired comparison. Evaluation of the semiquantitative histopathological scoring was analysed by Kruskal-Wallis followed by Dunn's multiple comparison test to observe intragroup differences by time, while Mann-Whitney test was performed to analyse intergroup differences at given time points.

3.2 Chronic gastritis model

3.2.1 Animals and ethics

Experiments were performed on 8-week-old male CD1 and C57Bl/6 mice weighing 18–25 g and Wistar rats weighing 180–220 g at the beginning of the study; each group consisted of 6 animals. Animals were bred and kept in the Laboratory Animal House of the Department of Pharmacology and Pharmacotherapy, University of Pécs, Pécs, Hungary at 24–25 °C, provided with standard rodent chow and water *ad libitum*, maintained under 12 h light-dark cycle. All procedures were carried out according to the 40/2013 (II.14.) Government Regulation on Animal Protection and Consideration Decree of Scientific Procedures of Animal Experiments and Directive 2010/63/EU of the European Parliament. They were approved by the Ethics Committee on Animal Research of University of Pécs according to the Ethical Codex of Animal Experiments (license no.: BA02/2000-20/2019, June, 2019).

3.2.2 Iodoacetamide (IAA)-induced gastritis model

Gastritis was induced by the administration of IAA (Sigma-Aldrich Inc., Darmstadt, Germany) to the drinking water. Since IAA is light-sensitive, IAA-containing drinking water was prepared freshly every day by dissolving 0.1, 0.2, 0.4, 0.6 or 1 g IAA in 200 mL tap water (0.05%, 0.1%, 0.2%, 0.3% and 0.5% concentration, respectively) for 7 or 14 days consecutively, depending on the experimental paradigm (Figures 4, 5).

Fluid intake and body weight were measured daily in each study. At the end of the study, animals were euthanised under ketamine (120 mg/kg ip.; Calypsol, Gedeon Richter Plc., Budapest, Hungary) and xylazine (6 mg/kg ip.; Sedaxylan, Eurovet Animal Health B.V., Bladel, Netherlands) anesthesia. The stomach was excised, opened along the greater curvature and rinsed with room temperature saline. After photo documentation of the macroscopic lesions, the stomach was cut in four sections: antrum and corpus specimens were fixed in 6% formaline and 5 μm sections were stained with hematoxylin and eosin (HE) for histopathologic and immunohistochemical evaluation. Other antral and corpus samples were snap-frozen for molecular biological assessments.

3.2.3 Experimental design for IAA-induced gastric injury model in rats

Rats were randomized into 8 groups of 6 animals in each, and received 0.05%, 0.1% or 0.2% IAA solution in the drinking water for 7 or 14 days consecutively. Littermates drinking IAA-free tap water served as control animals (Figure 4).

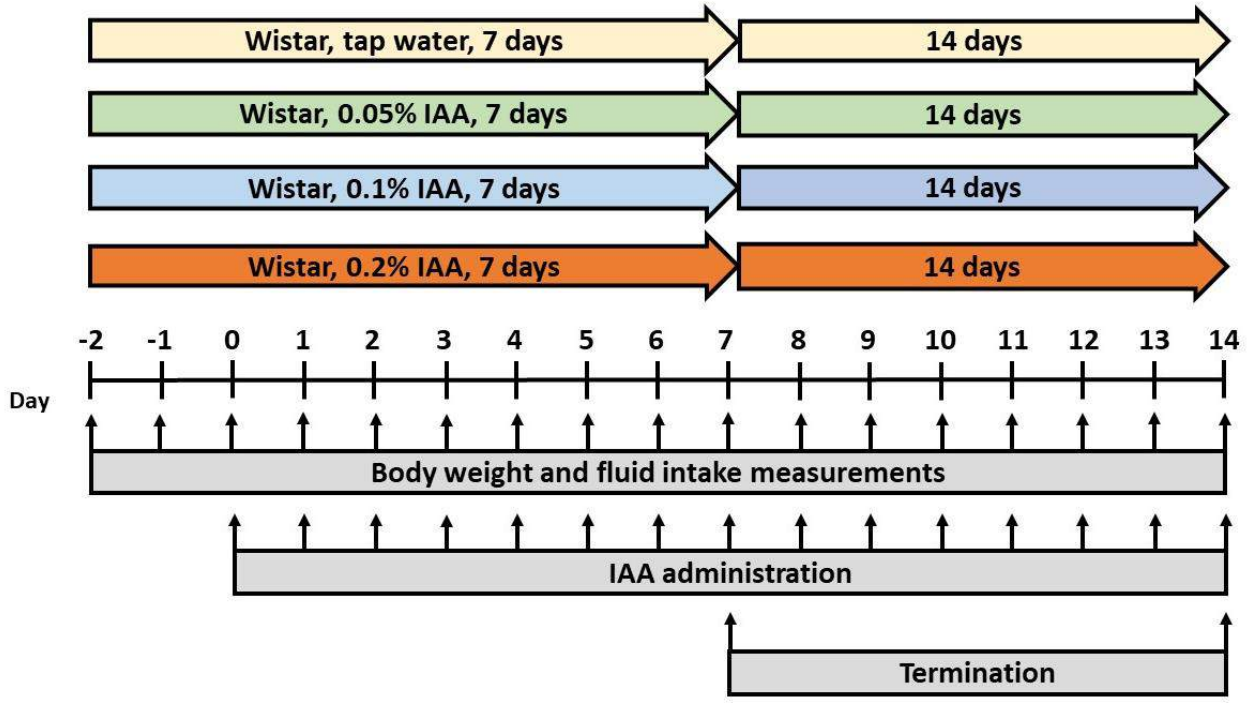

Figure 4. Experimental design of IAA gastritis. Male Wistar rats were divided into 8 groups according to the duration of the protocol (7 days or 14 days) and concentration (0.05%, 0.1% or 0.2%) of IAA dissolved in drinking water. Control rats received tap water. Body weight and fluid intake were monitored daily throughout the experiment. At the end of the protocol, rats were euthanised, and their stomachs were excised for macroscopic, microscopic evaluation and further molecular biological assessment.

3.2.4 Experimental design for IAA-induced gastric injury model in mice

In the first mouse study, CD1 mice were randomized into 4 groups: mice receiving 0.1% IAA for 7 and 14 days, with the respective control groups. Based on the negative results of this study, CD1 mice were randomized in 3 groups receiving 0.3% and 0.5% IAA for 7 days; the control group drank tap water. To investigate interstrain differences, C57Bl/6 mice were randomized into 4 groups receiving 1) 0.3% IAA-containing drinking water, 2) 0.3% IAA-containing drinking water, which also contained 2% sucrose, 3) a control group drinking tap water, and 4) a second control group receiving 2% sucrose dissolved in tap water (Figure 5).

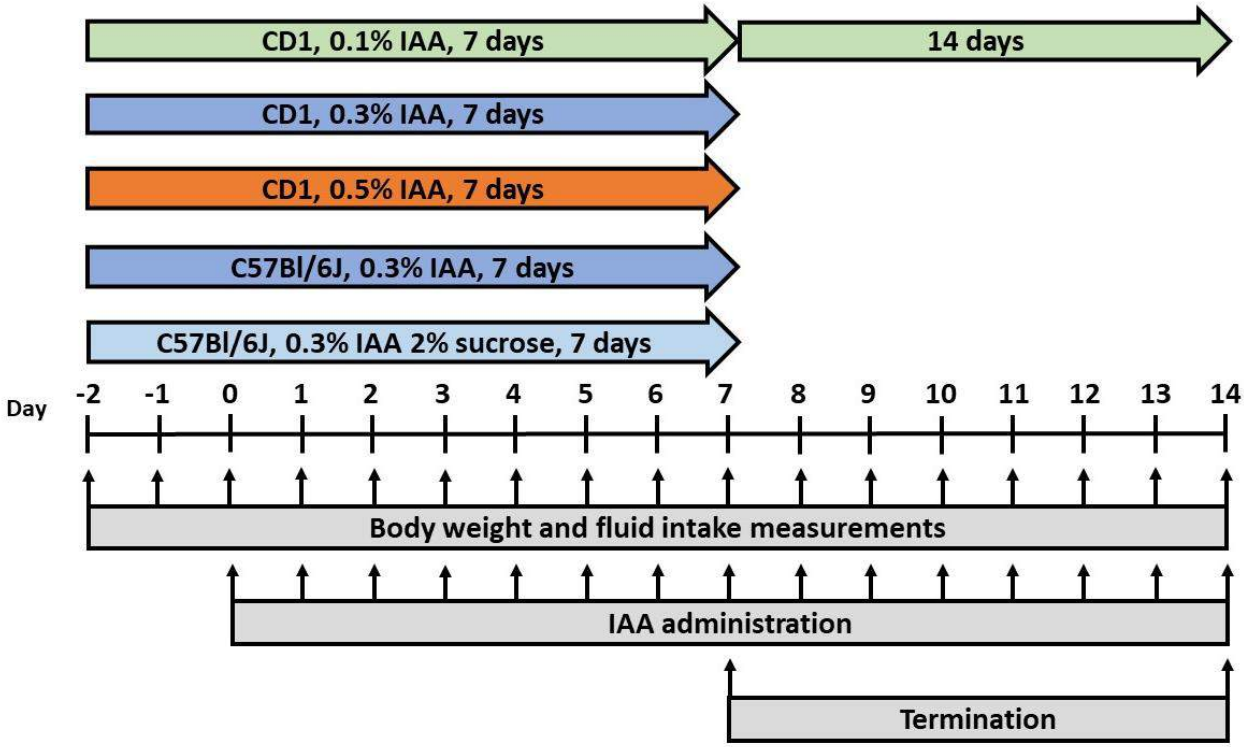

Figure 5. Experimental design of IAA gastritis with CD1 and C57Bl/6 mice. Male CD1 and C57Bl/6 mice were divided into groups receiving various concentrations (0.1%, 0.3% and 0.5%) of IAA dissolved in drinking water. Control mice received tap water. Body weight and fluid intake were monitored daily throughout the experiment. At the end of the protocol, mice were euthanised, and their stomachs were excised for macroscopic and microscopic evaluation.

3.2.5 Semiquantitative macroscopic and qualitative histopathological evaluation of gastric lesions

The extent and severity of the macroscopic lesions were evaluated by a semiquantitative scoring system based on the extent of hyperemia (0: none; 1: < 25%, 2: 25–50%; 3: > 50% of the total gastric mucosa) and the number of erosions/ulcerations (0: none; 1: 1-2; 2: 3-4; 3: ≥5). Excised gastric samples were paraformaldehyde-fixed (4%) and embedded in paraffin, 5 μm sections were cut and stained with HE for further qualitative histological analysis, i.e., the assessment of the extent of lesions, submucosal infiltration and capillarization.

3.2.6 Total glutathione concentration measurement

GSH was measured in gastric mucosa specimens by a specific high power liquid chromatography (HPLC) method after pre-column derivatisation with *ortho*-phthaldehyde (OPA) as described previously for erythrocytic GSH (111). Wet specimens weighing 122 to 241 mg were homogenized in 1-mL aliquots of ice-cooled PBS (0.1 M, pH 7.2) in precellys tubes (Bertin-Instruments, USA) four times each for 20 s at 5500 rpm. The homogenates were immediately centrifuged (5 min, 3345 g, 4°C), and the supernatants (500 µL) were ultrafiltered by centrifugation using Vivaspin 500 cartridges (15,000 g, 20 min, 4 °C; Sartorius, Germany). The ultrafiltrate samples (25 – 40 µL aliquots) were frozen immediately and kept stored at -20 °C until subsequent analysis. After thawing, 20 µL aliquots of the ultrafiltrates were diluted with 180 µL of ice-cooled PBS. Aliquots (50 µL) of the dilutions were treated with 900 µL borate buffer (0.4 M, pH 8.5) and 50 µL of the OPA reagent (111). HPLC analysis with UV absorbance detection (338 nm) was performed 2 min after derivatisation by injecting 20 µL aliquots of the samples.

The 5 µm RP 18 NUCLEOSHELL HPLC columns (guard column, 4 x 3 mm; analytical column, 250 x 4 mm) were from Macherey-Nagel (Düren, Germany) and were thermostated at 20 °C. Isocratic elution was performed with 10 vol% methanol-90 vol% sodium acetate (150 mM, pH 7.5) at a flow rate of 1 mL/min (111). The GSH-OPA derivative eluted from the column at 3.924±0.027 min (coefficient of variation, 0.7%). The concentration of GSH in the samples was calculated by using a calibration curve generated in the range 0-1000 µM upon sample dilution as performed for the ultrafiltrate samples. Plotting of the peak area of the GSH-OPA peak (y, mAU/min) versus the GSH concentration (x, µg/mL) resulted in a line (r^2=0.9987) with the regression equation y=1.38+0.31x. The calibration curve samples were re-analysed next day by HPLC and resulted in the regression equation y=0.53+0.33x (r^2=0.9997), indicating the high inter-assay precision of the method. This HPLC method can also analyze γ-glutamyl-cysteine (GluCys), but not cysteine and other cysteine-containing species (111). In some samples we observed a peak eluting in front of GSH-OPA peak (retention time, 2.964±0.156 min) and is likely to be the GluCys-OPA derivative (112,113). HPLC analysis of the GSH calibration curve samples did not reveal presence of GluCys in the GSH preparation. Incubation of biological samples including human erythrocytes with *N*-acetylcysteine ethyl ester (NACET) allows for the measurement of total GSH (tGSH) (111) and total GluCys (tGluCys) (112). tGluCys includes free GluCys and GluCys released by NACET from symmetric and asymmetric disulfides (R-GluCys). Analogous, tGSH includes free GSH and GSH released by NACET from the symmetric GSH disulfide (i.e., GSSG) and from asymmetric disulfides (R-GSH). The GSH concentration in the homogenate samples was corrected by the protein concentration in the homogenates as measured by the BCA method and is reported as nmol GSH per mg wet protein. Due to the lack of a GluCys reference

compound, the concentration of GluCys in the samples was not measured. Yet, it is assumed that GSH and GluCys, at a molar basis, yield closely similar peak areas.

3.2.7 TRPV1 and TRPA1 immunohistochemistry and scoring

For antigen recovery, the paraformaldehyde-fixed and paraffin-embedded tissue samples were deparaffinised, rehydrated and incubated in acidic citrate buffer (pH 6) in a microwave oven. Endogenous peroxidase activity was quenched 3% hydrogen peroxide. The sections were washed and incubated in blocking solution, then treated with a 1:1000 dilution of rabbit polyclonal anti-TRPA1 (ab68848; Abcam, Cambridge, UK) and anti-TRPV1 (GP14100; Neuromics, Edina, MN, USA) antibodies. Slides were incubated with anti-rabbit secondary antibody conjugated with horseradish peroxidase (HRP) (DakoCytomation, Carpinteria, CA, USA) with the EnVision system. The reaction was visualised by 0.01% hydrogen peroxide containing 3,3-diaminobenzidine tetrachloride, and histological counterstaining was performed with hematoxylin (114). Quantitative assessment of TRPA1 and TRPV1 immunopositivity was performed based on the % ratio of the immunopositive cells on 10 fields of vision/slide/animal by an expert pathologist blinded to the study. Pannoramic Digital Slide Scanner with CaseViewer software (3DHISTECH Ltd., Budapest, Hungary) was used for both the evaluation and taking the representative photos of the slides. Incubating untreated rat gastric mucosa with Tris-buffered saline instead of the primary antibodies served as the negative control, while sections of rat dorsal root ganglia expressing TRPA1 and TRPV1 abundantly were used as positive controls. Antibody selectivity was validated by the lack of immunopositivity after the respective blocking peptides (ab150297 for TRPA1; Abcam, Cambridge, UK and P14100 for TRPV1; Neuromics, Edina, MN, USA) and was also based on literature data (115).

3.2.8 *Trpv1* and *Trpa1* real-time qPCR analysis

Total RNA was purified by TRI Reagent (Molecular Research Center Inc., Cincinnati, OH, USA) with Direct-Zol RNA MiniPrep isolation kit (Zymo Research, Irvine, CA) following the manufacturer's protocol. The quantity and purity of RNA samples were assessed by NanoDrop ND-1000 spectrophotometer (NanoDrop Technologies Inc., Wilmington, DE) and then treated with deoxyribonuclease I enzyme (Zymo Research, Irvine, CA, USA). Purified total RNA (100 ng) was reverse transcribed with Maxima First Strand cDNA Synthesis Kit (Thermo Fisher Scientific,

Waltham, MA, USA) according to the manufacturer's instructions. Real-time qPCR was conducted on a Stratagene M×3000P qPCRSystem (Agilent Technologies, Santa Clara, CA, USA) using Luminaris HiGreen LowROX qPCR Master Mix (Thermo Fisher Scientific, Waltham, MA, USA) to amplify transcripts. The following primer pairs were used: the reference gene glyceraldehyde 3-phosphate dehydrogenase (*Gapdh*) (NM_017008.4) (sense): 5′-TGCACCACCAACTGCTTAGC-3′ and (antisense): 5′-GGCATGGACTGTGGTCATGAG-3′; *Trpv1* (NM_031982.1) (sense): 5'-AATACACCATCGCTCTGCT-3' and (antisense): 5'-CAATGTGCAGTGCTGTCTGG-3'; *Trpa1* (NM_207608.1) (sense): 5'-ATCCAAATAGACCCAGGCACG-3' and (antisense): 5'-CAAGCATGTGTCAATGTTTGGTACT-3'. Primers with similar efficiencies were used. In order to verify primer specificity, dissociation curve analyses were performed. All reactions were measured in triplicates, and the geometric mean of their Ct values were calculated. The determination of relative mRNA expression levels was performed according to the comparative DDCt method using samples of control animals as calibrator.

3.2.9 Statistical analysis

Statistical analysis was performed by using GraphPad Prism v6 software. Values for all measurements are expressed as means ± SEM of n = 6 animals in each group. Evaluation of body weight change and fluid intake was performed by repeated-measures ANOVA followed by Bonferroni's modified t-test. Semiquantitative macroscopic scoring was analysed by the non-parametric Kruskal–Wallis method followed by Dunn's multiple comparison test to observe intergroup differences at given timepoints, while Mann–Whitney test was performed to analyse intragroup differences by time. GSH measurements were analysed by one-way ANOVA, while TRPA1 and TRPV1 immunopositivities were evaluated by ordinary two-way ANOVA followed by Dunn's multiple comparisons test. qPCR measurements were evaluated by Student's unpaired t-test.

4 Results

4.1 Characterization of CS-induced chronic pulmonary inflammation model

4.1.1 Follow-up measurement of respiratory functions by unrestrained WBP

Pulmonary functions were determined at the end of each month in conscious mice by unrestrained whole-body plethysmography in a self-controlled manner. None of the parameters determined by this technique (RT, f, TV, MV, Ti, Te, PIF, PEF) were different between the smoking and non-smoking groups at any time-points during the 6-month-period (Figure 6). This is in agreement with the findings of Vanoirbeek and colleagues, who demonstrated that the non-invasive method is not appropriate to determine functional alterations especially in emphysema (116).

4.1.2 Invasive respiratory function parameters at the end of the 6-month-long protocol

At the end of the 6^{th} month, restrained whole-body plethysmography was performed in tracheotomised, anaesthetised and mechanically ventilated mice. Significant decrease of Rl, EEW, EEP, Te, as well as increase of EF50 and Ti/(Ti+Te) ratio were observed, whereas dynamic compliance did not change in response to chronic smoke exposure as compared to the non-smoking group (Figure 7).

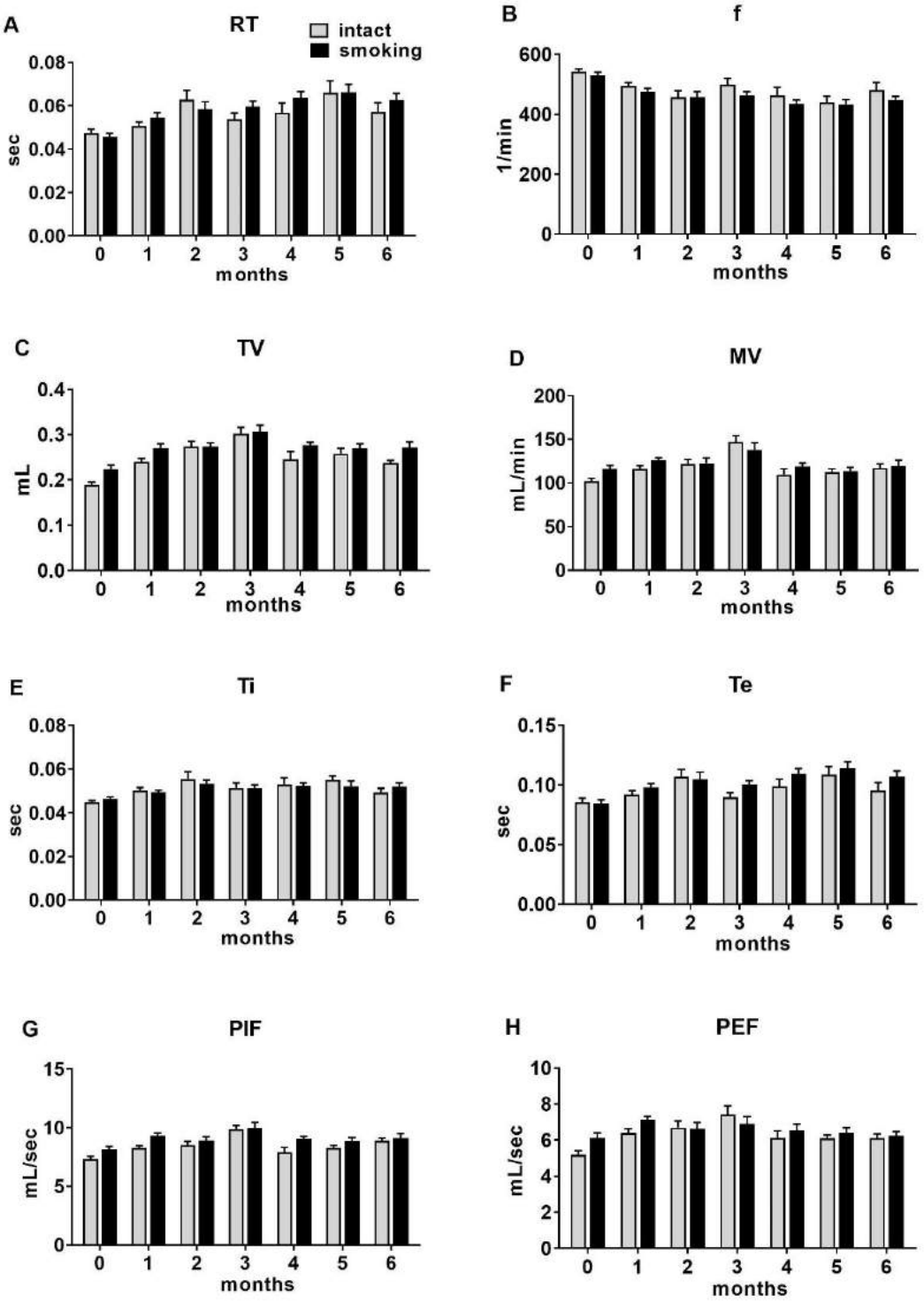

Figure 6. Unrestrained WBP parameters before the treatment period (0 month) and at the end of each month during the 6-month CSE period. A) relaxation time (RT). B) frequency (f), C) tidal volume (TV), D) minute ventilation (MV) E) time of inspiration (Ti), F) time of expiration (Te), G) peak inspiratory flow (PIF) and H) peak expiratory flow (PEF). n = 6 / group.

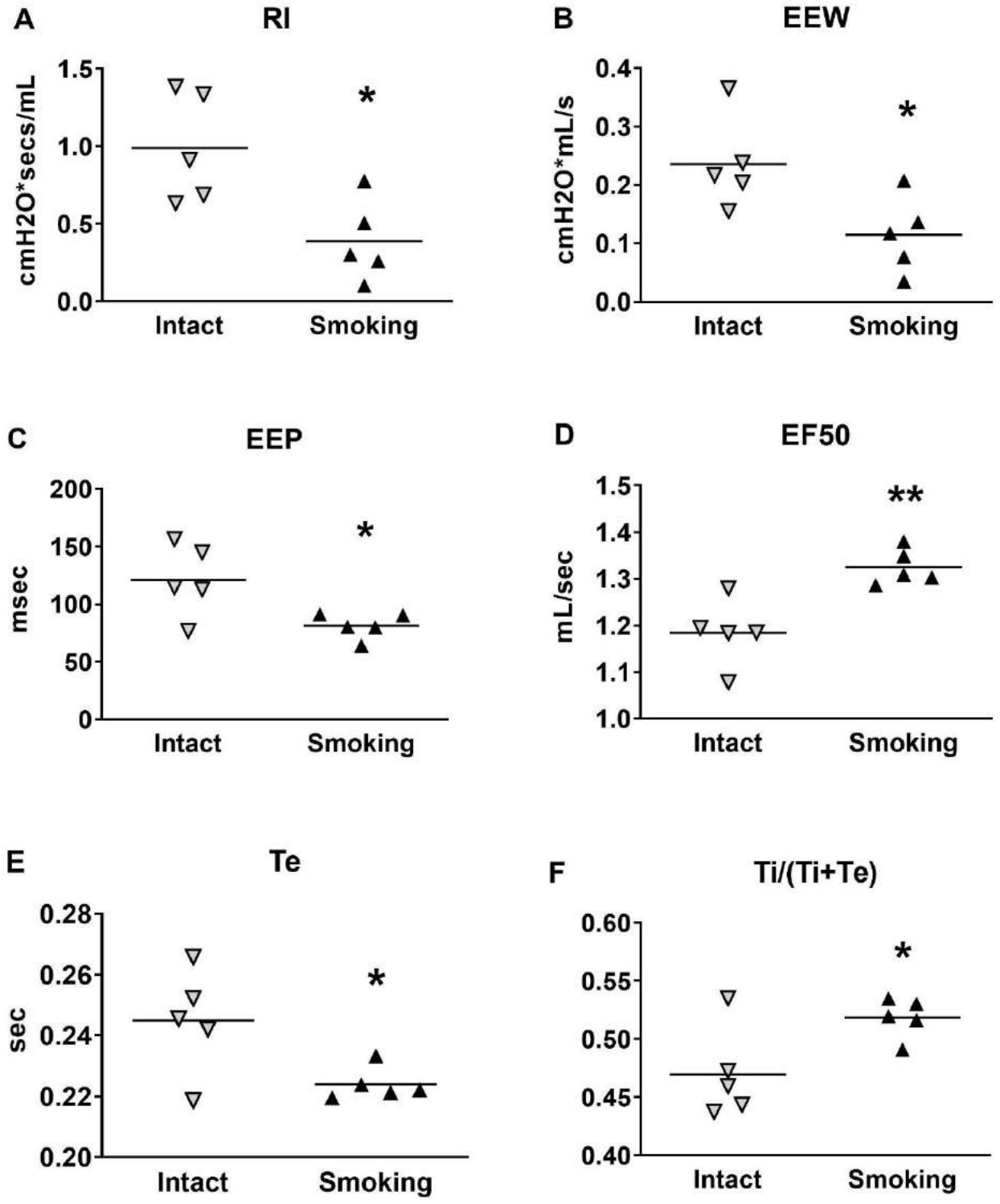

Figure 7. Respiratory parameters measured by restrained WBP at the end of the 6th month. A) airway resistance (Rl), B) end expiratory work (EEW), C) end expiratory pause (EEP), D) tidal mid-expiratory flow (EF50), E) time of expiration (Te) and F) time of inspiration (Ti) andTi/(Ti+ Te) ratio. n = 5 / group (Student's t-test for unpaired comparison, *p<0.05; **p< 0.005; vs. the intact, non-smoking group).

4.1.3 Emphysema evaluation by micro-CT and mean linear intercept analysis

Dynamic structural changes of the lung were investigated by *in vivo* micro-CT during the 6-month smoking period. Emphysema formation, as the most important sign of tissue destruction, was clearly observed on the reconstructed 3D images (Figure 8A). According to our morphometric analysis the LAA/TLV%, a quantitative indicator of emphysema showed significant increase by the end of the 5th month that was further increased by the end of the 6th month (Figure 8B).

Remarkable alveolar space enlargement (L_m) was observed already after 1 month of CSE in comparison with the non-smoking group (Figure 8C). This parameter mainly characteristic to emphysema progressively increased parallelly to our micro-CT findings. By the end of the 5th month the distal air space was significantly expanded in smoking mice as compared to the L_m after the 1st month.

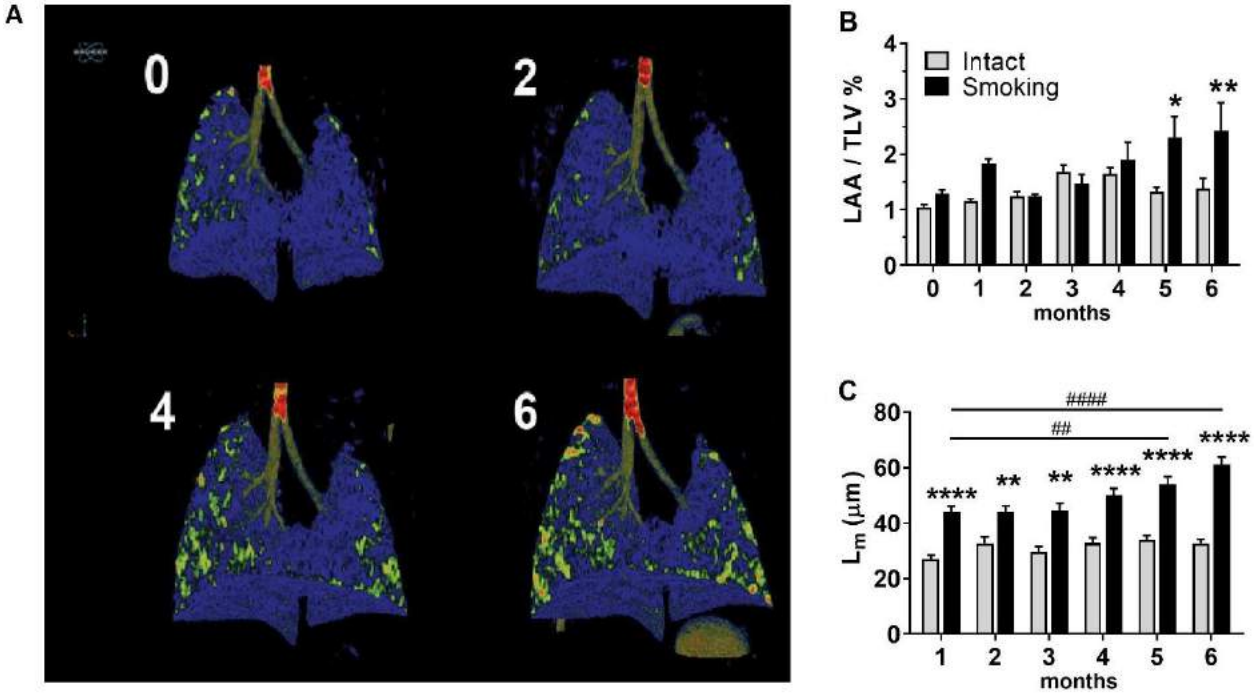

Figure 8. Evaluation of emphysema by micro-CT measurement and histological assessment of mean linear intercept (L_m) length. A) Representative 3D pictures of mouse lung before the treatment (0) and after 2, 4 and 6 months of smoking period. Light green and yellow areas represent the air-filled spaces. B) Calculated percentage of emphysema by the ratio of low-attenuation area (LAA) and total lung volume (TLV). n = 6 / group (two-way ANOVA followed by Bonferroni's post-test, *p< 0.05; **p< 0.005 vs. the intact, non-smoking group). C) Lm measured on formalin fixed lung sections at the end of each month. N=80-100 chords per animal (two-way ANOVA followed by Bonferroni's post-test, **p< 0.005; ****p< 0.0001 vs. the intact, non-smoking group; ## p< 0.005; ####p< 0.0001 vs 1 month of smoking).

4.1.4 Qualitative and semiquantitative histopathological analysis

As compared to the intact, normal lung structure of a 3-month-old mouse (Figure 9A), one month of CSE induced a minimal peribronchial and moderate perivascular oedema formation, and slightly increased numbers of granulocytes and macrophages in the lung parenchyma (Figure 9B). After 2 months of smoking, there was an extensive perivascular and peribronchial oedema with large number of granulocytes, macrophages and lymphocytes infiltrating these regions. Inflammation was characteristic both to the interstitial and peribronchial areas, in addition, the bronchiolar epithelial cell layer became irregular, the bronchiolar and alveolar epithelium showed signs of damage, and the number of interepithelial mucus-producing cells was increased (Figure 9C, D). Interestingly, this massive inflammatory reaction showed a decreasing tendency from the 3-month-timepoint, the peribronchial oedema was still present, but less extensive, the number of immune cells was reduced and were mostly lymphocytes, which moved from the peribronchial spaces to the interstitial regions. Meanwhile, the bronchiolar epithelial destruction was remarkably greater (Figure 9E). At the 4-month CSE, the irregularity and damage of the bronchial epithelium was further aggravated. Tissue destruction became more severe, mild emphysema (enlargement of airspaces throughout the parenchyma) and atelectasis developed particularly on the peripheral regions. However, mild oedema was limited to the perivascular spaces and the number of inflammatory cells remarkably decreased (Figure 9F). After 5-6 months of smoking emphysema dominated the histological picture, first mainly in the peripheral areas, then also in the central parts of the lung. Inflammatory reaction at this stage was minimal, only few macrophages and lymphocytes could be noticed in the remaining parenchyma, while irregularity of the bronchial epithelium and hyperplasia of the mucus producing cells could be observed (Figure 9G, H). The semiquantitative histopathological scoring results throughout the 6-month study are shown in Figure 10.

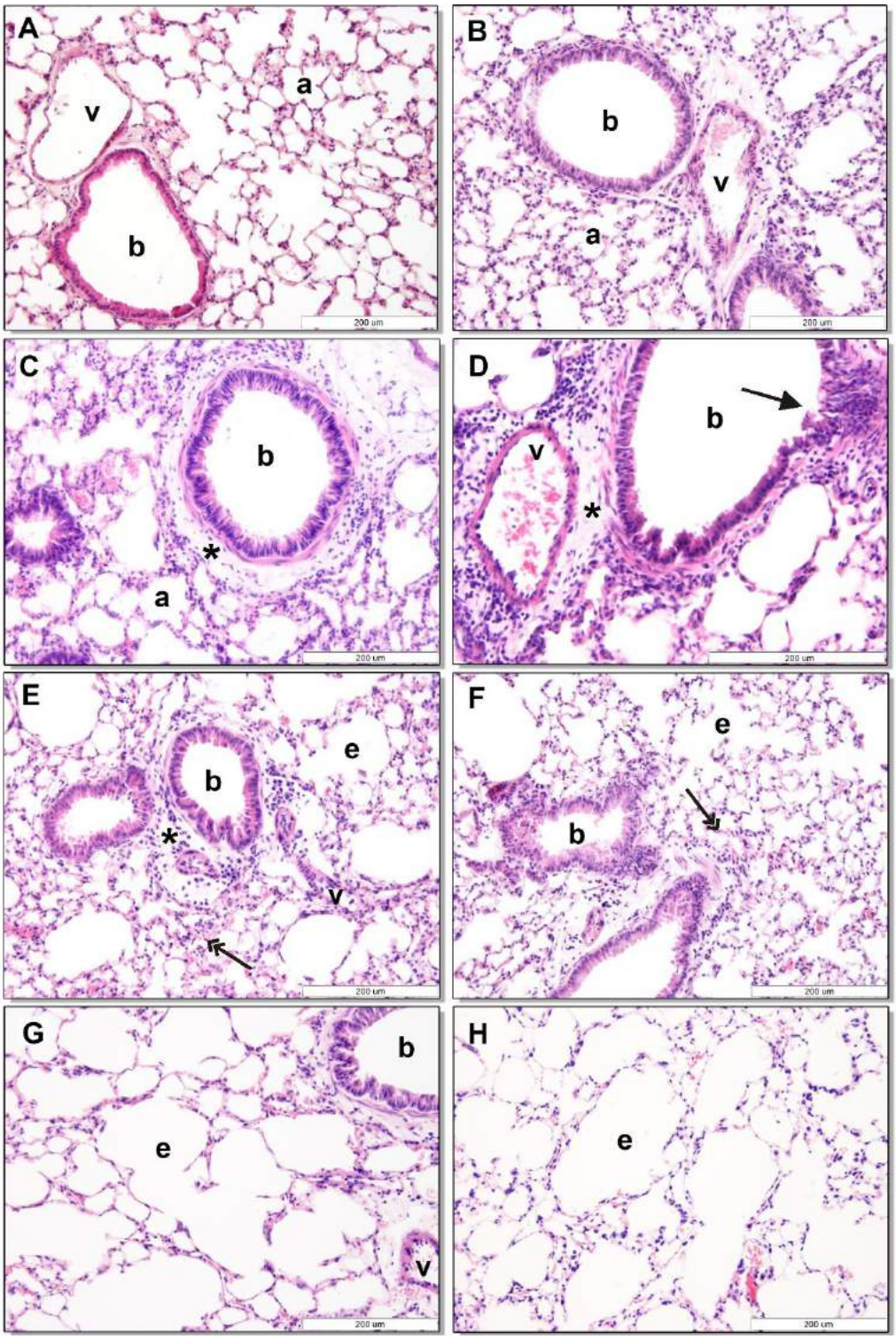

Figure 9. Representative histopathological pictures of the lung samples obtained A) before the treatment and B) after 1 month, C,D) 2 months, E) 3 months F), 4 months G), 5 months H) and 6 months. HE staining, magnification: 200x, except panel D: 400x; b: bronchioles, v: vessels; a: alveoli, *: peribronchiolar oedema, black arrow: disruption of bronchi wall, double headed arrows: granulocyte accumulation, e: emphysema.

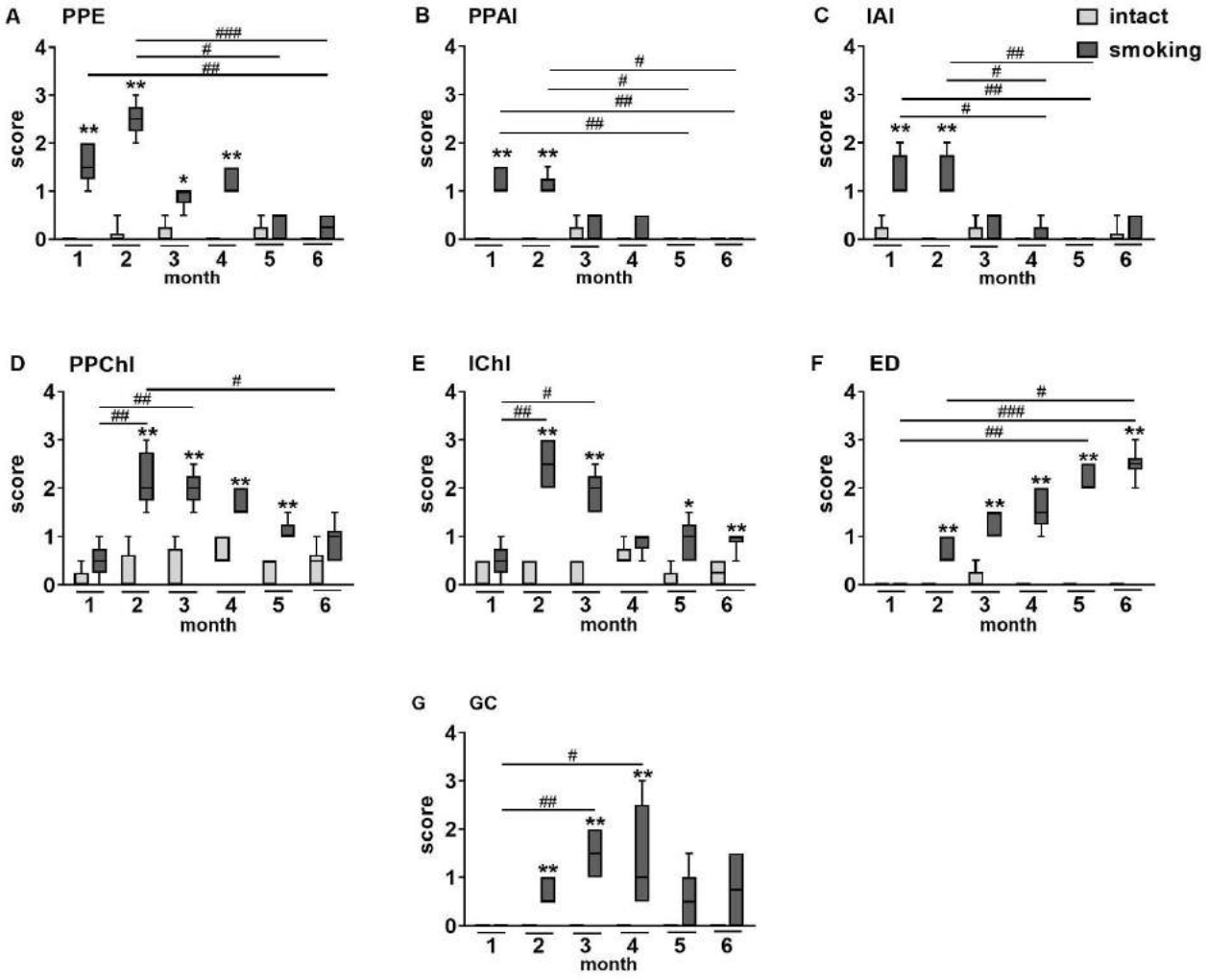

Figure 10. Semiquantitative histopathological evaluation of lung sections. Box plots representing lesion extent on a range from 0-3 (mean ± minimal-maximal values) of A) perivascular/ peribronchial oedema (PPE); B) perivascular/peribronchial acute inflammation (PPAI); C) interstitial acute inflammation (IAI); D) perivascular/peribronchial chronic inflammation (PPChI), E) interstitial chronic inflammation (IChI); F), epithelial damage (ED); G) and goblet cells (GC) at the end of each month. n = 6 / group (Kruskal-Wallis followed by Dunn's multiple comparison test to observe intragroup differences by time #p< 0.05, ##p< 0.005, ###p< 0.0005 vs. same group; Mann Whitney test to analyse intergroup differences at given time points *p< 0.05, **p< 0.005 smoking vs. intact group.

4.1.5 Inflammatory cell count in the BALF

At the end of the 1st month flow cytometric analysis revealed no difference in the granulocyte, macrophage and lymphocyte numbers of BALF samples obtained from smoke-exposed and intact mice. In contrast, 2 months of CSE induced an enormous increase in the number of all these cells in the BALF, which gradually decreased afterwards. The total number and the composition of BALF cells did not differ from the values of the non-smoker mice from the 3rd month. A tendency of increase in granulocyte and lymphocyte numbers was observed in the smoking group at the end of the 3rd month, but it did not reach statistical significance (Figure 11).

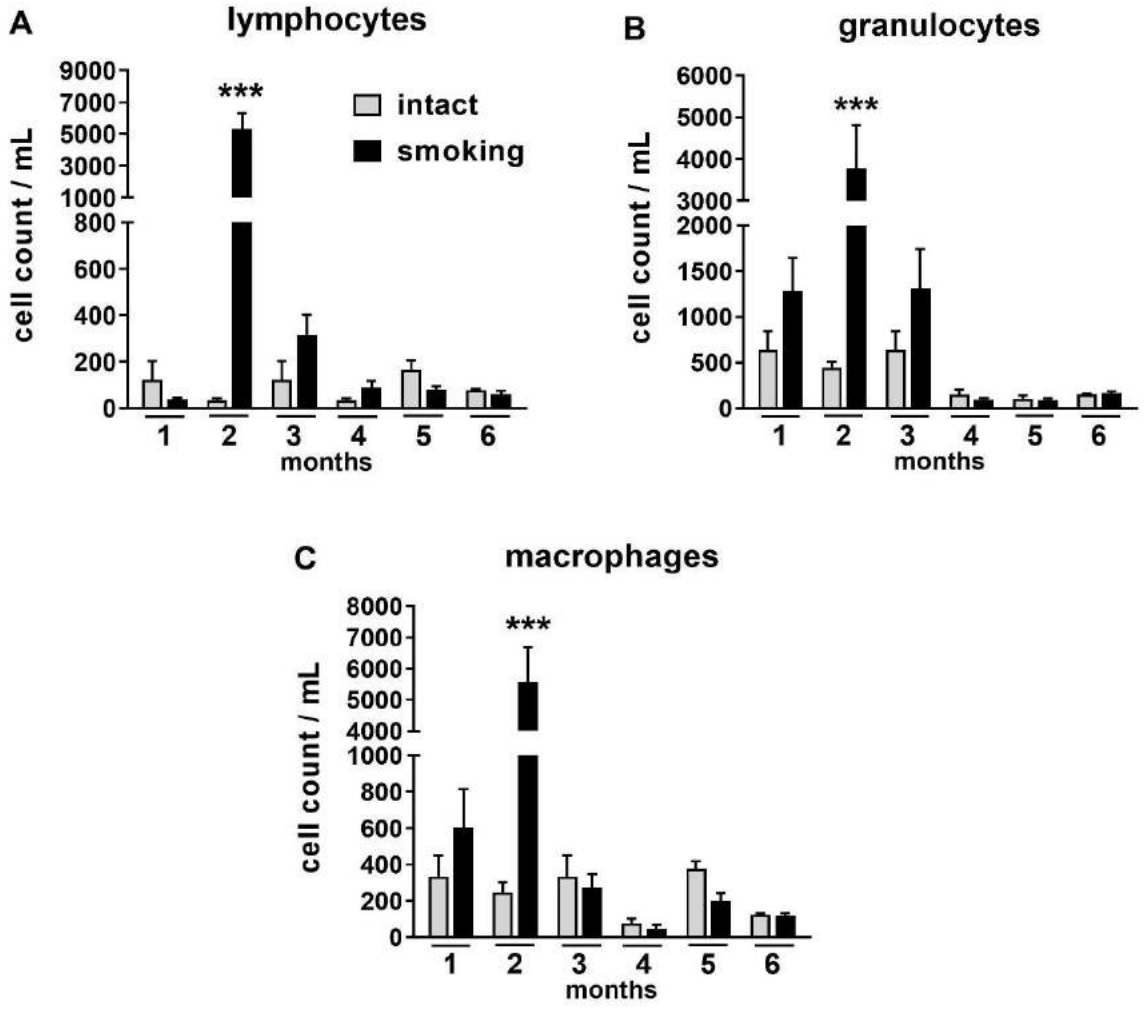

Figure 11. Inflammatory cell concentrations in the BALF. The number of A) lymphocytes, B) granulocytes, and C) macrophages in BALF samples were analysed with flow cytometry after each month. n = 6 / group (two-way ANOVA followed by Sidak's multiple comparison test, ***p< 0.001 vs. the intact, non-smoking group)

4.1.6 Chronic tobacco smoke increases MMP-2 and MMP-9 activities in the lung

Gelatine zymography showed a significant increase in pulmonary activity for MMP-2 as well as for MMP-9 in the lung samples of mice subjected to 6-month CSE as compared either to 1-month smokers or to non-smoker age-matched control mice (Figure 12).

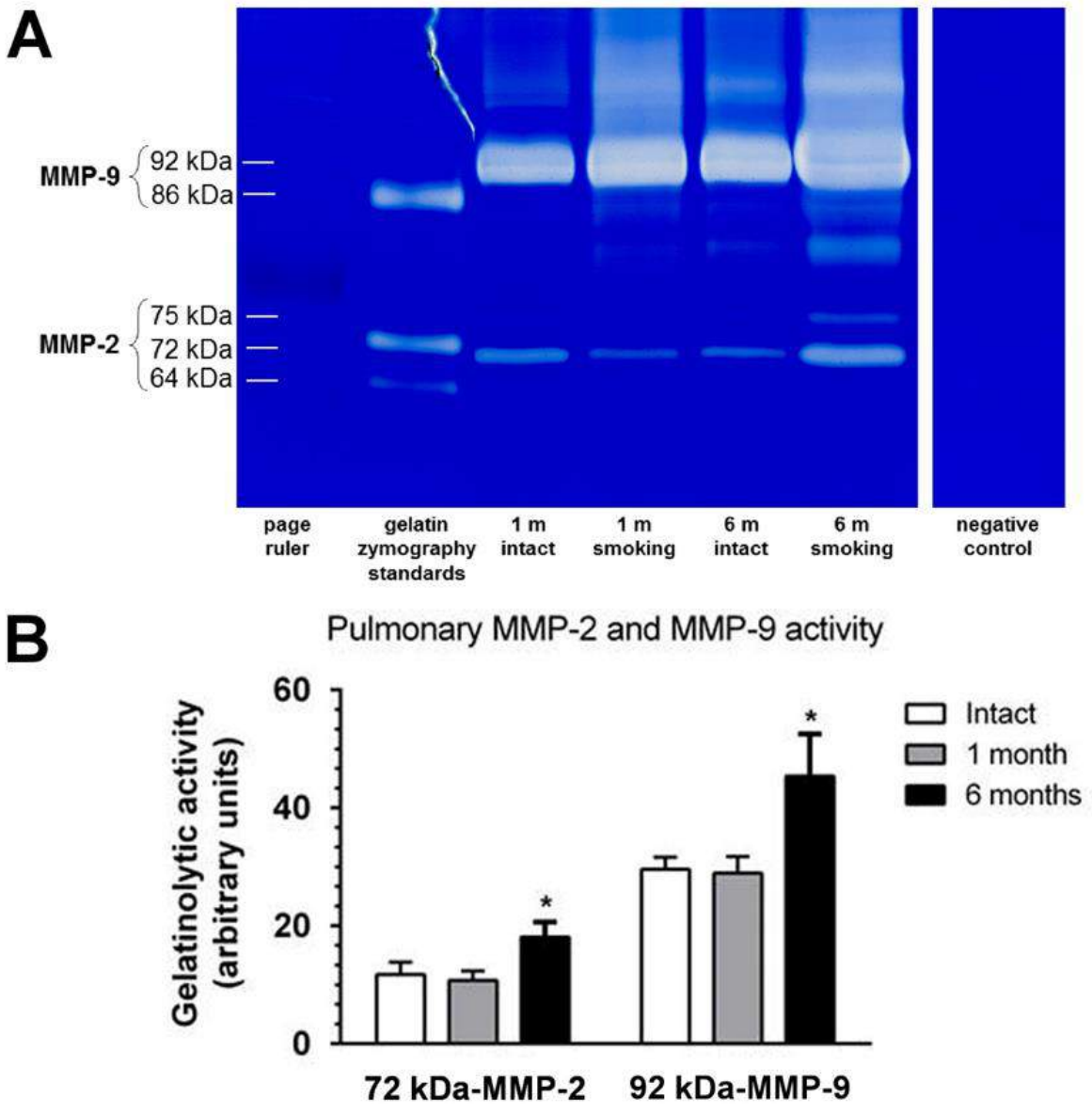

Figure 12. MMP-2 and MMP-9 activities in the mouse lung measured by gelatine zymography. A) Representative zymograms of the lung samples obtained after 1 or 6 months of CSE in comparison with the non-smoking intact. B) Gelatinolytic activity represented by the mean arbitrary units ± SEM of n = 6 mice / group. (Student's t-test for unpaired comparison, *$p<0.05$ vs. the intact, non-smoking group)

4.1.7 Cytokine expressions in the lung and serum

Among the 40 investigated inflammatory cytokines and chemokines 26 proteins were detectable in lung homogenates throughout the 6-month experiment. At the end of the 1st month, interleukin-1β (IL-1β), IL-10 and monocyte chemoattractant protein-5 (MCP-5) increased significantly, but none of them were detectable later. The triggering receptor expressed on myeloid cells-1 (TREM-1) showed a peak expression at this time-point. The C5a complement component, interleukin-1 receptor antagonist (IL-1ra) produced by several immune cells and epithelial cells, interleukin-16 (IL-16), interferon-gamma inducible protein-10 (IP-10), keratinocyte chemoattractant (KC), macrophage colony-stimulating factor (M-CSF), monocyte chemoattractant protein-1 (MCP-1 or JE), monokine induced by gamma interferon (MIG), regulated on activation, normal T cell expressed and secreted (RANTES), and tissue inhibitor of metalloproteinase-1 (TIMP-1) cytokines and chemokines reached their maximum expression at the 2nd month. Meanwhile, the concentration of the soluble intercellular adhesion molecule-1 (sICAM-1) was high in the intact lung homogenate and remained at a similarly high level during the whole 6-month smoking period (Figure 13A, B). In the serum of non-smoking mice B-lymphocyte chemoattractant (BLC), stromal cell-derived factor 1 (SDF-1), C5a, interleukin-1 alpha (IL-1α, IL-1ra, IL-16, JE, M-CSF, TIMP-1, TNF-α, and TREM-1 were detectable. The first two were not present in the intact lung, and they decreased by the end of the 6-month smoking period similarly to IL-16. KC remarkably, JE slightly increased by this time point, while the expression of the other cytokines remained unchanged in the serum (Figure 13C).

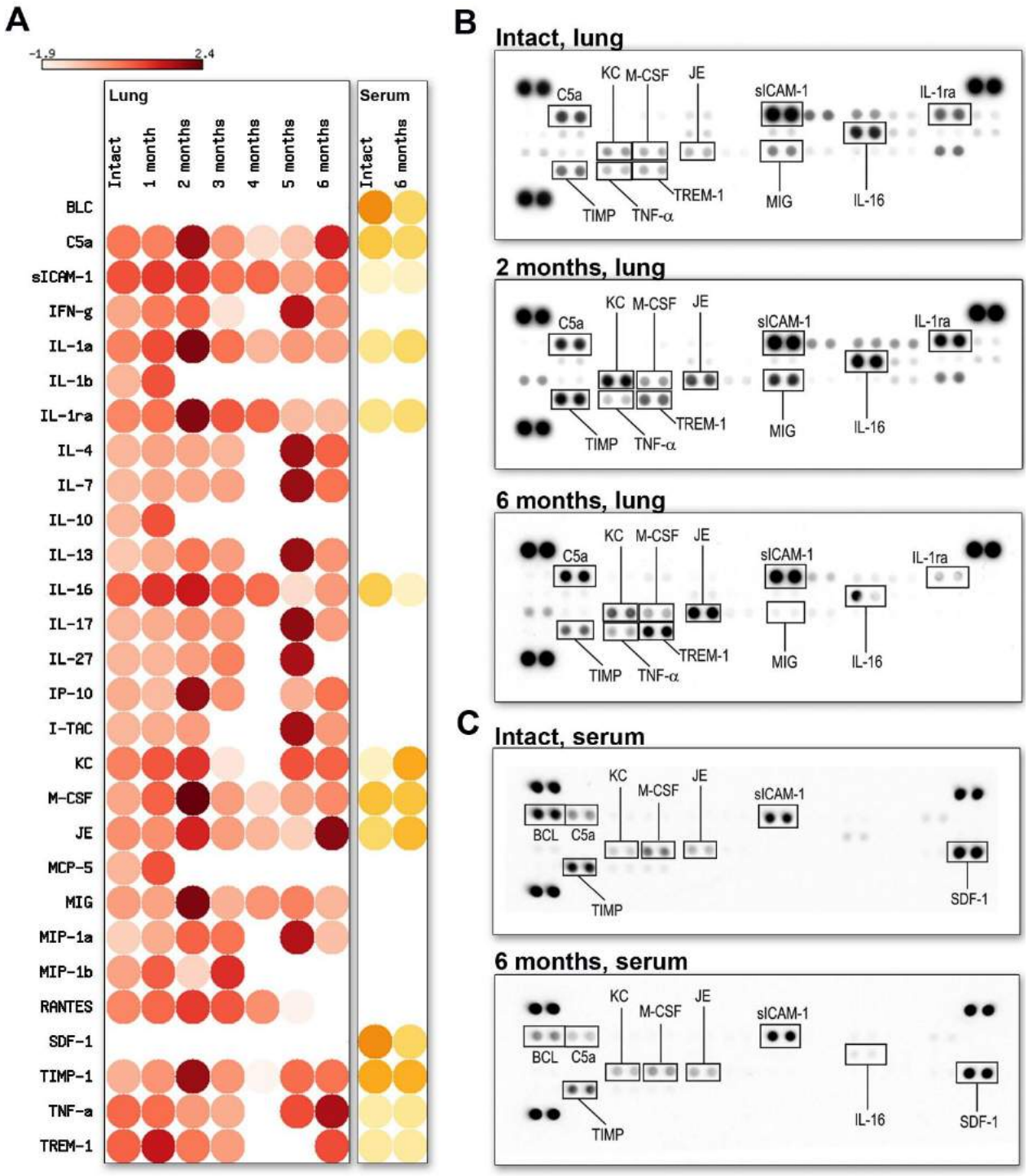

Figure 13. Cytokine determinations in the lung homogenates and serum samples. A) Heat map of cytokine expression in intact and smoking lung samples during the 6-month treatment period (red dots) and intact and 6-month smoking serum samples (yellow dots). B) Representative picture of the membranes after chemiluminescent detection of cytokines in lung tissue homogenates and C) in serum samples. The most important cytokine signals in duplicates are labelled. n = 3 / group.

4.2 Investigating the role of TRPA1 in CS-induced chronic airway inflammation

4.2.1 Comparison of basal airway function of *Trpa1* wildtype and gene-deficient mice

Under intact conditions, f, MV, PIF and PEF were significantly greater; TV, Ti, Te and RT were significantly smaller, while no difference was detected in the Penh value of *Trpa1*$^{-/-}$ mice compared to their wildtype counterparts, measured by unrestrained WBP (Figure 14).

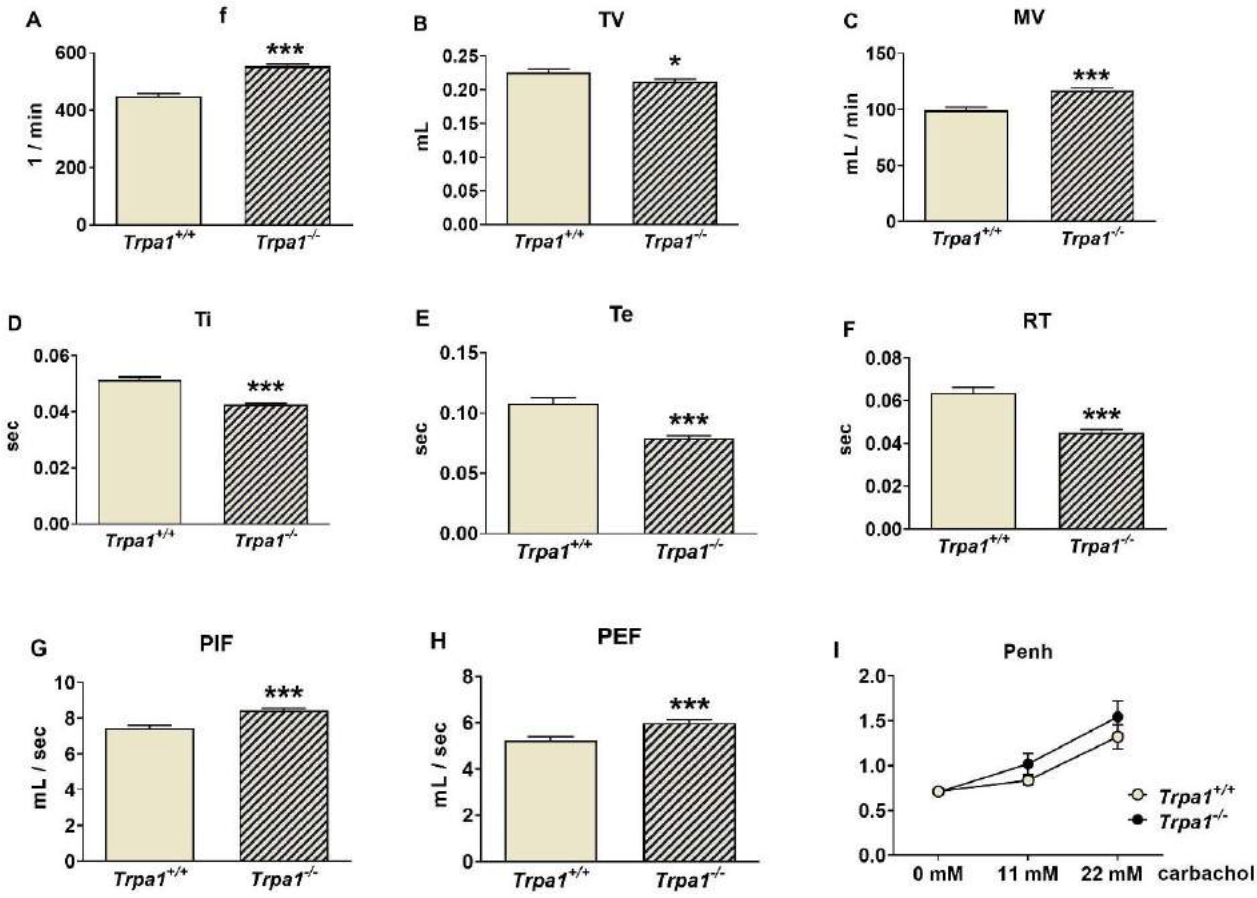

Figure 14. Comparison of the basal airway functions of intact *Trpa1*$^{+/+}$ and *Trpa1*$^{-/-}$ mice measured by unrestrained WBP. A) Breathing frequency (f), B) tidal volume (TV), C) minute ventilation (MV), D) inspiratory time (Ti), E) expiratory time (Te), F) relaxation time (RT), G) peak inspiratory flow (PIF) and H) peak expiratory flow (PEF) were measured in conscious, spontaneously breathing mice. I) Enhanced pause (Penh) correlating with bronchial responsiveness was assessed by the nebulization of the muscarinic receptor agonist, carbachol in increasing concentrations. Values represent the means ± SEM, n = 30–35 mice / group; Student's t-test for unpaired comparison; * $p < 0.05$; *** $p < 0.001$.

4.2.2 Respiratory functions of *Trpa1*$^{+/+}$ and *Trpa1*$^{-/-}$ mice after 4 months of CSE

Respiratory functions were measured in a follow-up design before and at the end of each month in the 4-month long protocol of cigarette smoke exposure. CSE induced a gradual and significant decrease in TV, MV, PIF and PEF in *Trpa1*$^{+/+}$ mice with a peak at 3 months, which was not present in the *Trpa1*$^{-/-}$ animals (Figure 15). The significant differences in f, Ti, Te and RT measured in the *Trpa1*$^{-/-}$ mice were attributable to the significant differences between the wildtype and gene-deficient mice observed already in the intact animals, before CSE.

4.2.3 Qualitative and semiquantitative histopathological analysis

After one month of CSE remarkable perivascular oedema developed (Figure 16C, E) that significantly decreased by time in both strains, and almost completely resolved at the end of the 4th month (Figure 17A). However, the accumulation of perivascular and peribronchial, as well as interstitial neutrophil granulocytes, macrophages and lymphocytes remained moderately increased throughout the experimental protocol (Figure 17B, C). At the end of the 3rd month of CSE, structural destruction characteristic to emphysema (Figure 16G–J) already developed.

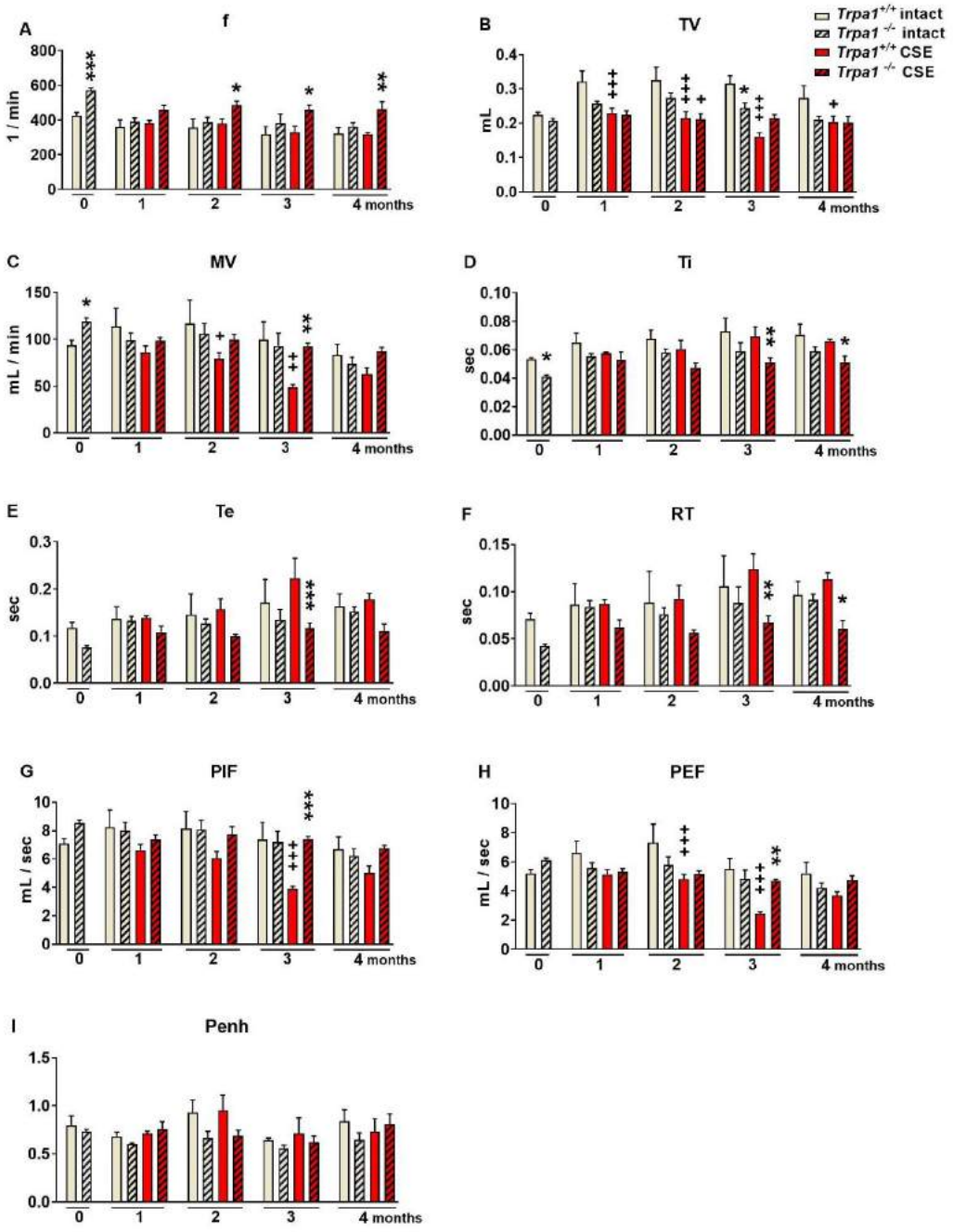

Figure 15. Respiratory functions of *Trpa1*$^{+/+}$ and *Trpa1*$^{-/-}$ intact (beige and red columns, respectively) and CS-exposed (beige and red striped columns, respectively). B) Tidal volume (TV), C) minute ventilation (MV), G) peak inspiratory flow (PIF) and H) peak expiratory flow (PEF) significantly decreased after CSE with a peak at 3 months in *Trpa1*$^{+/+}$ mice. The significant strain differences in A) frequency, D) inspiratory time (Ti), E) expiratory time (Te) and F) relaxation time (RT) observed already in intact mice were not influenced by CSE. I) Enhanced pause did not show any differences either by treatment or by strain. Values represent means ± SEM, n = 6–7 mice / group; two-way ANOVA followed by Tukey's post-test; +p< 0.05, ++p< 0.005, +++p< 0.001 vs. intact respective group; *p< 0.05, **p< 0.005, ***p< 0.001 vs. CSE-treated *Trpa1*$^{+/+}$.

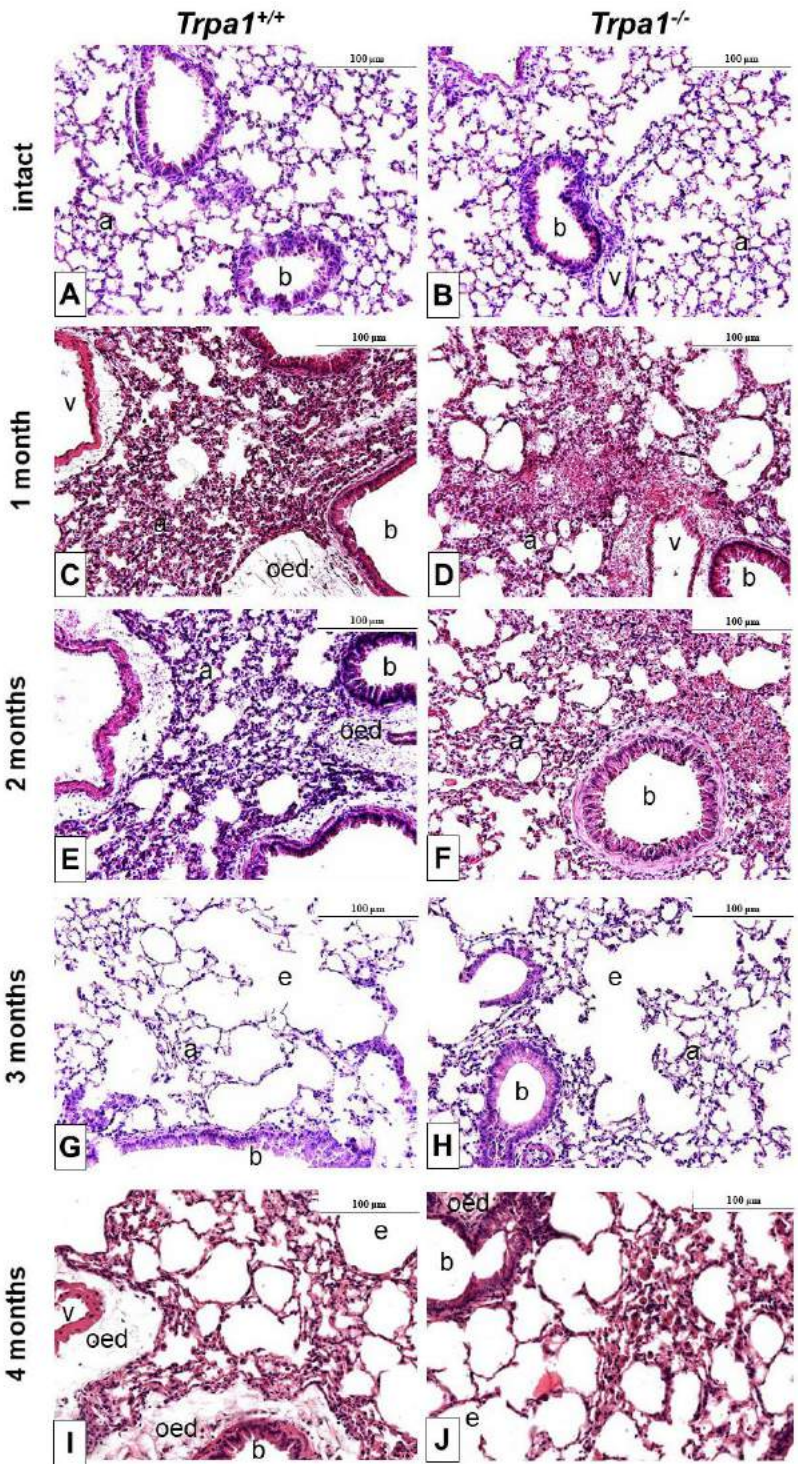

Figure 16. Representative histological pictures of the lungs of *Trpa1*$^{+/+}$ (A, C, E, G, I) and *Trpa1*$^{-/-}$ (B, D, F, H, J) mice under intact conditions (A,B), and after 1-4 months of CSE (C–J). 1 month of CSE induced perivascular and peribronchial oedema formation with inflammatory cell infiltration, that gradually subsided. After the 3rd month of CSE, emphysema formation was observed in both *Trpa1*$^{+/+}$ and *Trpa1*$^{-/-}$ mice. (HE staining; 200× magnification; a: alveolus, b: bronchiolus, v: venule, oed: oedema, e: emphysema).

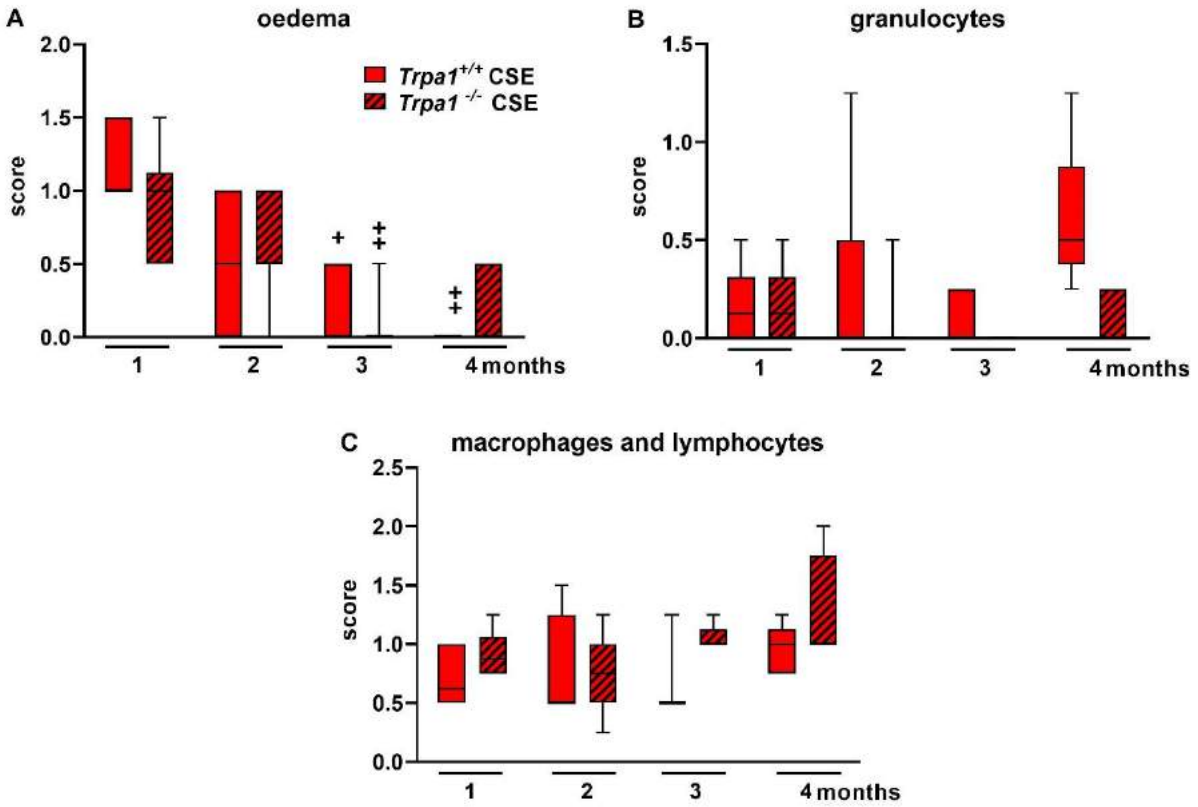

Figure 17. Semiquantitative evaluation of the histopathological changes in the lung of *Trpa1*$^{+/+}$ (red) and *Trpa1*$^{-/-}$ (striped red) mice after chronic CSE. A) Perivascular/peribronchial oedema developed after 1 month of CSE, which significantly decreased by time in both strains. The accumulation of perivascular and peribronchial, as well as interstitial B) neutrophil granulocytes, C) macrophages and lymphocytes did not differ in either group significantly. Boxplots represent the minimum, first quartile, mean, third quartile and maximum values, n = 5–13 / group, Kruskal–Wallis followed by Dunn's post-test; +p< 0.05, ++p< 0.005 vs. 1st month of CSE of respective strains.

4.2.4 Emphysema evaluation by micro-CT and mean linear intercept analysis

Emphysema was quantified by *in vivo* micro-CT by the ratio of LAA and TLV before and after 2 and 4 months of CSE. The ratio correlating with the extent of air-filled regions did not show alterations either by CSE treatment or time (Figure 18A). However, the more sensitive L_m measurement revealed that in *Trpa1*$^{+/+}$ mice emphysema already started to develop at an earlier timepoint compared to the gene-deleted counterparts; L_m was significantly increased in the wildtypes after 2 months of CSE, however, not in the *Trpa1*$^{-/-}$. At the end of the 4th month, L_m was elevated in both strains exposed to CS (Figure 18F).

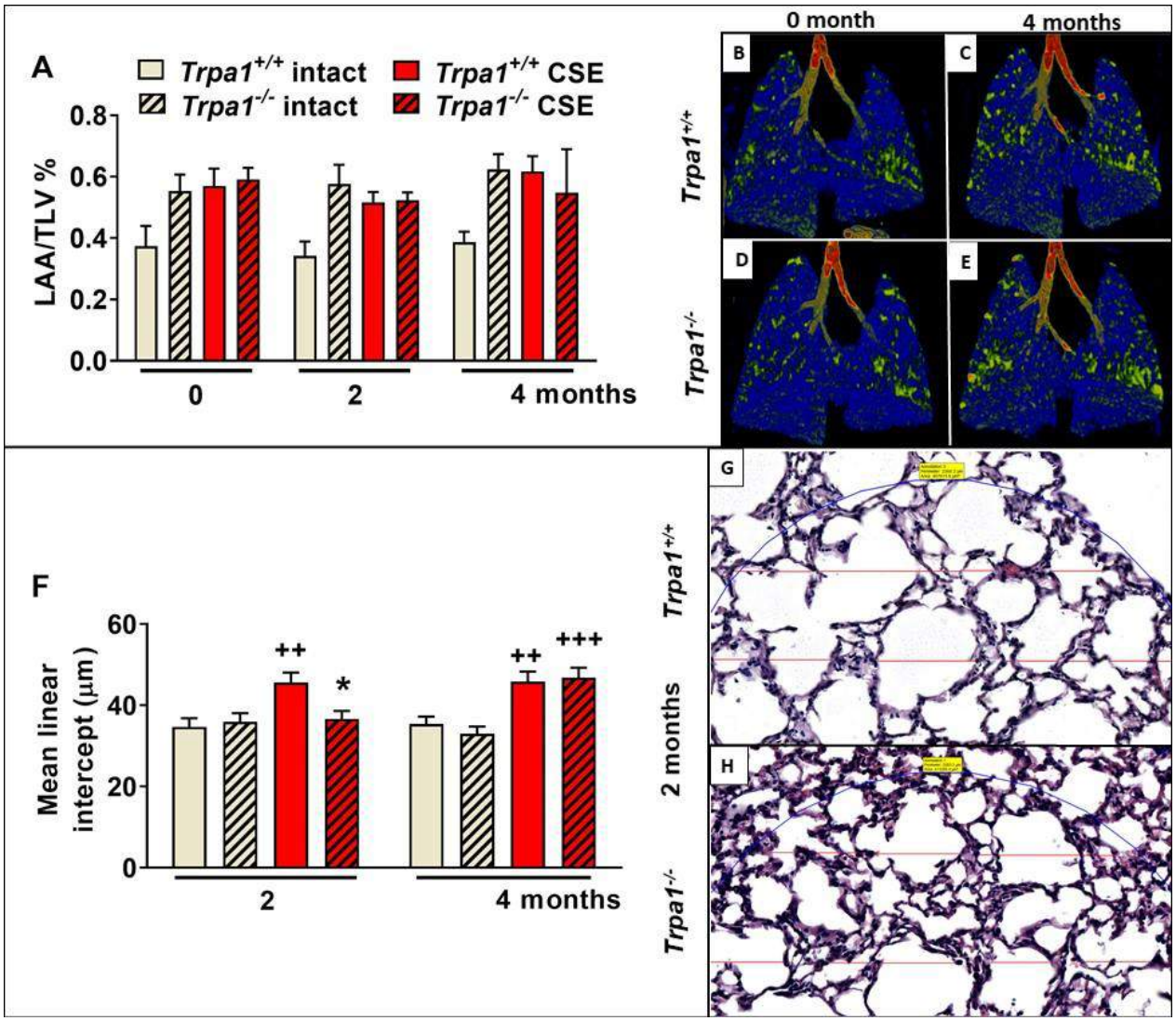

Figure 18. Quantitative evaluation of emphysema. (A) LAA/TLV ratio correlating with air-filled regions of the lungs exposed to CSE showed no significant alterations. Representative micro-CT pictures of lungs B,D) before and C,E) after 4 months of CSE in *Trpa1*$^{+/+}$ and *Trpa1*$^{-/-}$ mice, respectively. F) Microscopic quantitative assessment of L_m showed a significant increase in *Trpa1*$^{+/+}$ already after 2 months of CSE, but not in the *Trpa1*$^{-/-}$. Values represent means ± SEM, n = 6–7 mice / group; repeated measures two-way ANOVA followed by Tukey's post-test. Representative microscopic pictures of G) *Trpa1*$^{+/+}$ and H) *Trpa1*$^{-/-}$ mouse lung tissues after 2 months of CSE. Values represent means ± SEM, n = 60–100 measurements / group; two-way ANOVA followed by Tukey's post-test; ++p< 0.005, +++p< 0.001 vs. PBS-treated respective group; *p< 0.05 vs. CSE-treated *Trpa1*$^{+/+}$. (The blue circle indicates the region of interest in which Lm was measured. The measured chord lengths are represented by red lines and were expressed in µm on the scanned slides).

4.2.5 Inflammatory cell count in the BALF

CSE induced massive accumulations of granulocytes, macrophages and lymphocytes measured in the BALF of both *Trpa1*$^{+/+}$ and *Trpa1*$^{-/-}$ mice. In agreement with our previous findings (105), the number of inflammatory cells reduced by the end of the 3rd month of CSE. There was no biologically relevant difference between the wildtype and gene-deficient mice in either inflammatory cell components (Figure 19).

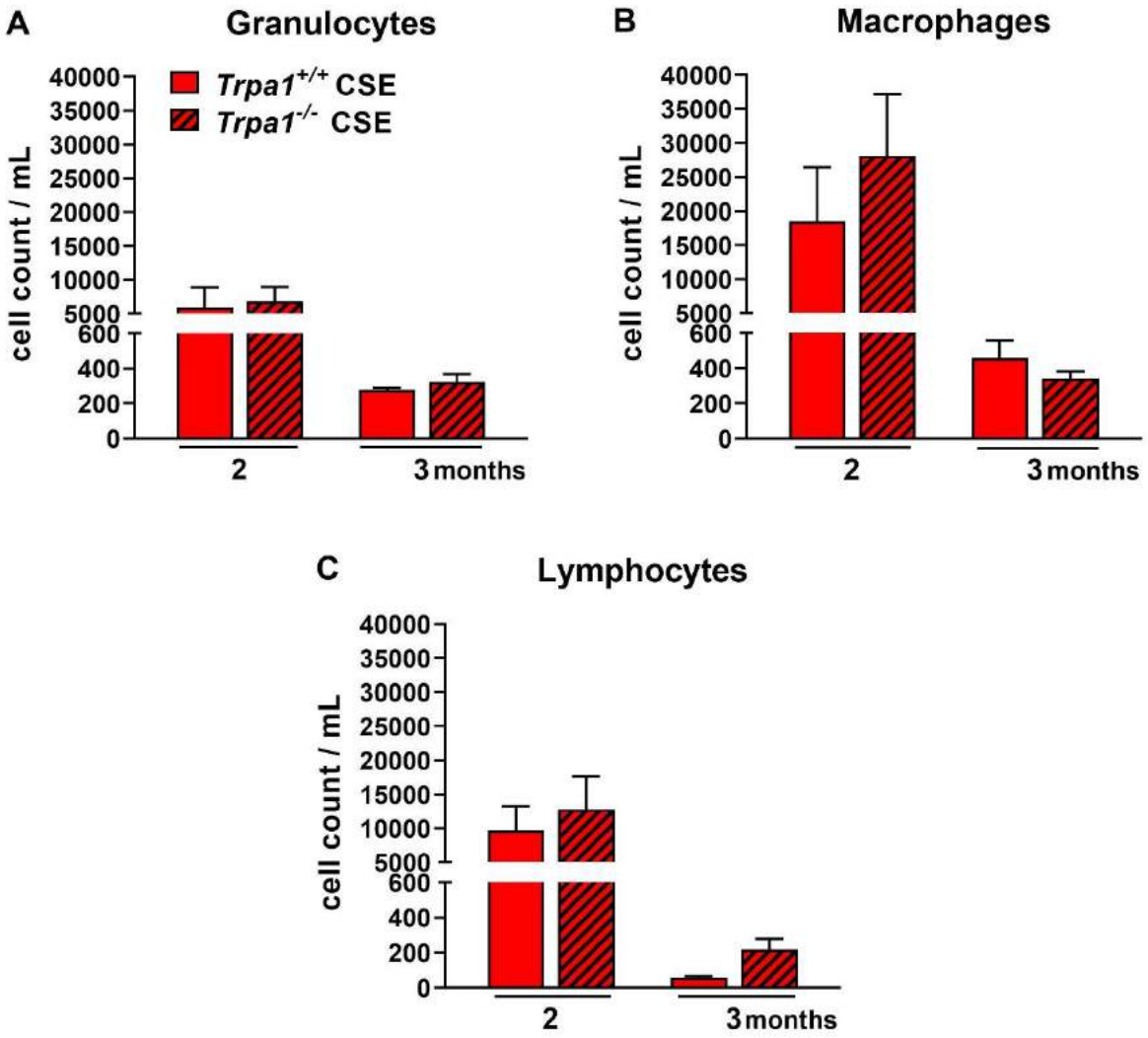

Figure 19. Number of inflammatory cells in the BALF after 2–3 months of CSE in *Trpa1*$^{+/+}$ and *Trpa1*$^{-/-}$ mice. After the peak of inflammatory cell infiltration at a 2-month timepoint, the number of A) granulocytes, B) macrophages and C) lymphocytes remarkably decreased by the end of the 3rd month in both *Trpa1*$^{+/+}$ and *Trpa1*$^{-/-}$ mice. Values represent means ± SEM, n = 6–7 mice / group; two-way ANOVA followed by Tukey's post-test.

4.3 IAA-induced chronic gastritis

4.3.1 Weight change and fluid consumption

Gastritis was induced by the administration of 0.05%, 0.1% or 0.2% IAA solution in the drinking water of Wistar rats, littermates drinking IAA-free tap water served as control animals. Rats were euthanised at days 7 and 14, their stomachs were harvested and opened along the greater curvature. In Wistar rats, IAA induced a concentration-dependent weight change. Similar to vehicle-treated animals, low concentration (0.05%) of IAA resulted in ~15% weight gain by the end of the 14-day experiment. Meanwhile, 0.1% and 0.2% IAA induced a concentration-dependent, gradual weight loss with a maximum of 13.4 ± 1.2% and 32.5 ± 3.3%, respectively (Figure 20A). The total water consumption of the 0.05% and the 0.1% IAA-treated groups was halved compared to the control group, and it was even more decreased to around 9 mL daily in the case of 0.2% concentration (Figure 20B).

4.3.2 Macroscopic evaluation of IAA-induced gastric lesions

Extensive hyperaemia, mucosal haemorrhage and several erosions or superficial ulcers were observed at both timepoints in all three examined concentrations. Semi-quantitative analysis showed significant hyperaemic areas and erosions in both 0.05% and 0.2% IAA-treated groups at day 7 compared to the controls. At day 14, lesions, especially the extent of the hyperaemic area in the 0.1% and 0.2% IAA-treated groups were significantly greater. Macroscopic changes showed no significant difference either by the increasing concentrations of ingested IAA or by time; however, ulcerations were more pronounced after 14 days of IAA-drinking (Figures 21 and 22).

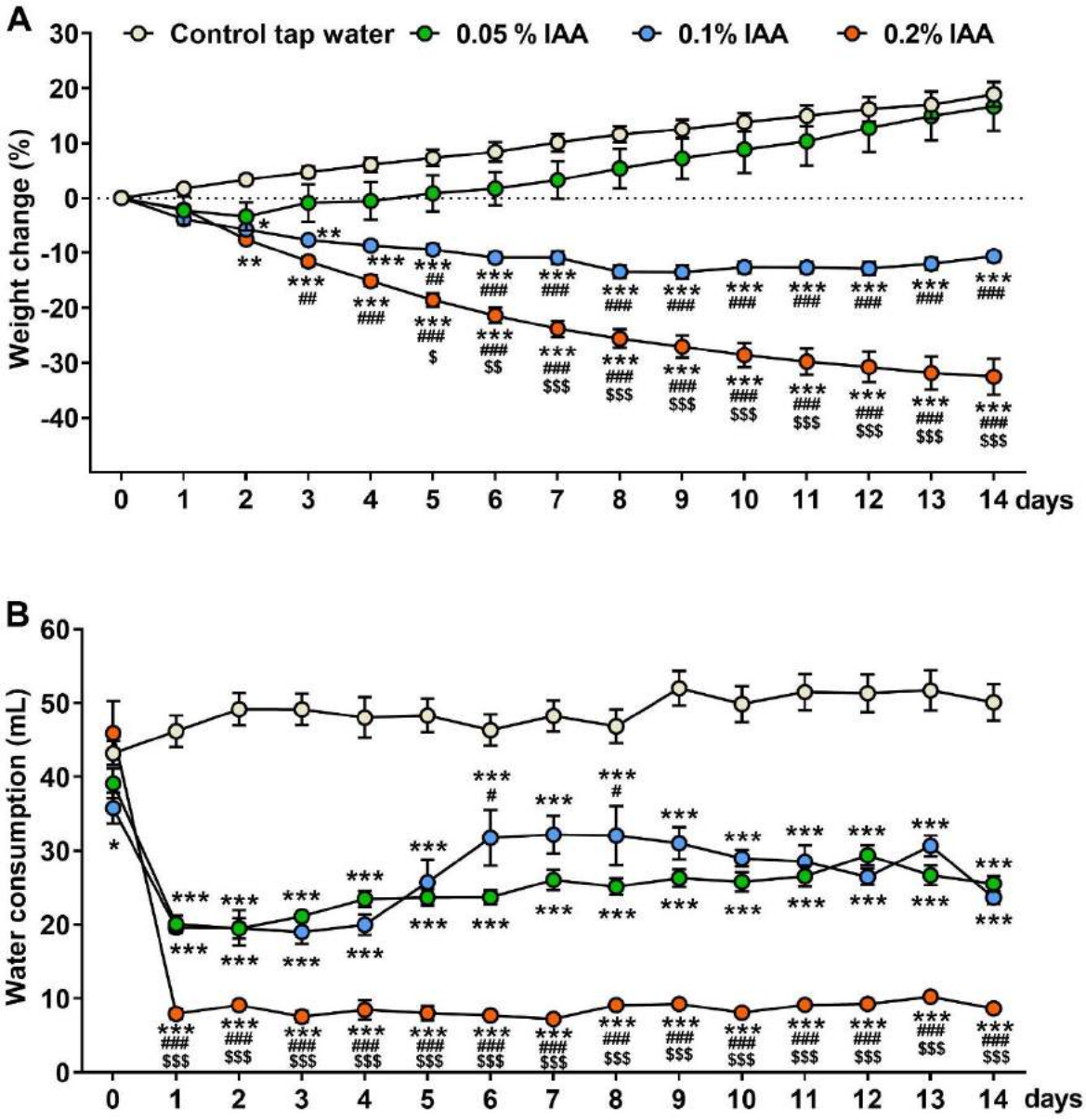

Figure 20. IAA-induced body weight change and water intake in Wistar rats. A) IAA administration resulted in a dose-dependent weight loss and B) reduced water intake in Wistar rats. Data are shown as means ± SEM; n = 6 / group (repeated measures two-way ANOVA followed by Bonferroni's modified t-test; *p < 0.05, **p < 0.005, ***p < 0.001 vs. control group; #p < 0.05 ##p < 0.005 ###p < 0.001 vs. 0.05% IAA group; $p < 0.05 $$p < 0.05 $$$p < 0.001 vs. 0.1% IAA group).

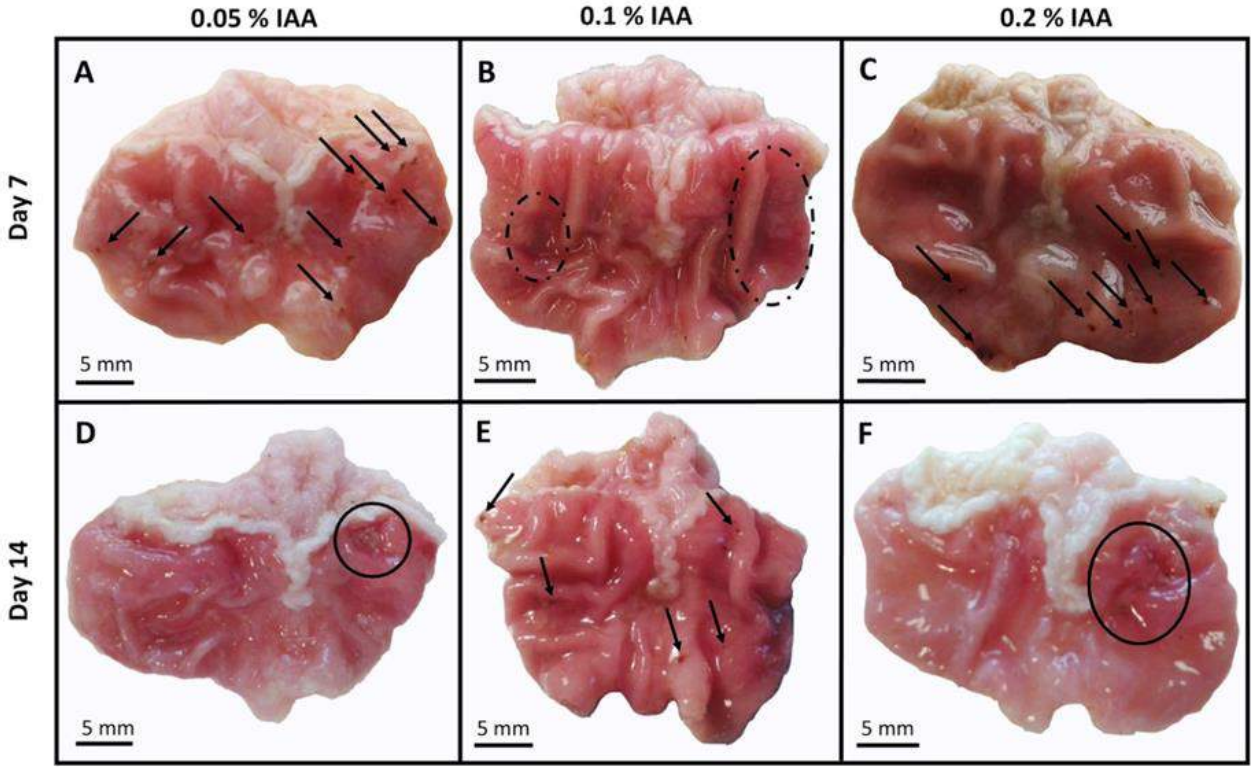

Figure 21. Representative macroscopic pictures of IAA-induced gastric mucosal inflammation in Wistar rats receiving A) 0.05%, B) 0.1%, C) 0.2% IAA for 7 and D–F) for 14 days, respectively. After 7 days, diffuse hyperaemia (dashed circles) and several superficial mucosal erosions (black arrows) developed, while by the end of the 14-day-long protocol, chronic ulcers were also observable in some animals (circles on panel D) and F)).

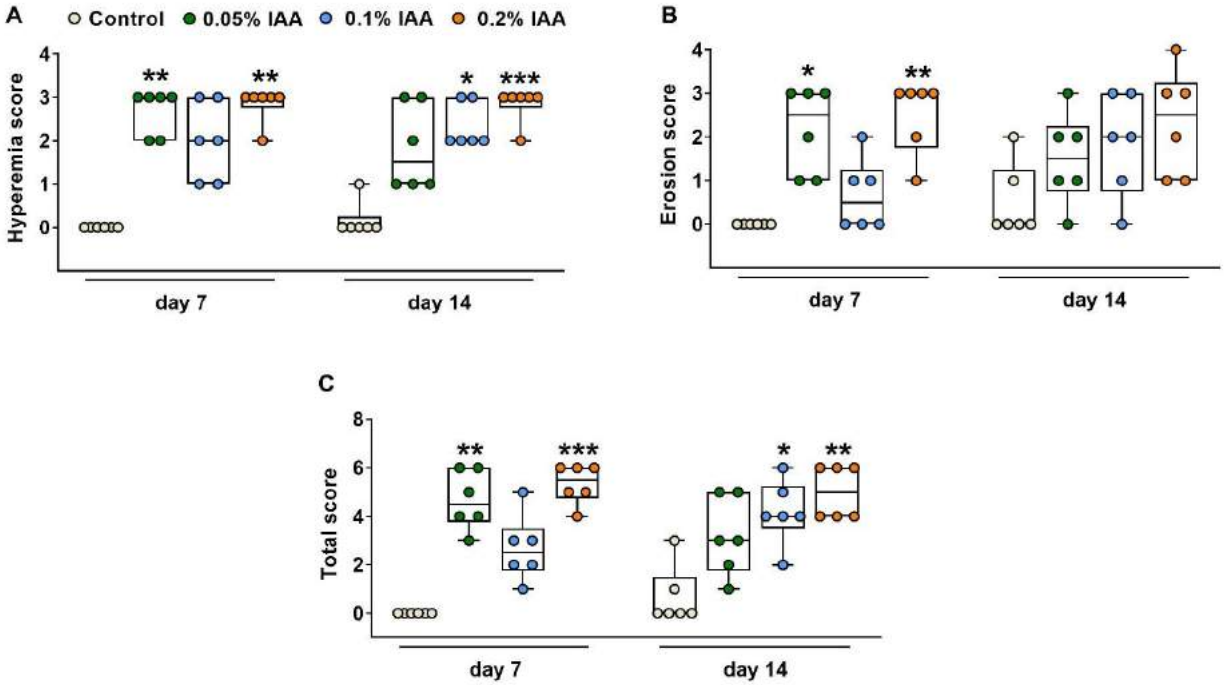

Figure 22. Semi-quantitative macroscopic evaluation of A) hyperaemia, B) superficial erosions/ulcers and C) total score in the gastric mucosa of Wistar rats. Box plots represent minimum, first quartile, median, third quartile, and maximum values with individual data plots; n = 6 / group (Kruskal–Wallis followed by Dunn's multiple comparison test to observe intergroup differences at given timepoints, *p< 0.05, **p< 0.005, ***p< 0.001 vs. control group; Mann–Whitney test was performed to analyse intragroup differences by time—not significant).

4.3.3 Qualitative microscopic evaluation of gastric mucosa

Seven days of IAA treatment resulted in submucosal widening due to massive oedema. In higher concentrations, extensive inflammatory cell infiltration was also observed. After 14 days, focal epithelial cell sloughing/erosions, and in some areas, almost total mucosal necrosis involving the muscularis mucosae were seen, admixed with acute and chronic inflammatory cells, both in the mucosa and the submucosa (Figure 23).

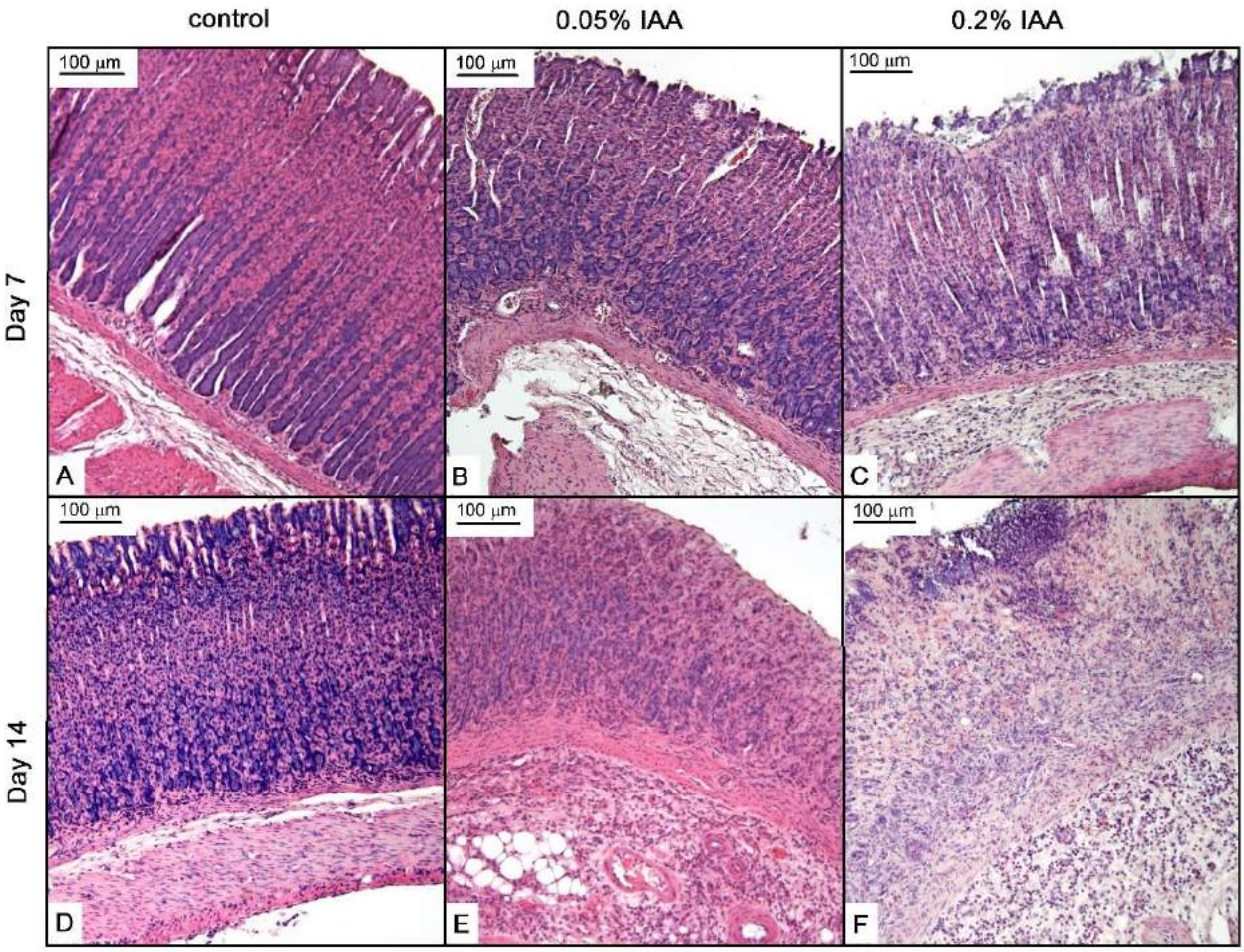

Figure 23. IAA treatment induced microscopic alterations in Wistar rat gastric mucosa. Representative HE-stained microscopic pictures of A, D) control; B, E) 0.05% IAA-treated, and C, F) 0.2% IAA-treated rat gastric mucosa at days 7 and 14, respectively.

4.3.4 Total glutathione concentration of rat gastric mucosa

The GSH content of the rat gastric mucosa was measured to be (mean ± standard deviation) 3.64 ± 1.91 nmol/mg protein in the control group, 5.82 ± 3.94 nmol/mg protein in the group receiving 0.1% IAA for 7 days, and 5.71 ± 2.07 nmol/mg protein in the group receiving 0.1% IAA for 14 days (data not shown). There were no statistically significant differences between the groups ($p = 0.343$, one-way ANOVA).

IAA treatment increased tGSH, but not significantly: 2.55 ± 0.85 in the control group; 3.15 ± 1.21 in the group treated with 0.1% IAA for 7 days; and 3.25 ± 0.82 in the group treated with 0.1% IAA for 14 days (Figure 24B). tGluCys increased significantly (between one week and two weeks: 5.78 ± 0.18; 5.97 ± 0.23; 6.18 ± 0.20, respectively) (Figure 24A). These changes resulted in a decrease in the tGluCys/tGSH molar ratio, which was not significant: 2.43 ± 0.72; 2.13 ± 0.77; 1.98 ± 0.39, respectively (data not shown).

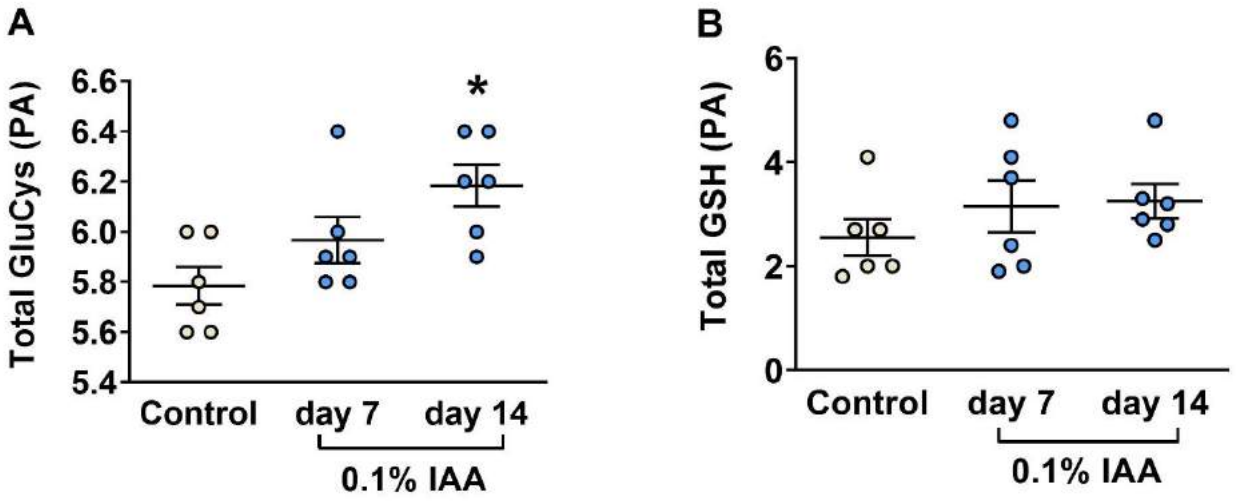

Figure 24. A) Total glutathione (GSH) and B) Total GSH (tGSH) γ-glutamyl-cysteine levels of the rat gastric mucosa measured by HPLC analysis. Data are shown as mean ± SEM; n = 6/group (ordinary one-way ANOVA; *$p < 0.05$).

4.3.5 Quantitative analysis of TRPA1 and TRPV1 immunohistochemistry

Mild TRPA1 and strong TRPV1 immunopositivity was detected on the epithelial cells in the intact control samples (Figure 25A,D). Quantification, as shown by the ratio of immunopositive cells, revealed a significant upregulation of TRPA1 after both 0.05% and 0.2% IAA administration by day 14 in both the antrum and corpus epithelial cells. Although TRPV1 immunopositivity also increased in the corpus, but did not change in the antrum in the case of 0.05% IAA, it significantly decreased in both localizations after 0.2% IAA treatment (Figure 25).

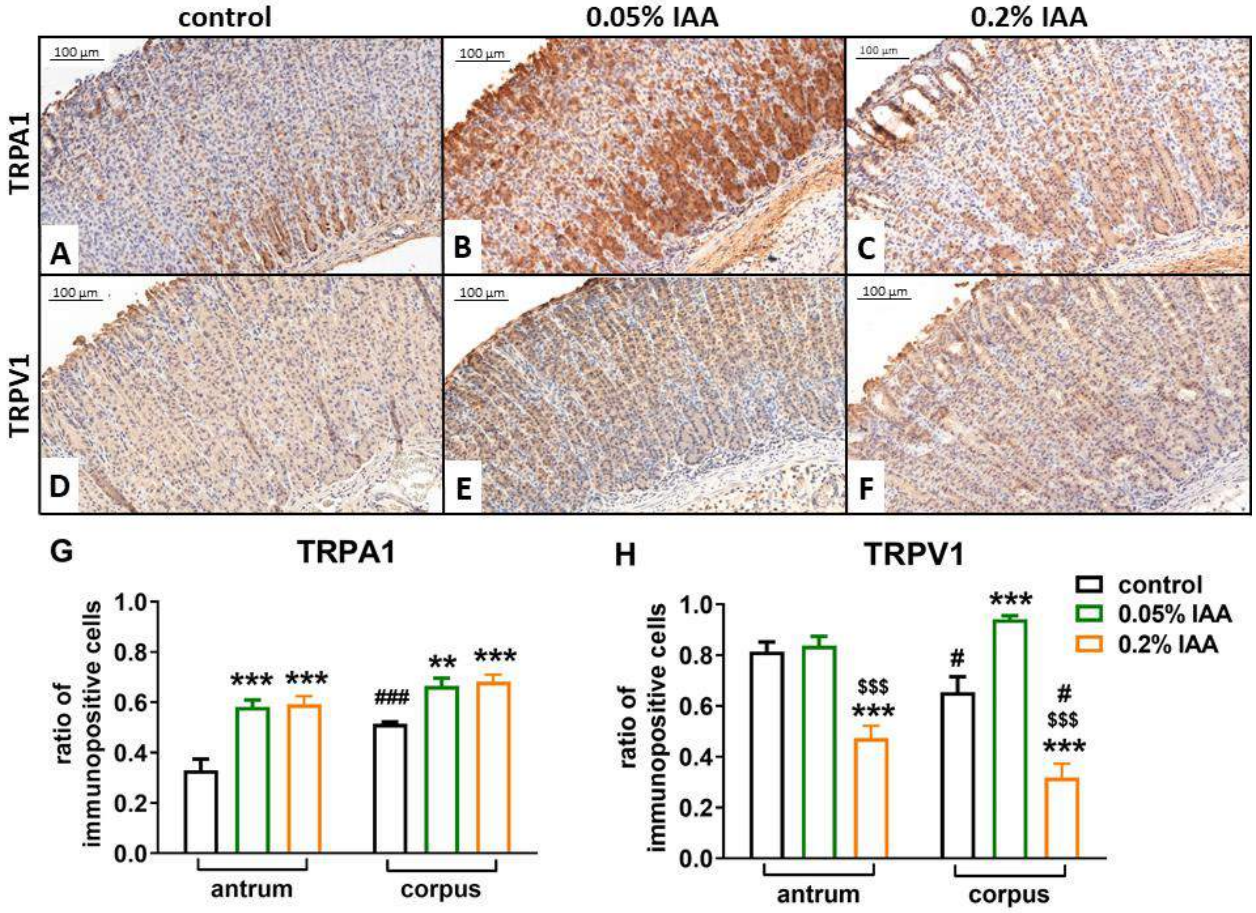

Figure 25. Quantitative analysis of TRPA1 and TRPV1 immunohistochemistry. Representative pictures of A–C) TRPA1 (antrum) and D–F) TRPV1 (corpus) immunohistochemistry of rat gastric mucosa A,D) under control conditions, and 14 days after B,E) 0.05% IAA, and C,F) 0.2% IAA treatment. Panel (G) and (H) demonstrates the quantitative histopathological analysis of TRPA1 and TRPV1 immunohistochemistry, respectively, calculated by the ratio of immunopositive cells/total cell number. Data are shown as means ± SEM; n = 6 animals / group, 10 fields of vision/slide/animal; ordinary two-way ANOVA followed by Dunn's multiple comparisons test **p< 0.005, ***p< 0.001 vs. control group; $$$p< 0.001 vs. 0.05% IAA-treated group; #p< 0.05, ###p< 0.001 vs. respective antrum samples.

4.3.6 *Trpa1* and *Trpv1* relative gene expression in the inflamed rat mucosa

In agreement with the TRPA1 protein expression, *Trpa1* mRNA was significantly upregulated in both 0.05% and 0.2% IAA-treated groups after 7 and 14 days as well, however, there was no detectable alteration in *Trpv1* relative gene expression either by time, dose, or localisation (Figure 26).

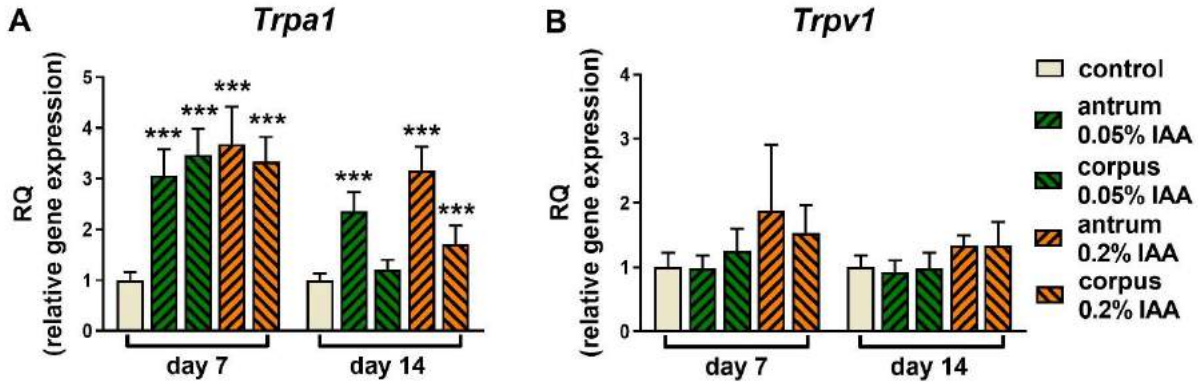

Figure 26. Relative gene expression of *Trpa1* and *Trpv1*. mRNA levels of A) *Trpa1* were significantly upregulated after 0.05% and 0.2% IAA treatment, whereas B) *Trpv1* gene expression did not show significant alterations either by time, concentration, or localisation. Data are shown as means ± SEM; n = 6 / group; Student's unpaired t-probe ***p< 0.001 vs. control group.

4.3.7 IAA-induced alterations in mice

CD1 and C57Bl/6 mice were administered 0.1%, 0.3%, or 0.5% IAA solution in the drinking water for 7 or 14 days; littermates drinking IAA-free tap water served as control animals. In CD1 mice, we observed an IAA dose-dependent continuous, gradual weight loss; in the 0.3% and 0.5% IAA-treated groups, weight reduction was so severe at the end of the 7-day-long protocol, that a 14-day-long protocol could not be performed due to the ethical considerations of humane endpoints (Figure 27A, C). Although water intake was significantly reduced in all IAA-treated groups, it showed no concentration-dependence, and could not explain the remarkable dose-dependent weight loss of these animals. C57Bl/6 mice proved to be more resistant to 0.3% IAA, which induced ~14% weight loss after 7 days, half as much as the same concentration in CD1 mice (~28%). Interestingly, adding 2% sucrose to 0.3% IAA significantly reduced both the fluid intake, as well as the weight (~21%) of C57Bl/6 mice compared to the 0.3% IAA-drinking group (Figure 27B, D). Surprisingly, in contrast to Wistar rats, where we observed similar body weight change and decreased water intake,

no macroscopic lesions or microscopic alterations were present in either of the mouse groups drinking IAA (Table 8).

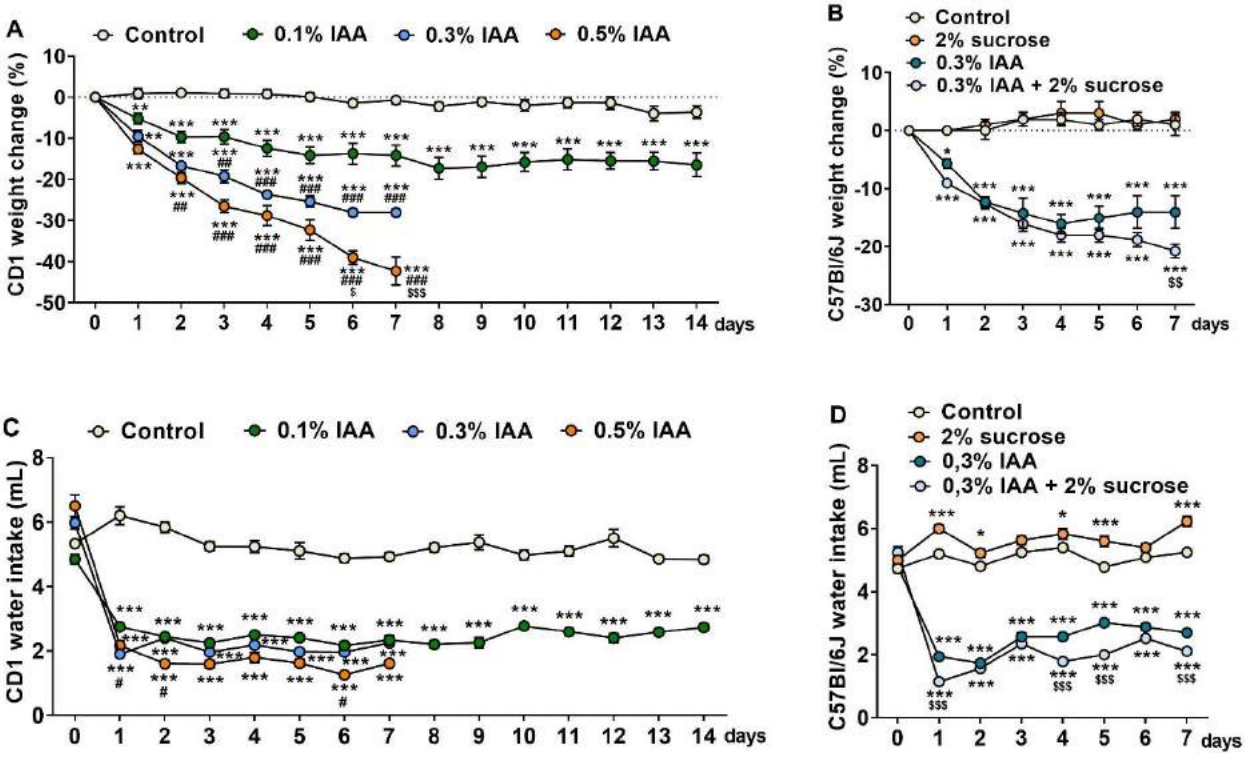

Figure 27. IAA-induced weight change and water intake in mice. IAA administration resulted in A,B) a dose-dependent weight loss and C,D) significantly reduced water intake in both CD1 and C57Bl/6 mice, respectively. Data are shown as means ± SEM; n = 6/group (repeated-measures ANOVA followed by Bonferroni's modified t-test; *p< 0.05, **p< 0.005, ***p< 0.0005 vs. control group; # vs. 0.1% IAA group, $ vs. 0.3% IAA group).

Table 5. Summary of IAA-induced alterations in mice.

Strain	IAA conc.	Duration	Weight loss	Water intake	Macroscopic and microscopic picture
CD1	0.1%	14 days	~17%	↓	negative
CD1	0.1%	7 days	~14%	↓	negative
CD1	0.3%	7 days	~28%	↓	negative
CD1	0.5%	7 days	~42%	↓↓	negative
C57Bl/6J	0.3%	7 days	~14%	↓	negative
C57Bl/6J	0.3% + 2% sucrose	7 days	~21%	↓↓	negative

5 Discussion

The present results provide the first experimental evidence in a chronic mouse model that cigarette smoke induces characteristic pulmonary inflammation, emphysema and atelectasis. We proved with functional, morphological and immunological techniques that these well-defined pathophysiological alterations from the inflammatory reactions to the tissue destruction are dependent on the duration of the smoke exposure and COPD-like structural and functional changes develop only after the fourth month.

Respiratory function determined by invasive WBP in anaesthetised, tracheotomised and mechanically ventilated mice showed a significant decrease in airway resistance, interestingly along with a decrease in the expiratory parameters, such as EF50 characteristic to bronchoconstriction, EEW, EEP and Te (117). Emphysema in humans is characterised by increase of expiratory parameters, since in most cases at the stage when COPD is diagnosed, it is associated with chronic bronchitis, thus smooth muscle hypertrophy together with emphysema are present in patients (118). The histopathological picture we found in mice after 6 months of smoke exposure did not show any inflammatory reaction with bronchial narrowing, only extensive emphysema and atelectasis, which can explain these functional differences compared to the human condition.

Inflammatory signs determined by the histopathological evaluation were clearly dependent on the duration of smoking. In the first two months peribronchial/perivascular oedema, neutrophil and macrophage infiltration were characteristic, from the third and fourth months macrophages and lymphocytes accumulated predominantly in the interstitial areas, and epithelial irregularity and hyperplasia developed. From the 5^{th} month, the extent of inflammatory reaction decreased, and tissue destruction dominated as shown by remarkable development of emphysema and atelectasis. Vascular endothelial proliferation, destructed bronchi with desquamated epithelial cells, fibrosis and a loss of the alveolar structure were detected by the end of the 6-month experiment. The histologically observed peak of peribronchial inflammation at 2 months of smoking was strongly supported by the drastically elevated numbers of granulocytes, macrophages, and lymphocytes in the BALF. At later time-points cell counts in BALF were not changed, which is not surprising, since at this stage interstitial localisation of the inflammation (at month 3) and the destruction of the bronchial epithelium (from month 4) were observed on histology. The development of emphysema after 5-6 months of smoke exposure was also clearly detected by micro-CT in complete agreement with the histological picture. Therefore, one major message of our study is that duration

of smoking strongly determines pathophysiological alterations that develop sequentially in the lung as a cascade from different types of inflammatory processes to tissue destruction. We described a transient inflammation in contrast to a persistent process caused by chronic exposure of the same type of cigarette demonstrated by others (73). It should be emphasised that they targeted a 4 times higher TPM and 3 times daily exposure and used female mice being more sensitive to oxidative stress and transforming growth factor- β (TGF-β) pathways in the small airways compared to males (74). It is crucial to choose the correct experimental paradigm depending on which mechanisms and phase of the chronic disease model are aimed to be investigated (61).

According to the well-established involvement of MMPs in COPD and emphysema even proposing a potential approach for pharmacological intervention (119), we measured MMP-2 and MMP-9 activities in the mouse lung and found a significant increase after 6 months of smoking. Similar to our findings, intraperitoneal administration of a cigarette smoke extract in mice also showed increased pulmonary expressions and activities of these gelatinases (120). In contrast, another recent mouse experiment of 6-month-long cigarette smoke exposure presented no differences either in MMP-2 or in MMP-9 mRNA levels in lung samples (121). However, without any alterations in gene expressions, MMP-2 and -9 may exert increased activities in case they are activated by enhanced oxidative stress as a result of cigarette smoke exposure (122,123). Regarding the role of MMP-9 in cigarette smoke-induced pathophysiological alterations in the lung, MMP-9-deficient mice developed similar emphysema, but they were protected from small airway fibrosis (57). Clinical data revealed elevated MMP-1, -9 and -12 levels in the BALF and plasma of patients with severe COPD (124), as well as increased MMP-9 in the plasma and emphysematous lung of smokers (125). Furthermore, enhanced release of MMP-9 and its endogenous inhibitor, TIMP-1 were detected from isolated human macrophages obtained from the BALF of smokers (126), and the BALF concentrations and macrophage expression of MMP-9 and MMP-1 (collagenase) also increased in COPD-emphysema patients (57). Increased activity of the active 64kDa MMP-2 isoform was shown in pneumocytes and alveolar macrophages isolated from COPD patients with emphysema (127). Furthermore, in a coronary artery disease patient group a significantly increased serum MMP-2 activity was found in a smoking subgroup of patients as compared to non-smoking patients with the same selection criteria (128). However, in another study, the increased MMP levels in the plasma, BALF, and lung did not correlate with the disease severity and were not predictive of the progression (124). Therefore, our MMP results can point out a similarity between

the mechanisms in the mouse model and the human disease supporting its translational relevance, but specific inhibition of MMP-9 is not likely to be an effective therapy for cigarette smoke-induced emphysema (125).

The cytokine panel measured from the lung homogenates showed a 2-phase pattern during the 6-month-smoke exposure: a characteristic profile was seen at the end of the second month when the inflammatory reaction reached its maximum, and another group of cytokines increased at 5-6 months related to the definitive tissue destruction and emphysema. The inflammatory burst at month 2 clearly suggests an IL-1-driven cascade with the elevation of C5a, IL-1α, IL-1ra, IL-16, IP-10, M-CSF, KC, MIG, RANTES, TIMP-1 (129). IL-1β remarkably increased at month 1 and IL-1α at months 1-2, but then the massive elevation of IL-1ra seems to down-regulate their production. However, the increased inflammatory cytokines demonstrate an IL-1-downstream profile (130). Several members of the IL-1 family including IL-1β are important mediators of lung inflammation. The expression of an inactive IL-1β precursor is induced in immune cells via activation of signalling pathways upstream of the nuclear factor-kappa B (NF-κB). Cigarette smoking leads to IL-1β release in the human lung (131). Mice overexpressing IL-1β in the lung present a phenotype similar to COPD including lung inflammation, emphysema and fibrosis (132). IL-1β increases the production of neutrophil chemoattractant factors, and the activity of MMP-2 and MMP-9 by alveolar macrophages, and these gelatinases are also able to activate IL-1β (133). The importance of the IL-1β cascade in lung pathology is shown by the fact that an IL-1-blocking monoclonal antibody (canakinumab) has recently been investigated for the treatment of several conditions including COPD (134). The complement component C5a is a potent inflammatory peptide, which is suggested to be involved in the pathogenesis of COPD. Plasma C5a concentrations in COPD patients were significantly higher than in healthy smokers. Elevated C5a and C3a levels were also measured in the sputum of stable COPD patients suggesting that the complement system is continuously activated during stable phase of the disease. Besides its chemotactic function, it enhances the production of various cytokines, regulate vascular permeability and influence the adaptive immune system by stimulating Th1 response. As a result of its action, abnormal inflammation could eventually lead to structural changes in the lungs (135). C5a induces autophagy in mouse alveolar macrophages promoting their apoptosis (136). Both cigarette smoke extract and C5a induce increased expression of ICAM-1 on airway epithelial monolayers (137). Clinical findings show that the Th1-attracting chemokine IP-10/CXCL10 was

increased in the bronchial mucosa and BALF of moderate/severe asthma and COPD patients. IP-10 is produced by epithelial cells and acts as the ligand for the CXCR3 receptor expressed on Th1 cells (138,139). The number of receptor-positive cells was increased in smokers with COPD as compared to non-smoking subjects, but not as compared with smokers of normal lung function, suggesting its pro-inflammatory role (140). Our interesting experimental finding showing a remarkably increased IP-10 level in the lung perfectly correlate with these data, therefore, emphasise the translational relevance of our results.

In the tissue destruction phase of our model at months 5-6 C5a, IFN-γ, IL-4, IL-7, IL-13, IL-17, IL-27, tumour necrosis factor-α (TNF-α), macrophage inflammatory protein-1α (MIP-1α), JE, TIMP-1, interferon-inducible T-cell chemoattractant (I-TAC) and TREM-1 cytokine levels increased. An adaptive immune reaction mediated by CD4+ and CD8+ T cells and a Th1 cell-regulated chemokine-cytokine profile might be important factors of emphysema in susceptible animals. There is a great upregulation of the inflammatory mediators pointing towards a Th1-adaptive inflammatory response in mice with significant increases in MIP-1α (141). Both natural killer (NK) and T cells use MIP-1α along with interferon-γ (IFN- γ), RANTES and the I-TAC as a "functional unit" to drive the Th1 response (142). TIMP-1 specifically interacts with proMMP-9, its expression is regulated by growth factors and cytokines (143). TIMP-1 does not only inhibit MMP activities, but also acts as a cytokine by promoting cell growth in a wide range of cell types including fibroblasts, epithelial cells and the SV40 transformed human lung cell line (144). TNF-α is also a key factor implicated in emphysema pathogenesis, its type 2 receptor plays a critical role in the pro-inflammatory pathway (145). IFN-γ is a potent stimulator of MMP-9 and CCR5 ligands (MIP-1α, MIP-1β, RANTES) which ultimately results in DNA damage, apoptosis and emphysema (146).

In contrast to asthma studies, Bowler and co-workers found that subjects with emphysema had decreased IL-16 protein in plasma and decreased IL-16 mRNA expression in peripheral blood mononuclear cells (147). Our results correlate with these finding as IL-16 expression decreased at months 5-6 when emphysema developed.

ICAM-1 is a central molecule in inflammatory processes and functions as a co-stimulatory signal being important for the trans-endothelial migration of leukocytes and the activation of T cells. Increased circulating levels of sICAM-1 are highly associated with major cardiovascular complications (e.g.: increased risk of myocardial infarction (148), in addition chronic smokers have

elevated levels of sICAM-1 (149). Furthermore, significant increase in sICAM-1 was associated with the extent of emphysema in patients involved in the Multi-Ethnic Study of Atherosclerosis Lung study (150). MMPs are responsible for the cleavage and generation of soluble adhesion molecules, including sICAM-1 and sVCAM-1 from the endothelium, and could act as mediators beyond the lung to establish and sustain low-grade inflammation and aggravate the cardiovascular complications (151).

The chronic moderate cigarette smoke exposure-induced mouse model therefore is appropriate to investigate smoking-induced time-dependent characteristic alterations and mechanisms in the lung. The pathophysiological alterations we described here appear to be similar to that observed in the clinics, which highlights the translational value of our model in relation to the human morbidity seen in COPD.

In this characterised and optimised model, we have investigated the involvement of TRPA1 in chronic airway inflammation. We provided the first evidence that the TRPA1 channel has a complex role in basal airway function regulation and inflammatory mechanisms by triggering chronic CSE-evoked emphysema formation and respiratory deterioration, such as MV, TV, PIF and PEF decrease with a peak after 3 months.

These data are supported by findings, that 4-week CSE increases *Trpa1* mRNA level in the nodose and jugular ganglia, positively correlating with the inflammatory cell infiltration in the BALF (152). Moreover, CS extract also increased the expression of TRPA1 in airway epithelial cells in a hypoxia-inducible factor-1α-mediated manner (12,153). Mostly *in vitro* data using cigarette smoke extract are available about the role of TRPA1 in CS-induced airway inflammation. Isolated bronchi experiments suggested that CS extract, as well as its components (acrolein and crotonaldehyde) caused Ca^{2+}-dependent CGRP- and SP-release from the capsaicin-sensitive nerve endings, and TRPA1 was involved in the CS extract-induced tracheal plasma extravasation and bronchoconstriction (20). Cigarette smoke-induced CGRP release in the trachea were predominantly mediated by TRPA1 rather than nicotinic receptors (23). CS and acrolein released keratinocyte chemoattractant (CXCL1/KC, mouse analogue of IL-8), which was attenuated by TRPA1 antagonists and TRPA1-deficiency (37). Furthermore, CS extract-induced and TRPA1-mediated IL-8 release was shown to develop via NADPH-oxidase activation and the MAPKs/NFκB signaling pathway-related Ca^{2+} influx (12). TRPA1 is involved in CS extract-

evoked alveolar and bronchial epithelial damage (154). Nicotine directly activates the TRPA1 receptor (22,24) which might mediate bronchoconstriction (37). Similarly, ROS and several lipid peroxidation products also stimulate TRPA1, which is likely to contribute to oxidative stress-evoked airway pathologies induced by CSE (12,16,21), such as emphysema, for which we provided the first data here.

The extent of perivascular/peribronchial oedema was the most severe after 1 month and gradually decreasing afterwards, and the inflammatory cell infiltration reached its maximum after 2 months of CSE in both groups, which is in agreement with our earlier findings in the same model (105). TRPA1 deficiency did not result in significant changes of the cellular components of these chronic inflammatory processes, as shown by both the histopathological results and BALF analysis.

Increasing data have suggested the involvement of the TRPA1 receptor in the pathophysiological mechanisms of several airway diseases, such as asthma, COPD and allergic/irritative cough (21,36,46,51,155–157), but little is known about its activation mechanisms and its potential as a drug target in lung inflammation is still controversial. Interestingly, our group has also demonstrated the protective role of TRPA1 in the LPS-induced acute pneumonitis model including decreased bronchial hyperreactivity, as well as neutrophil- and macrophage-derived myeloperoxidase (MPO) activity in *Trpa1* wildtype mice compared to their gene-deficient counterparts (173). Our results demonstrating the deteriorating role of TRPA1 in the CSE-induced chronic model seemingly oppose its protective regulatory effect in the acute LPS model (158). This can be explained by the multiple localisations of TRPA1 that might evoke different responses. Neuronal TRPA1 in the airways is expressed almost exclusively on vagal afferents that are a subpopulation of sensory afferents. It is co-localised with TRPV1 on capsaicin-sensitive vagal bronchopulmonary nociceptive C-fibers originating from the jugular ganglion. Most of these peptidergic bronchopulmonary C-fibers modulate the inflammatory process and induce defensive reflexes, shallow breathing, mucus secretion (159,160). However, TRPA1-mediated effects via the sensory trigeminal afferentation of the upper airways also might contribute to our results in both chronic and acute models (161). Besides the neuronal expression, TRPA1 is also located on epithelial, inflammatory and bronchial smooth muscle cells (20,37–39).

The virtually contradicting role of TRPA1 might also be explained by the very distinct pathophysiological mechanisms of the CSE and LPS models involving different signalling pathways in different cell types. Moreover, endotoxin and cigarette smoke components are able to

directly activate TRPA1 among other exogenous irritants reaching the airways, besides a variety of endogenous inflammatory mediators (protons, hydrogen peroxide, prostaglandins etc.) (13,15,19,22,24).

Since the activation of TRPA1 exerts protective effects in LPS-induced acute pneumonitis and subsequent bronchial hyperreactivity, our findings clearly support the concept that short-term activation of TRPA1 results in defensive effects presumably via sensory nerves and consequently released protective neuropeptides. However, permanent stimulation of the receptor under chronic inflammatory conditions of the airways results in complex regulatory functions due to the diverse localisation of TRPA1 also on non-neural cells and its broad range of both exogenous and endogenous activators.

The genetic deletion of the receptor does not directly predict prophylactic or therapeutic potential of TRPA1 agonists or antagonists. However, the activation of TRPA1 by commonly inhaled substances, e.g., cinnamaldehyde or carvacrol (21) (components of cinnamon or thyme essential oils) could be beneficial against acute inflammatory changes of the lung, additionally considering their antimicrobial potentials against pathogens predominant in airway infections [85].

Therefore, further research is needed to determine TRPA1 potential as a pharmacological target in the lung.

In order to investigate the potential role of TRPA1 and TRPV1 in gastritis we characterised a translationally relevant model of diffuse gastric injury. This was the first comprehensive and comparative acute and chronic diffuse gastritis model study, in which IAA-induced concentration- and duration-dependent changes were described in Wistar rats. IAA induced concentration-dependent weight loss and gastric erosions developed already after 7-day ingestion of IAA in drinking water accompanied by massive submucosal oedema and extensive infiltration of acute and chronic inflammatory cells, and subsequently, haemorrhagic erosions. After 14 days, ulcers were observed as deep necrosis involving the muscularis mucosae, which was more severe and more extensive in rats with high (0.2%) IAA concentration in their drinking water.

IAA is a sulfhydryl alkylating agent, which inhibits free radical scavenging by depleting reduced GSH, thus inducing gastric injury (92). However, although this mechanism of action is the state of the art, GSH concentrations are rarely measured directly in the stomach mucosa. In our present study, we did not find GSH reduction in response to IAA application. This might be due to the fact

that we measured it after 7 or 14 days of IAA ingestion when the lesions were already fully developed or started to heal. Furthermore, we used the whole stomach tissue, not only the mucosa. Nevertheless, the small, but significant increase in tGluCys also supports the onset of the healing phase with the elevation of oxidative stress and/or GSH synthesis enzyme activity. IAA-induced rapid GSH depletion was demonstrated in cultured Wistar rat astrocytes (173), rat hepatocytes (174,175), and in human erythrocytes as well (175). GSH content from *in vivo* experiments are highly influenced by the complex inflammatory/oxidative/antioxidant regulatory system of the animal, as well as the differences in sampling protocols. In an IAA-induced gastritis model, 0.1% IAA induced a robust, almost 4-fold increase in gastric mucosal GSH after one week, whereas in the same experimental paradigm, an approximately 50% decrease was measured after two weeks of IAA administration (176). The robust GSH increase was accompanied by a similarly elevated MPO activity, which is a reliable indicator of inflammatory cell infiltration/activation, suggesting that at the time of lesion formation, the fine regulation is also activated to counteract the imbalance of the aggressive/defensive factors. Similar rebound GSH increase was reported on alveolar epithelial cells (177), where genes involved in GSH synthesis, such as γ-glutamylcysteine transpeptidase, and activator protein-1 (AP-1) were upregulated as an adaptive mechanism.

Only a few studies have used the IAA gastritis model, but with different paradigms: 1) various durations (5 days–25 weeks) (178–181), 2) rats weighing 100–500 g (179,182), 3) different strains (178,180,182), 4) different IAA concentrations (112,180,181,183), 5) routes of administration, even with additional sucrose in drinking water (112,113,180,183). Therefore, the comparison of the outcomes and conclusions of these different studies is not easy, but they are consistent in MPO elevation and macroscopic/microscopic alterations characteristic to diffuse gastritis with haemorrhages. We did not observe significant changes in the severity of lesions regarding hyperaemia and erosions between 7 and 14 administration days in agreement with the literature (97), although ulcer formation was more pronounced after 14 days.

In this well-characterised gastric erosion/ulcer inflammatory model, our major finding is that both 0.05% and 0.2% IAA ingestion induced *Trpa1*, but not *Trpv1* mRNA upregulation in the rat antrum and corpus after 7 days—that remained elevated by the end of the 14-day period.

Most activators of the TRPA1 channel are structurally diverse molecules, which suggests that their effect is not exerted based on the conventional lock-and-key principle. They act as reactive electrophile compounds (allylisothiocyanate, cinnamaldehyde) inducing covalent reversible

modifications of the cytoplasmic N terminal of the receptor (184,185). IAA being a cysteine-modifying alkylating compound is able to bind covalently to the reactive cytoplasmic cysteine residues, thus inducing TRPA1 activation as demonstrated in HEK cell culture by Ca^{2+} imaging (184). However, TRPA1 upregulation in our experiments is not explained simply by direct IAA-evoked receptor activation or desensitisation, since prolonged administration of IAA to human TRPA1-expressing cells was described not to induce receptor desensitisation (186). Moreover, IAA acts as a partial TRPA1 agonist, since after its continuous administration, a subsequently applied other agonist (para-benzoquinone) that induce rapid desensitisation by itself further increased TRPA1-mediated Ca^{2+} current (186). Therefore, IAA-induced TRPA1 expression increase in the stomach is more likely due to the inflammatory cascade, which is further supported by its upregulation in water immersion restraint, stress-induced acute gastric mucosal ulcerations in rats (187).

There are no data on the expression and function of the TRPA1 channel in gastritis and only little information is available on TRPV1. The distribution of TRPV1 immunopositivity was reported to be increased in chronic gastritis biopsies, however, in that study, control samples were collected from patients with functional dyspepsia (188).

TRPV1/A1 expression on capsaicin-sensitive peptidergic nerve endings and non-neural cells, such as gastric epithelial and inflammatory cells (34,35,40,41), also shown by our present results detecting *Trpa1* mRNA in the stomach, make the interpretation of their roles much more complex. Several endogenous inflammatory mediators activating TRPV1 (protons, lipoxygenase products) are produced during the IAA-induced inflammatory reaction, which might also influence TRPA1 function and expression since their interactions have been described (4,29,40).

The role of capsaicin-sensitive sensory nerves in IAA-induced gastritis has been investigated by defunctionalising these neurons with high doses of capsaicin (183). The role of these peptidergic afferents depends on the experimental paradigm and the consequent pathophysiological mechanisms - they can both inhibit (e.g., ethanol-induced gastritis) or aggravate the inflammation presumably via SP and CGRP release (e.g., IAA-induced gastritis), underlining the role of neurogenic component in inflammation (183). The role of TRPA1 and TRPV1 in gastritis might also be attributed to the mediation of inflammatory visceral hyperalgesia and abdominal pain. IAA was shown to significantly increase Na^{+} current in the DRG of T9 and T10 afferent neurons (189),

and enhanced visceromotor responses primarily by increased activity of the splanchnic nerves (182).

Surprisingly, mice (both CD1 and C57Bl/6 strains) proved to be resistant to all applied concentrations of IAA, even higher than the most damaging one in the rat. Although they also exhibited concentration-dependent weight loss similar to the rat, no macroscopic or microscopic changes have been found in the stomach. The few studies coming from one group point out the lack of IAA-induced macroscopic lesions in mice supporting our present results, but describe a mixed inflammatory infiltration, characteristic to mild gastritis (190). Interestingly, most of these studies showed that after an initial weight loss, mice recovered by the third day of administration, although their water intake was reduced by approximately 50% throughout the study (191–193). This is also in agreement with our observation, that body weight loss cannot be explained solely by less drinking in IAA-treated animals. The concentration-dependent reduction in fluid consumption suggests an oral aversion that might be due to the potential gastro-irritating effect of the colourless, odourless IAA solution.

Since TRPA1 is activated by IAA, it raises the question whether the known species differences in sequence homology, as well as its selectivity to a range of ligands, might contribute to the observed species differences in the IAA model. As discussed above, IAA contains a highly reactive electrophilic moiety lacking structural selectivity, that forms alkylation adducts by binding to the cysteine residues on the N-terminal of TRPA1 (185), which might potentially lead to its activation (184). Therefore, it is more likely, that species differences in the IAA-induced diffuse gastritis model is not due to the heterogeneity in TRPA1 ion channel sequence, and that TRPA1 upregulation is rather a consequence of tissue injury. Determining resistance mechanisms was beyond the scope of our study; however, it might provide valuable information on gastroprotective mechanisms yet not fully known. As a general limitation of all immunohistochemical techniques, TRPA1- and TRPV1-like immunopositivity determined on the histopathological sections in our study might not provide direct evidence for the receptor protein expression. However, (i) the parallel receptor mRNA changes, (ii) the positive control with dorsal root ganglia samples, (iii) the lack of immunopositivity with the blocking peptides provided by the producers, (iv) as well as the extensive use of both antibodies in the literature (194,195) and in our earlier studies (30,196,197) suggest the reliability and validity of our IHC results supporting our conclusion.

The role of TRPV1 and TRPA1 in gastrointestinal mucosal defense mechanisms is virtually controversial, but the overall function is likely to be protective (82). Their investigation is more thorough in inflammatory bowel disease (IBD). Studies with *Trpv1* and *Trpa1* gene-deficient mice show contradictory data about their roles in colitis, most likely depending on the key pathophysiological mechanisms of the different colitis models (82). Several studies have focused on elucidating the mechanism by which these channels might mediate pro-inflammatory and/or anti-inflammatory effects (Tables 6-8).

Goso and co-workers provided the first evidence for a protective role of TRPV1-expressing peptidergic sensory nerves via the release of the protective neurotransmitter CGRP upon acute co-administration of capsaicin in a TNBS-induced colitis model (179). Administration of TRPV1 agonists, resiniferatoxin (RTX) or high dose capsaicin, induces a sustained functional denervation of TRPV1-expressing extrinsic neurons, thus it provides a method in animal models for the investigation of these sensory afferents and the released neurotransmitters. The results of this chemical desensitisation are not coherent, since pro-inflammatory and protective roles have also been described. Neonatal capsaicin desensitisation, as well as the administration of the TRPV1 antagonist capsazepine have been reported to significantly attenuate macroscopic damage score, MPO activity increase and inflammatory histopathological alterations compared to normal DSS-treated rats attributing the colitogenic effect to SP released from the nerve terminals of TRPV1-expressing sensory fibres (180). Meanwhile, Utsumi and co-workers found opposing results in the same model after adult treatment by high doses of capsaicin, which exacerbated colitis and reduced the inflammation-induced upregulation of both SP- and CGRP-positive fibres (181). However, they described that *Trpv1* and *Trpa1* gene deletion decreased colitis severity and the upregulation of SP-positive nerve fibres without influencing protective CGRP-positive nerves. Similarly, neonatal capsaicin denervation resulted in more severe colitis in the oxazolon-induced model, but exacerbation was not accompanied by changes in the expression and distribution of CGRP- and SP-immunoreactive nerves in the colon (182). These virtually contradictory pro- and anti-inflammatory effects of neuropeptides released from the TRPV1/A1-expressing fibres during chemically-induced colitis were further investigated in the TNBS model, where abrogated CGRP release in the isolated colon preparations and DRG were observed in *Trpa1*, but not in *Trpv1* gene-deficient mice. They showed that this mechanism is mediated via the sustained sensitisation of TRPA1 by TNBS covalently binding to the cysteine and lysine residues in the cytoplasmic N-

terminus of the receptor protein. TNBS induces similar severe acute colitis in wildtype and *Trpv1*$^{-/-}$, but reduced inflammation in *Trpa1*$^{-/-}$ mice or wildtype animals treated with the TRPA1 antagonist HC-030031. Sensory denervation, as well as SP gene-deletion abolished both TNBS and DSS-induced colitis, while in CGRP-deficient mice TNBS induced a more severe colitis further supporting the opposing actions of the sensory neuropeptides released from the same nerve terminals (79,183). *Trpv1*-deficiency did not affect disease severity, only prevented chronic pain development during the recovery phase of DSS-induced colitis (184). However, this result was challenged by other studies demonstrating the pathogenic role of TRPV1 by gene-deleted mice exhibiting less severe DSS-induced colitis, concluding that inflammatory mediators activate the TRPV1 receptor and induce neurogenic inflammatory components by releasing SP, neurotensin, vasoactive intestinal polypeptide and galanin (109,181). Meanwhile, Massa and co-workers found more severe DNBS-induced colitis in *Trpv1*$^{-/-}$ mice, suggesting a protective role of TRPV1 (185). Bertin and co-workers proposed non-neuronal TRPV1 and TRPA1-mediated proinflammatory mechanisms in colitis. They showed that both channels are present on mouse and human CD4+ T cells and play an important regulatory role in their activation and the production of proinflammatory cytokines, such as IFN-γ, IL-2, IL-10 and TNF-α. In a spontaneous *IL10*$^{-/-}$ colitis model both genetic deletion and pharmacologic inhibition of TRPV1 resulted in attenuated inflammation. They provided clear experimental evidence in a T cell adoptive transfer model that TRPV1-expressing CD4+ T cells are involved in colitis pathogenesis (41). In the same experimental paradigm TRPA1 was described to exert protective actions by restraining TRPV1 activity on these immune cells, thus controlling their activation and inflammatory functions (40). The protective role of TRPA1 was also supported by TRPA1-mediated downregulation of proinflammatory neuropeptides SP, neurokinins A, B (NKA, NKB) and NK1 receptor, as well as cytokines and chemokines like TNFα, IL-1β, MIG and MCP-1 (34).

Table 6. Role of TRPV1 in animal models of colitis (*Trpv1*$^{-/-}$ gene deleted mice were bred on C57Bl/6 background; DSS: dextrane sulfate sodium; TNBS: trinitrobenzene sulfonic acid; DNBS: dinitrobenzene sulphonic acid).

Approaches	**Results**	**Animal species/ strain**	**Model**	**Ref**
TRPV1 antagonist	reduces colitis severity	Sprague-Dawley rats	5% DSS + capsazepine	(180)
		female BALB/c mice	5% DSS + capsazepine/ JNJ 10185734	(193)
		Sprague-Dawley rats	TNBS + capsazepine	(194)
		female Wistar rats	TNBS + BCTC	(195)
		Il10$^{-/-}$*Trpv1*$^{-/-}$ mice	*Il10*$^{-/-}$-induced spontaneous colitis + SB366791	(41)
TRPV1 agonist	attenuates colitis/ visceral hyperalgesia	male Sprague-Dawley rats	TNBS + capsaicin	(179)
		male BALB/c mice	DNBS + curcumin	(186)
		male Sprague-Dawley rats	5% DSS + curcumin	(187)
TRPV1 gene deletion	decreases colitis	female *Trpv1*$^{-/-}$ mice	2% DSS	(196)
		Il10$^{-/-}$*Trpv1*$^{-/-}$ mice	*Il10*$^{-/-}$-induced spontaneous colitis	(41)
		male *Trpv1*$^{-/-}$ mice	2% DSS	(181)
	aggravates colitis	female *Trpv1*$^{-/-}$ mice	DNBS	(185)
	does not affect colitis severity	female *Trpv1*$^{-/-}$ mice	5% DSS	(196)
		Trpv1$^{-/-}$ mice	TNBS	(183)
		Trpv1$^{-/-}$ mice	2.5% DSS	(184)
	protects against chronic pain during recovery	*Trpv1*$^{-/-}$ mice	2.5% DSS	(184)
	decreases CD4+ T cell activation and cytokine production	*Il10*$^{-/-}$*Trpv1*$^{-/-}$ mice	*Il10*$^{-/-}$-induced spontaneous colitis	(41)

Table 7. Role of TRPA1 in animal models of colitis (*Trpa1*$^{-/-}$ gene deleted mice were bred on C57Bl/6 background; DSS: dextrane sulfate sodium; TNBS: trinitrobenzene sulfonic acid; DNBS: dinitrobenzene sulphonic acid).

Approaches	Results	Animal species/ strain	Model	Ref
TRPA1 antagonist	reduces colitis severity	C57Bl/6 mice	TNBS + HC-030031; DSS + HC-030031	(183)
	reverses visceromotor response	female Wistar rats	TNBS/ethanol + TCS-5861528	(195)
TRPA1 gene deletion	decreases colitis	*Trpa1*$^{-/-}$ mice	TNBS, 2% DSS	(183)
		male *Trpa1*$^{-/-}$ mice	2% DSS	(181)
	aggravates colitis	male *Trpa1*$^{-/-}$ mice	2% DSS	(197)
		Il10$^{-/-}$*Trpa1*$^{-/-}$ mice	*Il10*$^{-/-}$-induced spontaneous colitis	(40)
	increases TRPV1 channel activity in CD4+ T cells, increases CD4+ T cell activation and proinflammatory cytokine production	*Il10*$^{-/-}$*Trpa1*$^{-/-}$ mice	*Il10*$^{-/-}$-induced spontaneous colitis	(40)

Table 8. Role of capsaicin-senstive sensory neurons in animal models of colitis (*Trpv1*$^{-/-}$, *Trpa1*$^{-/-}$ gene deleted mice were bred on C57Bl/6 background; DSS: dextrane sulfate sodium; TNBS: trinitrobenzene sulfonic acid; DNBS: dinitrobenzene sulphonic acid).

Approaches	Results	Animal species/ strain	Model	Ref
Capsaicin-induced sensory desensitization	aggravates colitis	female BALB/c mice	oxazolone	(182)
		male *Trpv1*$^{-/-}$, *Trpa1*$^{-/-}$ mice	2% DSS	(181)
	alleviates colitis	Sprague-Dawley rats	5% DSS	(180)
RTX- denervation	alleviates colitis	C57Bl/6 mice	TNBS, 2% DSS	(183)

Pharmacological interventions with curcumin had anti-inflammatory and anti-hyperalgesic effects in colitis models (186,187). Although in these studies curcumin was interpreted and discussed as a TRPV1 agonist, it is important to note that curcumin is a non-selective compound having a typical pleiotropic effect including direct antioxidant activity, anticancer and antimicrobial properties mediated by a wide range of targets, even the TRPA1 receptor (188–190). Considering that TRPA1 is almost exclusively expressed in TRPV1-positive neurons and both channels are known to interact (29,30), cross-desensitisation could have a role in the actions of curcumin. Furthermore,

curcumin was also described as a TRPV1 antagonist, because it inhibited capsaicin-evoked potentials (191). In a clinical study, curcumin was reported to significantly reduce relapse rate in UC patients not via the activation, but the inhibition of TRPV1 either directly or by ways of cross-desensitisation of TRPA1 (192). Therefore, we should be cautious when drawing conclusions regarding TRPV1 involvement based on the results of curcumin administration.

Other TRPV1 and TRPA1 antagonists also showed mainly protective actions. TRPV1 blockade by the non-selective antagonist capsazepine, JNJ 10185734, BCTC and SB366791 in various models of colitis exerted anti-inflammatory actions supporting the pathogenic role of TRPV1 in experimental IBD (41,180,193–195). Moreover, both intraperitoneal and intrathecal administrations of TRPV1 and TRPA1 antagonists exerted analgesic actions in rat colitis models highlighting central nervous system mechanisms (195).

TRPV1 and TRPA1 expression, and experimental data regarding its role in colitis appears to be virtually inconsistent. Activation of these receptors on sensory nerve terminals mediates neurogenic inflammation via the release of SP and CGRP, resulting in increased vascular permeability, plasma protein extravasation and inflammatory cell activation. Meanwhile, anti-inflammatory sensory neuropeptides, such as somatostatin and opioid peptides released simultaneously from the same nerve ending exert anti-inflammatory and analgesic actions both locally and systemically through getting into the circulation. Furthermore, these ion channels on vascular smooth muscle and inflammatory cells such as macrophages and T helper cells mediate both pro- and anti-inflammatory functions. Therefore, the overall role of TRPV1 and TRPA1 in experimental colitis is dependent on 1) the diversity of the expression of these ion channels on sensory nerves, immune cells, epithelial cells and vascular smooth muscle cells (4), 2) the consequent activation-induced release of broad range of pro- and anti-inflammatory mediators including sensory neuropeptides and cytokines exerting divergent mechanisms, 3) the complex interactions of the co-expressed TRPV1 and TRPA1 receptors (Figure 1), 4) differences of the experimental models, protocols and paradigms (species, strain, concentration and composition of the chemicals, duration, intensity, complex mechanisms of the injury), as well as several limitations of the models (198).

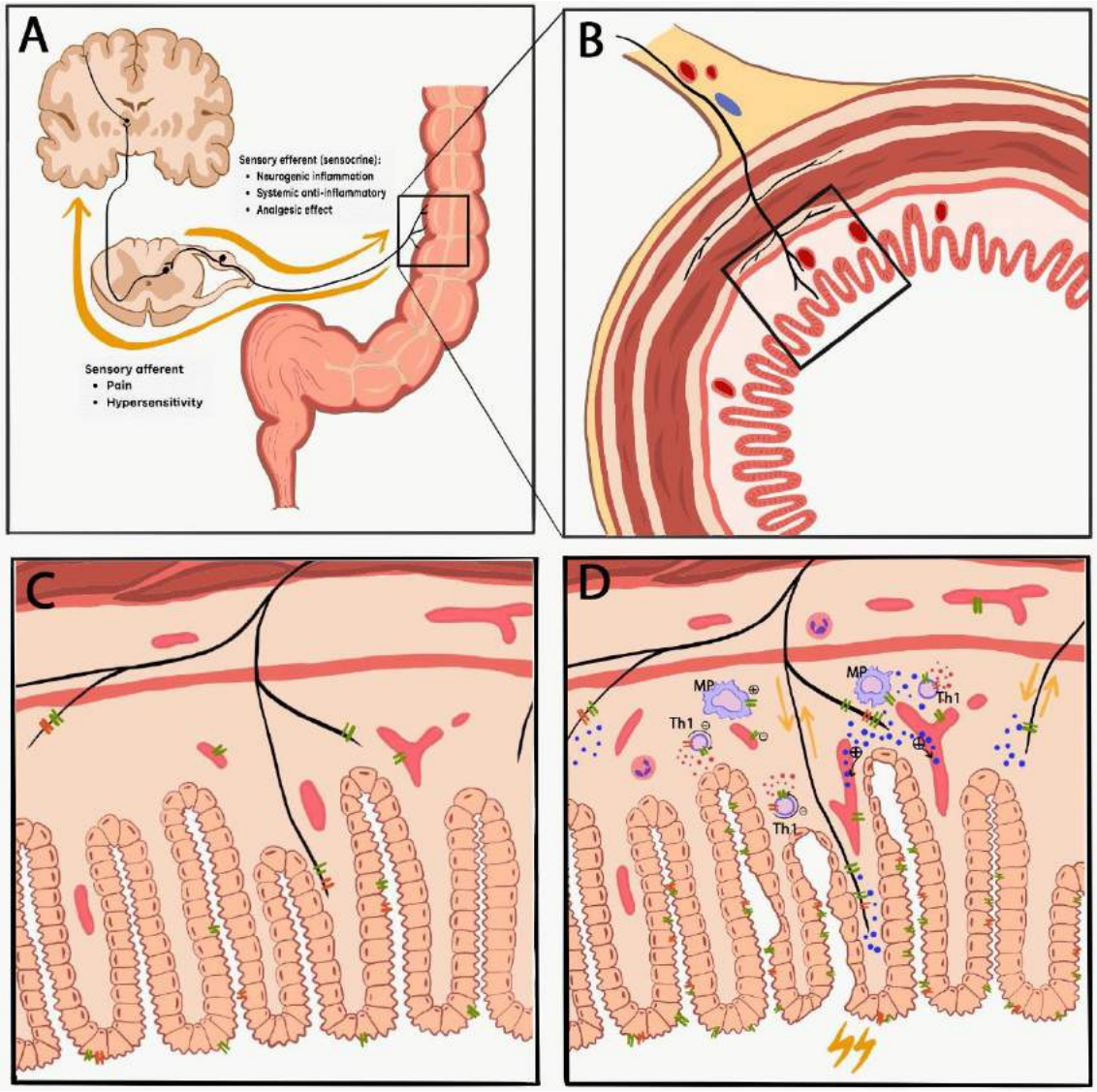

Figure 28. The complex interactions of TRPV1 and TRPA1 and their virtually contradictory role in colitis. A) The afferent and efferent (sensocrine) functions (yellow arrows) of the capsaicin-sensitive sensory nerve fibers. Panel C (without inflammation) and D (during inflammation) depict an enlarged schematic section of the colon cross section (panel B) focusing on the expression and interaction of TRPV1 (green double lines) and TRPA1 (orange double lines) in the colon mucosa. Neurogenic inflammation is mediated via the release of SP and CGRP (blue dots represent neurotransmitters, such as SP, CGRP and somatostatin), resulting in increased vascular permeability, plasma protein extravasation and inflammatory cell activation. Meanwhile, anti-inflammatory sensory neuropeptides, such as somatostatin and opioid peptides released simultaneously from the same nerve ending exert anti-inflammatory and analgesic actions both locally and systemically through getting into the circulation. Furthermore, these ion channels on vascular smooth muscle and inflammatory cell such as macrophages (MP) and T helper cells (Th1) mediate both pro- (+) and anti-inflammatory (-) effects by regulating the release of cytokines (IFN-γ, IL-2, IL-10, TNFα are represented as red dots) (82).

6 Summary of new results, conclusions

1) We provided evidence with functional, morphological and immunological techniques that chronic moderate cigarette smoke induces characteristic pulmonary inflammation, emphysema and atelectasis. These well-defined pathophysiological alterations from the inflammatory reactions to the tissue destruction are dependent on the duration of the smoke exposure and COPD-like structural and functional changes develop only after the fourth month (Figure 28) and are similar to that observed in the clinics, which highlights the translational value of our model in relation to the human morbidity seen in COPD. Therefore, this mouse model is appropriate to investigate smoking-induced time-dependent characteristic alterations and mechanisms in the lung.

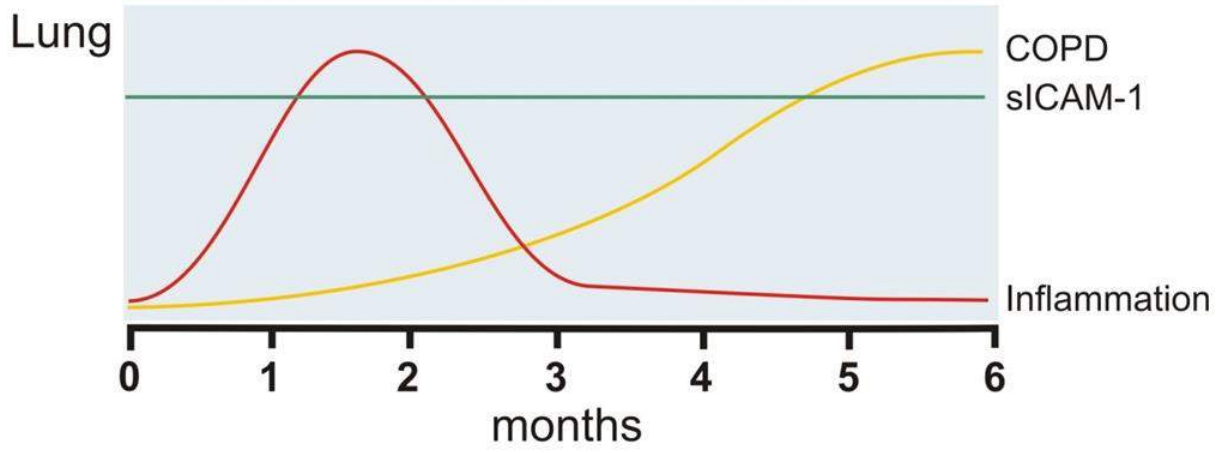

Figure 29. Time-dependent characteristic pulmonary and cardiac pathophysiological alterations in relation to tissue sICAM-1 levels in the chronic cigarette smoke-exposure-induced mouse COPD model.

2) We provided the first evidence that TRPA1 channel has a complex role in basal airway function regulation and inflammatory mechanisms by triggering chronic CSE-evoked emphysema formation and respiratory deterioration, such as MV, TV, PIF and PEF decrease with a peak after 3 months (Table 9).

Table 9. The deteriorating role of TRPA1 in chronic airway inflammation (ns: non-significant; arrows indicate change compared to non-inflamed intact mice, ++p<0.005, +++p<0.001; asteriks indicate strain difference, *p<0.05, **p<0.005 vs *Trpa1*$^{+/+}$).

CSE-induced chronic inflammation	***Trpa1*$^{+/+}$**	***Trpa1*$^{-/-}$**	***Trpa1*$^{+/+}$ vs *Trpa1*$^{-/-}$ CSE-treated inflamed**
	compared to intact control		
TV, MV, PIF, PEF	**↓ (++/+++)**	**ns**	*****
Oedema	↑	↑	**ns**
Inflammatory cell infiltration	↑	↑	**ns**
Emphysema	**earlier**	**later**	*****

3) We provided the first results on the upregulation of the TRPA1 ion channel in a well-characterized translational gastric injury model in correlation with IAA-induced concentration- and duration-dependent macroscopic and microscopic lesions. These data will provide a good basis for evaluating the effect of TRPA1-targeting pharmacological interventions on the different components of the gastric injury.

Table 10. Summary of novel results in the IAA-induced gastritis model (na: data not available).

		0.05% IAA		**0.1% IAA**		**0.2% IAA**	
		day 7	**day 14**	**day 7**	**day 14**	**day 7**	**day 14**
weight change		-	-	↓	↓	↓↓	↓↓
water consumption		↓	↓	↓	↓	↓↓	↓↓
macroscopic lesions		↑	-	-	↑	↑	↑
GSH	**total GluCys**	**na**	**na**	-	↑	**na**	**na**
	total GSH	**na**	**na**	-	-	**na**	**na**
		antrum / corpus					
IHC	**TRPA1**	**na**	↑ / ↑	**na**	**na**	**na**	↑ / ↑
	TRPV1	**na**	- / ↓	**na**	**na**	**na**	↓ / ↓
mRNA	**Trpa1**	↑ / ↑	↑ / -	**na**	**na**	↑ / ↑	↑ / ↑
	Trpv1	- / -	- / -	**na**	**na**	- / -	- / -

7 References

1. Pedersen SF, Owsianik G, Nilius B. TRP channels: an overview. Cell Calcium. 2005;38(3–4):233–52.
2. Abramowitz J, Yildirim E, Birnbaumer L. The TRPC Family of Ion Channels: Relation to the TRP Superfamily and Role in Receptor- and Store-Operated Calcium Entry. In: Liedtke W, Heller S, editors. TRP Ion Channel Function in Sensory Transduction and Cellular Signaling Cascades. Broca Raton, FL, USA: CRC Press/Taylor & Francis; 2007.
3. Latorre R, Zaelzer C, Brauchi S. Structure-functional intimacies of transient receptor potential channels. Q Rev Biophys. 2009;42(3):201–46.
4. Fernandes ES, Fernandes MA, Keeble JE. The functions of TRPA1 and TRPV1: Moving away from sensory nerves. British Journal of Pharmacology. 2012;166(2):510–21.
5. Caterina MJ, Park U. TRPV1: A Polymodal Sensor in the Nociceptor Terminal. Current Topics in Membranes. 2006;57(06):113–50.
6. Geppetti P, Nassini R, Materazzi S, Benemei S. The concept of neurogenic inflammation. BJU International. 2008;101(Suppl 3):2–6.
7. Szolcsányi J. Forty years in capsaicin research for sensory pharmacology and physiology. Neuropeptides. 2004;38(6):377–84.
8. Szolcsányi J, Helyes Z, Oroszi G, Németh J, Pintér E. Release of somatostatin and its role in the mediation of the anti-inflammatory effect induced by antidromic stimulation of sensory fibres of rat sciatic nerve. British Journal of Pharmacology. 1998;123(5):936–42.
9. Szolcsányi J. Capsaicin-sensitive sensory nerve terminals with local and systemic efferent functions: facts and scopes of an unorthodox neuroregulatory mechanism. Progress in Brain Research. 1996;113:343–59.
10. Helyes Z, Pintér E, Sándor K, Elekes K, Bánvölgyi Á, Keszthelyi D, et al. Impaired defense mechanism against inflammation, hyperalgesia, and airway hyperreactivity in somatostatin 4 receptor gene-deleted mice. PNAS. 2009;106(31):13088–93.
11. Sgouros SN, Bergele C, Viazis N, Avgerinos A. Somatostatin and its analogues in peptic ulcer bleeding: Facts and pathophysiological aspects. Digestive and Liver Disease. 2006;38(2):143–8.
12. Lin A-H, Liu M-H, Ko H-K, Perng D-W, Lee T-S, Kou YR. Lung Epithelial TRPA1 Transduces the Extracellular ROS into Transcriptional Regulation of Lung Inflammation Induced by Cigarette Smoke: The Role of Influxed Ca2+. Mediators of Inlfammation. 2015;2015(148367).
13. Taylor-Clark TE, Undem BJ, MacGlashan DW, Ghatta S, Carr MJ, McAlexander MA. Prostaglandin-Induced Activation of Nociceptive Neurons via Direct Interaction with Transient Receptor Potential A1 (TRPA1). Molecular Pharmacology. 2008;73(2):274–81.
14. Al-Shamlan F, El-Hashim AZ. Bradykinin sensitizes the cough reflex via a B2 receptor dependent activation of TRPV1 and TRPA1 channels through metabolites of cyclooxygenase and 12-lipoxygenase. Respiratory Research. 2019;20(110).
15. Bandell M, Story GM, Hwang SW, Viswanath V, Eid SR, Petrus MJ, et al. Noxious Cold Ion Channel TRPA1 Is Activated by Pungent Compounds and Bradykinin. Neuron. 2004;41:849–57.
16. Viana F. TRPA1 channels: molecular sentinels of cellular stress and tissue damage. J Physiol. 2016;594(15):4151–69.

17. Talavera K, Startek JB, Alvarez-Collazo J, Boonen B, Alpizar YA, Sanchez A, et al. Mammalian Transient Receptor Potential TRPA1 Channels: from Structure to Disease. Physiological Reviews [Internet]. 2020;100(2):725–803. Available from: www.physiology.org/journal/physrev
18. McNamara FN, Randall A, Gunthorpe MJ. Effects of piperine, the pungent component of black pepper, at the human vanilloid receptor (TRPV1). British Journal of Pharmacology. 2005 Mar;144(6):781–90.
19. Meseguer V, Alpizar YA, Luis E, Tajada S, Denlinger B, Fajardo O, et al. TRPA1 channels mediate acute neurogenic inflammation and pain produced by bacterial endotoxins. Nature Communications. 2014;5(3125).
20. Andrè E, Campi B, Materazzi S, Trevisani M, Amadesi S, Massi D, et al. Cigarette smoke – induced neurogenic inflammation is mediated by α,β-unsaturated aldehydes and the TRPA1 receptor in rodents. The Journal of Clinical Investigation. 2008;118(7):2574–82.
21. Bessac BF, Jordt S-E. Breathtaking TRP Channels : TRPA1 and TRPV1 in Airway Chemosensation and Reflex Control. Physiology. 2008;23:360–70.
22. Chung S, Baumlin N, Dennis JS, Moore R, Salathe SF, Whitney PL, et al. Electronic cigarette vapor with nicotine causes airway mucociliary dysfunction preferentially via TRPA1 receptors. American Journal of Respiratory and Critical Care Medicine. 2019;200(9):1134–45.
23. Kichko TI, Kobal G, Reeh PW. Cigarette smoke has sensory effects through nicotinic and TRPA1 but not TRPV1 receptors on the isolated mouse trachea and larynx. American Journal of Physiology Lung Cellular and Molecular Physiology. 2015;309:L812–20.
24. Talavera K, Gees M, Karashima Y, Meseguer VM, Vanoirbeek JAJ, Damann N, et al. Nicotine activates the chemosensory cation channel TRPA1. Nature Neuroscience [Internet]. 2009;12(10):1293–9. Available from: http://dx.doi.org/10.1038/nn.2379
25. Shapiro D, Deering-Rice CE, Romero EG, Hughen RW, Light AR, Veranth JM, et al. Activation of Transient Receptor Potential Ankyrin-1 (TRPA1) in Lung Cells by Wood Smoke Particulate Material. Chemical Research in Toxicology. 2013;26(5):750–8.
26. Deering-Rice CE, Memon T, Lu Z, Romero EG, Cox J, Taylor-Clark T, et al. Differential Activation of TRPA1 by Diesel Exhaust Particles: Relationships between Chemical Composition, Potency, and Lung Toxicity. Chemical Research in Toxicology. 2019;32:1040–50.
27. Memon TA, Nguyen ND, Burrell KL, Scott AF, Almestica-Roberts M, Rapp E, et al. Wood Smoke Particles Stimulate MUC5AC Overproduction by Human Bronchial Epithelial Cells through TRPA1 and EGFR Signaling. Toxicological Sciences. 2020;174(2):278–90.
28. Gouin O, L'Herondelle K, Lebonvallet N, le Gall-Ianotto C, Sakka M, Buhé V, et al. TRPV1 and TRPA1 in cutaneous neurogenic and chronic inflammation: pro-inflammatory response induced by their activation and their sensitization. Vol. 8, Protein and Cell. Higher Education Press; 2017. p. 644–61.
29. Ruparel NB, Patwardhan AM, Akopian AN, Hargreaves KM. Homologous and Heterologous Desensitization of Capsaicin and Mustard Oil Responses Utilize Different Cellular Pathways in Nociceptors. Pain. 2008;135(3):271–9.
30. Story GM, Peier AM, Reeve AJ, Eid SR, Mosbacher J, Hricik TR, et al. ANKTM1, a TRP-like Channel Expressed in Nociceptive Neurons, Is Activated by Cold Temperatures. Cell. 2003;112:819–29.
31. Amadesi S, Nie J, Vergnolle N, Cottrell GS, Grady EF, Trevisani M, et al. Protease-Activated Receptor 2 Sensitizes the Capsaicin Receptor Transient Receptor Potential

Vanilloid Receptor 1 to Induce Hyperalgesia. Journal of Neuroscience. 2004 May 5;24(18):4300–12.
32. Cattaruzza F, Lyo V, Jones E, Pham D, Hawkins J, Kirkwood K, et al. Cathepsin S is activated during colitis and causes visceral hyperalgesia by a PAR2-dependent mechanism in mice. Gastroenterology. 2011;141(5):1864-1874.e3.
33. Faussone-Pellegrini MS, Taddei A, Bizzoco E, Lazzeri M, Vannucchi MG, Bechi P. Distribution of the vanilloid (capsaicin) receptor type 1 in the human stomach. Histochemistry and Cell Biology. 2005;124(1):61–8.
34. Kun J, Szitter I, Kemény Á, Perkecz A, Kereskai L, Pohóczky K, et al. Upregulation of the Transient Receptor Potential Ankyrin 1 Ion Channel in the Inflamed Human and Mouse Colon and Its Protective Roles. PLoS ONE. 2014;9(9):e108164.
35. Poole DP, Pelayo JC, Cattaruzza F, Kuo Y, Gai G, Chiu J v., et al. Transient receptor potential ankyrin 1 is expressed by inhibitory motoneurons of the mouse intestine. Gastroenterology. 2011;141:565–75.
36. Mukhopadhyay I, Kulkarni A, Khairatkar-Joshi N. Blocking TRPA1 in Respiratory Disorders: Does It Hold a Promise? Pharmaceuticals. 2016;9(4):E70.
37. Nassini R, Pedretti P, Moretto N, Fusi C, Carnini C, Facchinetti F, et al. Transient Receptor Potential Ankyrin 1 Channel Localized to Non-Neuronal Airway Cells Promotes Non-Neurogenic Inflammation. PLoS ONE. 2012;7(8):e42454.
38. Kannler M, Lüling R, Yildirim AÖ, Gudermann T, Steinritz D, Dietrich A. TRPA1 channels: expression in non-neuronal murine lung tissues and dispensability for hyperoxia-induced alveolar epithelial hyperplasia. Pflügers Archiv - European Journal of Physiology. 2018;470(8):1231–41.
39. Yap MJG, Ueda T, Takeda N, Fukumitsu K, Fukuda S, Uemura T, et al. Cytokine An inflammatory stimulus sensitizes TRPA1 channel to increase cytokine release in human lung fibroblasts. Cytokine [Internet]. 2020;129:155027. Available from: https://doi.org/10.1016/j.cyto.2020.155027
40. Bertin S, Aoki-Nonaka Y, Lee J, de Jong PR, Kim P, Han T, et al. The TRPA1 ion channel is expressed in CD4+ T cells and restrains T cell-mediated colitis through inhibition of TRPV1. Gut. 2017;66(9):1584–96.
41. Bertin S, Aoki-Nonaka Y, de Jong PR, Nohara LL, Xu H, Stanwood SR, et al. The ion channel TRPV1 regulates the activation and proinflammatory properties of CD4+ T cells. Nature Immunology. 2014;15(11):1055–63.
42. Giorgi S, Nikolaeva-Koleva M, Alarcón-Alarcón D, Butrón L, González-Rodríguez S. Is TRPA1 burning down TRPV1 as druggable target for the treatment of chronic pain? International Journal of Molecular Sciences. 2019;20(12):1–20.
43. Nilius B, Appendino G, Owsianik G. The transient receptor potential channel TRPA1: from gene to pathophysiology. Pflügers Archiv - European Journal of Physiology. 2012;464:425–58.
44. López-Requena A, Boonen B, van Greven L, Hellings PW, Alpizar YA, Talavera K. Roles of Neuronal TRP Channels in Neuroimmune Interactions. In: Emir TLR, editor. Neurobiology of TRP Channels. 2nd ed. CRC Press/Taylor & Francis; 2017.
45. Chen J, McGaraughty S, Kym P. TRPA1 in drug discovery. In: Szallasi A, Bíró T, editors. TRP Channels in drug discovery. Humana Press, Springer; 2012. p. 43–59.
46. Grace MS, Baxter M, Dubuis E, Birrell MA, Belvisi MG. Transient receptor potential (TRP) channels in the airway: role in airway disease. British Journal of Pharmacology. 2014;171:2593–607.

47. Chen J, Hackos DH. TRPA1 as a drug target - Promise and challenges. Naunyn-Schmiedeberg's Archives of Pharmacology. 2015;388(4):451–63.
48. Banner HK, Igney F, Poll C. TRP channels: Emerging targets for respiratory disease. Pharmacology & Therapeutics [Internet]. 2011;130(3):371–84. Available from: http://dx.doi.org/10.1016/j.pharmthera.2011.03.005
49. Yang H, Li S. Transient Receptor Potential Ankyrin 1 (TRPA1) Channel and Neurogenic Inflammation in Pathogenesis of Asthma. Medical Science Monitor. 2016;22:2917–23.
50. Bonvini SJ, Belvisi MG. Cough and airway disease: The role of ion channels. Pulmonary Pharmacology and Therapeutics [Internet]. 2017;47:21–8. Available from: http://dx.doi.org/10.1016/j.pupt.2017.06.009
51. Wallace H. Airway Pathogenesis Is Linked to TRP Channels. In: Emir TLR, editor. Neurobiology of TRP Channels. 2nd ed. Boca Raton (FL): CRC Press/Taylor & Francis; 2017.
52. Prandini P, de Logu F, Fusi C, Provezza L, Nassini R, Montagner G, et al. Transient Receptor Potential Ankyrin 1 Channels Modulate Inflammatory Response in Respiratory Cells from Patients with Cystic Fibrosis. American Journal of Respiratory Cell and Molecular Biology. 2016;55(5):645–56.
53. Dietrich A. Modulators of Transient Receptor Potential (TRP) Channels as Therapeutic Options in Lung Disease. Pharmaceuticals. 2019;12(23).
54. Vestbo J, Hurd SS, Agustí AG, Jones PW, Vogelmeier C, Anzueto A, et al. Global strategy for the diagnosis, management, and prevention of chronic obstructive pulmonary disease GOLD executive summary. American Journal of Respiratory and Critical Care Medicine. 2013;187(4):347–65.
55. Salvi SS, Barnes PJ. Chronic obstructive pulmonary disease in non-smokers. Lancet. 2009 Aug;374(9691):733–43.
56. Restrepo RD. Year in Review 2014: COPD. Respir Care. 2015 Jul;60(7):1057–60.
57. Barnes PJ, Shapiro SD, Pauwels R a. Chronic obstructive pulmonary disease: Molecular and cellular mechanisms. European Respiratory Journal. 2003;22(4):672–88.
58. Yao H, Hwang J, Sundar IK, Friedman AE, McBurney MW, Guarente L, et al. SIRT1 redresses the imbalance of tissue inhibitor of matrix metalloproteinase-1 and matrix metalloproteinase-9 in the development of mouse emphysema and human COPD. Am J Physiol Lung Cell Mol Physiol. 2013;305(9):L615-24.
59. Canning BJ, Spina D. Sensory nerves and airway irritability. Handb Exp Pharmacol. 2009 Jan;(194):139–83.
60. Helyes Z, Hajna Z. Endotoxin-induced airway inflammation and asthma models. In: Szallasi A, Bíró T, editors. TRP Channels in drug discovery. Humana Press; 2012. p. 301–42.
61. Leberl M, Kratzer A, Taraseviciene-Stewart L. Tobacco smoke induced COPD/emphysema in the animal model-are we all on the same page? Frontiers in Physiology. 2013;4 MAY(May):1–23.
62. Wright JL, Churg A. Animal models of COPD: Barriers, successes, and challenges. Pulmonary Pharmacology and Therapeutics. 2008;21(5):696–8.
63. Martorana P a., Cavarra E, Lucattelli M, Lungarella G. Models for COPD involving cigarette smoke. Drug Discovery Today: Disease Models. 2006;3(3):225–30.
64. Mercer PF, Abbott-Banner K, Adcock IM, Knowles RG. Translational models of lung disease. Clinical Science. 2015;128(4):235–56.
65. Vlahos R, Bozinovski S, Gualano RC, Ernst M, Anderson GP. Modelling COPD in mice. Pulmonary Pharmacology and Therapeutics. 2006;19(1):12–7.

66. Beeh KM, Beier J, Kornmann O, Buhl R. Sputum matrix metalloproteinase-9, tissue inhibitor of metalloprotinease-1, and their molar ratio in patients with chronic obstructive pulmonary disease, idiopathic pulmonary fibrosis and healthy subjects. Respir Med. 2003 Jun;97(6):634–9.
67. Shapiro SD, Goldstein NM, Houghton a M, Kobayashi DK, Kelley D, Belaaouaj A. Neutrophil elastase contributes to cigarette smoke-induced emphysema in mice. Am J Pathol. 2003;163(6):2329–35.
68. Sinden NJ, Baker MJ, Smith DJ, Kreft J-U, Dafforn TR, Stockley RA. α-1-antitrypsin variants and the proteinase/antiproteinase imbalance in chronic obstructive pulmonary disease. Am J Physiol Lung Cell Mol Physiol. 2015 Jan;308(2):L179-90.
69. Fricker M, Deane A, Hansbro PM. Animal models of chronic obstructive pulmonary disease. Expert Opin Drug Discov. 2014 Jun;9(6):629–45.
70. Luo F, Liu J, Yan T, Miao M. Salidroside alleviates cigarette smoke-induced COPD in mice. Biomedicine & Pharmacotherapy. 2017;86:155–61.
71. Bartalesi B, Cavarra E, Fineschi S, Lucattelli M, Lunghi B, Martorana P a., et al. Different lung responses to cigarette smoke in two strains of mice sensitive to oxidants. European Respiratory Journal. 2005;25(1):15–22.
72. Phillips B, Veljkovic E, Boué S, Schlage WK, Vuillaume G, Martin F, et al. An 8-month systems toxicology inhalation/cessation study in Apoe-/- mice to investigate cardiovascular and respiratory exposure effects of a candidate modified risk tobacco product, THS 2.2, compared with conventional cigarettes. Toxicological Sciences. 2016;149(2):411–32.
73. Phillips B, Veljkovic E, Peck MJ, Buettner A, Elamin A, Guedj E, et al. A 7-month cigarette smoke inhalation study in C57BL/6 mice demonstrates reduced lung inflammation and emphysema following smoking cessation or aerosol exposure from a prototypic modified risk tobacco product. Food and Chemical Toxicology. 2015;80:328–45.
74. Tam A, Churg A, Wright JL, Zhou S, Kirby M, Coxson HO, et al. Sex Differences in Airway Remodeling in a Mouse Model of Chronic Obstructive Pulmonary Disease. AJRCCM Articles in Press. 2015;201503–487.
75. Low D, Nguyen DD, Mizoguchi E. Animal models of ulcerative colitis and their application in drug research. Vol. 7, Drug Design, Development and Therapy. 2013. p. 1341–56.
76. Kawada M, Arihiro A, Mizoguchi E, Yamamoto-Furusho JK, Submissions O, Com WW. Insights from advances in research of chemically induced experimental models of human inflammatory bowel disease. World J Gastroenterol [Internet]. 2007;13(42):5581–93. Available from: www.wjgnet.comwww.wjgnet.com
77. Panwala CM, Jones JC, Viney JL. A Novel Model of Inflammatory Bowel Disease: Mice Deficient for the Multiple Drug Resistance Gene, mdr1a, Spontaneously Develop Colitis. The Journal of Immunology [Internet]. 1998;161:5733–44. Available from: http://www.jimmunol.org/content/161/10/5733
78. Matsumoto K, Kurosawa E, Terui H, Hosoya T, Tashima K, Murayama T, et al. Localization of TRPV1 and contractile effect of capsaicin in mouse large intestine: high abundance and sensitivity in rectum and distal colon. Am J Physiol Gastrointest Liver Physiol [Internet]. 2009;297:348–60. Available from: http://www.ajpgi.org
79. Engel MA, Khalil M, Mueller-Tribbensee SM, Becker C, Neuhuber WL, Neurath MF, et al. The proximodistal aggravation of colitis depends on substance P released from TRPV1-expressing sensory neurons. Journal of Gastroenterology. 2012 Mar;47(3):256–65.
80. Anavi-Goffer S, Mckay NG, Ashford MLJ, Coutts AA. Vanilloid receptor type 1-immunoreactivity is expressed by intrinsic afferent neurones in the guinea-pig myenteric

plexus. Neuroscience Letters [Internet]. 2002 Nov 6;319:53–7. Available from: www.elsevier.com/locate/neulet
81. Kaji I, Yasuoka Y, Karaki S-I, Kuwahara A. Activation of TRPA1 by luminal stimuli induces EP 4-mediated anion secretion in human and rat colon. Am J Physiol Gastrointest Liver Physiol [Internet]. 2012;302:690–701. Available from: http://www.ajpgi.org
82. Csekő K, Beckers B, Keszthelyi D, Helyes Z. Role of TRPV1 and TRPA1 ion channels in inflammatory bowel diseases: Potential therapeutic targets? Pharmaceuticals. 2019;12(2):1–19.
83. Szolcsanyi J, Barthó L. Impaired defense mechanism to peptic ulcer in the capsaicin-desensitized rat. In: Mózsik G, Hanninen O, Jávor T, editors. Advances in Physiological Science. Oxford: Akadémiai Kiadó-Pergamon Press, Budapest; 1981. p. 39–51.
84. Mózsik G, Szolcsányi J, Rácz I. Gastroprotection induced by capsaicin in healthy human subjects. World Journal of Gastroenterology. 2005;11(33):5180–4.
85. Mózsik G. Capsaicin as new orally applicable gastroprotective and therapeutic drug alone or in combination with nonsteroidal anti-inflammatory drugs in healthy human subjects and in patients. Progress i. Abdel-Salam OME, editor. Vol. 68, Progress in Drug Research. Spriger Basel; 2014. 209–258 p.
86. Yu X, Yu M, Liu Y, Yu S. TRP channel functions in the gastrointestinal tract. Seminars in Immunopathology. 2015;38(3):385–96.
87. Szabo IL, Cseko K, Czimmer J, Mozsik G. Diagnosis of Gastritis – Review from Early Pathological Evaluation to Present Day Management. In: Mozsik G, editor. InTech Open Access Publisher. Rijeka; 2013. p. 3–20.
88. Lu CL, Chang SS, Wang SS, Chang FY, Lee SD. Silent peptic ulcer disease: frequency, factors leading to "silence," and implications regarding the pathogenesis of visceral symptoms. Gastrointestinal Endoscopy. 2004;60(1):34–8.
89. Appelman HD. Gastritis: Terminology, Etiology, and Clinicopathological Correlations: Another Biased View. Human Pathology. 1994;25(10):1006–19.
90. McColl KEL. Helicobacter pylori-Negative Nonsteroidal Anti-Inflammatory Drug-Negative Ulcer. Gastroenterology Clinics of North America [Internet]. 2009;38(2):353–61. Available from: http://dx.doi.org/10.1016/j.gtc.2009.03.004
91. Kavitt RT, Lipowska AM, Anyane-Yeboa A, Gralnek IM. Diagnosis and Treatment of Peptic Ulcer Disease. American Journal of Medicine [Internet]. 2019;132(4):447–56. Available from: https://doi.org/10.1016/j.amjmed.2018.12.009
92. Szabo S, Trier JS, Brown A, Schnoor J. Sulfhydryl blockers induce severe inflammatory gastritis in the rat. Gastroenterology. 1984;86:1271.
93. Szabo S, Trier JS, Frankel PW. Sulfhydryl compounds may mediate gastric cytoprotection. Science (1979). 1981;214(October):200–2.
94. Pihan G, Majzoubi D, Haudenschild C, Trier JS, Szabo S. Early microcirculatory stasis in acute gastric mucosal injury in the rat and prevention by 16,16-dimethyl prostaglandin E2 or sodium thiosulfate. Gastroenterology. 1986;91(6):1415–26.
95. Szabo S, Brown A. Prevention of ethanol-induced vascular injury and gastric mucosal lesions by sucralfate and its components: possible role of endogenous sulfhydryls. Proc Soc Expl Biol Med. 1987;185:493–397.
96. Lee SE, Song HJ, Park SY, Nam Y, Min CH, Lee DY, et al. Effect of ECQ on iodoacetamide-induced chronic gastritis in rats. Korean Journal of Physiology and Pharmacology. 2013;17(5):469–77.

97. Karmeli F, Okon E, Rachmilewitz D. Sulphydryl blocker induced gastric damage is ameliorated by scavenging of free radicals. Gut. 1996;38(6):826–31.
98. Bautista DM, Jordt S-E, Nikai T, Tsuruda PR, Read AJ, Poblete J, et al. TRPA1 Mediates the Inflammatory Actions of Environmental Irritants and Proalgesic Agents. Cells. 2006;124:1269–82.
99. Roemer E, Schramke H, Weiler H, Buettner A, Kausche S, Weber S, et al. Mainstream smoke chemistry and in vitro and in vivo toxicity of the reference cigarettes 3R4F and 2R4F. Beitrage zur Tabakforschung International/ Contributions to Tobacco Research. 2012;25(1):316–35.
100. Elekes K, Helyes Z, Kereskai L, Sándor K, Pintér E, Pozsgai G, et al. Inhibitory effects of synthetic somatostatin receptor subtype 4 agonists on acute and chronic airway inflammation and hyperreactivity in the mouse. European Journal of Pharmacology. 2008;578(2–3):313–22.
101. de Langhe E, vande Velde G, Hostens J, Himmelreich U, Nemery B, Luyten FP, et al. Quantification of lung fibrosis and emphysema in mice using automated micro-computed tomography. PLoS ONE. 2012;7(8).
102. Kobayashi S, Fujinawa R, Ota F, Kobayashi S, Angata T, Ueno M, et al. A single dose of lipopolysaccharide into mice with emphysema mimics human Chronic obstructive pulmonary disease exacerbation as assessed by micro-computed tomography. American Journal of Respiratory Cell and Molecular Biology. 2013;49(6):971–7.
103. Calvelli T, Denny TN, Paxton H, Gelman R, Kagan J. Guideline for flow cytometric immunophenotyping: A report from the national institute of allergy and infectious diseases, division of AIDS. Cytometry. 1993;14(7):702–15.
104. Ma W, Cui W, Lin Q. Improved immnunophenotyping of lymphocytes in bronchoalveolar lavage fluid (BALF) by flow cytometry. Clinica Chimica Acta. 2001;313(1–2):133–8.
105. Kemény Á, Csekő K, Szitter I, Varga Z v, Bencsik P, Kiss K, et al. Integrative characterization of chronic cigarette smoke-induced cardiopulmonary comorbidities in a mouse model. Environmental Pollution. 2017;229:746–59.
106. Knudsen L, Weibel ER, Gundersen HJG, Weinstein F v, Ochs M. Assessment of air space size characteristics by intercept (chord) measurement: an accurate and efficient stereological approach. J Appl Physiol (1985). 2010;108(2):412–21.
107. DeCoux A, Lindsey ML, Villarreal F, Garcia RA, Schulz R. Myocardial matrix metalloproteinase-2: inside out and upside down. J Mol Cell Cardiol. 2014 Dec;77:64–72.
108. Kupai K, Szucs G, Cseh S, Hajdu I, Csonka C, Csont T, et al. Matrix metalloproteinase activity assays: Importance of zymography. Journal of Pharmacological and Toxicological Methods. 2010;61(2):205–9.
109. Szitter I, Pintér E, Perkecz A, Kemény Á, Kun J, Kereskai L, et al. Role of neurokinin 1 receptors in dextran sulfate-induced colitis: Studies with gene-deleted mice and the selective receptor antagonist netupitant. Inflammation Research. 2014;63(5):399–409.
110. Pavlidis P, Noble WS. Matrix2png: a utility for visualizing matrix data. Bioinformatics. 2003 Jan;19(2):295–6.
111. Michaelsen JT, Dehnert S, Giustarini D, Beckmann B, Tsikas D. HPLC analysis of human erythrocytic glutathione forms using OPA and N-acetyl-cysteine ethyl ester: Evidence for nitrite-induced GSH oxidation to GSSG. Journal of Chromatography B. 2009;877(28):3405–17.

112. Neuschwander-Teri BA, Roll FJ. Glutathione measurement by HPLC separation and fluorometric detection of the glutathione Orthophthalaldehyde adduct. Analytical Biochemistry. 1989;179:236–41.
113. Parmentier C, Leroy P, Wellman M, Nicolas A. Determination of cellular thiols and glutathione-related enzyme activities: Versatility of high-performance liquid chromatography-spectrofluorimetric detection. Journal of Chromatography B. 1998;719(1–2):37–46.
114. Kun J, Helyes Z, Perkecz A, Ban A, Polgar B, Szolcsanyi J, et al. Effect of surgical and chemical sensory denervation on non-neural expression of the transient receptor potential vanilloid 1 (TRPV1) receptors in the rat. Journal of Molecular Neuroscience. 2012;48(3):795–803.
115. Potolicchio I, Santambrogio L, Strominger JL. Molecular interaction and enzymatic activity of macrophage migration inhibitory factor with immunorelevant peptides. Journal of Biological Chemistry. 2003;278(33):30889–95.
116. Vanoirbeek J a J, Rinaldi M, de Vooght V, Haenen S, Bobic S, Gayan-Ramirez G, et al. Noninvasive and invasive pulmonary function in mouse models of obstructive and restrictive respiratory diseases. American Journal of Respiratory Cell and Molecular Biology. 2010;42(1):96–104.
117. Hoymann HG. Invasive and noninvasive lung function measurements in rodents. Journal of Pharmacological and Toxicological Methods. 2007;55(1):16–26.
118. Caramori G, Adcock IM, di Stefano A, Chung KF. Cytokine inhibition in the treatment of COPD. International Journal of COPD. 2014;9:397–412.
119. Gueders MM, Foidart J-M, Noel A, Cataldo DD. Matrix metalloproteinases (MMPs) and tissue inhibitors of MMPs in the respiratory tract: potential implications in asthma and other lung diseases. Eur J Pharmacol. 2006;533(1–3):133–44.
120. Zhang Y, Cao J, Chen Y, Chen P, Peng H, Cai S, et al. Intraperitoneal injection of cigarette smoke extract induced emphysema, and injury of cardiac and skeletal muscles in BALB/C mice. Exp Lung Res. 2013 Feb;39(1):18–31.
121. Eurlings IMJ, Dentener MA, Mercken EM, de Cabo R, Bracke KR, Vernooy JHJ, et al. A comparative study of matrix remodeling in chronic models for COPD; mechanistic insights into the role of TNF-α. Am J Physiol Lung Cell Mol Physiol. 2014 Oct;307(7):L557-65.
122. Bencsik P, Kupai K, Giricz Z, Görbe A, Huliák I, Fürst S, et al. Cardiac capsaicin-sensitive sensory nerves regulate myocardial relaxation via S-nitrosylation of SERCA: role of peroxynitrite. Br J Pharmacol. 2008 Feb;153(3):488–96.
123. Viappiani S, Nicolescu AC, Holt A, Sawicki G, Crawford BD, León H, et al. Activation and modulation of 72 kDa matrix metalloproteinase-2 by peroxynitrite and glutathione. Biochemical Pharmacology. 2009;77(5):826–34.
124. D'Armiento JM, Goldklang MP, Hardigan A a., Geraghty P, Roth MD, Connett JE, et al. Increased Matrix Metalloproteinase (MMPs) Levels Do Not Predict Disease Severity or Progression in Emphysema. PLoS ONE. 2013;8(2).
125. Atkinson JJ, Lutey B a., Suzuki Y, Toennies HM, Kelley DG, Kobayashi DK, et al. The role of matrix metalloproteinase-9 in cigarette smoke-induced emphysema. American Journal of Respiratory and Critical Care Medicine. 2011;183(7):876–84.
126. Sam L, Roche N, Oliver BG, Mattos W, Barnes PJ, Fan Chung K. Balance of matrix metalloprotease-9 and tissue inhibitor of metalloprotease-1 from alveolar macrophages in cigarette smokers: Regulation by interleukin-10. American Journal of Respiratory and Critical Care Medicine. 2000;162(4 I):1355–60.

127. Ohnishi K, Takagi M, Kurokawa Y, Satomi S, Konttinen YT. Matrix metalloproteinase-mediated extracellular matrix protein degradation in human pulmonary emphysema. Lab Invest. 1998 Sep;78(9):1077–87.
128. Bencsik P, Sasi V, Kiss K, Kupai K, Kolossváry M, Maurovich-Horvat P, et al. Serum lipids and cardiac function correlate with nitrotyrosine and MMP activity in coronary artery disease patients. Eur J Clin Invest. 2015 Jul;45(7):692–701.
129. Dinarello C a. A clinical perspective of IL-1β as the gatekeeper of inflammation. European Journal of Immunology. 2011;41(5):1203–17.
130. Barksby HE, Lea SR, Preshaw PM, Taylor JJ. The expanding family of interleukin-1 cytokines and their role in destructive inflammatory disorders. Clin Exp Immunol. 2007 Aug;149(2):217–25.
131. Kuschner WG, D'Alessandro a., Wong H, Blanc PD. Dose-dependent cigarette smoking-related inflammatory responses in healthy adults. European Respiratory Journal. 1996;9(10):1989–94.
132. Lappalainen U, Whitsett J a., Wert SE, Tichelaar JW, Bry K. Interleukin-1beta causes pulmonary inflammation, emphysema, and airway remodeling in the adult murine lung. American Journal of Respiratory Cell and Molecular Biology. 2005;32(4):311–8.
133. Chakrabarti S, Patel KD. Matrix metalloproteinase-2 (MMP-2) and MMP-9 in pulmonary pathology. Exp Lung Res. 2009 Jan;31(6):599–621.
134. Rogliani P, Calzetta L, Ora J, Matera MG. Canakinumab for the treatment of chronic obstructive pulmonary disease. Pulmonary Pharmacology & Therapeutics. 2015;31:15–27.
135. Marc MM, Kristan SS, Rozman a., Kern I, Flezar M, Kosnik M, et al. Complement factor C5a in acute exacerbation of chronic obstructive pulmonary disease. Scandinavian Journal of Immunology. 2010;71(5):386–91.
136. Hu R, Chen Z-F, Yan J, Li Q-F, Huang Y, Xu H, et al. Complement C5a exacerbates acute lung injury induced through autophagy-mediated alveolar macrophage apoptosis. Cell Death Dis. 2014;5(639):e1330.
137. Floreani A a., Wyatt T a., Stoner J, Sanderson SD, Thompson EG, Allen-Gipson D, et al. Smoke and C5a induce airway epithelial intercellular adhesion molecule-1 and cell adhesion. American Journal of Respiratory Cell and Molecular Biology. 2003;29(4):472–82.
138. Takaku Y, Soma T, Uchida Y, Kobayashi T, Nakagome K, Nagata M. CXC chemokine superfamily induced by Interferon-γ in asthma: a cross-sectional observational study. Asthma Res Pract. 2016;2:6.
139. Ying S, O'Connor B, Ratoff J, Meng Q, Fang C, Cousins D, et al. Expression and cellular provenance of thymic stromal lymphopoietin and chemokines in patients with severe asthma and chronic obstructive pulmonary disease. J Immunol. 2008;181(4):2790–8.
140. Saetta M, Mariani M, Panina-Bordignon P, Turato G, Buonsanti C, Baraldo S, et al. Increased expression of the chemokine receptor CXCR3 and its ligand CXCL10 in peripheral airways of smokers with chronic obstructive pulmonary disease. American Journal of Respiratory and Critical Care Medicine. 2002;165(10):1404–9.
141. Guerassimov A, Hoshino Y, Takubo Y, Turcotte A, Yamamoto M, Ghezzo H, et al. The development of emphysema in cigarette smoke-exposed mice is strain dependent. Am J Respir Crit Care Med. 2004 Nov;170(9):974–80.
142. Dorner BG, Scheffold A, Rolph MS, Huser MB, Kaufmann SHE, Radbruch A, et al. MIP-1alpha, MIP-1beta, RANTES, and ATAC/lymphotactin function together with IFN-gamma as type 1 cytokines. Proc Natl Acad Sci U S A. 2002;99(9):6181–6.

143. Ries C. Cytokine functions of TIMP-1. Cellular and Molecular Life Sciences. 2014;71(4):659–72.
144. Hayakawa T, Yamashita K, Tanzawa K, Uchijima E, Iwata K. Growth-promoting activity of tissue inhibitor of metalloproteinases-1 (TIMP-1) for a wide range of cells. A possible new growth factor in serum. FEBS Lett. 1992;298(1):29–32.
145. Goldklang MP, Marks SM, D'Armiento JM. Second hand smoke and COPD: Lessons from animal studies. Frontiers in Physiology. 2013;4 FEB(February):1–8.
146. Ma B, Kang M-J, Lee CG, Chapoval S, Liu W, Chen Q, et al. Role of CCR5 in IFN-gamma-induced and cigarette smoke-induced emphysema. J Clin Invest. 2005 Dec;115(12):3460–72.
147. Bowler RP, Bahr TM, Hughes G, Lutz S, Kim Y-I, Coldren CD, et al. Integrative omics approach identifies interleukin-16 as a biomarker of emphysema. Omics: A Journal of Integrative Biology. 2013;17(12):619–26.
148. Ridker PM, Hennekens CH, Roitman-Johnson B, Stampfer MJ, Allen J. Plasma concentration of soluble intercellular adhesion molecule 1 and risks of future myocardial infarction in apparently healthy men. Lancet. 1998;351(9096):88–92.
149. Rohde LE, Hennekens CH, Ridker PM. Cross-sectional study of soluble intercellular adhesion molecule-1 and cardiovascular risk factors in apparently healthy men. Arterioscler Thromb Vasc Biol. 1999;19(7):1595–9.
150. Aaron CP, Schwartz JE, Bielinski SJ, Hoffman E a., Austin JHM, Oelsner EC, et al. Intercellular adhesion molecule 1 and progression of percent emphysema: The MESA Lung Study. Respiratory Medicine. 2015;109(2):255–64.
151. Pope CA, Bhatnagar A, McCracken J, Abplanalp WT, Conklin DJ, O'Toole TE. Exposure to Fine Particulate Air Pollution Is Associated with Endothelial Injury and Systemic Inflammation. Circ Res. 2016;
152. Dupont LL, Alpizar YA, Brusselle GG, Bracke KR, K T, Joos GF, et al. Expression of transient receptor potential (TRP) channels in a murine model of cigarette smoke exposure. In: Proceedings of the C34 Insights into COPD Pathogenesis from Pre-Clinical Studies San Diego, CA, USA, 16-21 May. Am J Resp Crit Care Med; 2014. p. Volume 189, A4286.
153. Nie Y, Huang C, Zhong S, Wortley MA, Luo Y, Luo W, et al. Cigarette smoke extract (CSE) induces transient receptor potential ankyrin 1 (TRPA1) expression via activation of HIF1αin A549 cells. Free Radical Biology and Medicine [Internet]. 2016;99:498–507. Available from: http://dx.doi.org/10.1016/j.freeradbiomed.2016.07.028
154. Wang M, Zhang Y, Xu M, Zhang H, Chen Y, Fan K, et al. Free Radical Biology and Medicine Roles of TRPA1 and TRPV1 in cigarette smoke -induced airway epithelial cell injury model. Free Radical Biology and Medicine [Internet]. 2019;134(January):229–38. Available from: https://doi.org/10.1016/j.freeradbiomed.2019.01.004
155. Caceres AI, Brackmann M, Elia MD, Bessac BF, del Camino D, D'Amours M, et al. A sensory neuronal ion channel essential for airway inflammation and hyperreactivity in asthma. PNAS. 2009;106(22):9099–104.
156. Raemdonck K, de Alba J, Birrell MA, Grace M, Maher SA, Irvin CG, et al. A role for sensory nerves in the late asthmatic response. Thorax. 2012;67(19–25):19–25.
157. Geppetti P, Patacchini R, Nassini R, Materazzi S. Cough: The Emerging Role of the TRPA1 Channel. Lung. 2010;188(Suppl1):S63–8.
158. Hajna Z, Csekő K, Kemény Á, Kereskai L, Kiss T, Perkecz A, et al. Complex regulatory role of the trpa1 receptor in acute and chronic airway inflammation mouse models. International Journal of Molecular Sciences. 2020 Jun 1;21(11):1–21.

159. Mazzone SB, Undem BJ. Vagal afferent innervation of the airways in health and disease. Physiological Reviews. 2016;96(3):975–1024.
160. Undem BJ, Kollarik M. The role of vagal afferent nerves in chronic obstructive pulmonary disease. Proc Am Thorac Soc. 2005;2(4):355–60.
161. Canning BJ. Afferent nerves regulating the cough reflex: Mechanisms and Mediators of Cough in Disease. Otolaryngol Clin North Am. 2010;43(1):15–vii.
162. Schmidt MM, Dringen R. Differential effects of iodoacetamide and iodoacetate on glycolysis and glutathione metabolism of cultured astrocytes. Frontiers in Neuroenergetics. 2009;1:1–10.
163. Mitchell DB, Acosta D, Bruckner J v. Role of glutathione depletion in the cytotoxicity of acetaminophen in a primary culture system of rat hepatocytes. Toxicology. 1985;37:127–46.
164. Palmen NGM, Evelo CTA. Glutathione depletion in human erythrocytes and rat liver: A study on the interplay between bioactivation and inactivation functions of liver and blood. Toxicology in Vitro. 1996;10(3):273–81.
165. Elseweidy MM, Younis NN, Amin RS, Abdallah FR, Fathy AM, Yousif ZA. Effect of some natural products either alone or in combination on gastritis induced in experimental rats. Digestive Diseases and Sciences. 2008;53:1774–84.
166. Rahman I, Antonicelli F, MacNee W. Molecular mechanism of the regulation of glutathione synthesis by tumour necrosis factor-a and dexamethasone in human alveolar epithelial cells. The Journal of Biological Chemistry. 1999;274(8):5088–96.
167. Yasin R, Leese CL. The production of chronic gastritis and ulceration in the glandular stomach of rats by iodoacetamide (IAM). European Journal of Cancer. 1970;6(5):425–32.
168. Dial EJ, Hall LR, Romero JJ, Lichtenberger LM. Rats with gastritis have increased sensitivity to the gastrin stimulatory effects of luminal ammonia. Gastroenterology. 1996;110(3):801–8.
169. Barnett K, Bell CJ, McKnight W, Dicay M, Sharkey KA, Wallace JL. Role of cyclooxygenase-2 in modulating gastric acid secretion in the normal and inflamed rat stomach. American Journal of Physiology - Gastrointestinal and Liver Physiology. 2000;279(6 42-6):1292–7.
170. Lalich JJ. Iodoacetamide induced gastric ulcers in rats. Proc Soc Expl Biol Med. 1962;109:905–8.
171. Ozaki N, Bielefeldt K, Sengupta JN, Gebhart GF. Models of gastric hyperalgesia in the rat. American Journal of Physiology - Gastrointestinal and Liver Physiology. 2002;283:666–76.
172. Larauche M, Anton PM, Peiro G, Eutamène H, Buéno L, Fioramonti J. Role of capsaicin-sensitive afferent nerves in different models of gastric inflammation in rats. Autonomic Neuroscience: Basic and Clinical. 2004;110(2):89–97.
173. Macpherson LJ, Dubin AE, Evans MJ, Marr F, Schultz PG, Cravatt BF, et al. Noxious compounds activate TRPA1 ion channels through covalent modification of cysteines. Nature. 2007;445(7127):541–5.
174. Hinman A, Chuang HH, Bautista DM, Julius D. TRP channel activation by reversible covalent modification. PNAS. 2006;103(51):19564–8.
175. Ibarra Y, Blair NT. Benzoquinone reveals a cysteine-dependent desensitization mechanism of TRPA1. Molecular Pharmacology. 2013;83(5):1120–32.
176. Xu Y, Jia J, Xie C, Wu Y, Tu W. Transient Receptor Potential Ankyrin 1 and Substance P Mediate the Development of Gastric Mucosal Lesions in a Water Immersion Restraint Stress Rat Model. Digestion. 2018;97(3):228–39.

177. Dömötör A, Kereskay L, Szekeres G, Hunyady B, Szolcsányi J, Mózsik G. Participation of capsaicin-sensitive afferent nerves in the gastric mucosa of patients with Helicobacter pylori-positive or-negative chronic gastritis. Digestive Diseases and Sciences. 2007;52(2):411–7.
178. Bielefeldt K, Ozaki N, Gebhart GF. Mild Gastritis Alters Voltage-Sensitive Sodium Currents in Gastric Sensory Neurons in Rats. Gastroenterology. 2002;122(3):752–61.
179. Goso C, Evangelista S, Tramontana M, Manzini S, Blumberg PM, Szallasi A. Topical capsaicin administration protects against trinitrobenzene sulfonic acid-induced colitis in the rat. European Journal of Pharmacology. 1993;249:185–90.
180. Kihara N, de la Fuente SG, Fujino K, Takahashi T, Pappas TN, Mantyh CR. Vanilloid receptor-1 containing primary sensory neurones mediate dextran sulphate sodium induced colitis in rats. Gut [Internet]. 2003 Oct 1;52:713–9. Available from: www.gutjnl.com
181. Utsumi D, Matsumoto K, Tsukahara T, Amagase K, Tominaga M, Kato S. Transient receptor potential vanilloid 1 and transient receptor potential ankyrin 1 contribute to the progression of colonic inflammation in dextran sulfate sodium-induced colitis in mice : Links to calcitonin gene-related peptide and substance P. Journal of Pharmacological Sciences. 2018;136:121–32.
182. Lee J, Yamamoto T, Kuramoto H, Kadowaki M. TRPV1 expressing extrinsic primary sensory neurons play a protective role in mouse oxazolone-induced colitis. Autonomic Neuroscience: Basic and Clinical. 2012 Jan 26;166(1–2):72–6.
183. Engel MA, Leffler A, Niedermirtl F, Babes A, Zimmermann K, Filipovic MR, et al. TRPA1 and Substance P Mediate Colitis in Mice. Gastroenterology. 2011;141(4):1346–58.
184. Lapointe TK, Basso L, Iftinca MC, Flynn R, Chapman K, Dietrich G, et al. TRPV1 sensitization mediates postinflammatory visceral pain following acute colitis. Am J Physiol Gastrointest Liver Physiol [Internet]. 2015;309:87–99. Available from: http://www.ajpgi.org
185. Massa F, Sibaev A, Marsicano G, Blaudzun H, Storr M, Lutz B. Vanilloid receptor (TRPV1)-deficient mice show increased susceptibility to dinitrobenzene sulfonic acid induced colitis. Journal of Molecular Medicine. 2006 Feb;84(2):142–6.
186. Martelli L, Ragazzi E, di Mario F, Martelli M, Castagliuolo I, Dal Maschio M, et al. A potential role for the vanilloid receptor TRPV1 in the therapeutic effect of curcumin in dinitrobenzene sulphonic acid-induced colitis in mice. Neurogastroenterology and Motility. 2007 Aug;19(8):668–74.
187. Yang M, Wang J, Yang C, Han H, Rong W, Zhang G. Oral administration of curcumin attenuates visceral hyperalgesia through inhibiting phosphorylation of TRPV1 in rat model of ulcerative colitis. Mol Pain. 2017;13(1744806917726416).
188. Nalli M, Ortar G, Schiano Moriello A, di Marzo V, de Petrocellis L. Effects of curcumin and curcumin analogues on TRP channels. Fitoterapia. 2017 Oct 1;122:126–31.
189. Leamy AW, Shukla P, McAlexander MA, Carr MJ, Ghatta S. Curcumin ((E,E)-1,7-bis(4-hydroxy-3-methoxyphenyl)-1,6-heptadiene-3,5-dione) activates and desensitizes the nociceptor ion channel TRPA1. Neuroscience Letters. 2011 Oct 10;503(3):157–62.
190. Larmonier CB, Midura-Kiela MT, Ramalingam R, Laubitz D, Janikashvili N, Larmonier N, et al. Modulation of neutrophil motility by curcumin: Implications for inflammatory bowel disease. Inflammatory Bowel Diseases. 2011 Feb;17(2):503–15.
191. Zhi L, Dong L, Kong D, Sun B, Sun Q, Grundy D, et al. Curcumin acts via transient receptor potential vanilloid-1 receptors to inhibit gut nociception and reverses visceral hyperalgesia. Neurogastroenterology and Motility. 2013 Jun;25(6):e429–40.

192. Hanai H, Iida T, Takeuchi K, Watanabe F, Maruyama Y, Andoh A, et al. Curcumin Maintenance Therapy for Ulcerative Colitis: Randomized, Multicenter, Double-Blind, Placebo-Controlled Trial. Clinical Gastroenterology and Hepatology. 2006 Dec;4(12):1502–6.
193. Kimball ES, Wallace NH, Schneider CR, D'Andrea MR, Hornby PJ. Vanilloid receptor 1 antagonists attenuate disease severity in dextran sulphate sodium-induced colitis in mice. Neurogastroenterology and Motility. 2004 Dec;16(6):811–8.
194. Fujino K, Takami Y, de La Fuente SG, Ludwig KA, Mantyh CR, Becker J, et al. Inhibition of the Vanilloid Receptor Subtype-1 Attenuates TNBS-Colitis. Journal of Gastrointestinal Surgery. 2004;8(7):842–8.
195. Vermeulen W, de Man J, de Schepper HU, Bult H, Moreels TG, Pelckmans PA, et al. Role of TRPV1 and TRPA1 in visceral hypersensitivity to colorectal distension during experimental colitis in rats. European Journal of Pharmacology [Internet]. 2013;698(1–3):404–12. Available from: http://dx.doi.org/10.1016/j.ejphar.2012.10.014
196. Szitter I, Pozsgai G, Sandor K, Elekes K, Kemeny A, Perkecz A, et al. The role of transient receptor potential vanilloid 1 (Trpv1) receptors in dextran sulfate-induced colitis in mice. Journal of Molecular Neuroscience. 2010 Sep;42(1):80–8.
197. Kun J, Perkecz A, Knie L, Sétáló Jr G, Tornóczki T, Pintér E, et al. TRPA1 receptor is upregulated in human oral lichen planus. Oral Dis. 2017;23(2):189–98.
198. Perše M, Cerar A. Dextran sodium sulphate colitis mouse model: Traps and tricks. Journal of Biomedicine and Biotechnology. 2012;2012:718617.
199. Piqueras L, Corpa JM, Martínez J, Martínez V. Gastric hypersecretion associated to iodoacetamide-induced mild gastritis in mice. Naunyn-Schmiedeberg's Archives of Pharmacology. 2003;367(2):140–50.
200. Holzer P, Wultsch T, Edelsbrunner M, Mitrovic M, Shahbazian A, Painsipp E, et al. Increase in Gastric Acid-Induced Afferent Input to the Brainstem in Mice with Gastritis. Neuroscience. 2007;145(3):1108–19.
201. Wultsch T, Painsipp E, Shahbazian A, Mitrovic M, Edelsbrunner M, Waldmann R, et al. Deletion of the acid-sensing ion channel ASIC3 prevents gastritis-induced acid hyperresponsiveness of the stomach – brainstem axis. Pain. 2008;134(3):245–53.
202. Painsipp E, Wultsch T, Shahbazian A, Edelsbrunner M, Kreissl MC, Schirbel A, et al. Experimental gastritis in mice enhances anxiety in a gender- related manner. Neuroscience. 2007;150(3):522–36.
203. Chen Z, Du S, Kong C, Zhang Z, Mokhtar A. Intrathecal administration of TRPA1 antagonists attenuate cyclophosphamide-induced cystitis in rats with hyper-reflexia micturition. BMC Urology [Internet]. 2016;16(33). Available from: http://dx.doi.org/10.1186/s12894-016-0150-x
204. Price TJ, Louria MD, Candelario-Soto D, Dussor GO, Jeske NA, Patwardhan AM, et al. Treatment of trigeminal ganglion neurons in vitro with NGF, GDNF or BDNF: Effects on neuronal survival, neurochemical properties and TRPV1-mediated neuropeptide secretion. BMC Neuroscience. 2005;6(4):1–15.
205. Kemény Á, Kodji X, Horváth S, Komlódi R, Szőke É, Sándor Z, et al. TRPA1 acts in a protective manner in imiquimod-induced psoriasiform dermatitis in mice. The Journal of Investigative Dermatology [Internet]. 2018;138(8):1774–84. Available from: https://doi.org/10.1016/j.jid.2018.02.040
206. Bohonyi N, Pohóczky K, Szalontai B, Perkecz A, Kovács K, Kajtár B, et al. Local upregulation of transient receptor potential ankyrin I and transient receptor potential

vanilloid I ion channels in rectosigmoid deep infiltrating endometriosis. Molecular Pain. 2017;13:1–13.

8 Acknowledgements

I would like to thank my supervisor, Prof. Dr. Zsuzsanna Helyes for her guidance, perseverance and positive attitude that inspired me throughout my PhD years and the years to follow. I would like to thank Prof. Dr. Erika Pintér, the head of department and leader of the Neuropharmacology doctoral program for giving me the opportunity to work and study in her school as well as providing a supportive and appreciative workplace. I would like to express my gratitude to Prof. Dr. János Szolcsányi, the founder of this research group who set an example for all of us with his professional calling.

I would like to express my special thank to the Gedeon Richter Talentum Foundation for its significant support in conducting my PhD research.

I would like to thank Prof. Dr. Sándor Szabó and Dr. Daniel Keszthelyi for their significant help throughout my PhD research as well as their major support to be able to actively participate in international collaborative work. I would like to thank Dr. Imre Szabó, my former research supervisor his guidance and advices, his role in taking this carrier path was decivise in my life, and for that I will ever be grateful.

I cannot thank enough my most supportive colleagues and friends, Dr. Éva Szőke, Dr. Krisztina Pohóczky, Dr. Maja Payrits, Dr. Tímea Aczél and Noémi Bencze whom I could always rely on on a professional level, as well as having always been there for me.

I am grateful to Dr. Ágnes Kemény, Dr. Zsófia Hajna, Dr. Dániel Pécsi and Dr. Bram Beckers for their significant help in writing the manuscripts.

Many thanks to our collaborators Prof. Dr. Péter Ferdinandy, Dr. Péter Bencsik, Dr. László Kereskai, Dr. Béla Kajtár, Dr. Dimitrios Tsikas, Dr. Alexander Bollenbach, Dr. Ivett Hegedűs for their important contributions and for providing us with valuable critical insights.

I would like to express my gratitude to Dr. Kata Bölcskei, Dr. Gábor Pethő, and Dr. Bálint Szalontai to whom I could always turn to for professional help. I would also like to thank Dóra Ömböli Gyuláné, Tamás Kiss, Anikó Perkecz, Lilla Draskóczi and Zöldhegyi Józsefné for their valuable technical assistance in the experiments.

I wish to thank all members of the institute for their varying but indispensable help.

Finally, I would like to thank my husband and my family for their love, support and patience through all these years.

9 List of publications

9.1 Publications related to the thesis:

Kata Csekő, Dániel Pécsi, Béla Kajtár, Ivett Hegedűs, Alexander Bollenbach, Dimitrios Tsikas, Imre László Szabó, Sándor Szabó, Zsuzsanna Helyes. Upregulation of the TRPA1 Ion Channel in the Gastric Mucosa after Iodoacetamide-Induced Gastritis in Rats: A Potential New Therapeutic Target. *Int J Mol Sci.* 2020; 21(16):5591. doi: 10.3390/ijms21165591.
IF: 5.924

Zsófia Hajna*, **Kata Csekő** *, Ágnes Kemény, László Kereskai, Tamás Kiss, Anikó Perkecz, István Szitter, Béla Kocsis, Erika Pintér, Zsuzsanna Helyes. Complex Regulatory Role of the TRPA1 Receptor in Acute and Chronic Airway Inflammation Mouse Models. *Int J Mol Sci.* 2020. 21(11):4109. doi: 10.3390/ijms21114109.
co-first authors*, **IF: 5.924

Kata Csekő*, Bram Beckers*, Daniel Keszthelyi, Zsuzsanna Helyes. Role of TRPV1 and TRPA1 ion channels in inflammatory bowel diseases: Potential Therapeutic Targets? *Pharmaceuticals (Basel)* 2019. 12(2):48. doi: 10.3390/ph12020048
co-first authors*, **IF: 4.46

Ágnes Kemény*, **Kata Csekő***, István Szitter, Zoltán V Varga, Péter Bencsik, Krisztina Kiss, Róbert Halmosi, László Deres, Krisztián Erős, Anikó Perkecz, László Kereskai, Tamás Kiss, Péter Ferdinandy, Zsuzsanna Helyes. Integrative characterization of chronic cigarette smoke-induced cardiopulmonary comorbidities in a mouse model. *Environ Pollut.* 2017; 229:746-759. doi: 10.1016/j.envpol.2017.04.098.
co-first authors*, **IF: 4.39

9.2 Publications not related to the thesis:

Kata Csekő, Dóra Hargitai, Lilla Draskóczi, Adrienn Kéri, Pongsiri Jaikumpun, Beáta Kerémi, Zsuzsanna Helyes, Ákos Zsembery. Safety of chronic hypertonic bicarbonate inhalation in a cigarette smoke-induced airway irritation guinea pig model. *BMC Pulmonary Medicine* 2022; 22:131 doi: 0.1186/s12890-022-01919-x

IF: 3.154*

A M E Alleleyn, Daniel Keszthelyi, N F Rinsma, **Kata Csekő**, Béla Kajtár, Zsuzsanna Helyes, B Winkens, A A Masclee, José M Conchillo. The potential role for impaired mucosal integrity in the generation of esophageal pain using capsaicin in humans: an explorative study. *Clin Transl Gastroenterol.* 2022; 10.14309/ctg.0000000000000488

IF: 4.488*

Kata Csekő*, Péter Maróti*, Zsuzsanna Helyes, Roland Told, Fanni Riegler, József Szalma, Zsuzsanna Gurdán. The effect of extrinsic factors on the mechanical behaviour and structure of elastic dental ligatures and chains. *Polymers* 2022; 14(11):38 doi: 10.3390/polym14010038

co-first authors,* **IF: 4.493*

Abraham B Beckers, Ellen Wilms, Zlatan Mujagic, Béla Kajtár, **Kata Csekő**, Zsa Zsa R M Weerts, Lisa Vork, Freddy J Troost, Joanna W Kruimel, José M Conchillo, Zsuzsanna Helyes, Ad A M Masclee, Daniel Keszthelyi, Daisy M A E Jonkers. Age-related decrease in abdominal pain and associated structural- and Functional Mechanism: An exploratory study in healthy individuals and irritable bowel syndrome patients. *Front Pharmacol.* 2021; 12:806002. doi: 10.3389/fphar.2021.806002

IF: 5.422*

Eszter Becsekeházi, Marietta Margaréta Korsós, Eleonóra Gál, László Tiszlavicz, Zsófia Hoyk, Mária A Deli, Zoltán Márton Köhler, Anikó Keller-Pintér, Attila Horváth, **Kata Csekő**, Zsuzsanna Helyes, Péter Hegyi, Viktória Venglovecz. Inhibition of NHE-1 increases smoke-induced proliferative activity of Barrett's esophageal cell line. *Int J Mol Sci.* 2021; 22(19):10581. doi: 10.3390/ijms221910581

IF: 6.132*

Valéria Tékus, Ádám István Horváth, **Kata Csekő**, Krisztina Szabadfi, Andrea Kovács-Valasek, Bese Dányádi, László Deres, Róbert Halmosi, Éva Sághy, Zoltán V Varga, Ernest Adeghate, Tamás Kőszegi, Péter Mátyus, Róbert Gábriel, Péter Ferdinandy, Erika Pintér, Zsuzsanna Helyes. Protective effects of the novel amine-oxidase inhibitor multi-target drug SZV 1287 on streptozotocin-induced beta cell damage and diabetic complications in rats. *Biomed Pharmacother.* 2021; 134:111105. doi:10.1016/j.biopha.2020.111105

IF: 5.979*

Eszter Csikós*, **Kata Csekő***, Amir Reza Ashraf, Ágnes Kemény, László Kereskai, Béla Kocsis, Andrea Böszörményi, Zsuzsanna Helyes, Györgyi Horváth. Effects of *Thymus vulgaris L., Cinnamomum verum J,Presl* and *Cymbopogon nardus* (L.) Rendle Essential Oils in the Endotoxin-induced Acute Airway Inflammation Mouse Model. *Molecules* 2020; 25(15):3553. doi: 10.3390/molecules25153553
co-first authors,* **IF: 4.412

Ádám Horváth, Bálint Botz, Tamás Kiss, **Kata Csekő**, Ibolya Kiss, Attila Felinger, Tamara Szabados, Éva Kenyeres, Péter Bencsik, Attila Mócsai, Péter Ferdinandy, Zsuzsanna Helyes. Subantimicrobial Dose Doxycycline Worsens Chronic Arthritis-Induced Bone Microarchitectural Alterations in a Mouse Model: Role of Matrix Metalloproteinases? *Front Pharmacol*. 2019; 10:233 doi: 10.3389/fphar.2019.00233
IF: 4.26

Kitti Rusznák*, **Kata Csekő***, Zsófia Varga, Dávid Csabai, Ágnes Bóna, Mátyás Mayer, Zsolt Kozma, Zsuzsanna Helyes, Boldizsár Czéh. Long-term stress and concomitant marijuana smoke exposure affect physiology, behavior and adult hippocampal neurogenesis *Front Pharmacol.* 2018; 9:786 (doi: 10.3389/fphar.2018.00786)
co-first authors,* **IF: 3.80

Bálint Scheich, **Kata Csekő**, Éva Borbély, István Ábrahám, Valér Csernus, Balázs Gaszner, Zsuzsanna Helyes. Higher susceptibility of male somatostatin 4 receptor gene-deleted mice to chronic stress-induced behavioural and neuroendocrine alterations. *Neuroscience* 2017; 346:320-336. doi: 10.1016/j.neuroscience.2017.01.039.
IF: 3.382

Zsuzsanna Helyes, Ágnes Kemény, **Kata Csekő**, Éva Szőke, Krisztián Elekes, Miklós Mester, Katalin Sándor, Anikó Perkecz, László Kereskai, László Márk, Ágnes Bóna, András Benkő, Erika Pintér, János Szolcsányi, Catherine Ledent, Beáta Sperlágh, F Tamás Molnár. Marijuana smoke induces pulmonary hyperresponsiveness, inflammation and emphysema in a predictive mouse model not via CB1 receptor. *Am J Physiol Lung Cell Mol Physiol.* 2017; 313(2):L267-L277. doi: 10.1152/ajplung.00354.2016
IF: 4.17

Maja Payrits, Éva Sághy, János Szolcsányi, Krisztina Pohóczky, **Kata Csekő**, Kata Bölcskei, Klaudia Barabás, Dávid Ernszt, István Ábrahám, Zsuzsanna Helyes, Éva Szőke. Evidence for the role of estradiol on gating of the Transient Receptor Potential Vanilloid 1 channels. *Endocrinology* 2017; 158(10):3249-3258. doi.org/10.1210/en.2017-00101
IF: 3.961

Imre L Szabó, Róbert Mátics, Péter Hegyi, András Garami, Anita Illés, Patrícia Sarlós, Judit Bajor, Ákos Szűcs, Dóra Mosztbacher, Katalin Márta, Kata Szemes, **Kata Csekő**, Bálint Kővári, Zoltán Rumbus, Áron Vincze. PPIs Prevent Aspirin-Induced Gastrointestinal Bleeding better than H2RAs. A Systemic review and Meta-analysis. J *Gastrointestin Liver Dis.* 2017; 26(4):395-402. doi: 10.15403/jgld.2014.1121.264.hra
IF: 2.033

Dávid Csabai, **Kata Csekő**, Lilla Szaiff, Zsófia Varga, Attila Miseta, Zsuzsanna Helyes, Boldizsár Czéh. Low intensity, long term exposure to tobacco smoke inhibits hippocampal neurogenesis in adult mice. *Behav Brain Res.* 2016; 302: pp. 44-52.
IF:3.002

Erzsébet Laczkó, Pál Riba, Zoltán Giricz, András Váradi, Laura Cornic, Mihály Balogh, Kornél Király, **Kata Csekő**, Shaaban A Mousa, Sándor Hosztafi, Michael Schäfer, Zoltán Zádori, Zsuzsanna Helyes, Péter Ferdinandy, Zsuzsanna Fürst, Mahmoud Al-Khrasani. New morphine analogues produce peripheral antinociception after systemic administration. *J Pharmacol Exp Ther*. 2016; 359(1):171-81. doi: 10.1124/jpet.116.233551
IF: 3.867

Imre L Szabó, **Kata Csekő**, József Czimmer, Gyula Mózsik. Diagnosis of gastritis: review from early pathological evaluation to present day management. In: Mózsik Gyula (editor) Current Topics in Gastritis - 2012. Rijeka: *InTech Open Access Publisher,* 2013. pp. 3-18. ISBN: 978-953-51-0907-5

(*5-year impact factor)

Cumulative impact factor (without citable abstracts): 83.253

Citations (MTMT): 188

Independent citations (MTMT): 161

Citations (Google Scholar): 263

H-index: 9

10 List of conference presentations

10.1 Oral presentations

Csekő, K.; Kormos, V.; Zelena, D.; Horváth, Á.; Kecskés, A.; Gaszner, B.; Sudalina, M.; Yarushkina, N.; Filaretova, L.; Helyes, Z. Somatostatin receptor subtype 4 alleviates indomethacin-induced gastrointestinal mucosal injury in mice. (*11th International Symposium on Cell/Tissue Injury and Cytoprotection/Organoprotection (ISCTICO) joint meeting of the Hungarian Society for Experimental and Clinical Pharmacology (HUPHAR) and the International Union of Basic and Clinical Pharmacology (IUPHAR) – October 27-30, 2021, Pécs* – **Best Young Researcher Award**)

Csekő, K.; Kormos, V.; Horváth, Á.; Sudalina, M.; Yarushkina, N.; Zelena, D.; Filaretova, L.; Helyes, Z. Protective role of the somatostatin receptor subtype 4 in the indomethacin-induced gastrointestinal mucosal injury model. (*Summer School on Stress – June 25-28, 2019, St. Petersburg, Russia*)

Csekő, K.; Szitter, I.; Hajna, Z.; Elekes, K.; Kemény, Á.; Kereskai, L.; Quinn, J. P.; Sándor, K.; Pintér, E.; Szolcsányi, J.; Helyes, Z. Role of neuro-immune interactions in a cigarette smoke-induced chronic airway inflammation mouse model. (*4th Conference of Association of Hungarian-American Academicians (AHAA/AMAT) Scientific and Business Meeting - April 4-6, 2019, Memphis, Tennessee, USA*)

Csekő, K.; Hargitai, D.; Kéri, A.; Pongsiri, J.; Kerémi, B.; Helyes, Z., Zsemebry, Á. A hipertóniás nátrium-bikarbonát inhaláció biztonságos krónikus dohányfüst-expozíciónak kitett tengerimalacoknak. (*FAMÉ 2019 – Magyar Kísérletes és Klinikai Farmakológiai Társaság, Magyar Anatómus Társaság, Magyar Mikrocirkulációs és Vaszkuláris Biológiai Társaság, Magyar Élettani Társaság Közös Vándorgyűlése - June 5-8, 2019, Budapest*)

Csekő, K.; Helyes, Z.; Zsembery, Á. Inhalation of sodium-bicarbonate – an animal study. (*EFOP-3.6.2-16-2017-00006 Translational interactive hands-on training and conference on epithelial ion transport - November 22-23, 2018, Budapest*)

Csekő, K.; Pécsi, D.; Hegedűs, I.; Perkecz, A.; Szabó, I.L.; Szabó, S.; Helyes, Z. Expressions and inflammation-induced alterations of Transient Receptor Potential Vanilloid 1 and Ankyrin 1 ion channels in the human and rat gastric mucosa. (*MGT58 - Magyar Gasztroenterológiai Társaság 58. Nagygyűlés – June 4-7, 2016, Siófok*)

Csekő, K.; Pécsi, D.; Hegedűs, I.; Perkecz, A.; Szabó, S.; Szabó, I.; Helyes, Z. A Tranziens Receptor Potenciál Vanilloid 1 és Ankyrin 1 ioncsatornák expressziója humán és patkány gyomornyálkahártyában, valamint változásainak vizsgálata jódacetamiddal kiváltott krónikus

gasztritisz patkány modellben. (*Magyar Farmakológiai, Anatómus, Mikrocirkulációs és Élettani Társaságos Közös Tudományos konferenciája, Ifjúsági Szekció – June 1-4, 2016, Pécs* – **Special award**)

10.2 Poster presentations

Csekő, K.; Szitter, I.; Hajna, Z.; Elekes, K.; Kemény, Á.; Kereskai, L.; Quinn, J. P.; Sándor, K.; Pintér, E.; Szolcsányi, J.; Helyes, Z. Role of neuro-immune interactions in a cigarette smoke-induced chronic airway inflammation mouse model. (*EB 2019 – Experimental Biology 2019 – April 6-9, 2019, Orlando, Florida, USA*)

Csekő, K., Kormos, V.; Horváth, Á.; Sudalina, M.; Iarushkina, N.; Zelena, D.; Filaretova, L.; Helyes, Z. Protective role of the somatostatin receptor subtype 4 in the indomethacin-induced gastrointestinal mucosal injury. (*EB 2019 – Experimental Biology 2019 – April 6-9, 2019, Orlando, Florida, USA*)

Csekő, K.; Csikós, E.; Ashraf, A. R.; Fard, S.; Draskóczi, L.; Kemény, Á.; Kereskai, L.; Böszörményi, A.; Horváth, G.; Helyes, Z. Thyme essential oil inhalation decreases endotoxin-induced acute airway inflammation in a mouse model via TRPA1/V1 ion channels. (*RegPep2018 - 22nd International Symposium on Regulatory Peptides – September 22-25, 2018, Acapulco, Mexico*)

Csekő, K.; Kemény, Á.; Szitter, I.; Varga, V. Z.; Bencsik, P.; Kiss, K.; Halmosi, R.; Deres, L.; Erős, K.; Perkecz, A.; Kereskai, L.; László, T.; Kiss, T.; Ferdinandy, P.; Helyes, Z. Integrative characterization of chronic cigarette smoke-induced cardiopulmonary comorbidities in a mouse model. (*Cardiovascular Research Days – March 1-3, 2018, Debrecen*)

Csekő, K.; Kemény, Á.; Horváth, Á.; Szőke, É.; Halmosi, R.; Deres, L.; Erős, K.; Nagy, Cs. T.; Bencsik, P.; Kiss, K.; Kiss, I.; Ferdinandy, P.; Helyes, Z. Doxycyclin kezelés hatása és a mátrix metalloproteinázok szerepe krónikus obstruktív tüdőbetegség dohányfüsttel kiváltott komorbiditás egérmodelljében. (*GYIK 2018 - Gyógyszer Innováció 2018 Konferenciája – April 9-11, 2018, Velence*)

Csekő, K.; Kemény, Á.; Kiss, T.; Hajna, Zs.; Deres, L.; Halmosi, R.; Kereskai, L.; Mayer, M.; Bóna, Á.; Márk, L.; Molnár, F. T.; Helyes, Z. A TRPA1 receptor szerepe krónikus légúti gyulladás egérmodelljeiben. (*MFT 2017 - A Magyar Kísérletes és Klinikai Farmakológiai Társaság Gyógyszerinnovációs Kongresszusa – May 7-9, 2017, Velence*)

Csekő, K.; Kemény, Á.; Szőke, É.; Nagy, Cs. T.; Bencsik, P.; Kiss, K.; Halmosi, R.; Deres, L.; Erős, K.; Perkecz, A.; Kereskai, L.; Kiss, T.; Ferdinandy, P.; Helyes, Z. Doxycyclin kezelés hatása és a mátrix metalloproteinázok szerepe krónikus obstruktív tüdőbetegség dohányfüsttel kiváltott komorbiditás egérmodelljében. (*ÉFM 2017 - A Magyar Élettani Társaság, A Magyar Kísérletes és Klinikai Farmakológiai Társaság és a Magyar Mikrocirkulációs és Vaszkuláris Biológiai Társaság közös Vándorgyűlése – June 13-16, 2017, Debrecen*)

Scheich, B.; **Csekő, K.**; Borbély, É.; Ábrahám, I.; Csernus, V.; Gaszner, B.; Helyes, Z. Higher susceptibility of somatostatin 4 receptor gene-deleted mice to chronic stress-induced behavioral and neuroendocrine alterations. (*FENS Regional Meeting – September 20-23, 2017, Pécs*)

Csekő, K.; Kemény, Á.; Kiss, T.; Deres, L.; Halmosi, R.; Kereskai, L.; Mayer, M.; Bóna, Á.; Márk, L.; Molnár, F. T.; Helyes, Z. The role of TRPA1 ion channels in a chronic pulmonary inflammation mouse model. (*13th International Symposium on VIP, PACAP and Related Peptides – December 3-7, 2017, HongKong*)

Csekő, K.; Pécsi, D.; Hegedűs, I.; Perkecz, A.; Szabó, I.; Helyes, Z.; Szabó, S. First animal model of diffuse mucosal injury. (*9th International Symposium on Cell/Tissue Injury and Cytoprotection / Organoprotection (ISCTICO) – September 15-17, 2016, Cracow, Poland*)

Csekő, K.; Pécsi, D.; Hegedűs, I.; Perkecz, A.; Szabó, S.; Szabó, I. L.; Helyes, Z. Transient Receptor Potential Vanilloid 1 and Ankyrin 1 ion channel expressions in human and rat intact and inflamed gastric mucosa. (*RegPep 2016 – July 12-14, 2016, Rouen, France, 2016*)

Csekő, K.; Szalontai, B.; Pohóczky, K.; Hegedűs, I.; Perkecz, A.; Illés, A.; Vincze, Á.; Czimmer, J.; Szabó, I. L.; Helyes, Z. Expression and inflammation-induced alterations of Transient Receptor Potential Vanilloid 1 (TRPV1) and Ankyrin 1 (TRPA1) ion channels in the human gastric mucosa. (*Neuropeptides 2015, - September 28 – October 1, 2015, Aberdeen, United Kingdom*)

Csekő, K.; Szalontai, B.; Pohóczky, K.; Hegedűs, I.; Perkecz, A.; Illés, A.; Vincze, Á.; Czimmer, J.; Helyes, Z.; Szabó, I. L. Non-neuronal expression of Transient Receptor Potential Vanilloid 1 (TRPV1) and Ankyrin 1 (TRPA1) receptors in the human gastric mucosa. (*MGT57 - Magyar Gasztroenterológus Társaság Éves Nagygyűlése – May 30 – June 2, 2015, Siófok*)

Csekő, K.; Kemény, Á.; Szitter, I.; Varga, Z.; Bencsik, P.; Kiss, K.; Halmosi, R.; Deres, L.; Erős, K.; Perkecz, A.; Kereskai, L.; Kiss, T.; Ferdinandy, P.; Helyes, Z. Patofiziológiai folyamatok és mechanizmusok komplex vizsgálata krónikus obstruktív tüdőbetegség dohányfüsttel kiváltott egérmodelljében. (*Transzlációs kutatások a neuro- és kardiovaszkuláris farmakológiában – March 26-28, 2015, Velence*)

Csekő, K.; Szalontai, B.; Pohóczky, K.; Hegedűs, I.; Perkecz, A.; Illés, A.; Vincze, Á.; Czimmer, J.; Szabó, I.L.; Helyes, Z. Expression of Transient Receptor Potential Vanilloid 1, 4 (TRPV1, TRPV4) and Ankyrin 1 (TRPA1) Ion Channels in the Human Gastric Mucosa. (*8th International Symposium on Cell/Tissue Injury and Cytoprotection / Organoprotection (ISCTICO) – September 24-26, 2014, Budapest*)

Csekő, K.; Szalontai, B.; Pohóczky, K.; Hegedűs, I.; Perkecz, A.; Illés, A.; Vincze, Á.; Czimmer, J.; Szabó, I. L.; Helyes, Z. The Transient Receptor Potential Vanilloid 1, 4 (TRPV1, TRPV4) and Ankyrin 1 (TRPA1) receptor mRNAs are expressed in the human gastric mucosa. (*Joint meeting of the Federation of European Physiological Societies (FEPS) and the Hungarian Physiological Society – August 27-30, 2014, Budapest*)

Environmental Pollution xxx (2017) 1–14

Contents lists available at ScienceDirect

Environmental Pollution

journal homepage: www.elsevier.com/locate/envpol

Integrative characterization of chronic cigarette smoke-induced cardiopulmonary comorbidities in a mouse model☆

Ágnes Kemény [a, b, c, 1], Kata Csekő [a, c, 1], István Szitter [a, c], Zoltán V. Varga [d], Péter Bencsik [e, f], Krisztina Kiss [e], Róbert Halmosi [c, g], László Deres [c, g], Krisztián Erős [c, g, k], Anikó Perkecz [a], László Kereskai [h], Terézia László [h], Tamás Kiss [c], Péter Ferdinandy [d, e, f], Zsuzsanna Helyes [a, c, i, j, *]

[a] Department of Pharmacology and Pharmacotherapy, University of Pécs, Faculty of Medicine, H-7624 Pécs, Szigeti út 12., Hungary
[b] Department of Medical Biology, University of Pécs, Faculty of Medicine, H-7624 Pécs, Szigeti út 12., Hungary
[c] Szentágothai Research Centre, University of Pécs, H-7624 Pécs, Ifjúság útja 20., Hungary
[d] Cardiometabolic Research Group, Department of Pharmacology and Pharmacotherapy, Semmelweis University, Faculty of Medicine, H-1089 Budapest, Nagyvárad tér 4., Hungary
[e] Cardiovascular Research Group, Department of Biochemistry, University of Szeged, Faculty of Medicine, H-6720 Szeged, Dóm tér 9., Hungary
[f] Pharmahungary Group, H-6722 Szeged, Hajnóczy u. 6., Hungary
[g] I[st] Department of Internal Medicine, University of Pécs, Faculty of Medicine, H-7624 Pécs, Ifjúság útja 13., Hungary
[h] Department of Pathology, University of Pécs, Faculty of Medicine, H-7624 Pécs, Szigeti út 12., Hungary
[i] MTA-PTE NAP B Chronic Pain Research Group, University of Pécs, Faculty of Medicine, H-7624 Pécs, Szigeti út 12., Hungary
[j] PharmInVivo Ltd, H-7629 Pécs, Szondi György út 10., Hungary
[k] Department of Biochemistry and Medical Chemistry, University of Pécs, Faculty of Medicine, H-7624 Pécs, Szigeti út 12., Hungary

ARTICLE INFO

Article history:
Received 28 September 2016
Received in revised form
24 February 2017
Accepted 6 April 2017
Available online xxx

Keywords:
Pneumonitis
Emphysema
Whole-body plethysmography
Echocardiography
Inflammatory cytokines

ABSTRACT

Cigarette smoke-triggered inflammatory cascades and consequent tissue damage are the main causes of chronic obstructive pulmonary disease (COPD). There is no effective therapy and the key mediators of COPD are not identified due to the lack of translational animal models with complex characterization. This integrative chronic study investigated cardiopulmonary pathophysiological alterations and mechanisms with functional, morphological and biochemical techniques in a 6-month-long cigarette smoke exposure mouse model. Some respiratory alterations characteristic of emphysema (decreased airway resistance: Rl; end-expiratory work and pause: EEW, EEP; expiration time: Te; increased tidal mid-expiratory flow: EF50) were detected in anaesthetized C57BL/6 mice, unrestrained plethysmography did not show changes. Typical histopathological signs were peribronchial/perivascular (PB/PV) edema at month 1, neutrophil/macrophage infiltration at month 2, interstitial leukocyte accumulation at months 3–4, and emphysema/atelectasis at months 5–6 quantified by mean linear intercept measurement. Emphysema was proven by micro-CT quantification. Leukocyte number in the bronchoalveolar lavage at month 2 and lung matrix metalloproteinases-2 and 9 (MMP-2/MMP-9) activities in months 5–6 significantly increased. Smoking triggered complex cytokine profile change in the lung with one characteristic inflammatory peak of C5a, interleukin-1α and its receptor antagonist (IL-1α, IL-1ra), monokine induced by gamma interferon (MIG), macrophage colony-stimulating factor (M-CSF), tissue inhibitor of matrix metalloproteinase-1 (TIMP-1) at months 2–3, and another peak of interferon-γ (IFN-γ), IL-4, 7, 13, 17, 27 related to tissue destruction. Transient systolic and diastolic ventricular dysfunction developed after 1–2 months shown by significantly decreased ejection fraction (EF%) and deceleration time, respectively. These parameters together with the tricuspid annular plane systolic excursion (TAPSE) decreased again after 5–6 months. Soluble intercellular adhesion molecule-1 (sICAM-1) significantly increased in the heart homogenates at month 6, while other inflammatory cytokines were undetectable.

☆ This paper has been recommended for acceptance by David Carpenter.

* Corresponding author. Department of Pharmacology and Pharmacotherapy, University of Pécs, H-7624 Pécs, Szigeti út 12., Hungary.
E-mail addresses: agnes.kemeny@aok.pte.hu (Á. Kemény), cseko.kata@pte.hu (K. Csekő), szitteristvan@gmail.com (I. Szitter), varga.zoltan@med.semmelweis-univ.hu (Z.V. Varga), peter.bencsik@pharmahungary.com (P. Bencsik), kiss.krisztina.1@med.u-szeged.hu (K. Kiss), halmosi.robert@pte.hu (R. Halmosi), laszlo.deres@aok.pte.hu (L. Deres), krisztian.eros@aok.pte.hu (K. Erős), aniko.perkecz@aok.pte.hu (A. Perkecz), kereskai.laszlo@pte.hu (L. Kereskai), laszlo.terezia@pte.hu (T. László), tamas.kiss2@aok.pte.hu (T. Kiss), peter.ferdinandy@pharmahungary.com (P. Ferdinandy), zsuzsanna.helyes@aok.pte.hu (Z. Helyes).

[1] Á. Kemény and K. Csekő equally contributed to the present work.

http://dx.doi.org/10.1016/j.envpol.2017.04.098

This is the first study demonstrating smoking duration-dependent, complex cardiopulmonary alterations characteristic to COPD, in which inflammatory cytokine cascades and MMP-2/9 might be responsible for pulmonary destruction and sICAM-1 for heart dysfunction.

List of abbreviations

BALF	bronchoalveolar lavage fluid
BLC	B-lymphocyte chemoattractant
COPD	chronic obstructive pulmonary disease
EEP	end-expiratory pause
EEW	end-expiratory work
EF%	ejection fraction
EF50	tidal mid-expiratory flow
f	frequency
IL-1α	interleukin-1 alpha
IL-1ra	interleukin-1 receptor antagonist
IL-16	interleukin-16
I-TAC	interferon-inducible T-cell chemoattractant
KC	keratinocyte chemoattractant
LAA/TLV	low attenuation area/total lung volume ratio
L_m	mean linear intercept (chord) length
LV	left ventricular
MCP-1	monocyte chemoattractant protein-1 (JE)
M-CSF	macrophage colony-stimulating factor
MIG	monokine induced by gamma interferon
MMP	matrix metalloproteinase
MV	minute ventilation
PB/PV	peribronchial/perivascular
PEF	peak expiratory flow
PIF	peak inspiratory flow
RANTES	regulated on activation normal T cell expressed and secreted
Rl	airway resistance
RT	relaxation time
SDF-1	stromal cell-derived factor 1
sICAM-1	soluble intercellular adhesion molecule-1
TAPSE	tricuspid annular plane systolic excursion
Te	expiratory time
Ti	inspiratory time
TIMP-1	tissue inhibitor of metalloproteinase-1
TNF-α	tumor necrosis factor-alpha
TREM-1	triggering receptor expressed on myeloid cells-1
TV	tidal volume
WBP	whole-body plethysmography

1. Introduction

Chronic obstructive pulmonary disease (COPD) is a major global health problem that in 2020 is projected to rank fifth worldwide in terms of economic and social burden of disease and third in terms of mortality. According to the most recent definition and description of the Global Initiative for Chronic Obstructive Lung Disease (GOLD 2017) from the Global Strategy for the Diagnosis, Management and Prevention of COPD, it is characterized by persistent respiratory functions and airflow limitation. It is usually progressive and associated with an enhanced chronic inflammatory response in the airways and the lung due to airway and/or alveolar abnormalities usually caused by noxious particles or gases. Exacerbations and comorbidities contribute to the overall severity (Vestbo et al., 2013). Functional respiratory disorders result from chronic obstructive bronchiolitis narrowing the small airways and emphysema due to lung parenchymal destruction. COPD adversely affects both the structure and function of the right ventricle due to pulmonary arterial hypertension, the phenomena known as *cor pulmonale*. It is known that chronic hypoxia leads to pulmonary arteriolar constriction that represents an increased afterload for the right ventricle. In addition chronic hypoxia may induce functional contractile impairment of the left ventricle as well. Therefore, the potential effect of carbon-monoxide, an important toxic compound of cigarette smoke should also be emphasized, which may greatly contribute to the development of hypoxic conditions and related diseases. Cigarette smoking is the most common cause of COPD accounting for approximately 95% of cases in developed countries besides other predisposing factors, such as air pollutants and occupational exposure (Salvi and Barnes, 2009).

There is no curative treatment, the available therapy is restricted to corticosteroids, adrenergic β_2 receptor agonists and acetylcholine muscarinic receptor antagonists that can only slow down the progression and alleviate the symptoms (Vestbo et al., 2013). However, these have limited effect in a relatively small patient population (Restrepo, 2015). Therefore, there is an urgent need to find novel therapeutic targets in COPD. Due to the extensive interest in this area of research, our knowledge of the underlying mechanisms has remarkably expanded. Cigarette smoke and other airway irritants induce an abnormal inflammatory response involving $CD8^+$ lymphocytes, neutrophils and macrophages. These immune cells release chemotactic factors, colony stimulating factors and proinflammatory cytokines, thus sustain and enhance inflammation and immune cell recruitment. Furthermore, proteases like neutrophil elastase, cathepsins and matrix metalloproteinases (MMPs) are responsible for elastin destruction resulting in emphysema formation (Barnes et al., 2003; Yao et al., 2013). However, the complex pathophysiological mechanism, the inflammatory cascades and the role of the immune cells, sensory nerves and neuro-immune interactions, as well as the key mediators need to be determined to identify potential novel therapeutic targets (Canning and Spina, 2009).

Besides human studies to analyse tissue samples, translational animal models are particularly important to define the pathophysiological processes underlying the molecular pathways. Many species like rodents, sheep, dogs, guinea pigs, and monkeys have been investigated for modeling COPD (Helyes and Hajna, 2012; Leberl et al., 2013; Wright and Churg, 2008), but considering the possibilities of genetic engineering, easier handling and less compound requirement, mouse models seem to be most suitable and promising to elucidate the pathophysiological pathways and the complexity of the mechanisms (Martorana et al., 2006; Mercer

Please cite this article in press as: Kemény, Á., et al., Integrative characterization of chronic cigarette smoke-induced cardiopulmonary comorbidities in a mouse model, Environmental Pollution (2017), http://dx.doi.org/10.1016/j.envpol.2017.04.098

et al., 2015; Vlahos et al., 2006).

Several studies focus on the protease-antiprotease imbalance and use only short-lasting models of various types of elastases, such as pancreatic elastase, neutrophil elastase, proteinase-3 (Beeh et al., 2003; Shapiro et al., 2003; Sinden et al., 2015; Yao et al., 2013), or lipopolysaccharides and inorganic dusts to investigate their role in the development of emphysema. These models have been proved to be useful, however, they focus only on one factor that is an intermediate player of the pathophysiological cascade. Meanwhile, cigarette smoke, which is the most common initial triggering stimulus in the human disease, switches on a variety of other pathways and mechanisms that are upstream mediators (Shapiro et al., 2003). In order to investigate the whole complexity of the chronic persistent inflammatory process, the only authentic translational model for COPD is the chronic cigarette smoke exposure (Fricker et al., 2014; Luo et al., 2017). This model has been used by several groups so far, but their broad conclusive potential is limited by the facts that they 1) applied different protocols, experimental paradigms, exposure durations and intensities, 2) did not have a longitudinal self-control follow-up design, 3) did not aim to use an integrative methodological approach to investigate the complexity of the disease, only focused on certain specific parameters, 4) used different strains, and 5) did not take the common cardiovascular comorbidities into consideration. It is important to note that genetic variance, sex and different cigarette types have a great influence on the outcome of chronic cigarette smoke exposure (Bartalesi et al., 2005; Phillips et al., 2016, 2015; Tam et al., 2015). Since C57Bl/6 mice are the most widely used one for genetic manipulations, and it is very sensitive to cigarette smoke (Martorana et al., 2006) it would be the most important to set up, characterize and optimize a model in this strain. Therefore, we aimed to establish a translational mouse model for complex functional, morphological, immunological and biochemical investigation of chronic cardiopulmonary pathophysiological changes characteristic to COPD. This helps to analyse the mechanisms in different stages of the disease, and identify key targets for pharmacological research.

2. Materials and methods

For detailed description of materials, methods and statistics please see the online supplementary material.

2.1. Animals

Experiments were performed on 8-week-old male C57BL/6 mice to avoid potential variations related to the estrus cycle-induced hormonal changes (Yoshizaki et al., 2017) weighing 20–25 g at the beginning of the study; each group consisted of 6 mice. Animals were bred and kept in the Laboratory Animal House of the Department of Pharmacology and Pharmacotherapy, University of Pécs, at 24–25 °C, provided with standard chow and water ad libitum, maintained under 12 h light-dark cycle. All procedures were carried out according to the 40/2013 (II.14.) Government Regulation on Animal Protection and Consideration Decree of Scientific Procedures of Animal Experiments and Directive 2010/63/EU of the European Parliament. They were approved by the Ethics Committee on Animal Research of University of Pécs according to the Ethical Codex of Animal Experiments (licence No.: BA02/2000-5/2011).

2.2. Experimental protocol and investigational techniques

Animals were exposed to cigarette smoke (3R4F Kentucky Research Cigarette; University of Kentucky, USA) in a two-port TE-2 whole-body smoke exposure chamber (Teague Enterprise, USA) twice daily, 10 times/week for 6 months. Two cigarettes were smoked at a time for 10 min with a puff duration of 2 s and a puff frequency of 1/min/cigarette, mice were exposed to smoke for 30 min followed by a ventilation period of 30 min during which smoke was driven from the chamber. The total particulate matter (TPM 154.97 ± 5.18 mg/m^3), nicotine (9.86 ± 0.33 mg/m^3) and carbon-monoxide (147.57 ± 4.93 ppm) concentrations were determined every week. Age-matched non-smoking mice kept under the same circumstances served as controls. The precise composition of the mainstream smoke is well established and described in detail (Roemer et al., 2012).

Before the treatment period and at the end of each month, body weight was measured (see Suppl. Fig. E2) and 6 smoking and 6 intact animals were sacrificed after ketamine and xylazine anesthesia. Lungs and hearts were excised and rinsed with cold phosphate-buffered saline. Lungs were dissected into 3 pieces: 2 pieces were snap frozen and one part was placed in 6% formaldehyde solution.

At the end of the 6th month blood samples were collected and restrained whole body plethysmography was performed by invasive methodology. Some functional parameters (airway resistance (Rl), end-expiratory work (EEW), tidal mid-expiratory flow (EF50), end-expiratory pause (EEP), expiratory time (Te) and inspiratory time (Ti)) were measured by restrained whole-body plethysmography (PLY4111, Buxco Europe Ltd., Winchester, UK) in anaesthetized, tracheotomized and ventilated mice.

Airway responsiveness was determined at the end of each month by unrestrained whole-body plethysmography (WBP) with Buxco instrument (PLY3211, Buxco Europe Ltd., Winchester, UK) in conscious, spontaneously breathing animals. Breathing function parameters (relaxation time: RT, frequency: f, tidal volume: TV, minute ventilation: MV, inspiratory time: Ti, expiratory time: Te, peak inspiratory and expiratory flows: PIF, PEF) were calculated by the Buxco software (Elekes et al., 2008).

Pulmonary structural changes were imaged by a Skyscan 1176 high resolution microtomograph (Skyscan, Kontich, Belgium) at the end of each month. Emphysema was calculated by the ratio of LAA (low-attenuation area) and total lung volume (TLV) (Kobayashi et al., 2013).

Excised lung tissue samples were formalin-fixed (6%) and embedded in paraffin, 5 μm sections were cut and stained with haematoxylin-eosin for further histological analysis. Emphysema was quantified by measuring the mean linear intercept (chord; L_m) length (Knudsen et al., 2010) using CaseViewer software (3DHISTECH Ltd., Hungary) (n = 80–100 chords in 400.000 μm^2 area per animal). Histopathological analysis was performed by a pathologist in a blind manner in order to evaluate perivascular/peribronchial edema, acute and chronic inflammation, interstitial acute and chronic inflammation, epithelial damage and goblet cells on a semiquantitative scale ranging from 0 to 3.

Total cell count and the ratio of lymphocytes, monocytes and granulocytes of the bronchoalveolar lavage fluids were analysed with CyFlow Space flow cytometer (Partec, Germany) at the end of each month (Ma et al., 2001).

Pulmonary MMP-2 and MMP-9 activities from lung samples were measured by gelatin zymography. Gelatinolytic activities of MMPs were examined as previously described (Kupai et al., 2010). Band intensities were quantified and expressed as the ratio to the internal standard.

Forty inflammatory cytokines from lung and heart homogenates as well as serum samples were determined simultaneously with Mouse Cytokine Array Panel A (R&D Systems). To eliminate the interassay variability all data were re-calculated with the same control-spot densities (Szitter et al., 2014). Cytokine heat map was generated by Matrix2png 1.2.1 online freeware (Pavlidis and Noble,

Please cite this article in press as: Kemény, Á., et al., Integrative characterization of chronic cigarette smoke-induced cardiopulmonary comorbidities in a mouse model, Environmental Pollution (2017), http://dx.doi.org/10.1016/j.envpol.2017.04.098

2003).

Transthoracic echocardiography was performed by a VEVO 770 high-resolution ultrasound imaging system (VisualSonics Vevo 770® High-Resolution Imaging System, Toronto, Canada) equipped with a mouse cardiac transducer (30 MHz), and ejection fraction (EF%), tricuspid annular plane systolic excursion (TAPSE) and deceleration time were determined at the end of each month (Respress and Wehrens, 2010).

3. Results

3.1. Chronic cigarette smoke exposure impairs respiratory functions

Pulmonary functions were determined at the end of each month in conscious mice by unrestrained whole-body plethysmography in a self-controlled manner. None of the parameters determined by this technique (RT, f, TV, MV, Ti, Te, PIF, PEF) were different between the smoking and non-smoking groups at any time-points during the 6-month-period (see Suppl. Fig. E1). This is in complete agreement with the findings of Vanoirbeek and colleagues, who demonstrated that the non-invasive method is irrelevant and not appropriate to determine functional alterations in mouse disease models, especially in emphysema (Vanoirbeek et al., 2010). At the end of the sixth month, restrained whole-body plethysmography was performed in tracheotomized, anaesthetized and mechanically ventilated mice. Significant decrease of Rl, EEW, EEP, Te, as well as increase of EF50 and Ti/(Ti + Te) ratio were observed, whereas dynamic compliance did not change in response to chronic smoke exposure as compared to the non-smoking group (Fig. 1).

3.2. Cigarette smoke induces emphysema formation shown by in vivo micro-CT

Dynamic structural changes of the lung were investigated by *in vivo* micro-CT during the 6-months smoking period. Emphysema formation, as the most important sign of tissue destruction, was clearly observed on the reconstructed 3D images (Fig. 2A). According to our morphometric analysis the low attenuation area/total lung volume ratio (LAA/TLV%), a quantitative indicator showed significant increase by the end of the 5th month that was further increased by the end of the 6th month (Fig. 2B).

3.3. Smoke exposure induces characteristic histopathological alterations in the lung

As compared to the intact, normal lung structure of a 3-month-old mouse (Fig. 3A), one month of cigarette smoke exposure induced a minimal peribronchial and moderate perivascular edema formation, and slightly increased numbers of granulocytes and macrophages in the lung parenchyma (Fig. 3B). After 2 months of smoking, there was an extensive perivascular and peribronchial edema with a large number of granulocytes, macrophages and lymphocytes infiltrating these regions. Inflammation was characteristic both in the interstitial and peribronchial areas, in addition the bronchiolar epithelial cell layer became irregular, the bronchiolar and alveolar epithelium showed signs of damage, and the number of interepithelial mucus-producing cells was increased (Fig. 3C and D). Interestingly, this massive inflammatory reaction showed a decreasing tendency from the 3-month-timepoint, the peribronchial edema was still present, but less extensive, the number of immune cells was reduced and were mostly lymphocytes, which moved from the peribronchial spaces to the interstitial regions. Meanwhile, the bronchiolar epithelium destruction was remarkably greater (Fig. 3E). At the 4-month-smoke exposure, the irregularity and damage of the bronchial epithelium was further aggravated. Tissue destruction became more severe, mild emphysema (enlargement of airspaces throughout the parenchyma) and atelectasis developed particularly on the peripheral regions. However, mild edema was limited to the perivascular spaces and the number of inflammatory cells remarkably decreased (Fig. 3F). After 5–6 months of smoking emphysema dominated the histological picture, first mainly in the peripheral areas, then also in the central parts of the lung. Inflammatory reaction at this stage was minimal, only few macrophages and lymphocytes could be noticed in the remaining parenchyma, while irregularity of the bronchial epithelium and hyperplasia of the mucus producing cells could be observed (Fig. 3G and H). The semiquantitative histopathological scoring results throughout the 6-month study are shown in Fig. 4. Remarkable alveolar space enlargement (L_m) was observed already after 1 month of smoke exposure in comparison with the non-smoking group (Fig. 2C). This parameter mainly characteristic to emphysema progressively increased, by the end of the 5th month the distal air space was significantly expanded in smoking mice as compared to the L_m after the 1st month parallelly to our micro-CT findings.

3.4. Inflammatory cell profile analysis of the bronchoalveolar lavage fluid (BALF)

Flow cytometric analysis revealed no difference between the granulocyte, macrophage and lymphocyte numbers of the BALF samples obtained from smoke-exposed and intact mice at the end of the first month. In contrast, 2 months of smoke exposure induced an enormous increase in the number of all these cells in the BALF, which gradually decreased afterwards. The total number and the composition of BALF cells did not differ from the values of the non-smoker mice from the 3rd month. A tendency of increase in granulo- and lymphocyte numbers was observed in the smoking group at the end of the 3rd month, but it did not reach statistical significance (Fig. 5).

3.5. Chronic tobacco smoke increases MMP-2 and MMP-9 activities in the lung

Gelatin zymography showed a significant increase in pulmonary activity for MMP-2 as well as for MMP-9 in the lung samples of mice subjected to 6-month cigarette smoke exposure as compared either to 1-month smokers or to non-smoker age-matched control mice (Fig. 6).

3.6. Cytokine expressions in the lung, serum and heart

Among the 40 investigated inflammatory cytokines and chemokines 26 proteins were detectable in lung homogenates throughout the 6-month experiment. At the end of the first month, interleukin-1β (IL-1β), IL-10 and monocyte chemoattractant protein-5 (MCP-5) increased significantly, but none of them were detectable later. The triggering receptor expressed on myeloid cells-1 (TREM-1) showed a peak expression at this time-point. The C5a complement component, interleukin-1 receptor antagonist (IL-1ra) produced by several immune cells and epithelial cells, interleukin-16 (IL-16), interferon-gamma inducible protein-10 (IP-10), keratinocyte chemoattractant (KC), macrophage colony-stimulating factor (M-CSF), monocyte chemoattractant protein-1 (MCP-1 or JE), monokine induced by gamma interferon (MIG), regulated on activation, normal T cell expressed and secreted (RANTES), and tissue inhibitor of metalloproteinase-1 (TIMP-1) cytokines and chemokines reached their maximum expression at the 2nd month. Meanwhile, the concentration of the soluble intercellular adhesion molecule-1 (sICAM-1) was high in the intact

Please cite this article in press as: Kemény, Á., et al., Integrative characterization of chronic cigarette smoke-induced cardiopulmonary comorbidities in a mouse model, Environmental Pollution (2017), http://dx.doi.org/10.1016/j.envpol.2017.04.098

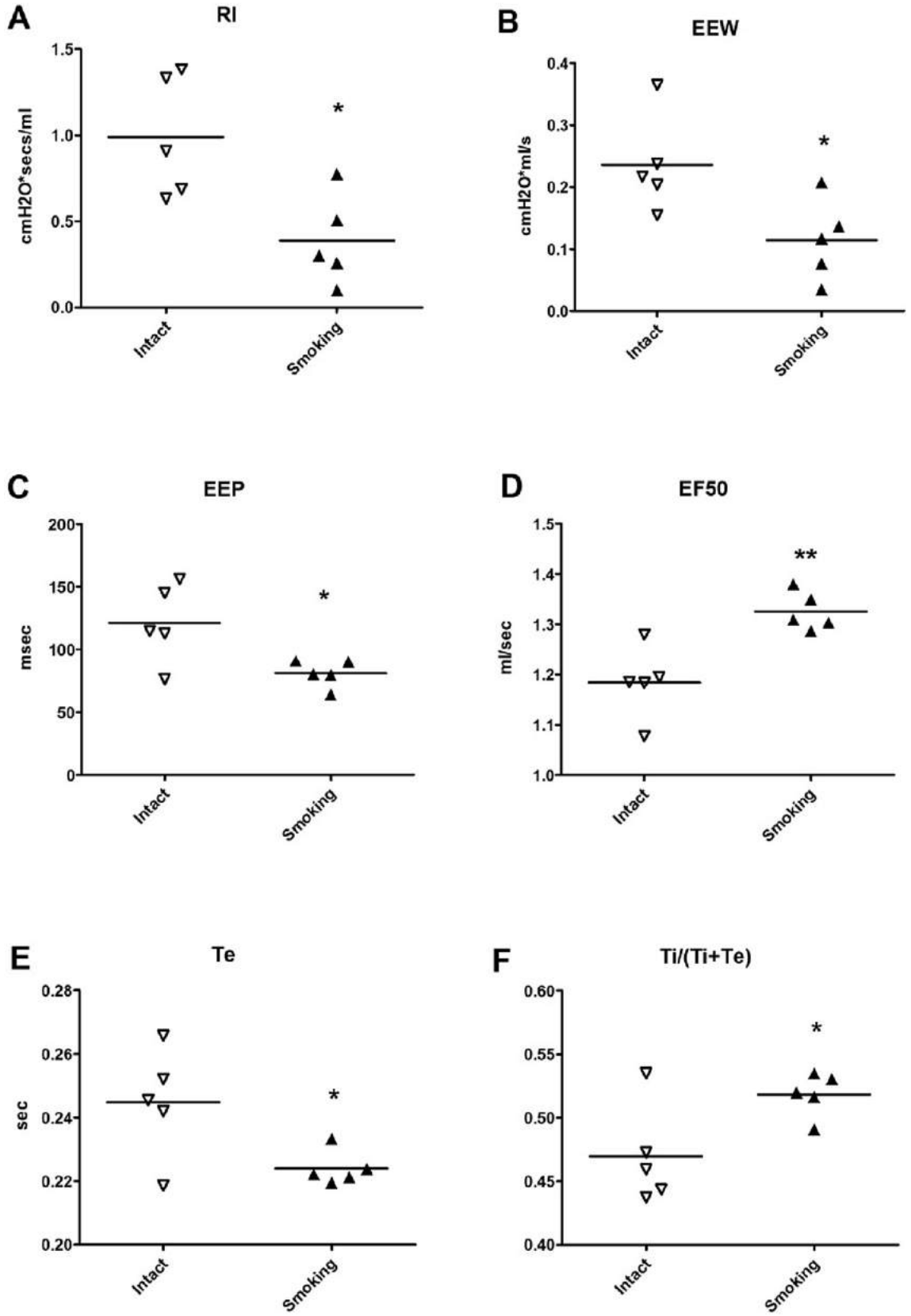

Fig. 1. Respiratory functions. Restrained whole-body plethysmography (WBP) parameters at the end of the 6th month. Panel A shows the airway resistance (RI), B: end expiratory work (EEW), C: end expiratory pause (EEP), D: tidal mid-expiratory flow (EF50), E: time of expiration (Te) and F: time of inspiration (Ti) and Te ratio at the end of the 6th month. N = 5 per group (Student's t-test for unpaired comparison, *$p < 0.05$; **$p < 0.005$; vs. the intact, non-smoking group).

Please cite this article in press as: Kemény, Á., et al., Integrative characterization of chronic cigarette smoke-induced cardiopulmonary comorbidities in a mouse model, Environmental Pollution (2017), http://dx.doi.org/10.1016/j.envpol.2017.04.098

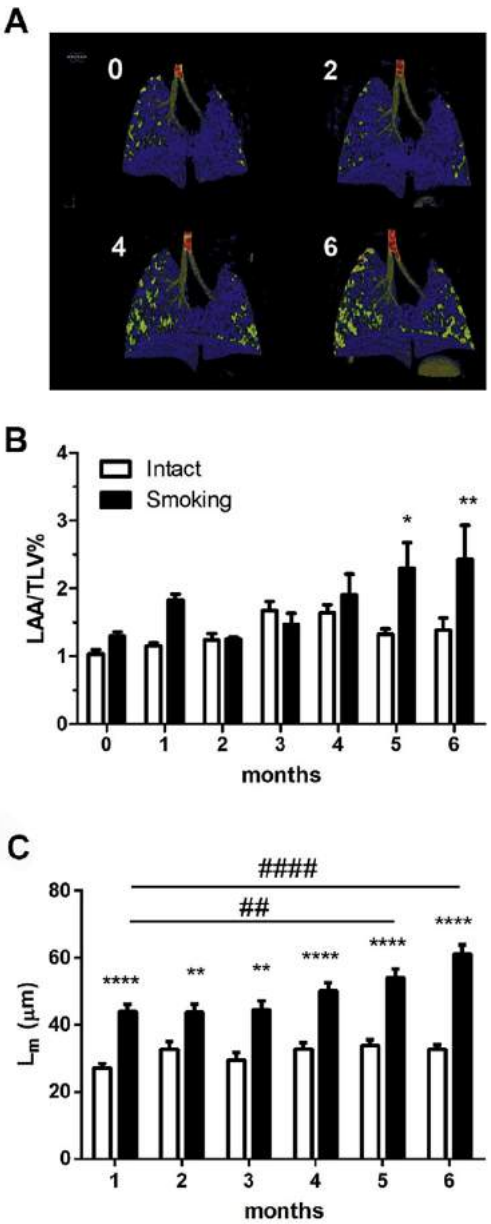

Fig. 2. Evaluation of emphysema by micro-CT measurement and histological assessment of mean linear intercept (chord) length. Structural changes of the lungs were imaged by breath-gated tomography on a Skyscan 1176 high resolution microtomograph. Panel A: representative 3D pictures of mouse lung before the treatment (0) and after 2-, 4- and 6-month smoking period. Light green and yellow areas represent the air-filled spaces. Panel B shows the calculated percentage of emphysema by the ratio of low-attenuation area (LAA) and total lung volume (TLV). N = 6 per group (two-way ANOVA followed by Bonferroni's post-test, *p < 0.05; **p < 0.005 vs. the intact, non-smoking group). Panel C: mean linear intercept length (L_m) measured on formalin fixed lung sections at the end of each month. N = 80–100 per group (two-way ANOVA followed by Bonferroni's post-test, **p < 0.005; ****p < 0.0001 vs. the intact, non-smoking group; ##p < 0.005; ####p < 0.0001 vs 1 month of smoking).

lung homogenate, and remained at a similarly high level during the whole 6-month smoking period (Fig. 7A and B). In the serum of non-smoking mice B-lymphocyte chemoattractant (BLC), stromal cell-derived factor 1 (SDF-1), C5a, interleukin-1 alpha (IL-1α), IL-1ra, IL-16, JE, M-CSF, TIMP-1, TNF-α, and TREM-1 were detectable. The first two were not present in the intact lung, and they decreased by the end of the 6-month smoking period similarly to IL-16. KC remarkably, JE slightly increased by this time point, while the expression of the other cytokines remained unchanged in the serum (Fig. 7C). In contrast, in the heart homogenates only granulocyte-monocyte colony-stimulating factor (GM-CSF) and sICAM-1 were detectable at relatively low levels, and sICAM-1 showed an approximately 2-fold elevation at the end of the 6th month of smoke exposure as compared to the time-matched intact heart samples (Fig. 7D).

3.7. Chronic tobacco smoke deteriorates cardiac function

Non-invasive echocardiographic evaluation and quantification were performed at the end of each month in a self-controlled manner during the 6-month experimental period. Heart rate did not differ significantly during anesthesia among the groups (data not shown). At the beginning of the study echocardiographic parameters of the two groups were not significantly different from each other (Fig. 8). Moreover, there were no significant intergroup differences in the case of left ventricular (LV) wall thicknesses (septum, posterior wall) and LV end-diastolic volume during the treatment period (data not shown). The results of the non-smoking intact animals did not change significantly during the 6 months of the experiment. In contrast, there were moderate, but significant pathophysiological functional alterations in mice exposed to chronic tobacco smoke transiently at 1–2 month, and also by the end of the study.

Echocardiography revealed that left ventricular ejection fraction (EF%) significantly decreased at the end of the first month, and then from the 5th month of smoke exposure as compared to the age-matched non-smoking controls (Fig. 8A and B). The diastolic LV function (deceleration time) deteriorated markedly from the 2nd month in the smoking group (Fig. 8C). TAPSE, which is a parameter of the systolic right ventricular function also significantly decreased after 4–6 months of chronic tobacco smoke exposure compared to non-smoking mice of the same age (Fig. 8D).

4. Discussion

The present results provide the first experimental evidence in a predictive chronic mouse model that cigarette smoke induces characteristic pulmonary inflammation, emphysema and atelectasis, as well as simultaneous development of left and right ventricular dysfunction. We proved with functional, morphological and immunological techniques that these well-defined pathophysiological alterations from the inflammatory reactions to the tissue destruction are dependent on the duration of the smoke exposure and COPD-like structural and functional changes develop only after the fourth month.

Respiratory function determined by invasive WBP in anaesthetized, tracheotomized and mechanically ventilated mice showed a significant decrease in airway resistance, interestingly along with a decrease in the expiratory parameters, such as EF50 characteristic to bronchoconstriction, EEW, EEP and Te (Hoymann, 2007). Emphysema in humans is characterized by increase of expiratory parameters, since in most cases at the stage when COPD is diagnosed, it is associated with chronic bronchitis, thus smooth muscle hypertrophy together with emphysema are present in patients (Caramori et al., 2014). The histopathological picture we found in mice after 6 months of smoke exposure did not show any inflammatory reaction with bronchial narrowing, only extensive emphysema and atelectasis, which can explain these functional differences compared to the human condition.

Inflammatory signs determined by the histopathological evaluation were clearly dependent on the duration of smoking. In the first two months peribronchial/perivascular edema, neutrophil and macrophage infiltration were characteristic, from the third and fourth months macrophages and lymphocytes accumulated

Please cite this article in press as: Kemény, Á., et al., Integrative characterization of chronic cigarette smoke-induced cardiopulmonary comorbidities in a mouse model, Environmental Pollution (2017), http://dx.doi.org/10.1016/j.envpol.2017.04.098

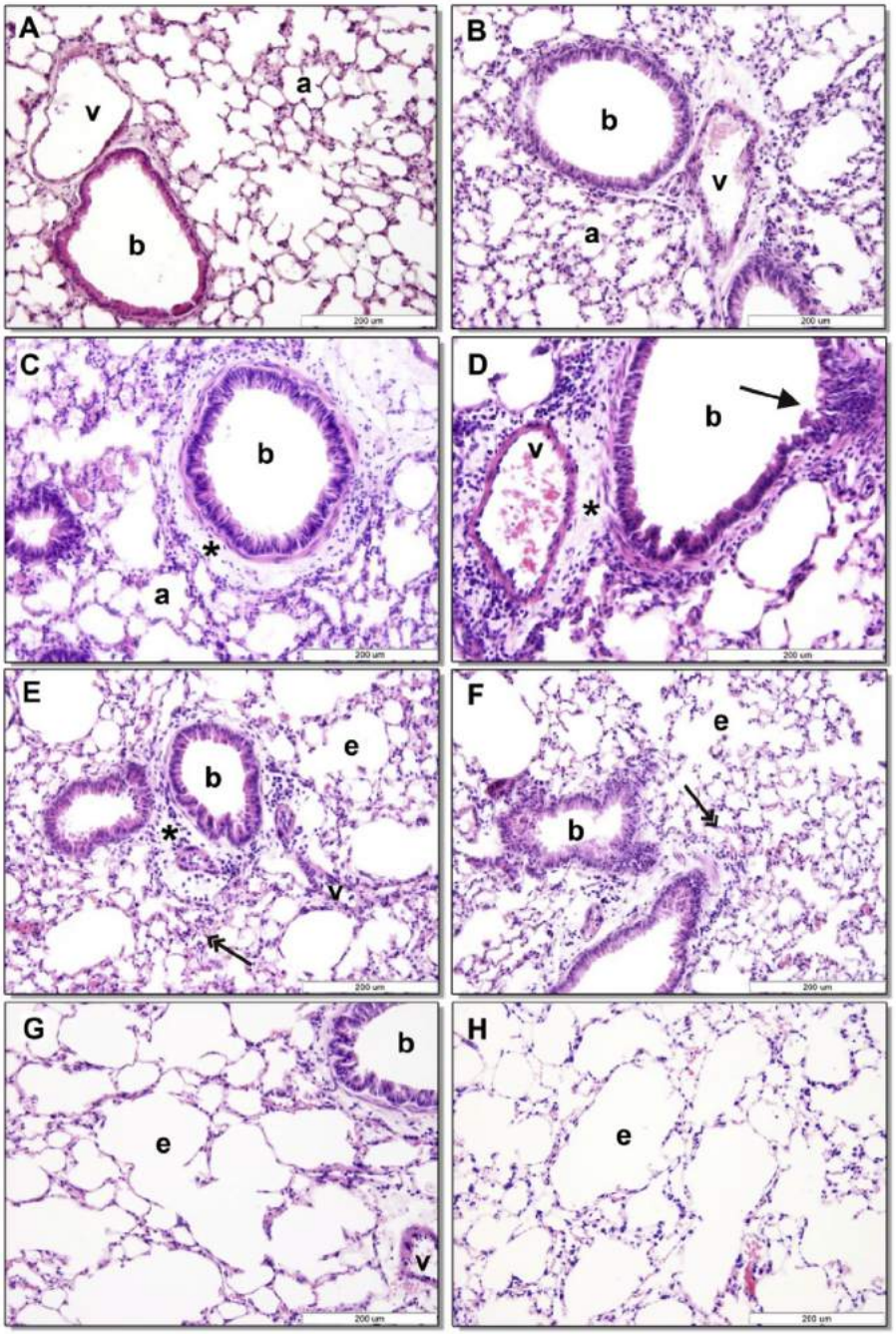

Fig. 3. Histopathological alterations in the lung. Representative histopathological pictures of the lung samples obtained before the treatment (A) and after 1 month (B), 2 months (C, D), 3 months (E), 4 months (F), 5 months (G) and 6 months (H). HE staining, magnification: 200×, except panel D: 400×; b: bronchioles, v: vessels; a: alveoli, *: peribronchiolar edema, black arrow: disruption of bronchi wall, double headed arrows: granulocyte accumulation, e: emphysema.

predominantly in the interstitial areas, and epithelial irregularity and hyperplasia developed. From the 5th month, the extent of inflammatory reaction decreased and tissue destruction dominated as shown by remarkable development of emphysema and atelectasis. Vascular endothelial proliferation, destructed bronchi with desquamated epithelial cells, fibrosis and a loss of the alveolar structure were detected by the end of the 6-month experiment. The histologically observed peak of peribronchial inflammation at 2 months of smoking was strongly supported by the drastically elevated numbers of granulocytes, macrophages and lymphocytes in the BALF. At later time-points cell counts in BALF were not changed, which is not surprising, since at this stage interstitial localization of the inflammation (at month 3) and the destruction of the bronchial epithelium (from month 4) were observed on histology. The development of emphysema after 5–6 months of smoke exposure was also clearly detected by micro-CT in complete agreement with the histological picture. Therefore, one major message of our study is that duration of smoking strongly determines pathophysiological alterations that develop sequentially in the lung as a cascade from different types of inflammatory processes to tissue destruction. We described a transient inflammation in contrast to a persistent process caused by chronic

Please cite this article in press as: Kemény, Á., et al., Integrative characterization of chronic cigarette smoke-induced cardiopulmonary comorbidities in a mouse model, Environmental Pollution (2017), http://dx.doi.org/10.1016/j.envpol.2017.04.098

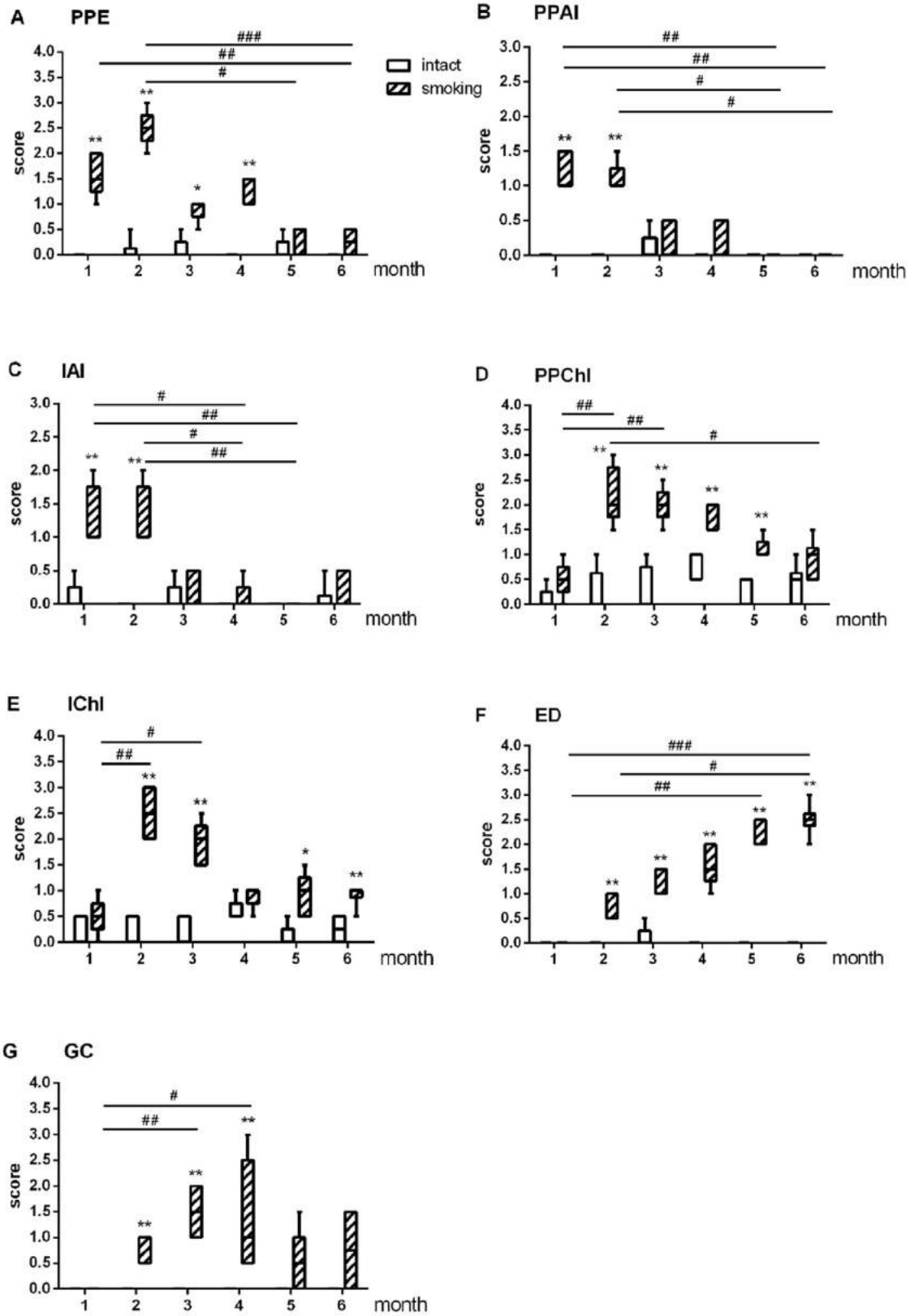

Fig. 4. Semiquantitative histopathological evaluation of lung sections. Box plots representing lesion extent on a range from 0 to 3 (mean ± minimal-maximal values) of perivascular/peribronchial edema (PPE) (A), perivascular/peribronchial acute inflammation (PPAI) (B), interstitial acute inflammation (IAI) (C), perivascular/peribronchial chronic inflammation (PPChI) (D), interstitial chronic inflammation (IChI) (E), epithelial damage (ED) (F) and goblet cells (GC) (G) at the end of each month. N = 6 per group (Kruskal-Wallis followed by Dunn's multiple comparison test to observe intragroup differences by time #$p < 0.05$, ##$p < 0.005$, ###$p < 0.0005$ vs. same group; Mann Whitney test to analyse intergroup differences at given time points *$p < 0.05$, **$p < 0.005$ smoking vs. intact group.

Please cite this article in press as: Kemény, Á., et al., Integrative characterization of chronic cigarette smoke-induced cardiopulmonary comorbidities in a mouse model, Environmental Pollution (2017), http://dx.doi.org/10.1016/j.envpol.2017.04.098

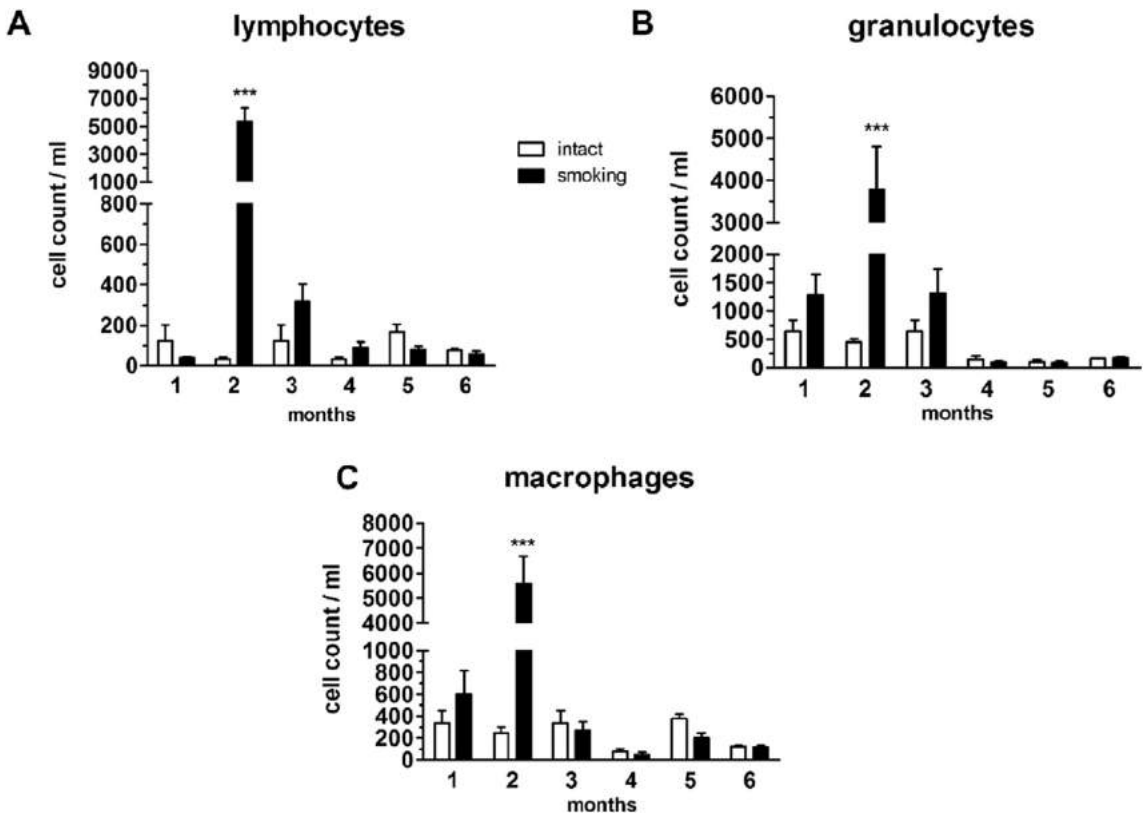

Fig. 5. Inflammatory cell concentrations in the BALF. The number of lymphocytes (A), granulocytes (B) and macrophages (C) in bronchoalveolar lavage fluid (BALF) samples were analysed with flow cytometry after each month. N = 6 per group (two-way ANOVA followed by Sidak's multiple comparison test, ***$p < 0.001$ vs. the intact, non-smoking group).

exposure of the same type of cigarette demonstrated by others (Phillips et al., 2015). It should be emphasized that they targeted a 4 times higher TPM and 3 times daily exposure and used female mice being more sensitive to oxidative stress and TGF-β pathways in the small airways compared to males (Tam et al., 2015). It is crucial to choose the correct experimental paradigm depending on which mechanisms and phase of the chronic disease model are aimed to be investigated (Leberl et al., 2013).

Our present study demonstrates for the first time in the literature the alterations of myocardial functions, as well as cardiac cytokine and MMP profiles in response to chronic smoke exposure (Suppl. Fig. E3). Recently, smoking-induced COPD models have been in the focus of respiratory research (Eltom et al., 2013; Luo et al., 2017; Wang et al., 2014), but none of these studies investigated the effects of chronic cigarette smoking on cardiac alterations. Although Wang et al. investigated the alterations of the right ventricle in a rat model of smoking-induced COPD, they did not determine either cardiac functional parameters or MMPs activity and inflammatory cytokines, but only right ventricular hypertrophy index (Wang et al., 2014). Therefore, the present study provides novel insight into the functional and molecular changes in the heart, especially in the left ventricle, during the development of COPD induced by chronic cigarette smoking. The transient impairment of the cardiovascular functions after 1 and 2 months of smoke exposure is likely to be due to the massive edema formation and inflammation in the lung, as described by the histopathological evaluation. Since the measured cardiovascular alterations are closely and sensitively related to the pulmonary pathophysiology, the observed mild, but significant systolic and diastolic dysfunctions at these earlier time points. CO could potentially be involved in the cardiac changes as a direct or indirect pathogenic factor in our model, and might explain -at least partially- the ejection fraction decrease.

According to the well-established involvement of MMPs in COPD and emphysema even proposing a potential approach for pharmacological intervention (Gueders et al., 2006), we measured MMP-2 and MMP-9 activities in the mouse lung and found a significant increase after 6 months of smoking. Similarly to our findings, intraperitoneal administration of a cigarette smoke extract in mice also showed increased pulmonary expressions and activities of these gelatinases (Zhang et al., 2013). In contrast, another recent mouse experiment of 6-month-long cigarette smoke exposure presented no differences either in MMP-2 or in MMP-9 mRNA levels in lung samples (Eurlings et al., 2014). However, without any alterations in gene expressions, MMP-2 and -9 may exert increased activities in case they are activated by enhanced oxidative stress as a result of cigarette smoke exposure (Bencsik et al., 2008; Viappiani et al., 2009; Zhang et al., 2005). Regarding the role of MMP-9 in cigarette smoke-induced pathophysiological alterations in the lung, MMP-9-deficient mice developed similar emphysema, but they were protected from small airway fibrosis (Barnes et al., 2003). Clinical data revealed elevated MMP-1, -9 and -12 levels in the BALF and plasma of patients with severe COPD (D'Armiento et al., 2013), as well as increased MMP-9 in the plasma and emphysematous lung of smokers (Atkinson et al., 2011). Furthermore, enhanced release of MMP-9 and its endogenous inhibitor, TIMP-1 were detected from isolated human macrophages obtained from the BALF of smokers (Sam et al., 2000), and the BALF concentrations and macrophage expression of MMP-9 and MMP-1 (collagenase) also increased in COPD-emphysema patients (Barnes et al., 2003). Increased activity of the active 64 kDa MMP-2 isoform was shown in pneumocytes and alveolar macrophages isolated from COPD

Please cite this article in press as: Kemény, Á., et al., Integrative characterization of chronic cigarette smoke-induced cardiopulmonary comorbidities in a mouse model, Environmental Pollution (2017), http://dx.doi.org/10.1016/j.envpol.2017.04.098

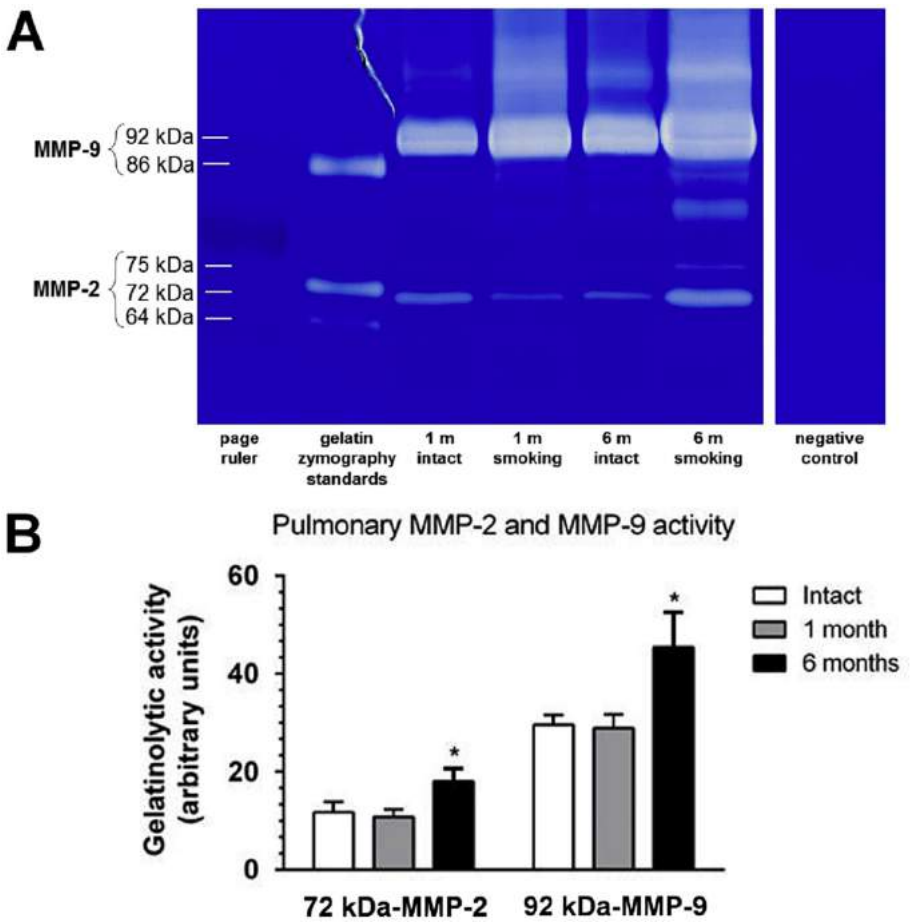

Fig. 6. MMP-2 and MMP-9 activities in the mouse lung. Panel A shows representative zymograms of the lung samples obtained after 1 or 6 months of tobacco smoke exposure in comparison with the non-smoking intact. Panel B represents the mean arbitrary units±S.E.M. of N = 6 mice per group. (Student's t-test for unpaired comparison, *$p < 0.05$ vs. the intact, non-smoking group).

patients with emphysema (Ohnishi et al., 1998). Furthermore, in a coronary artery disease patient group we have previously found a significantly increased activity of serum MMP-2 in a smoking subgroup of patients as compared to non-smoking patients with the same selection criteria (severity of disease, other co-morbidities, medications, etc.; 50.5 ± 9.8 vs. 26.2 ± 5.0; n = 8–13, $p < 0.05$ with Student's t-test for unpaired comparison) (Bencsik et al., 2015). Plasma MMP-9 activity was also higher, but it did not reach the level of statistical significance (193.3 ± 74.2 vs. 122.6 ± 34.4). However, in another study, the increased MMP levels in the plasma, BALF, and lung did not correlate with the disease severity and were not predictive of the progression (D'Armiento et al., 2013). Therefore, our MMP results can point out a similarity between the mechanisms in the mouse model and the human disease supporting its translational relevance, but specific inhibition of MMP-9 is not likely to be an effective therapy for cigarette smoke-induced emphysema (Atkinson et al., 2011).

The cytokine panel measured from the lung homogenates showed a 2-phase pattern during the 6-month-smoke exposure: a characteristic profile was seen at the end of the second month when the inflammatory reaction reached its maximum, and another group of cytokines increased at 5–6 months related to the definitive tissue destruction and emphysema. The inflammatory burst at month 2 clearly suggests an IL-1-driven cascade with the elevation of C5a, IL-1α, IL-1ra, IL-16, IP-10, M-CSF, KC, MIG, RANTES, TIMP-1 (Dinarello, 2011). IL-1β remarkably increased at month 1 and IL-1α at months 1–2, but then the massive elevation of IL-1ra seems to down-regulate their production. However, the increased inflammatory cytokines demonstrate an IL-1-downstream profile (Barksby et al., 2007). Several members of the IL-1 family including IL-1β are important mediators of lung inflammation. The expression of an inactive IL-1β precursor is induced in immune cells via activation of signaling pathways upstream of the transcription factor NFκB. Cigarette smoking leads to IL-1β release in the human lung (Kuschner et al., 1996). Mice overexpressing IL-1β in the lung present a phenotype similar to COPD including lung inflammation, emphysema and fibrosis (Lappalainen et al., 2005). IL-1β increases the production of neutrophil chemoattractant factors, and the activity of MMP-2 and MMP-9 by alveolar macrophages, and these gelatinases are also able to activate the active form of IL-1β from its inactive form (Chakrabarti and Patel, 2009). The importance of the IL-β cascade in lung pathology is shown by the fact that an IL-1-blocking monoclonal antibody (canakinumab) is currently being investigated for the treatment of several conditions including COPD (Rogliani et al., 2015). The complement component C5a is a potent inflammatory peptide, which is suggested to be involved in the pathogenesis of COPD. Plasma C5a concentrations in COPD patients were significantly higher than in healthy smokers. Elevated C5a and C3a levels were also measured in the sputum of stable COPD patients suggesting that the complement system is continuously activated during stable phase of the disease. Besides its chemotactic function, it enhances the production of various cytokines, regulate

Please cite this article in press as: Kemény, Á., et al., Integrative characterization of chronic cigarette smoke-induced cardiopulmonary comorbidities in a mouse model, Environmental Pollution (2017), http://dx.doi.org/10.1016/j.envpol.2017.04.098

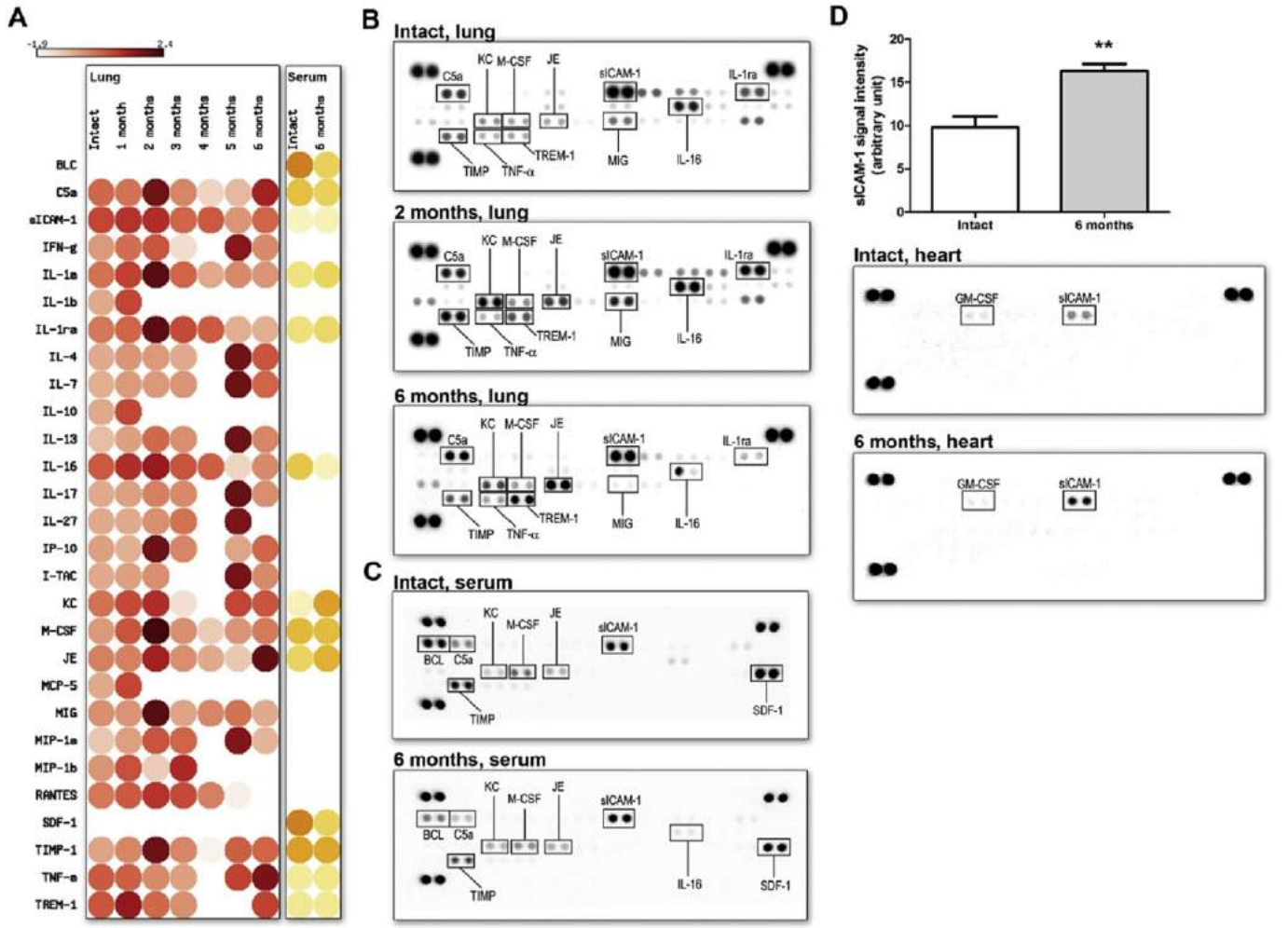

Fig. 7. Cytokine determinations in the lung and the heart homogenates. A: heat map of cytokine expression in intact and smoking lung samples during the six-month treatment period (red dots) and intact and 6-month smoking serum samples (yellow dots), B: representative picture of the membranes after chemiluminescent detection of cytokines in lung tissue homogenates. C: representative picture of the membranes after chemiluminescent detection of cytokines in serum samples. The most important cytokine signals in duplicate are labeled. D: Expression of sICAM-1 cell adhesion molecule in intact and 6-month smoking heart tissues (upper panel). Representative picture of the membranes after chemiluminescent detection of cytokines in heart tissues (lower panel). The most important cytokine signals in duplicate are labeled. N = 3 per group (two-way ANOVA followed by Bonferroni's post-test, $^{**}p < 0{,}005$ vs. the intact, non-smoking group).

vascular permeability and influence the adaptive immune system by stimulating Th1 response. As a result of its action, abnormal inflammation could eventually lead to structural changes in the lungs (Marc et al., 2010). C5a induces autophagy in mouse alveolar macrophages promoting their apoptosis (Hu et al., 2014). Both cigarette smoke extract and C5a induce increased expression of ICAM-1 on airway epithelial monolayers (Floreani et al., 2003). Clinical findings showing that the Th1-attracting chemokine IP-10/CXCL10 was increased in the bronchial mucosa and bronchoalveolar lavage fluid of moderate/severe asthma and COPD patients. IP-10 is produced by epithelial cells and act as the ligands for the CXCR3 receptor expressed on Th1 cells (Takaku et al., 2016; Ying et al., 2008). The number of receptor-positive cells was increased in smokers with COPD as compared to non-smoking subjects, but not as compared with smokers of normal lung function, suggesting its pro-inflammatory role (Saetta et al., 2002). Our interesting experimental finding showing a remarkably increased IP-10 level in the lung perfectly correlate with these data, therefore, emphasize the translational relevance of our results.

In the tissue destruction phase of our model at months 5–6, the increased cytokines were C5a, IFN-γ, IL-4, IL-7, IL-13, IL-17, IL-27, TNF-α, MIP-1α, JE, TIMP-1, interferon-inducible T-cell chemoattractant (I-TAC) and TREM-1. An adaptive immune reaction mediated by $CD4^+$ and $CD8^+$ T cells and a Th1 cell-regulated chemokine-cytokine profile might be important factors of emphysema in susceptible animals. There is a great upregulation of the inflammatory mediators pointing towards a Th1-adaptive inflammatory response in mice with significant increases in MIP-1α (Guerassimov et al., 2004). Both natural killer (NK) and T cells use MIP-1α along with interferon-γ, RANTES and the I-TAC as a "functional unit" to drive the Th1 response (Dorner et al., 2002). TIMP-1 specifically interacts with proMMP-9, its expression is regulated by growth factors and cytokines (Ries, 2014). TIMP-1 does not only inhibit MMP activities, but also acts as a cytokine by promoting cell growth in a wide range of cell types including fibroblasts, epithelial cells and the SV40 transformed human lung cell line (Hayakawa et al., 1992). TNF-α is also a key factor implicated in emphysema pathogenesis, its type 2 receptor plays a critical role in the pro-inflammatory pathway (Goldklang et al., 2013). IFN-γ is a potent stimulator of MMP-9 and CCR5 ligands (MIP-1α, MIP-1β, RANTES)

Please cite this article in press as: Kemény, Á., et al., Integrative characterization of chronic cigarette smoke-induced cardiopulmonary comorbidities in a mouse model, Environmental Pollution (2017), http://dx.doi.org/10.1016/j.envpol.2017.04.098

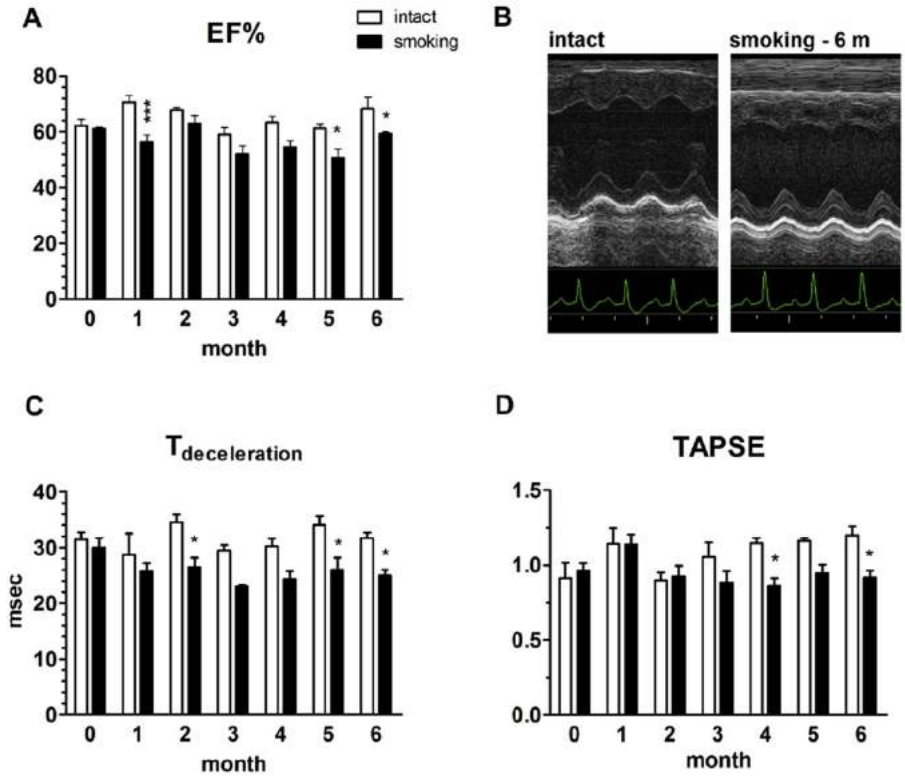

Fig. 8. Echocardiographic parameters. Evaluation of cardiac functions and dimensions. A: Ejection fraction (EF%), B: representative images of M-mode measurements, C: deceleration time ($T_{deceleration}$) and D: tricuspid annular plane systolic excursion (TAPSE). N = 6 mice per group (Student's t-test for unpaired comparison, *$p < 0.05$ vs. the intact, non-smoking groups of respective age).

which ultimately results in DNA damage, apoptosis and emphysema (Ma et al., 2005).

In contrast to asthma studies, Bowler and co-workers found that subjects with emphysema had decreased IL-16 protein in plasma and decreased IL-16 mRNA expression in peripheral blood mononuclear cells (Bowler et al., 2013). Our results correlate with these findings as IL-16 expression decreased at months 5–6 when emphysema developed.

ICAM-1 is a central molecule in inflammatory processes and functions as a co-stimulatory signal being important for the *trans*-endothelial migration of leukocytes and the activation of T cells. Increased circulating levels of sICAM-1 are highly associated with major cardiovascular complications (e.g.: increased risk of myocardial infarction (Ridker et al., 1998), in addition chronic smokers have elevated levels of sICAM-1 (Rohde et al., 1999). Furthermore, significant increase in sICAM-1 was associated with the extent of emphysema in patients involved in the Multi-Ethnic Study of Atherosclerosis Lung study (Aaron et al., 2015). Two clinical studies have found significant associations between increasing concentration of sICAM-1 and risk of myocardial infarction, especially among participants with baseline sICAM-1 concentrations in the highest quartile (Luc et al., 2003; Ridker et al., 1998; Sungprem et al., 2009). Vascular inflammation is crucial in pathophysiological processes underlying many cardiovascular diseases. ICAM-1 mediates vascular inflammation by promoting leukocyte adhesion to the activated endothelial cells (Badimon et al., 2012). MMPs are responsible for the cleavage and generation of soluble adhesion molecules, including sICAM-1 and sVCAM-1 from the endothelium, and could act as mediators beyond the lung to establish and sustain low-grade inflammation and aggravate the cardiovascular complications (Pope et al., 2016). The selective increase of sICAM-1 in the heart suggests that our mouse model can mimic this key mechanism in smoking-related cardiovascular alterations. However, the limitation of this study, besides that our facility is lacking the forced oscillation technique to determine airway mechanics in a non-invasive way, are that we did not determine specific biomarkers of the smoke exposure and could not directly prove the functional roles of either sICAM-1 in the heart or the other detected mediators in the lung.

In summary, the major conclusion of this study is that the chronic moderate cigarette smoke exposure-induced mouse model is appropriate to investigate smoking-induced time-dependent characteristic alterations and mechanisms simultaneously in the lung and the heart. Our primary focus was to show links with the human disease and to describe common mediators as potential markers and/or therapeutic targets. The pathophysiological alterations we described here appear to be similar to that observed in the clinics, which highlights the translational value of our model in relation to the human cardiopulmonary comorbidity seen in COPD.

Funding

This work was performed with the financial support of SROP-4.2.2.A-11/1/KONV-2012-0024 and National Research, Development and Innovations Office (TET_15_IN_1-2016-0068). P. Bencsik was supported by the János Bolyai Research Scholarship of the Hungarian Academy of Sciences, Zs. Helyes by the National Brain Research Programme B (KTIA_NAP_13-2014-0022, Research site ID number: 888819, Hungary) and Á. Kemény by the GINOP-2.3.2-15-2016-00050 – PEPSYS. K. Csekő was supported by the Richter Gedeon Talentum Foundation and GINOP-2.3.2 STAY ALIVE. We state hereby that no financial or other relationships exist which might lead to conflicts of interest.

Please cite this article in press as: Kemény, Á., et al., Integrative characterization of chronic cigarette smoke-induced cardiopulmonary comorbidities in a mouse model, Environmental Pollution (2017), http://dx.doi.org/10.1016/j.envpol.2017.04.098

Appendix A. Supplementary data

Supplementary data related to this article can be found at http://dx.doi.org/10.1016/j.envpol.2017.04.098.

References

Aaron, C.P., Schwartz, J.E., Bielinski, S.J., Hoffman, E.a., Austin, J.H.M., Oelsner, E.C., Donohue, K.M., Kalhan, R., Berardi, C., Kaufman, J.D., Jacobs, D.R., Tracy, R.P., Barr, R.G., 2015. Intercellular adhesion molecule 1 and progression of percent emphysema: the MESA Lung Study. Respir. Med. 109, 255–264. http://dx.doi.org/10.1016/j.rmed.2014.10.004.

Atkinson, J.J., Lutey, B.a., Suzuki, Y., Toennies, H.M., Kelley, D.G., Kobayashi, D.K., Ijem, W.G., Deslee, G., Moore, C.H., Jacobs, M.E., Conradi, S.H., Gierada, D.S., Pierce, R.a., Betsuyaku, T., Senior, R.M., 2011. The role of matrix metalloproteinase-9 in cigarette smoke-induced emphysema. Am. J. Respir. Crit. Care Med. 183, 876–884. http://dx.doi.org/10.1164/rccm.201005-0718OC.

Badimon, L., Romero, J.C., Cubedo, J., Borrell-Pagès, M., 2012. Circulating biomarkers. Thromb. Res. 130, S12–S15. http://dx.doi.org/10.1016/j.thromres.2012.08.262.

Barksby, H.E., Lea, S.R., Preshaw, P.M., Taylor, J.J., 2007. The expanding family of interleukin-1 cytokines and their role in destructive inflammatory disorders. Clin. Exp. Immunol. 149, 217–225. http://dx.doi.org/10.1111/j.1365-2249.2007.03441.x.

Barnes, P.J., Shapiro, S.D., Pauwels, R.a., 2003. Chronic obstructive pulmonary disease: molecular and cellular mechanisms. Eur. Respir. J. 22, 672–688. http://dx.doi.org/10.1183/09031936.03.00040703.

Bartalesi, B., Cavarra, E., Fineschi, S., Lucattelli, M., Lunghi, B., Martorana, P.a., Lungarella, G., 2005. Different lung responses to cigarette smoke in two strains of mice sensitive to oxidants. Eur. Respir. J. 25, 15–22. http://dx.doi.org/10.1183/09031936.04.00067204.

Beeh, K.M., Beier, J., Kornmann, O., Buhl, R., 2003. Sputum matrix metalloproteinase-9, tissue inhibitor of metalloprotinease-1, and their molar ratio in patients with chronic obstructive pulmonary disease, idiopathic pulmonary fibrosis and healthy subjects. Respir. Med. 97, 634–639.

Bencsik, P., Kupai, K., Giricz, Z., Görbe, A., Huliák, I., Fürst, S., Dux, L., Csont, T., Jancsó, G., Ferdinandy, P., 2008. Cardiac capsaicin-sensitive sensory nerves regulate myocardial relaxation via S-nitrosylation of SERCA: role of peroxynitrite. Br. J. Pharmacol. 153, 488–496. http://dx.doi.org/10.1038/sj.bjp.0707599.

Bencsik, P., Sasi, V., Kiss, K., Kupai, K., Kolossváry, M., Maurovich-Horvat, P., Csont, T., Ungi, I., Merkely, B., Ferdinandy, P., 2015. Serum lipids and cardiac function correlate with nitrotyrosine and MMP activity in coronary artery disease patients. Eur. J. Clin. Invest 45, 692–701. http://dx.doi.org/10.1111/eci.12458.

Bowler, R.P., Bahr, T.M., Hughes, G., Lutz, S., Kim, Y.-I., Coldren, C.D., Reisdorph, N., Kechris, K.J., 2013. Integrative omics approach identifies interleukin-16 as a biomarker of emphysema. OMICS 17, 619–626. http://dx.doi.org/10.1089/omi.2013.0038.

Canning, B.J., Spina, D., 2009. Sensory nerves and airway irritability. Handb. Exp. Pharmacol. 139–183. http://dx.doi.org/10.1007/978-3-540-79090-7_5.

Caramori, G., Adcock, I.M., Di Stefano, A., Chung, K.F., 2014. Cytokine inhibition in the treatment of COPD. Int. J. COPD 9, 397–412. http://dx.doi.org/10.2147/COPD.S42544.

Chakrabarti, S., Patel, K.D., 2009. Matrix metalloproteinase-2 (MMP-2) and MMP-9 in pulmonary pathology. Exp. Lung Res. 31, 599–621. http://dx.doi.org/10.1080/01902140944232.

D'Armiento, J.M., Goldklang, M.P., Hardigan, A.a., Geraghty, P., Roth, M.D., Connett, J.E., Wise, R.a., Sciurba, F.C., Scharf, S.M., Thankachen, J., Islam, M., Ghio, A.J., Foronjy, R.F., 2013. Increased matrix metalloproteinase (MMPs) levels do not predict disease severity or progression in emphysema. PLoS One 8. http://dx.doi.org/10.1371/journal.pone.0056352.

Dinarello, C.a., 2011. A clinical perspective of IL-1β as the gatekeeper of inflammation. Eur. J. Immunol. 41, 1203–1217. http://dx.doi.org/10.1002/eji.201141550.

Dorner, B.G., Scheffold, A., Rolph, M.S., Huser, M.B., Kaufmann, S.H.E., Radbruch, A., Flesch, I.E.a., Kroczek, R.a., 2002. MIP-1alpha, MIP-1beta, RANTES, and ATAC/lymphotactin function together with IFN-gamma as type 1 cytokines. Proc. Natl. Acad. Sci. U. S. A. 99, 6181–6186. http://dx.doi.org/10.1073/pnas.092141999.

Elekes, K., Helyes, Z., Kereskai, L., Sándor, K., Pintér, E., Pozsgai, G., Tékus, V., Bánvölgyi, Á., Németh, J., Szuts, T., Kéri, G., Szolcsányi, J., 2008. Inhibitory effects of synthetic somatostatin receptor subtype 4 agonists on acute and chronic airway inflammation and hyperreactivity in the mouse. Eur. J. Pharmacol. 578, 313–322. http://dx.doi.org/10.1016/j.ejphar.2007.09.033.

Eltom, S., Stevenson, C., Birrell, M.A., 2013. Cigarette smoke exposure as a model of inflammation associated with COPD. Curr. Protoc. Pharmacol. http://dx.doi.org/10.1002/0471141755.ph0564s60 (Chapter 5), Unit5.64.

Eurlings, I.M.J., Dentener, M.A., Mercken, E.M., de Cabo, R., Bracke, K.R., Vernooy, J.H.J., Wouters, E.F.M., Reynaert, N.L., 2014. A comparative study of matrix remodeling in chronic models for COPD; mechanistic insights into the role of TNF-α. Am. J. Physiol. Lung Cell. Mol. Physiol. 307, L557–L565. http://dx.doi.org/10.1152/ajplung.00116.2014.

Floreani, A.a., Wyatt, T.a., Stoner, J., Sanderson, S.D., Thompson, E.G., Allen-Gipson, D., Heires, A.J., 2003. Smoke and C5a induce airway epithelial intercellular adhesion molecule-1 and cell adhesion. Am. J. Respir. Cell Mol. Biol. 29, 472–482. http://dx.doi.org/10.1165/rcmb.2002-0143OC.

Fricker, M., Deane, A., Hansbro, P.M., 2014. Animal models of chronic obstructive pulmonary disease. Expert Opin. Drug Discov. 9, 629–645. http://dx.doi.org/10.1517/17460441.2014.909805.

Goldklang, M.P., Marks, S.M., D'Armiento, J.M., 2013. Second hand smoke and COPD: lessons from animal studies. Front. Physiol. 4 (FEB), 1–8. http://dx.doi.org/10.3389/fphys.2013.00030.

Gueders, M.M., Foidart, J.-M., Noel, A., Cataldo, D.D., 2006. Matrix metalloproteinases (MMPs) and tissue inhibitors of MMPs in the respiratory tract: potential implications in asthma and other lung diseases. Eur. J. Pharmacol. 533, 133–144. http://dx.doi.org/10.1016/j.ejphar.2005.12.082.

Guerassimov, A., Hoshino, Y., Takubo, Y., Turcotte, A., Yamamoto, M., Ghezzo, H., Triantafillopoulos, A., Whittaker, K., Hoidal, J.R., Cosio, M.G., 2004. The development of emphysema in cigarette smoke-exposed mice is strain dependent. Am. J. Respir. Crit. Care Med. 170, 974–980. http://dx.doi.org/10.1164/rccm.200309-1270OC.

Hayakawa, T., Yamashita, K., Tanzawa, K., Uchijima, E., Iwata, K., 1992. Growth-promoting activity of tissue inhibitor of metalloproteinases-1 (TIMP-1) for a wide range of cells. A possible new growth factor in serum. FEBS Lett. 298, 29–32. http://dx.doi.org/10.1016/0014-5793(92)80015-9.

Helyes, Z., Hajna, Z., 2012. Endotoxin-induced airway inflammation and asthma models. In: Szallasi, A., Bíró, T. (Eds.), TRP Channels in Drug Discovery. Humana Press, pp. 301–342. http://dx.doi.org/10.1007/978-1-62703-077-9.

Hoymann, H.G., 2007. Invasive and noninvasive lung function measurements in rodents. J. Pharmacol. Toxicol. Methods 55, 16–26. http://dx.doi.org/10.1016/j.vascn.2006.04.006.

Hu, R., Chen, Z.-F., Yan, J., Li, Q.-F., Huang, Y., Xu, H., Zhang, X., Jiang, H., 2014. Complement C5a exacerbates acute lung injury induced through autophagy-mediated alveolar macrophage apoptosis. Cell Death Dis. 5, e1330. http://dx.doi.org/10.1038/cddis.2014.274.

Knudsen, L., Weibel, E.R., Gundersen, H.J.G., Weinstein, F.V., Ochs, M., 2010. Assessment of air space size characteristics by intercept (chord) measurement: an accurate and efficient stereological approach. J. Appl. Physiol. 108, 412–421. http://dx.doi.org/10.1152/japplphysiol.01100.2009.

Kobayashi, S., Fujinawa, R., Ota, F., Kobayashi, S., Angata, T., Ueno, M., Maeno, T., Kitazume, S., Yoshida, K., Ishii, T., Gao, C., Ohtsubo, K., Yamaguchi, Y., Betsuyaku, T., Kida, K., Taniguchi, N., 2013. A single dose of lipopolysaccharide into mice with emphysema mimics human Chronic obstructive pulmonary disease exacerbation as assessed by micro-computed tomography. Am. J. Respir. Cell Mol. Biol. 49, 971–977. http://dx.doi.org/10.1165/rcmb.2013-0074OC.

Kupai, K., Szucs, G., Cseh, S., Hajdu, I., Csonka, C., Csont, T., Ferdinandy, P., 2010. Matrix metalloproteinase activity assays: importance of zymography. J. Pharmacol. Toxicol. Methods 61, 205–209. http://dx.doi.org/10.1016/j.vascn.2010.02.011.

Kuschner, W.G., D'Alessandro, a., Wong, H., Blanc, P.D., 1996. Dose-dependent cigarette smoking-related inflammatory responses in healthy adults. Eur. Respir. J. 9, 1989–1994. http://dx.doi.org/10.1183/09031936.96.09101989.

Lappalainen, U., Whitsett, J.a., Wert, S.E., Tichelaar, J.W., Bry, K., 2005. Interleukin-1beta causes pulmonary inflammation, emphysema, and airway remodeling in the adult murine lung. Am. J. Respir. Cell Mol. Biol. 32, 311–318. http://dx.doi.org/10.1165/rcmb.2004-0309OC.

Leberl, M., Kratzer, A., Taraseviciene-Stewart, L., 2013. Tobacco smoke induced COPD/emphysema in the animal model-are we all on the same page? Front. Physiol. 4 (MAY), 1–23. http://dx.doi.org/10.3389/fphys.2013.00091.

Luc, G., Arveiler, D., Evans, A., Amouyel, P., Ferrieres, J., Bard, J.M., Elkhalil, L., Fruchart, J.C., Ducimetiere, P., 2003. Circulating soluble adhesion molecules ICAM-1 and VCAM-1 and incident coronary heart disease: the PRIME Study. Atherosclerosis 170, 169–176. http://dx.doi.org/10.1016/S0021-9150(03)00280-6.

Luo, F., Liu, J., Yan, T., Miao, M., 2017. Salidroside alleviates cigarette smoke-induced COPD in mice. Biomed. Pharmacother. 86, 155–161. http://dx.doi.org/10.1016/j.biopha.2016.12.032.

Ma, B., Kang, M.-J., Lee, C.G., Chapoval, S., Liu, W., Chen, Q., Coyle, A.J., Lora, J.M., Picarella, D., Homer, R.J., Elias, J.A., 2005. Role of CCR5 in IFN-gamma-induced and cigarette smoke-induced emphysema. J. Clin. Invest 115, 3460–3472. http://dx.doi.org/10.1172/JCI24858.

Ma, W., Cui, W., Lin, Q., 2001. Improved immnunophenotyping of lymphocytes in bronchoalveolar lavage fluid (BALF) by flow cytometry. Clin. Chim. Acta 313, 133–138. http://dx.doi.org/10.1016/S0009-8981(01)00664-7.

Marc, M.M., Kristan, S.S., Rozman, a., Kern, I., Flezar, M., Kosnik, M., Korosec, P., 2010. Complement factor C5a in acute exacerbation of chronic obstructive pulmonary disease. Scand. J. Immunol. 71, 386–391. http://dx.doi.org/10.1111/j.1365-3083.2010.02385.x.

Martorana, P.a., Cavarra, E., Lucattelli, M., Lungarella, G., 2006. Models for COPD involving cigarette smoke. Drug Discov. Today Dis. Model 3, 225–230. http://dx.doi.org/10.1016/j.ddmod.2006.09.004.

Mercer, P.F., Abbott-Banner, K., Adcock, I.M., Knowles, R.G., 2015. Translational models of lung disease. Clin. Sci. 128, 235–256. http://dx.doi.org/10.1042/CS20140373.

Ohnishi, K., Takagi, M., Kurokawa, Y., Satomi, S., Konttinen, Y.T., 1998. Matrix metalloproteinase-mediated extracellular matrix protein degradation in human pulmonary emphysema. Lab. Invest 78, 1077–1087.

Pavlidis, P., Noble, W.S., 2003. Matrix2png: a utility for visualizing matrix data. Bioinformatics 19, 295–296. http://dx.doi.org/10.1093/bioinformatics/19.2.295.

Phillips, B., Veljkovic, E., Boué, S., Schlage, W.K., Vuillaume, G., Martin, F., Titz, B., Leroy, P., Buettner, A., Elamin, A., Oviedo, A., Cabanski, M., De León, H., Guedj, E., Schneider, T., Talikka, M., Ivanov, N.V., Vanscheeuwijck, P., Peitsch, M.C.,

Hoeng, J., 2016. An 8-month systems toxicology inhalation/cessation study in Apoe-/- mice to investigate cardiovascular and respiratory exposure effects of a candidate modified risk tobacco product, THS 2.2, compared with conventional cigarettes. Toxicol. Sci. 149, 411–432. http://dx.doi.org/10.1093/toxsci/kfv243.

Phillips, B., Veljkovic, E., Peck, M.J., Buettner, A., Elamin, A., Guedj, E., Vuillaume, G., Ivanov, N.V., Martin, F., Boué, S., Schlage, W.K., Schneider, T., Titz, B., Talikka, M., Vanscheeuwijck, P., Hoeng, J., Peitsch, M.C., 2015. A 7-month cigarette smoke inhalation study in C57BL/6 mice demonstrates reduced lung inflammation and emphysema following smoking cessation or aerosol exposure from a prototypic modified risk tobacco product. Food Chem. Toxicol. 80, 328–345. http://dx.doi.org/10.1016/j.fct.2015.03.009.

Pope, C.A., Bhatnagar, A., McCracken, J., Abplanalp, W.T., Conklin, D.J., O'Toole, T.E., 2016. Exposure to fine particulate air pollution is associated with endothelial injury and systemic inflammation. Circ. Res. http://dx.doi.org/10.1161/CIRCRESAHA.116.309279.

Respress, J.L., Wehrens, X.H.T., 2010. Transthoracic echocardiography in mice. J. Vis. Exp. 3–5. http://dx.doi.org/10.3791/1738.

Restrepo, R.D., 2015. Year in review 2014: COPD. Respir. Care 60, 1057–1060. http://dx.doi.org/10.4187/respcare.04227.

Ridker, P.M., Hennekens, C.H., Roitman-Johnson, B., Stampfer, M.J., Allen, J., 1998. Plasma concentration of soluble intercellular adhesion molecule 1 and risks of future myocardial infarction in apparently healthy men. Lancet 351, 88–92. http://dx.doi.org/10.1016/S0140-6736(97)09032-6.

Ries, C., 2014. Cytokine functions of TIMP-1. Cell. Mol. Life Sci. 71, 659–672. http://dx.doi.org/10.1007/s00018-013-1457-3.

Roemer, E., Schramke, H., Weiler, H., Buettner, A., Kausche, S., Weber, S., Berges, A., Stueber, M., Muench, M., Trelles-Sticken, E., Pype, J., Kohlgrueber, K., Voelkel, H., Wittke, S., 2012. Mainstream smoke chemistry and in vitro and in vivo toxicity of the reference cigarettes 3R4F and 2R4F. Beitrage zur Tab. Int. Contrib. Tob. Res. 25, 316–335. http://dx.doi.org/10.2478/cttr-2013-0912.

Rogliani, P., Calzetta, L., Ora, J., Matera, M.G., 2015. Canakinumab for the treatment of chronic obstructive pulmonary disease. Pulm. Pharmacol. Ther. 31, 15–27. http://dx.doi.org/10.1016/j.pupt.2015.01.005.

Rohde, L.E., Hennekens, C.H., Ridker, P.M., 1999. Cross-sectional study of soluble intercellular adhesion molecule-1 and cardiovascular risk factors in apparently healthy men. Arterioscler. Thromb. Vasc. Biol. 19, 1595–1599.

Saetta, M., Mariani, M., Panina-Bordignon, P., Turato, G., Buonsanti, C., Baraldo, S., Bellettato, C.M., Papi, A., Corbetta, L., Zuin, R., Sinigaglia, F., Fabbri, L.M., 2002. Increased expression of the chemokine receptor CXCR3 and its ligand CXCL10 in peripheral airways of smokers with chronic obstructive pulmonary disease. Am. J. Respir. Crit. Care Med. 165, 1404–1409. http://dx.doi.org/10.1164/rccm.2107139.

Salvi, S.S., Barnes, P.J., 2009. Chronic obstructive pulmonary disease in non-smokers. Lancet 374, 733–743. http://dx.doi.org/10.1016/S0140-6736(09)61303-9.

Sam, L., Roche, N., Oliver, B.G., Mattos, W., Barnes, P.J., Fan Chung, K., 2000. Balance of matrix metalloprotease-9 and tissue inhibitor of metalloprotease-1 from alveolar macrophages in cigarette smokers: Regulation by interleukin-10. Am. J. Respir. Crit. Care Med. 162, 1355–1360. http://dx.doi.org/10.1164/ajrccm.162.4.9910097.

Shapiro, S.D., Goldstein, N.M., Houghton, a.M., Kobayashi, D.K., Kelley, D., Belaaouaj, A., 2003. Neutrophil elastase contributes to cigarette smoke-induced emphysema in mice. Am. J. Pathol. 163, 2329–2335. http://dx.doi.org/10.1016/S0002-9440(10)63589-4.

Sinden, N.J., Baker, M.J., Smith, D.J., Kreft, J.-U., Dafforn, T.R., Stockley, R.A., 2015. α-1-antitrypsin variants and the proteinase/antiproteinase imbalance in chronic obstructive pulmonary disease. Am. J. Physiol. Lung Cell. Mol. Physiol. 308, L179–L190. http://dx.doi.org/10.1152/ajplung.00179.2014.

Sungprem, K., Khongphatthanayothin, A., Kiettisanpipop, P., Chotivitayatarakorn, P., Poovorawan, Y., Lertsapcharoen, P., 2009. Serum level of soluble intercellular adhesion molecule-1 correlates with pulmonary arterial pressure in children with congenital heart disease. Pediatr. Cardiol. 30, 472–476. http://dx.doi.org/10.1007/s00246-008-9374-1.

Szitter, I., Pintér, E., Perkecz, A., Kemény, Á., Kun, J., Kereskai, L., Pietra, C., Quinn, J.P., Zimmer, A., Berger, A., Paige, C.J., Helyes, Z., 2014. Role of neurokinin 1 receptors in dextran sulfate-induced colitis: studies with gene-deleted mice and the selective receptor antagonist netupitant. Inflamm. Res. 63, 399–409. http://dx.doi.org/10.1007/s00011-014-0712-x.

Takaku, Y., Soma, T., Uchida, Y., Kobayashi, T., Nakagome, K., Nagata, M., 2016. CXC chemokine superfamily induced by Interferon-γ in asthma: a cross-sectional observational study. Asthma Res. Pract. 2, 6. http://dx.doi.org/10.1186/s40733-016-0021-y.

Tam, A., Churg, A., Wright, J.L., Zhou, S., Kirby, M., Coxson, H.O., Lam, S., Man, S.F.P., Sin, D.D., 2015. Sex differences in airway remodeling in a mouse model of chronic obstructive pulmonary disease. Am. J. Respir. Crit. Care Med. 193, 825–834. http://dx.doi.org/10.1164/rccm.201503-0487OC.

Vanoirbeek, J.a.J., Rinaldi, M., De Vooght, V., Haenen, S., Bobic, S., Gayan-Ramirez, G., Hoet, P.H.M., Verbeken, E., Decramer, M., Nemery, B., Janssens, W., 2010. Noninvasive and invasive pulmonary function in mouse models of obstructive and restrictive respiratory diseases. Am. J. Respir. Cell Mol. Biol. 42, 96–104. http://dx.doi.org/10.1165/rcmb.2008-0487OC.

Vestbo, J., Hurd, S.S., Agustí, A.G., Jones, P.W., Vogelmeier, C., Anzueto, A., Barnes, P.J., Fabbri, L.M., Martinez, F.J., Nishimura, M., Stockley, R.a., Sin, D.D., Rodriguez-Roisin, R., 2013. Global strategy for the diagnosis, management, and prevention of chronic obstructive pulmonary disease GOLD executive summary. Am. J. Respir. Crit. Care Med. 187, 347–365. http://dx.doi.org/10.1164/rccm.201204-0596PP.

Viappiani, S., Nicolescu, A.C., Holt, A., Sawicki, G., Crawford, B.D., León, H., van Mulligen, T., Schulz, R., 2009. Activation and modulation of 72 kDa matrix metalloproteinase-2 by peroxynitrite and glutathione. Biochem. Pharmacol. 77, 826–834. http://dx.doi.org/10.1016/j.bcp.2008.11.004.

Vlahos, R., Bozinovski, S., Gualano, R.C., Ernst, M., Anderson, G.P., 2006. Modelling COPD in mice. Pulm. Pharmacol. Ther. 19, 12–17. http://dx.doi.org/10.1016/j.pupt.2005.02.006.

Wang, Y., Jiang, X., Zhang, L., Wang, L., Li, Z., Sun, W., 2014. Simvastatin mitigates functional and structural impairment of lung and right ventricle in a rat model of cigarette smoke-induced COPD. Int. J. Clin. Exp. Pathol. 7, 8553–8562.

Wright, J.L., Churg, A., 2008. Animal models of COPD: barriers, successes, and challenges. Pulm. Pharmacol. Ther. 21, 696–698. http://dx.doi.org/10.1016/j.pupt.2008.01.007.

Yao, H., Hwang, J., Sundar, I.K., Friedman, A.E., McBurney, M.W., Guarente, L., Gu, W., Kinnula, V.L., Rahman, I., 2013. SIRT1 redresses the imbalance of tissue inhibitor of matrix metalloproteinase-1 and matrix metalloproteinase-9 in the development of mouse emphysema and human COPD. Am. J. Physiol. Lung Cell. Mol. Physiol. 305, L615–L624. http://dx.doi.org/10.1152/ajplung.00249.2012.

Ying, S., O'Connor, B., Ratoff, J., Meng, Q., Fang, C., Cousins, D., Zhang, G., Gu, S., Gao, Z., Shamji, B., Edwards, M.J., Lee, T.H., Corrigan, C.J., 2008. Expression and cellular provenance of thymic stromal lymphopoietin and chemokines in patients with severe asthma and chronic obstructive pulmonary disease. J. Immunol. 181, 2790–2798. http://dx.doi.org/10.4049/jimmunol.181.4.2790.

Yoshizaki, K., Brito, J.M., Silva, L.F., Lino-dos-Santos-Franco, A., Frias, D.P., e Silva, R.C.R., Amato-Lourenço, L.F., Saldiva, P.H.N., de Fátima Lopes Calvo Tibério, I., Mauad, T., Macchione, M., 2017. The effects of particulate matter on inflammation of respiratory system: differences between male and female. Sci. Total Environ. http://dx.doi.org/10.1016/j.scitotenv.2017.01.221.

Zhang, N., Inan, S., Cowan, A., Sun, R., Wang, J.M., Rogers, T.J., Caterina, M., Oppenheim, J.J., 2005. A proinflammatory chemokine, CCL3, sensitizes the heat- and capsaicin-gated ion channel TRPV1. Proc. Natl. Acad. Sci. U. S. A. 102, 4536–4541. http://dx.doi.org/10.1073/pnas.0406030102.

Zhang, Y., Cao, J., Chen, Y., Chen, P., Peng, H., Cai, S., Luo, H., Wu, S.-J., 2013. Intraperitoneal injection of cigarette smoke extract induced emphysema, and injury of cardiac and skeletal muscles in BALB/C mice. Exp. Lung Res. 39, 18–31. http://dx.doi.org/10.3109/01902148.2012.745910.

Please cite this article in press as: Kemény, Á., et al., Integrative characterization of chronic cigarette smoke-induced cardiopulmonary comorbidities in a mouse model, Environmental Pollution (2017), http://dx.doi.org/10.1016/j.envpol.2017.04.098

Supplementary material

Integrative characterization of chronic cigarette smoke-induced cardiopulmonary comorbidities in a mouse model

Ágnes Kemény, Kata Csekő, István Szitter, Zoltán V. Varga, Péter Bencsik, Krisztina Kiss, Róbert Halmosi, László Deres, Krisztián Erős, Anikó Perkecz, László Kereskai, Terézia László, Tamás Kiss, Péter Ferdinandy, Zsuzsanna Helyes*

Running title: Chronic smoking-induced pulmonary and cardiac comorbidity mouse model

* Corresponding author: Zsuzsanna Helyes, M.D., Ph.D., D.Sc.
Department of Pharmacology and Pharmacotherapy,
University of Pécs, H-7624 Pécs, Szigeti út. 12., Hungary
Tel.: 36-72-536001/35591, 29043; Fax.: 36-72-536218
e-mail: zsuzsanna.helyes@aok.pte.hu

Author contributions:

Á. Kemény and K. Csekő equally contributed to the present work.

Materials and Methods

Pulmonary function measurement in conscious mice by unrestrained whole-body plethysmography

Airway responsiveness was determined by unrestrained whole-body plethysmography (WBP) with Buxco instrument (PLY3211, Buxco Europe Ltd., Winchester, UK) in conscious, spontaneously breathing animals before the treatment period serving as self-control values and at the end of each months during the 6 months cigarette smoke exposure period. (All measurements were performed on the same animals in a self-controlled manner.) We determined the relaxation time (RT), breathing frequency (f), tidal volume (TV), minute ventilation (MV), inspiratory time (Ti), expiratory time (Te), peak inspiratory flow (PIF) and peak expiratory flow (PEF). These parameters were measured every 10 seconds during a 2 minute acquisition period and were averaged by the BioSystem XA Software for Windows (Buxco Research Systems) (Elekes et al., 2008).

Pulmonary function measurement in anaesthetized tracheotomized mice by restrained whole-body plethysmography

At the end of the 6^{th} month mice were anaesthetized with intraperitoneal administration of ketamine and xylazine. Mice were tracheotomized and placed in a whole-body plethysmograph (PLY4111, Buxco Europe Ltd., Winchester, UK) for measuring invasive resistance and compliance. The tracheal tube was connected to a mouse ventilator (MiniVent Type 845, Hugo Sach Elektronik - Harvard apparatus GmbH, March-Hugstetten, Germany) with a frequency of 120 strokes/min, and a stroke volume of 200 μl. After loading the animal a water-coupled tube was inserted to the esophagus to isolate the airway in the resistance calculations. The flow and pressure transducers (TRD5700 and TRD4515 Buxco Europe Ltd., Winchester, UK) were

connected to the preamplifier module, which digitized the signals via an analog-to-digital converter (MAX2270 Buxco Europe Ltd., Winchester, UK). All respiratory parameters (airway resistance (RI), end-expiratory work (EEW), tidal mid-expiratory flow (EF50), end-expiratory pause (EEP), Te and Ti) were measured every 10 seconds during a 10 minute baseline reading period and were averaged by the BioSystem XA Software for Windows (Buxco Research Systems).

Computed lung microtomography (CT)

Structural changes of the lungs were imaged by breath-gated tomography on a Skyscan 1176 high resolution microtomograph (Skyscan, Kontich, Belgium) at the end of each month in a self-controlled manner. Mice were anaesthetized with pentobarbital (70 mg/kg) i.p. and placed in supine position on the bed of the scanner, a piece of paper was placed onto the chest with a high-contrast sign to enable the video gating of the breathing movements to eliminate motion artefacts. Scanning parameters were the following: 50kV tube voltage, 500 µA tube current, 0.5 mm Al filter, 180 degree scan, 0.7 degree rotation angle between each camera angle and 10 acquired images per step. Pixel size was kept on 35 µm. One field of view (FOV) covered the whole lung. With these settings one scan took about 12-15 minutes and provided a good combination of sufficient resolution, short scan time and low radiation. After sorting the images into 5 bins (stacks) of images, each bin contained at least 2 images, based on the video gating signal. The bins represent a certain phase of breathing cycle. One of the bins was chosen for reconstruction with following settings: ring artefact correction was set at 20, 35% beam hardening correction, smoothing was set at 5. Reconstruction and morphometric analysis were performed with a software package provided by the manufacturer. Image analysis was performed according to the manuscript of De Langhe et al. (de Langhe et al., 2012). Briefly, air-filled pixels outside the animals were excluded from reconstructed images using a

previously reconstructed image of a phantom with air-containing Eppendorf tube and using a "despeckle" command. The resulting images were reloaded and thresholding was repeated to determine the air filled areas within the lung (with an additional "despeckle" command). Emphysema was calculated by the ratio of LAA (low-attenuation area, from -750 to -1000 Hounsfield unit, representing the air-filled regions) and total lung volume (TLV) and was expressed in percentage (Kobayashi et al., 2013).

Histopathological evaluation: measurement of acinar air space complex and semiquantitative scoring of the lung sections

The mean linear intercept (chord) length (L_m), a widely used parameter to quantify distal air space enlargement, was measured to evaluate the size of the acinar air space complex related to emphysema (Knudsen et al., 2010). Slides were scanned by a Pannoramic DESK scanner (3DHISTECH Ltd., Hungary) and the alveolar space or alveolar and ductal air space together were measured along parallel test lines by using the Case Viewer software (3DHISTECH Ltd., Hungary). At least 3 sections were evaluated from each mouse from different depths to obtain reliable results, tissue shrinkage or integrity damage were not observed (n=80-100 measurements per mouse). Histopathological analysis of lung sections was performed by a pathologist in a blind manner in order to evaluate perivascular/peribronchial edema, acute and chronic inflammation, interstitial acute and chronic inflammation, epithelial damage and goblet cells. Scores were assessed by observing several representative microscopic fields on a semiquantitative scale ranging from scores 0-3 (0 - normal, 1 – mild, 2 – moderate and 3 – severe histopathological alterations in the examined parameters).

Bronchoalveolar lavage fluid (BALF) analysis with flow cytometry

After data collection at the end of each month of 6 months smoking period, mice were anaesthetized with pentobarbital (70 mg/kg i.p.), lungs were flushed with cold phosphate buffered saline (PBS, 5x1 ml) with the help of a trachea cannula and BALFs were collected. They were centrifuged at 1000 rpm for 5 minutes at room temperature, then stained and fixed for flow cytometry as follows: cells were resuspended in 500 µl staining solution (PBS with 0.1% BSA and 0.1% NaN_3) and incubated with 1 µl FITC-CD45 (mouse IgG1, Becton Dickinson, San Jose, CA) as a panleukocyte marker and 1 µl propidium iodine (PI, Sigma-Aldrich, Budapest, Hungary) to exclude cellular debris for 30 min at room temperature in the dark. After the incubation, samples were centrifuged and washed, then resuspended in PBS with 2% neutral-buffered formalin. Cell preparations were immediately analyzed with CyFlow Space flow cytometer (Partec, Germany). Total cell count and the ratio of lymphocytes, monocytes and granulocytes were calculated regarding their FSC/SSC feature. Gating was determined from mouse peripheral blood sample as control (Calvelli et al., 1993; Ma et al., 2001).

Detection of MMP-2 and MMP-9 activities by gelatin zymography in the lung

To measure pulmonary MMP-2 and MMP-9 activities, gelatin zymography was performed from mouse lung samples. MMP-2 has 2 major isoforms, 72 kDa and 64 kDa (DeCoux et al., 2014). Basically, the 64 kDa MMP-2 activated by limited proteolysis is the enzyme's active form, but via an alternative way, 72 kDa MMP-2 can also be activated. The same can be observed in case of MMP-9: 86 kDa MMP-9 is the cleaved active form, but 92 kDa MMP-9 can also gain activity. Gelatinolytic activities of these MMP isoforms were examined as previously described (Kupai et al., 2010). Briefly, 8% polyacrylamide gels were copolymerized with gelatin (2 mg/ml, type A from porcine skin, Sigma-Aldrich), and 50 µg of protein per lane

was loaded. An internal standard (American Type Culture Collection, Manassas, VA) was loaded into each gel to normalize activities between gels. After electrophoresis (90 V, 90 min), gels were washed with zymogram renaturation buffer (Bio-Rad Laboratories, Hercules, CA) for 40 min. Lung samples were incubated for 20 h and at 37°C in zymogram development buffer (Bio-Rad Laboratories, Hercules, CA). Gels were then stained with 0.05% Coomassie brilliant blue (G-250, Sigma-Aldrich) in a mixture of methanol-acetic acid-water [2.5:1:6.5 (vol/vol)] and destained in aqueous 4% methanol-8% acetic acid (vol/vol). For positive controls, gelatinase zymography standard containing human MMP-2 and -9 (Chemicon Europe Ltd., Southampton, UK) were used. For negative control, lanes containing tissue samples were cut off after renaturation of the gel and were separately incubated for 20 h at 37°C in development buffer in the presence of the calcium chelator EGTA (ethylene glycol-bis(2-aminoethylether)-N,N,N′,N′-tetraacetic acid; 10 mM). Gelatinolytic activities were detected as transparent bands against the dark-blue background. Gels were scanned in a transilluminator and band intensities were quantified, expressed as the ratio to the internal standard, and presented in arbitrary units.

Cytokine profile analysis

Excised lung and heart tissues were thawed, weighed and immediately homogenized in PBS containing 1% protease inhibitor phenylmethylsulfonyl fluoride (PMSF, Sigma-Aldrich, Budapest, Hungary), and centrifuged at 10,000 g for 5 min to remove cell debris. Triton X-100 was added to a final concentration of 1%. Blood samples from 6 months smoking and intact animals were left to clot in room temperature for 30 min, then centrifuged for 20 min at 2000g. Serum was removed and processed as follows. Total protein content of the homogenates and serum samples were determined prior to cytokine measurement with BioRad DC protein assay kit. Samples were diluted regarding their total protein content in 1 g wet tissue or in 1 ml serum. Forty different inflammatory cytokines were determined simultaneously with Mouse Cytokine

Array Panel A (R&D Systems) according to the manufacturer's instruction. Briefly, capture antibodies of forty pre-selected cytokines were spotted in duplicate on nitrocellulose membrane. Diluted samples and biotinylated detection antibody mixtures were incubated on the membranes overnight. Chemiluminescent detection was performed on the 2nd day and semiquantitative analysis based on densitometry was done with ImageJ freeware. To eliminate the interassay variability all data were re-calculated with the same control-spot densities (Szitter et al., 2014). Cytokine heat map was generated by Matrix2png 1.2.1 online freeware (Pavlidis and Noble, 2003).

Noninvasive evaluation of cardiac functions and dimensions

At the start of the experiment, all animals were examined by echocardiography to exclude mice with any heart abnormalities. Transthoracic echocardiography was performed under volatile/isoflurane anesthesia in every month during the 6-month-long period. Mice were slightly anesthetized with a mixture of 1.0% isoflurane (Forane, Abbott Laboratories, Hungary) and 99.0% oxygen. The chest of animals was shaved, acoustic coupling gel was applied and warming pad was used to maintain normothermia. Mice were imaged in the left lateral decubitus position by a VEVO 770 high-resolution ultrasound imaging system (VisualSonics Vevo 770® High-Resolution Imaging System, Toronto, Canada) equipped with a mouse cardiac transducer (30 MHz). LV ejection fraction (EF), LV end-diastolic volume (LVEDV), LV end-systolic volume (LVESV) and the thickness of septum and posterior wall were measured from the parasternal short- and long-axis views at the mid-papillary level. EF (%) was calculated from the M-mode images (100x(LVEDV-LVESV)/LVEDV). The tricuspid annular plane systolic excursion (TAPSE) - a parameter of the systolic right ventricular function - and deceleration time (DT) - a parameter of the diastolic left ventricular function - were determined from the apical 4 chamber view (Respress and Wehrens, 2010).

Statistics

Values for all measurements were expressed as the mean ±SEM of n=6 mice in each group with the exception of restrained WBP (n=5 per group) and cytokine determination of lung and heart homogenates (n=3 per group). Evaluation of the unrestrained WBP, echocardiography and micro-CT results have been performed by repeated measures ANOVA followed by Bonferroni's modified t-test to see statistical differences between different data sets and then between the respective data points. Data collected from BALF flow cytometry and mean linear intercept length (80-100 measurements/slides) were analyzed with two-way ANOVA followed by Sidak's multiple comparison test. Expression level of forty different cytokines was statistically compared to intact values with two-way ANOVA followed by Bonferroni's post-test. Restrained WBP and gelatin zymography results were analyzed by Student's t-test for unpaired comparison. Evaluation of the semiquantitative histopathological scoring was analyzed by Kruskal-Wallis followed by Dunn's multiple comparison test to observe intragroup differences by time, while Mann-Whitney test was performed to analyze intergroup differences at given time points.

Power of the study

The adequate sample size was calculated on the basis of the "resource equation" method (Charan and Kantharia, 2013). We used altogether 72 animals, 6 animals per time point and per group to suit the requirements of both the adequate scientific requirements and ethical considerations determined by the 3R regulation. To avoid systemic error all groups were handled simultaneously.

Reference

Calvelli, T., Denny, T.N., Paxton, H., Gelman, R., Kagan, J., 1993. Guideline for flow cytometric immunophenotyping: A report from the national institute of allergy and infectious diseases, division of AIDS. Cytometry 14, 702–715. doi:10.1002/cyto.990140703

Charan, J., Kantharia, N.D., 2013. How to calculate sample size in animal studies? J. Pharmacol. Pharmacother. 4, 303–6. doi:10.4103/0976-500X.119726

de Langhe, E., Vande Velde, G., Hostens, J., Himmelreich, U., Nemery, B., Luyten, F.P., Vanoirbeek, J., Lories, R.J., 2012. Quantification of lung fibrosis and emphysema in mice using automated micro-computed tomography. PLoS One 7. doi:10.1371/journal.pone.0043123

DeCoux, A., Lindsey, M.L., Villarreal, F., Garcia, R.A., Schulz, R., 2014. Myocardial matrix metalloproteinase-2: inside out and upside down. J. Mol. Cell. Cardiol. 77, 64–72. doi:10.1016/j.yjmcc.2014.09.016

Elekes, K., Helyes, Z., Kereskai, L., Sándor, K., Pintér, E., Pozsgai, G., Tékus, V., Bánvölgyi, Á., Németh, J., Szuts, T., Kéri, G., Szolcsányi, J., 2008. Inhibitory effects of synthetic somatostatin receptor subtype 4 agonists on acute and chronic airway inflammation and hyperreactivity in the mouse. Eur. J. Pharmacol. 578, 313–322. doi:10.1016/j.ejphar.2007.09.033

Knudsen, L., Weibel, E.R., Gundersen, H.J.G., Weinstein, F. V, Ochs, M., 2010. Assessment of air space size characteristics by intercept (chord) measurement: an accurate and efficient stereological approach. J. Appl. Physiol. 108, 412–421. doi:10.1152/japplphysiol.01100.2009

Kobayashi, S., Fujinawa, R., Ota, F., Kobayashi, S., Angata, T., Ueno, M., Maeno, T., Kitazume, S., Yoshida, K., Ishii, T., Gao, C., Ohtsubo, K., Yamaguchi, Y., Betsuyaku, T., Kida, K., Taniguchi, N., 2013. A single dose of lipopolysaccharide into mice with emphysema mimics human Chronic obstructive pulmonary disease exacerbation as assessed by micro-computed tomography. Am. J. Respir. Cell Mol. Biol. 49, 971–977. doi:10.1165/rcmb.2013-0074OC

Kupai, K., Szucs, G., Cseh, S., Hajdu, I., Csonka, C., Csont, T., Ferdinandy, P., 2010. Matrix metalloproteinase activity assays: Importance of zymography. J. Pharmacol. Toxicol. Methods 61, 205–209. doi:10.1016/j.vascn.2010.02.011

Ma, W., Cui, W., Lin, Q., 2001. Improved immnunophenotyping of lymphocytes in bronchoalveolar lavage fluid (BALF) by flow cytometry. Clin. Chim. Acta 313, 133–138. doi:10.1016/S0009-8981(01)00664-7

Pavlidis, P., Noble, W.S., 2003. Matrix2png: a utility for visualizing matrix data. Bioinformatics 19, 295–296. doi:10.1093/bioinformatics/19.2.295

Respress, J.L., Wehrens, X.H.T., 2010. Transthoracic echocardiography in mice. J. Vis. Exp. 3–5. doi:10.3791/1738

Szitter, I., Pintér, E., Perkecz, A., Kemény, Á., Kun, J., Kereskai, L., Pietra, C., Quinn, J.P., Zimmer, A., Berger, A., Paige, C.J., Helyes, Z., 2014. Role of neurokinin 1 receptors in dextran sulfate-induced colitis: Studies with gene-deleted mice and the selective receptor antagonist netupitant. Inflamm. Res. 63, 399–409. doi:10.1007/s00011-014-0712-x

Figure legends

Figure E1

Unrestrained whole-body plethysmography (WBP) parameters before the treatment period (0 month) and at the end of each month during the 6-month cigarette smoke exposure period. Panel A: relaxation time (RT). B: frequency (f), C: tidal volume (TV), D: minute ventilation (MV) E: time of inspiration (Ti), F: time of expiration (Te), G: peak inspiratory flow (PIF) and H: peak expiratory flow (PEF) during the 6-month experiment. N=6 per group.

Figure E2

Weight change in percentage correlated to the initial body weight measurement of the animals before the treatment period (0 month – 0%) and at the end of each month during the 6-month cigarette smoke exposure period. N=6 per group (****$p<0.0001$ vs. intact controls)

Figure E3

Time-dependent characteristic pulmonary and cardiac pathophysiological alterations in relation to tissue sICAM-1 levels in the chronic cigarette smoke-exposure-induced mouse COPD model.

Figures

Figure E1

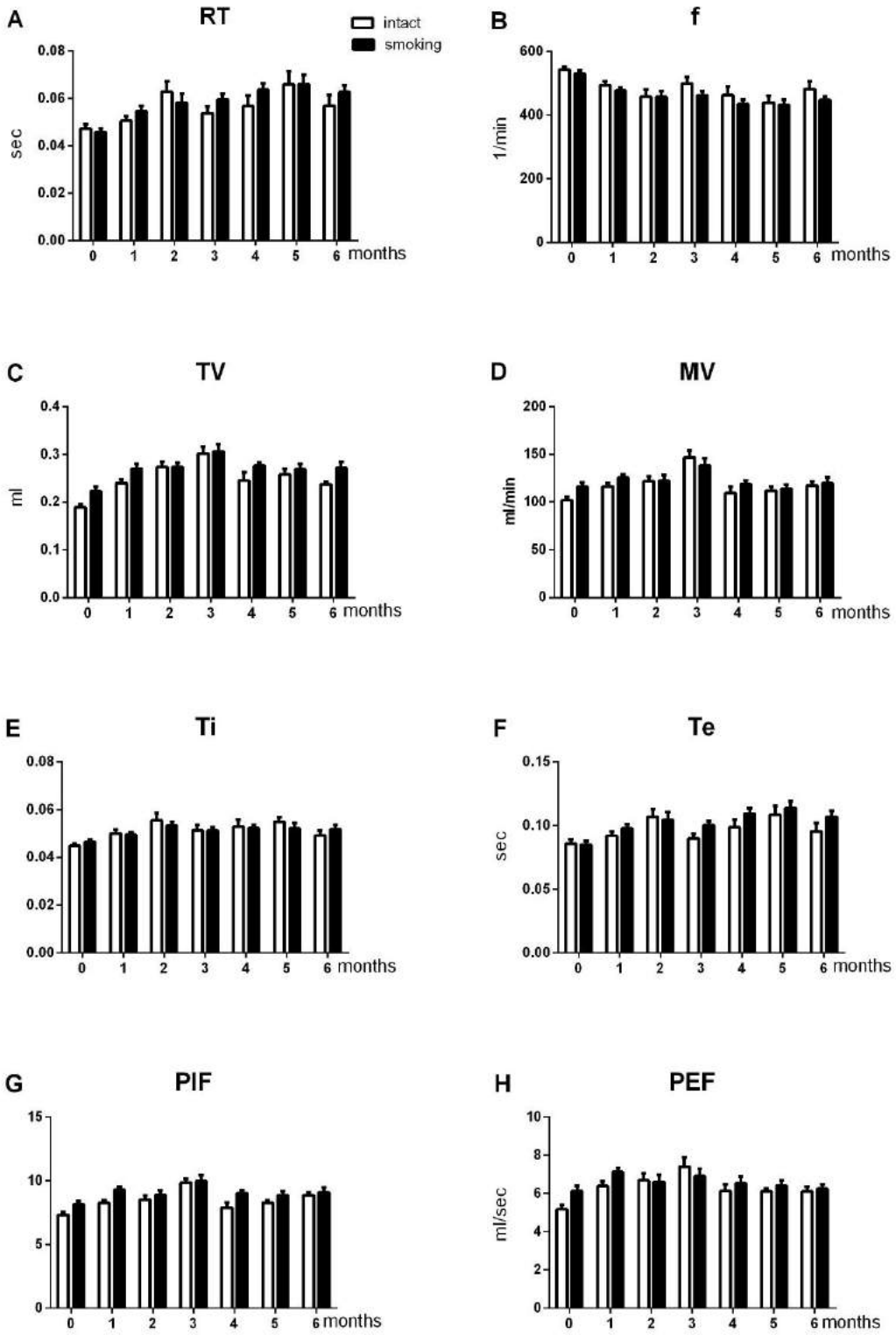

Figure E2

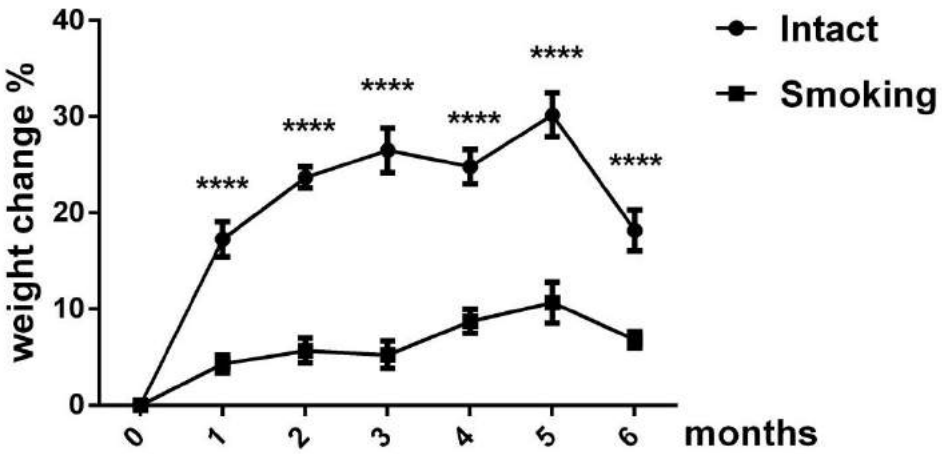

Figure E3

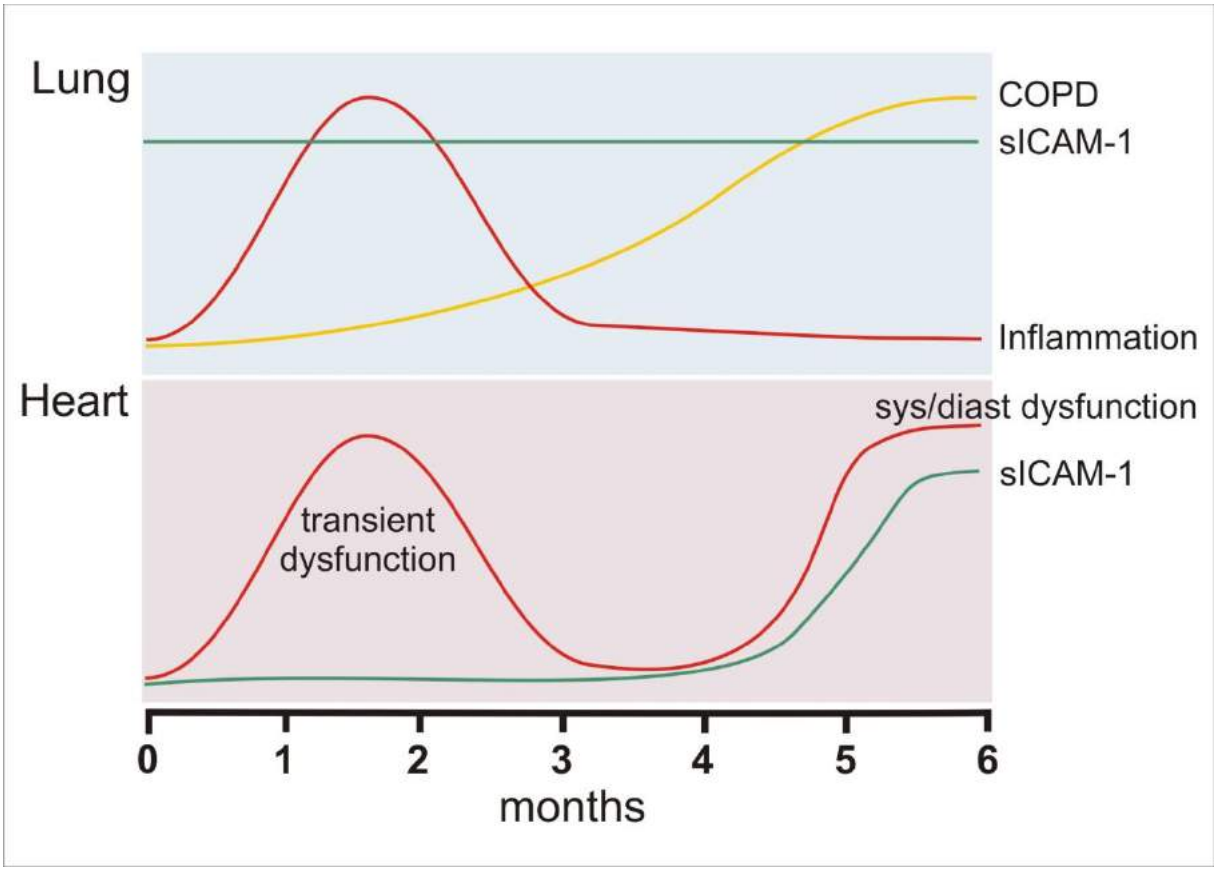

International Journal of
Molecular Sciences

MDPI

Article

Complex Regulatory Role of the TRPA1 Receptor in Acute and Chronic Airway Inflammation Mouse Models

Zsófia Hajna [1,†], Kata Csekő [1,*,†], Ágnes Kemény [1,2], László Kereskai [3], Tamás Kiss [1], Anikó Perkecz [1], István Szitter [1], Béla Kocsis [4], Erika Pintér [1,5] and Zsuzsanna Helyes [1,5]

1 Department of Pharmacology and Pharmacotherapy, Medical School and János Szentágothai Research Centre & Centre for Neuroscience, University of Pécs, H-7624 Pécs, Hungary; zsofia.hajna@aok.pte.hu (Z.H.); kemenyagnes1@gmail.com (Á.K.); kiss891012@gmail.com (T.K.); perkecz@gmail.com (A.P.); szitteristvan@gmail.com (I.S.); erika.pinter@aok.pte.hu (E.P.); zsuzsanna.helyes@aok.pte.hu (Z.H.)
2 Department of Medical Biology, University of Pécs, Medical School, H-7624 Pécs, Hungary
3 Department of Pathology, University of Pécs, Medical School, H-7624 Pécs, Hungary; kereskai.laszlo@pte.hu
4 Department of Medical Microbiology and Immunology, University of Pécs, Medical School, H-7624 Pécs, Hungary; kocsis.bela@pte.hu
5 PharmInVivo Ltd., H-7629 Pécs, Hungary
* Correspondence: csekoe.kata@gmail.com; Tel.: +36-72-536-000 (ext. 35386)
† These authors contributed equally to this work.

Received: 5 May 2020; Accepted: 7 June 2020; Published: 9 June 2020

Abstract: The Transient Receptor Potential Ankyrin 1 (TRPA1) cation channel expressed on capsaicin-sensitive afferents, immune and endothelial cells is activated by inflammatory mediators and exogenous irritants, e.g., endotoxins, nicotine, crotonaldehyde and acrolein. We investigated its involvement in acute and chronic pulmonary inflammation using *Trpa1* gene-deleted (*Trpa1*$^{-/-}$) mice. Acute pneumonitis was evoked by intranasal *Escherichia coli* endotoxin (lipopolysaccharide: LPS) administration, chronic bronchitis by daily cigarette smoke exposure (CSE) for 4 months. Frequency, peak inspiratory/expiratory flows, minute ventilation determined by unrestrained whole-body plethysmography were significantly greater, while tidal volume, inspiratory/expiratory/relaxation times were smaller in *Trpa1*$^{-/-}$ mice. LPS-induced bronchial hyperreactivity, myeloperoxidase activity, frequency-decrease were significantly greater in *Trpa1*$^{-/-}$ mice. CSE significantly decreased tidal volume, minute ventilation, peak inspiratory/expiratory flows in wildtypes, but not in *Trpa1*$^{-/-}$ mice. CSE remarkably increased the mean linear intercept (histopathology), as an emphysema indicator after 2 months in wildtypes, but only after 4 months in *Trpa1*$^{-/-}$ mice. Semiquantitative histopathological scores were not different between strains in either models. TRPA1 has a complex role in basal airway function regulation and inflammatory mechanisms. It protects against LPS-induced acute pneumonitis and hyperresponsiveness, but is required for CSE-evoked emphysema and respiratory deterioration. Further research is needed to determine TRPA1 as a potential pharmacological target in the lung.

Keywords: bronchitis; cigarette smoke; COPD; emphysema; LPS; pneumonitis; whole body plethysmography

1. Introduction

The Transient Receptor Potential Ankyrin 1 (TRPA1) receptor is the sole member of the "ankyrin" subfamily of the Transient Receptor Potential (TRP) receptors in mammals. It is predominantly

expressed on capsaicin-sensitive peptidergic sensory nerves densely innervating the lungs [1,2]. TRPA1 is a large transmembrane protein forming a ligand-gated non-selective cation channel [3,4].

TRPA1 is activated by several exogenous stimuli, such as bacterial endotoxin [5] and environmental irritants like acrolein, crotonaldehyde, nicotine and isocyanates [6–10], found in cigarette smoke, wood smoke, diesel exhaust and tear gas [6,7,10–13]. Moreover, several endogenous mediators produced during inflammation and oxidative stress, such as lipid peroxidation products, e.g., 4-hydroxynonenal (HNE) and 4-oxo-2-nonenal (4-ONE) [14–16], reactive oxygen species (ROS) [17], hydrogen sulfide, bradykinin and prostanoids stimulate TRPA1 [18–22]. Electrophilic compounds activate the receptor by covalently binding to the reactive cysteine residues at the intracellular N-terminal region [23–26]. Bradykinin and prostaglandins sensitize TRPA1 [22,27] through protein kinase A (PKA)-mediated phosphorylation [28,29]. Moreover, TRPA1 is also involved in protease activated receptor 1 (PAR1)/Gq-mediated increase of the intracellular Ca^{2+}-level [30,31].

Pro-inflammatory sensory neuropeptides, e.g., substance P (SP) and calcitonin gene-related peptide (CGRP) are released in response to TRPA1 activation leading to neurogenic inflammation (vasodilatation and plasma protein extravasation) [32]. Simultaneously with these pro-inflammatory mediators, anti-inflammatory neuropeptides, e.g., somatostatin and pituitary adenylate cyclase activating polypeptide are also released from the same terminals counteracting the inflammatory process [33,34].

TRPA1 is also expressed on several non-neuronal cells [35], e.g., keratinocytes, macrophages and CD4+ lymphocytes [36–38], epidermal melanocytes, fibroblasts [39,40], urothelial and endothelial cells, as well as primary human osteoarthritic chondrocytes [41–43]. In the airways, TRPA1 is expressed on fibroblasts, tracheal, bronchial and alveolar epithelial cells, bronchial smooth muscle cells (SMC), as well as lymphocytes [17,44–50].

Due to its polymodal chemosensor function and its wide expression pattern, TRPA1 has been addressed as having a key role in physiological and pathophysiological processes, particularly in neuro-immune interactions [51–53]. It is suggested to be a particularly important chemical sensor in the respiratory system, playing a role in physiological (protective reflexes, cough and sneeze) and pathophysiological responses (inflammation, bronchial hyperreactivity) [54–56]. Although increasing evidence suggests TRPA1 involvement in the pathogenesis of chronic obstructive pulmonary disease (COPD), asthma, chronic cough, cystic fibrosis etc., pointing to the important therapeutic potential of TRPA1 in the pharmacological treatment of chronic pulmonary diseases [26,46,54,57–62], there are few in vivo data concerning its function in airway inflammation. Therefore, the results are far from being conclusive and more information is needed to determine the significance of TRPA1 as a possible pharmacological target in inflammatory lung disease, pneumonitis and COPD.

Therefore, in the present study we investigated the involvement of TRPA1 in the in vivo models of endotoxin (lipopolisaccharide: LPS)-induced acute and cigarette smoke exposure-induced chronic pulmonary inflammation with the help of TRPA1 wildtype (*Trpa1*$^{+/+}$) and gene-deficient (*Trpa1*$^{-/-}$) mice.

2. Results

2.1. Differences in Basal Airway Function Parameters of *Trpa1*$^{+/+}$ and *Trpa1*$^{-/-}$ Mice

Under intact conditions, frequency (f), minute ventilation (MV), peak inspiratory flow (PIF) and peak expiratory flow (PEF) were significantly greater, tidal volume (TV), inspiratory time (Ti), expiratory time (Te) and relaxation time (RT) were significantly smaller, while no difference was detected in the enhanced pause (Penh) of *Trpa1*$^{-/-}$ mice compared to their wildtype counterparts, measured by unrestrained whole body plethysmography (WBP) (Figure 1).

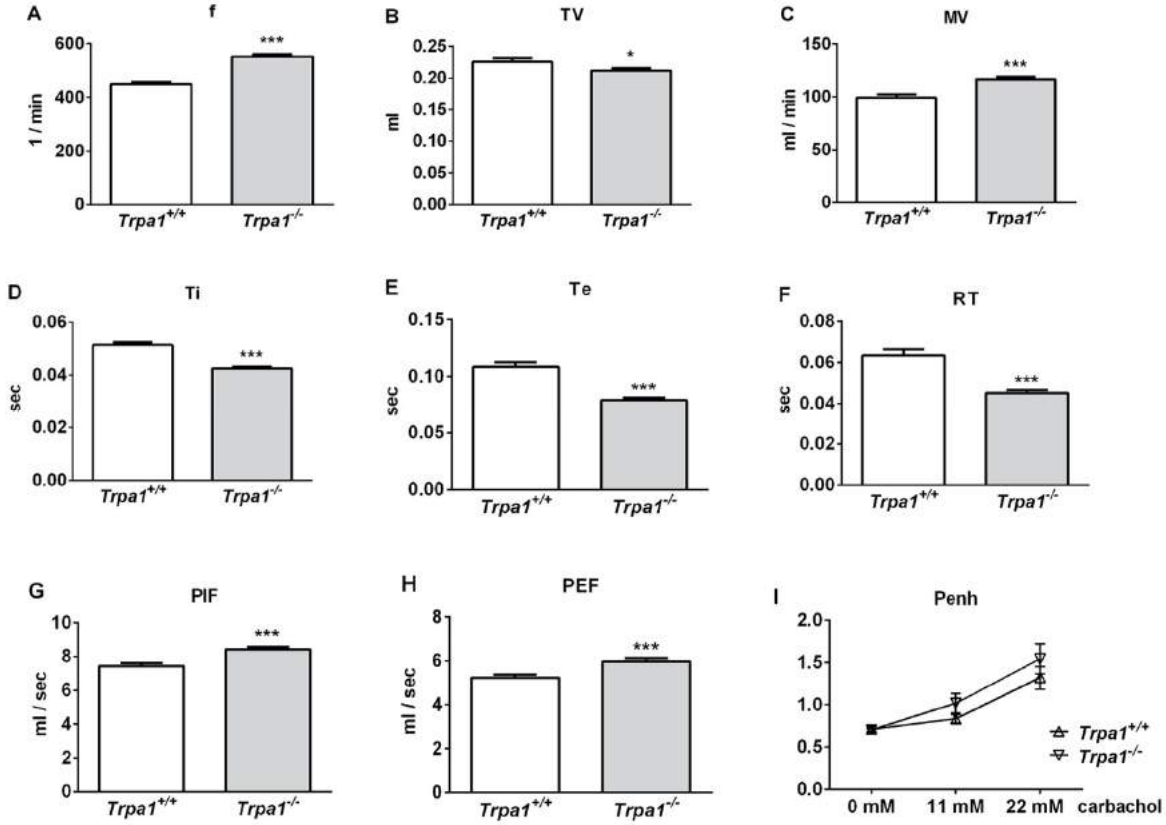

Figure 1. Comparison of the basal airway functions of intact *Trpa1*$^{+/+}$ and *Trpa1*$^{-/-}$ mice measured by unrestrained whole-body plethysmography. (**A**) Breathing frequency (f), (**B**) tidal volume (TV), (**C**) minute ventilation (MV), (**D**) inspiratory time (Ti), (**E**) expiratory time (Te), (**F**) relaxation time (RT), (**G**) peak inspiratory flow (PIF) and (**H**) peak expiratory flow (PEF) were measured in conscious, spontaneously breathing mice. (**I**) Enhanced pause (Penh) correlating with bronchial responsiveness was assessed by the nebulization of the muscarinic receptor agonist, carbachol. Values represent the means ± SEM, n = 30–35 mice/group; Student's t-test for unpaired comparison; * $p < 0.05$; *** $p < 0.001$.

2.2. Endotoxin-Induced Bronchial Hyperreactivity is Greater in *Trpa1*$^{-/-}$ Mice

Bronchial responsiveness characterized by the Penh parameter significantly and concentration-dependently elevated in the *Trpa1*$^{-/-}$ mice in response to increasing concentrations of the muscarinic receptor agonist carbachol 24 h after the administration of intranasal LPS. This indicates the development of inflammatory airway hyperreactivity, which was significantly greater in the TRPA1-deficient mice compared to the LPS-treated wildtypes (Figure 2A).

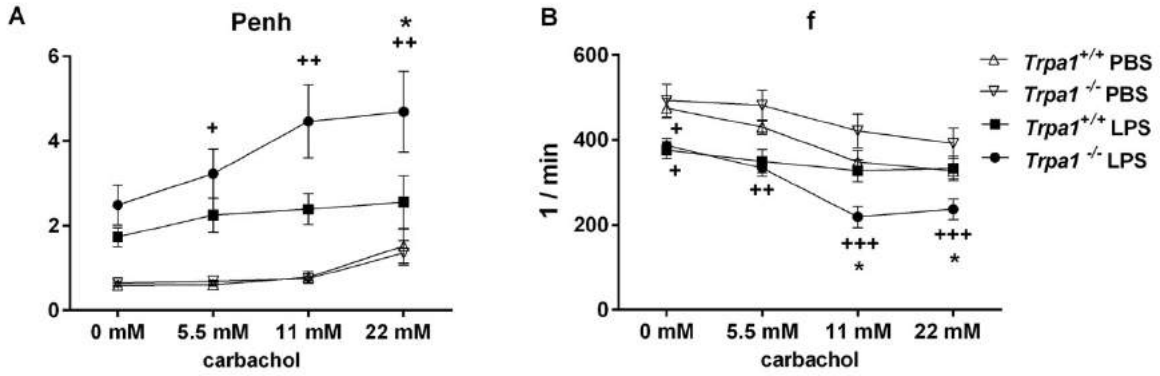

Figure 2. Inflammatory airway hyperreactivity: (**A**) carbachol-induced bronchoconstriction and (**B**) changes in breathing frequency. Carbachol-evoked bronchoconstriction remarkably increased, and the decrease in breathing frequency was significantly greater in *Trpa1*$^{-/-}$ mice 24 h after LPS administration, but not in the wildtypes. Values represent the means ± SEM, n = 5–10 mice/group; two-way ANOVA followed by Tukey's post-test; $^{+}$ $p < 0.05$, $^{++}$ $p < 0.005$, $^{+++}$ $p < 0.001$ vs. PBS-treated respective group; * $p < 0.05$ vs. LPS-treated *Trpa1*$^{+/+}$.

LPS inhalation significantly reduced basal f in both strains. In response to carbachol, f did not change in *Trpa1*$^{+/+}$ mice, but it significantly declined in a concentration-dependent manner in the *Trpa1*$^{-/-}$ ones, being significantly lower compared to the wildtypes at 11 and 22 mM carbachol stimuli (Figure 2B).

Interestingly, the mild, although significant breathing frequency difference between the wildtype and knockout groups found under intact conditions was not observable in this model, most probably because of the different study setting and the use of phosphate buffer saline (PBS) in the control group.

2.3. Endotoxin-Induced Histological Alterations Show No Difference in the Case of TRPA1-Deficiency

In comparison to the PBS-treated mouse groups (Figure 3A,B) LPS administration induced remarkable oedema formation and inflammatory cell infiltration (Figure 3C,D) in the lung tissue. Based on the semiquantitative histopathological evaluation perivascular/peribronchial oedema and neutrophil granulocyte infiltration (Figure 4A) were significantly higher 24 h after LPS treatment, and the extent of goblet cell hyperplasia also increased, although not significantly. There was no statistical difference in the extent of endotoxin-induced airway inflammation scores between *Trpa1*$^{+/+}$ and *Trpa1*$^{-/-}$ mice (Figure 4A,B).

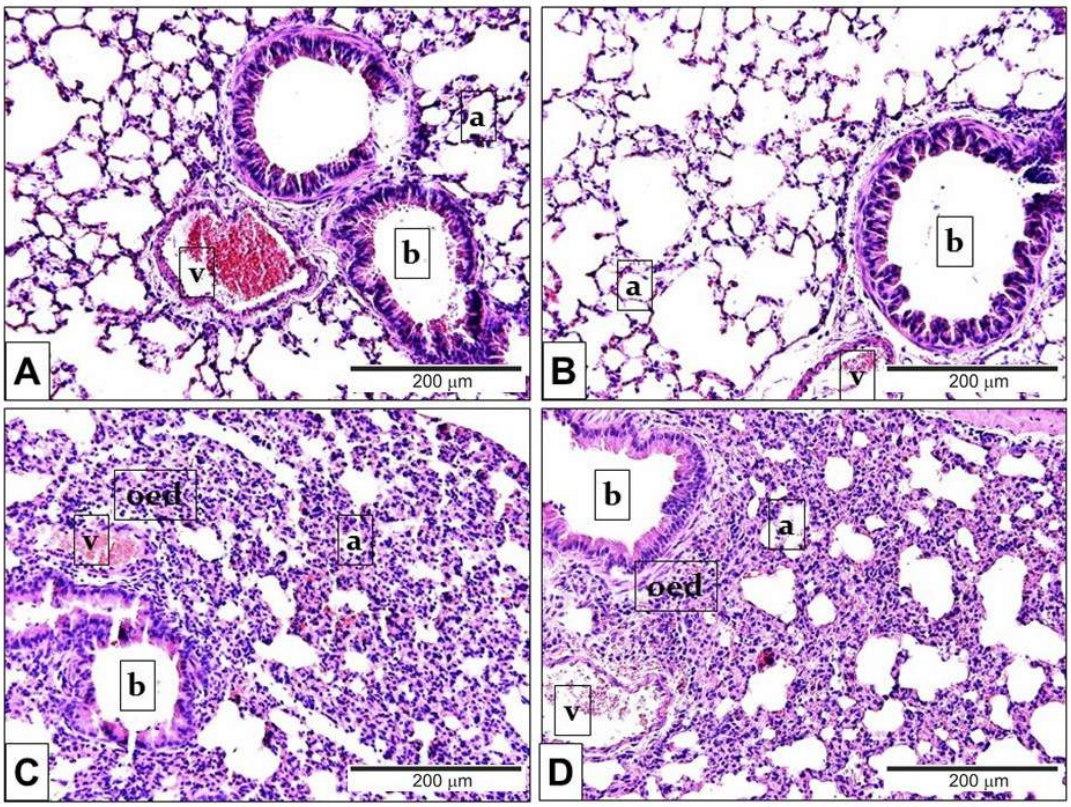

Figure 3. Representative histological pictures of LPS-induced pulmonary alterations. Compared to the PBS-treated (**A**) *Trpa1*$^{+/+}$ and (**B**) *Trpa1*$^{-/-}$ control groups, the lung tissue of LPS-treated (**C**) *Trpa1*$^{+/+}$ and (**D**) *Trpa1*$^{-/-}$ mice exhibited remarkable perivascular and peribronchial oedema, neutrophil granulocyte accumulation, macrophage infiltration and goblet cell hyperplasia (hematoxylin-eosin staining; 200× *g* magnification; a: alveolus, b: bronchiolus, v: venula, oed: oedema).

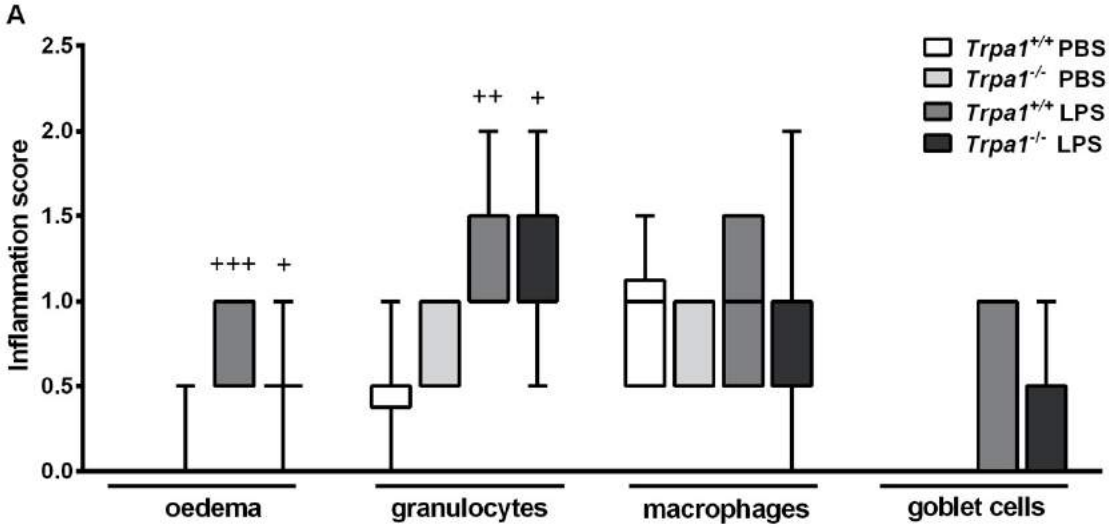

Figure 4. *Cont.*

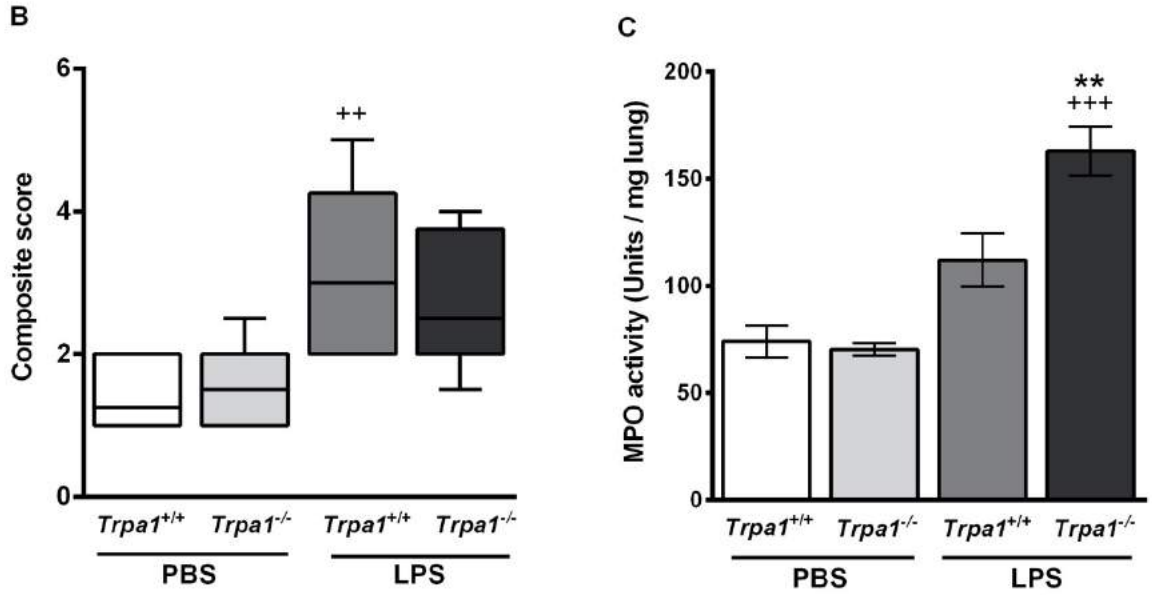

Figure 4. Semiquantitative histopathological evaluation and determination of the myeloperoxidase (MPO) activity of the lung 24 h after LPS inhalation. No significant difference was observed in the (**A**) detailed and (**B**) composite scores of histopathological inflammatory parameters between the *Trpa1*$^{+/+}$ and *Trpa1*$^{-/-}$ groups. Boxplots represent the minimum, first quartile, mean, third quartile and maximum values, n = 7–13/group, Kruskal–Wallis followed by Dunn's post-test; $^{+}$ $p < 0.05$, $^{++}$ $p < 0.005$, $^{+++}$ $p < 0.001$ vs. PBS-treated *Trpa1*$^{+/+}$. (**C**) LPS administration increased myeloperoxidase activity in the lung, which was significantly elevated in *Trpa1*$^{-/-}$ compared to the wildtypes. Values represent the means ± SEM, n = 5–8 mice/group; one-way ANOVA followed by Bonferroni's post-test; $^{+++}$ $p < 0.001$ vs. PBS-treated respective group; ** $p < 0.01$ vs. LPS-treated *Trpa1*$^{+/+}$.

2.4. Endotoxin-Induced Myeloperoxidase Activity in the Lung is Greater in Trpa1$^{-/-}$ *Mice*

Myeloperoxidase (MPO) enzyme activity correlating with the activated neutrophil granulocytes and macrophages increased 24 h after LPS-inhalation in both strains, however it was significantly greater in *Trpa1*$^{-/-}$ mice compared to the wildtypes (Figure 4C).

2.5. Chronic Cigarette Smoke Induces Respiratory Function Alterations in Trpa1$^{+/+}$*, but not in Trpa1*$^{-/-}$ *Mice*

Respiratory functions were measured in a follow-up design before and at the end of each month in the 4-month long protocol of cigarette smoke exposure (CSE). CSE induced a gradual and significant decrease in TV, MV, PIF and PEF in *Trpa1*$^{+/+}$ mice with a peak at 3 months, which was not present in the *Trpa1*$^{-/-}$ animals (Figure 5). The significant differences in f, Ti, Te and RT measured in the *Trpa1*$^{-/-}$ mice were attributable to the significant differences between the wildtype and gene-deficient mice observed already in the intact animals, before CSE.

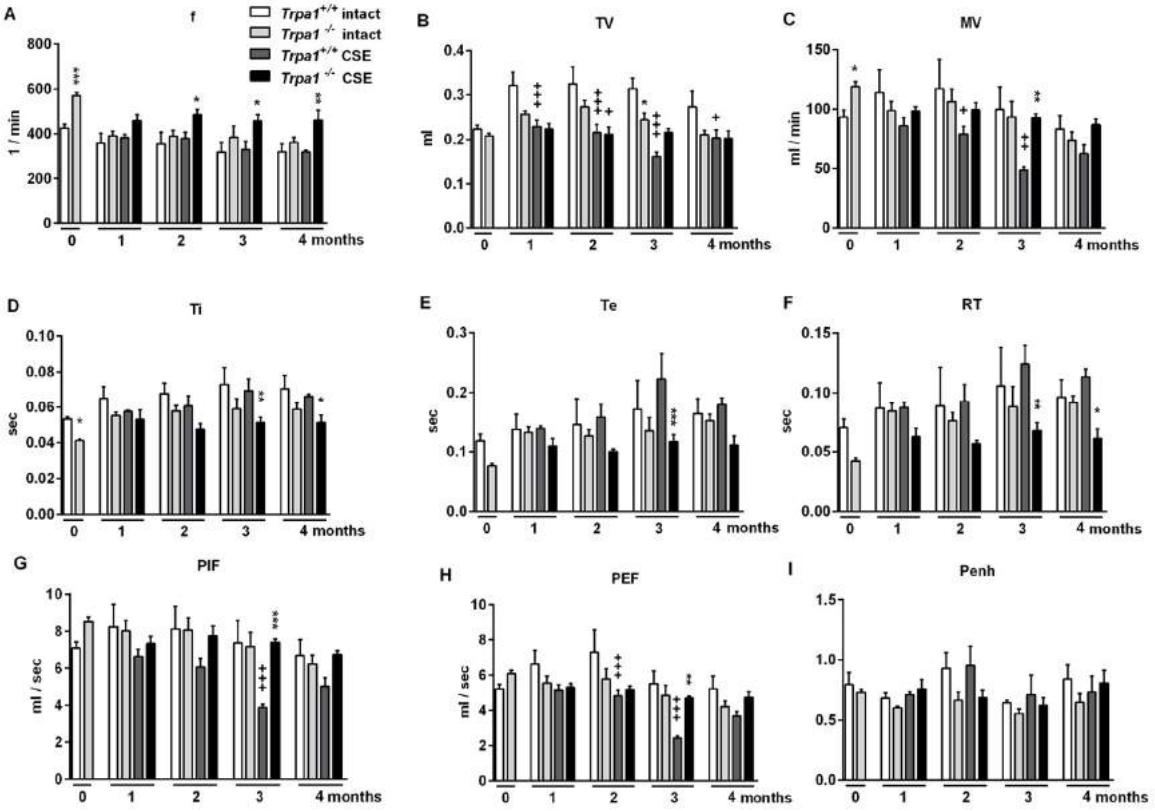

Figure 5. Respiratory functions during the 4 months of cigarette smoke exposure. (**B**) Tidal volume (TV), (**C**) minute ventilation (MV), (**G**) peak inspiratory flow (PIF) and (**H**) peak expiratory flow (PEF) significantly decreased after CSE with a peak at 3 months in *Trpa1*$^{+/+}$ mice. The significant strain differences in (**A**) frequency, (**D**) inspiratory time (Ti), (**E**) expiratory time (Te) and (**F**) relaxation time (RT) observed already in intact mice were not influenced by CSE. (**I**) Enhanced pause did not show any differences either by treatment or by strain. Values represent means ± SEM, n = 6–7 mice/group; two-way ANOVA followed by Tukey's post-test; $^{+}$ $p < 0.05$, $^{++}$ $p < 0.005$, $^{+++}$ $p < 0.001$ vs. PBS-treated respective group; * $p < 0.05$, ** $p < 0.005$, *** $p < 0.001$ vs. LPS-treated *Trpa1*$^{+/+}$.

2.6. CSE-Induced Inflammatory Histopathological Alterations are Similar in Trpa1$^{+/+}$ *and Trpa1*$^{-/-}$ *Mice*

After one month of CSE remarkable perivascular oedema developed (Figure 6C,E) that significantly decreased by time in both strains, and almost completely resolved at the end of the 4th month (Figure 7A). However, the accumulation of perivascular and peribronchial, as well as interstitial neutrophil granulocytes, macrophages and lymphocytes remained moderately increased throughout the experimental protocol (Figure 7B,C). At the end of the 3rd month of CSE, structural destruction characteristic to emphysema (Figure 6G–J) already developed.

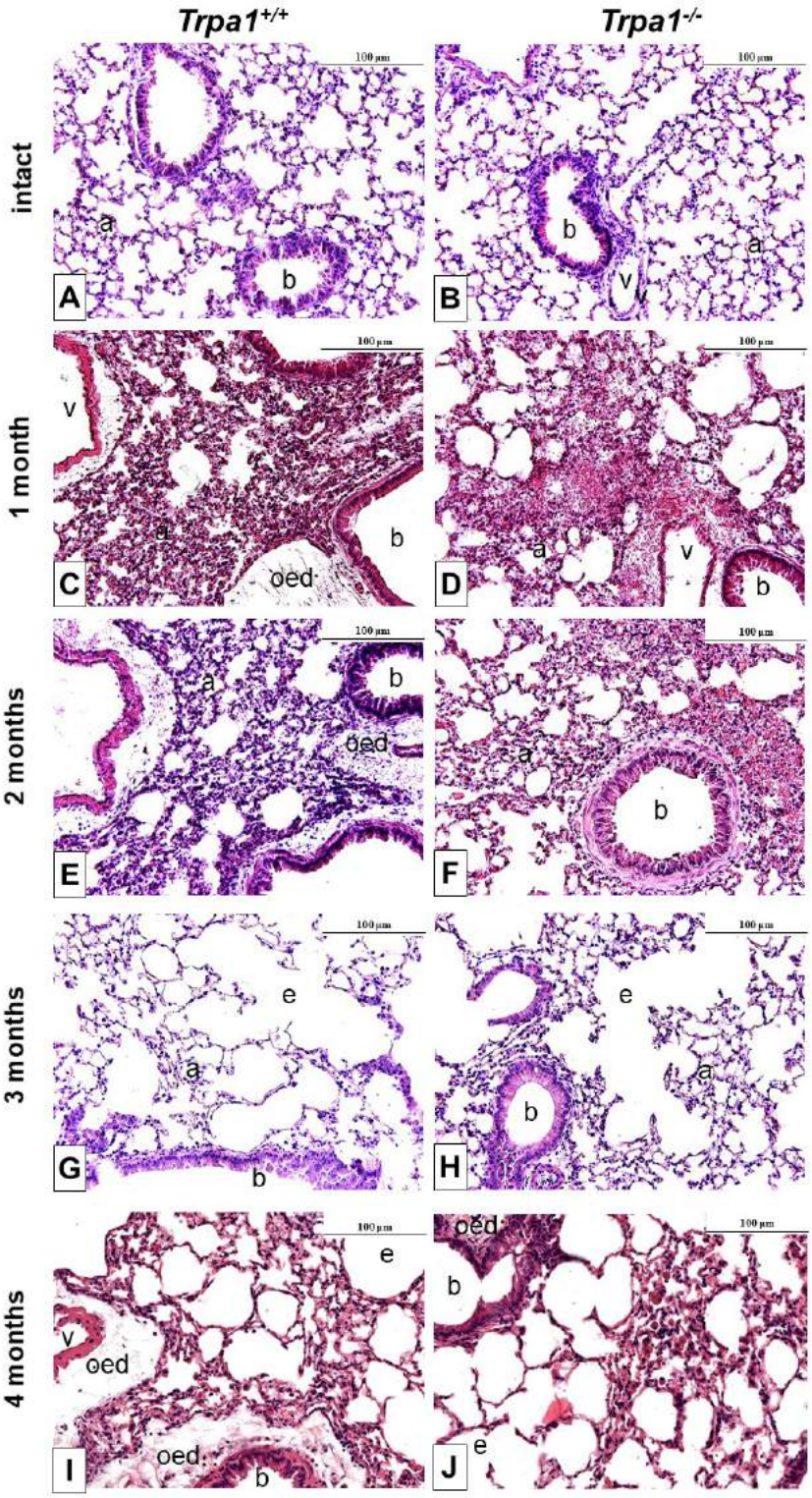

Figure 6. Representative histological pictures of the lungs of *Trpa1*$^{+/+}$ (**A**,**C**,**E**,**G**,**I**) and *Trpa1*$^{-/-}$ (**B**,**D**,**F**,**H**,**J**) mice under intact conditions (**A**,**B**), and after 1–4 months of CSE (**C**–**J**). One month of CSE induced a perivascular and peribronchial oedema formation associated with inflammatory cell infiltration, that gradually subsided over the 4-month long protocol. After the 3rd month of CSE, emphysema formation was observed in both wildtype and gene-deficient mice. (hematoxylin-eosin staining; 200× *g* magnification; a: alveolus, b: bronchiolus, v: venula, oed: oedema, e: emphysema).

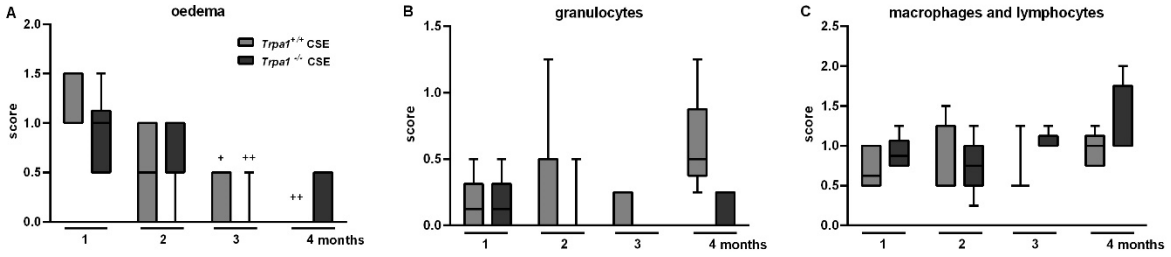

Figure 7. Semiquantitative evaluation of the histopathological changes of the lung after chronic cigarette smoke exposure. (**A**) Perivascular/peribronchial oedema developed after 1 month of CSE, which significantly decreased by time in both strains. The accumulation of perivascular and peribronchial, as well as interstitial (**B**) neutrophil granulocytes, (**C**) macrophages and lymphocytes did not differ in either groups significantly. Boxplots represent the minimum, first quartile, mean, third quartile and maximum values, n = 5–13/group, Kruskal–Wallis followed by Dunn's post-test; $^{+}$ $p < 0.05$, $^{++}$ $p < 0.005$ vs. 1st month of CSE.

2.7. Cigarette Smoke-Induced Emphysema Develops Earlier in Trpa1$^{+/+}$ Mice

Emphysema was quantified by in vivo microCT by the ratio of the low attenuation area (LAA) and total lung volume (TLV) before and after 2 and 4 months of CSE. The ratio correlating with the extent of air-filled regions did not show alterations either by CSE treatment or time (Figure 8A). However, the more sensitive mean linear intercept (Lm) measurement revealed that in *Trpa1*$^{+/+}$ mice emphysema already started to develop at an earlier timepoint compared to the gene-deleted counterparts, Lm was significantly increased in the wildtypes after 2 months of CSE, however, not in the *Trpa1*$^{-/-}$. At the end of the 4th month, Lm was elevated in both strains exposed to CS (Figure 8F).

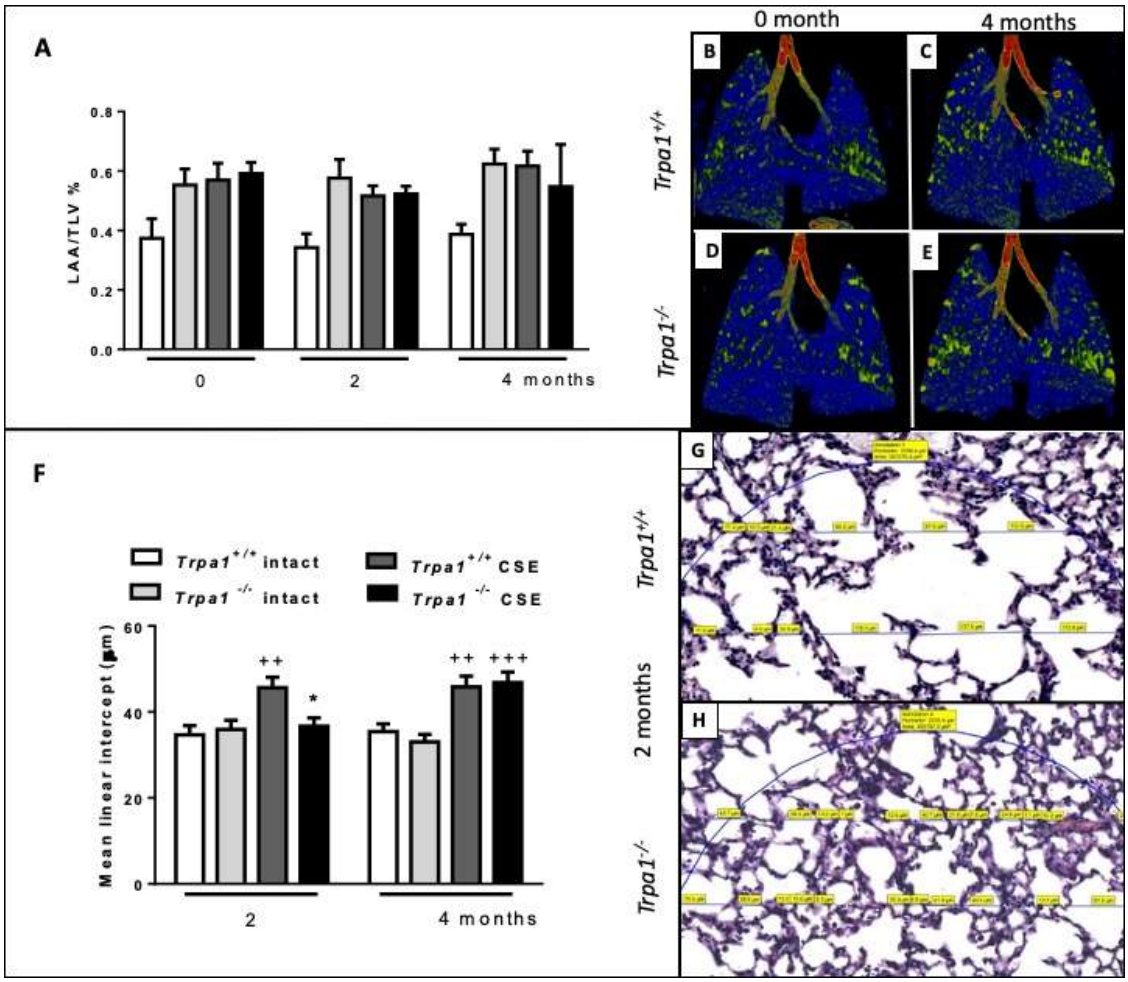

Figure 8. Quantitative evaluation of emphysema. (**A**) LAA/TLV ratio correlating with air-filled regions of the lungs exposed to CSE showed no significant alterations. Representative microCT pictures of lungs (**B**,**D**) before and (**C**,**E**) after 4 months of CSE in *Trpa1*$^{+/+}$ and *Trpa1*$^{-/-}$ mice, respectively. (**F**) Microscopic quantitative assessment of Lm showed a significant increase in *Trpa1*$^{+/+}$ already after 2 months of CSE, but not in the *Trpa1*$^{-/-}$. Values represent means ± SEM, n = 6–7 mice/group; repeated measures two-way ANOVA followed by Tukey's post-test. Representative microscopic pictures of (**G**) *Trpa1*$^{+/+}$ and (**H**) *Trpa1*$^{-/-}$ mouse lung tissues after 2 months of CSE. Values represent means ± SEM, n = 60–100 measurements/group; two-way ANOVA followed by Tukey's post-test; $^{++}$ $p < 0.005$, $^{+++}$ $p < 0.001$ vs. PBS-treated respective group; * $p < 0.05$ vs. CSE-treated *Trpa1*$^{+/+}$. (The blue circle indicates the region of interest in which Lm was measured. The measured chord lengths represented by blue lines were expressed in µm on the scanned slides and labelled in yellow.).

2.8. Chronic Cigarette Smoke-Induced Inflammatory Cell Accumulation in the BALF Shows No Strain Difference

CSE induced massive accumulations of granulocytes, macrophages and lymphocytes measured in the bronchoalveolar lavage fluid (BALF) of both *Trpa1*$^{+/+}$ and *Trpa1*$^{-/-}$ mice. In agreement with our previous findings [63], the number of inflammatory cells reduced by the end of the 3rd month of CSE. There was no biologically relevant difference between the wildtype and gene-deficient mice in either inflammatory cell component (Figure 9).

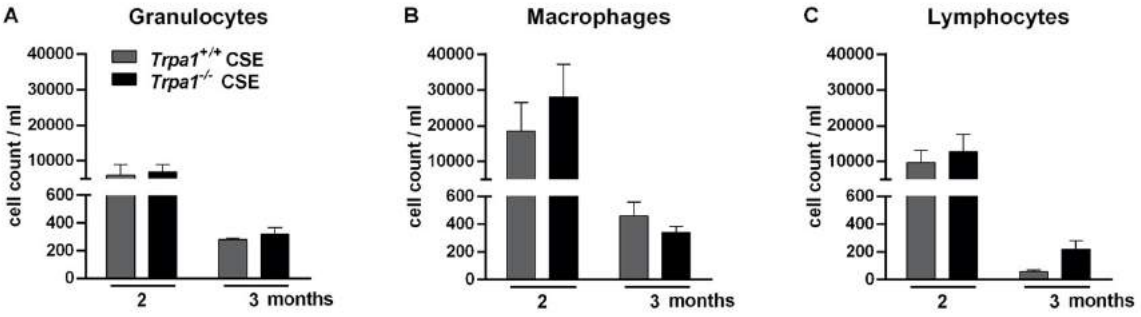

Figure 9. Number of inflammatory cells in the bronchoalveolar lavage fluid (BALF) after 2–3 months of CSE in *Trpa1*$^{+/+}$ and *Trpa1*$^{-/-}$ mice. After the peak of inflammatory cell infiltration at a 2-month timepoint, the number of (**A**) granulocytes, (**B**) macrophages and (**C**) lymphocytes remarkably decreased by the end of the 3rd month in both *Trpa1*$^{+/+}$ and *Trpa1*$^{-/-}$ mice. Values represent means ± SEM, n = 6–7 mice/group; two-way ANOVA followed by Tukey's post-test.

3. Discussion and Conclusion

We provide here the first evidence that the TRPA1 channel has a complex role in basal airway function regulation and inflammatory mechanisms. It protects against LPS-induced acute pneumonitis and hyperresponsiveness, but triggers chronic CSE-evoked emphysema formation and respiratory deterioration (Table 1).

Table 1. The complex regulatory role of TRPA1 in acute and chronic airway inflammation (ns: non-significant; arrows indicate change compared to control PBS-treated or non-inflamed intact mice, $^{++}$ $p < 0.005$, $^{+++}$ $p < 0.001$; asterisks indicate strain difference, * $p < 0.05$, ** $p < 0.005$ vs. *Trpa1*$^{+/+}$).

Endotoxin-Induced Acute Inflammation	***Trpa1*$^{+/+}$**	***Trpa1*$^{-/-}$**	***Trpa1*$^{+/+}$ vs. *Trpa1*$^{-/-}$ *LPS-Treated Inflamed***
	Compared to PBS-Treated Control		
Bronchial hyperreactivity	**ns.**	↑(++)	*
Myeloperoxidase activity	ns.	↑(+++)	**
Inflammatory histopathological changes	↑(++)	ns	ns
CSE-induced Chronic Inflammation	***Trpa1*$^{+/+}$**	***Trpa1*$^{-/-}$**	***Trpa1*$^{+/+}$ vs. *Trpa1*$^{-/-}$ *CSE-Treated Inflamed***
	Compared to Intact Control		
TV, MV, PIF, PEF	↓(++/+++)	ns	*
Oedema	↑	↑	ns.
Inflammatory cell infiltration	↑	↑	ns.
Emphysema	earlier	later	*

Increasing data have suggested the involvement of the TRPA1 receptor in the pathophysiological mechanisms of several airway diseases, such as asthma, COPD and allergic/irritative cough [7,46,56–60,62,64–67], but little is known about its activation mechanisms and its potential as a drug target in lung inflammation is still controversial. Our results demonstrating seemingly opposing regulatory functions of TRPA1 in the acute and chronic models can be explained by its multiple localizations that might evoke different responses. Neuronal TRPA1 in the airways is expressed almost exclusively on vagal afferents that are a subpopulation of sensory afferents. It is co-localized with Transient Receptor Potential Vanilloid 1 (TRPV1) on capsaicin-sensitive vagal bronchopulmonary nociceptive C-fibers originating from the jugular ganglion. Most of these peptidergic bronchopulmonary C-fibers modulate the inflammatory process and induce defensive reflexes, shallow breathing, mucus secretion [68,69]. However, TRPA1-mediated effects via the sensory trigeminal afferentation of the upper airways also might contribute to our results in both models [70]. Besides the neuronal expression, TRPA1 is also located on epithelial, inflammatory and bronchial smooth muscle cells [6,47,48,50].

The virtually contradicting role of TRPA1 might also be explained by the very distinct pathophysiological mechanisms of the LPS and CSE models involving different signaling pathways in different cell types. Moreover, endotoxin and cigarette smoke components are able to directly activate TRPA1 among other exogenous irritants reaching the airways, besides a variety of endogenous inflammatory mediators (protons, hydrogen peroxide, prostaglandins etc.) [5,8,10,18,22].

Direct interactions between endotoxins and TRPA1 [71,72] has been described in LPS-induced acute inflammatory pain, CGRP-release and vascular response that developed via the activation of TRPA1 on nociceptive sensory fibers, independently from TLR4 signaling [5]. The TRPA1 agonist cinnamaldehyde exerts complex immunomodulatory effects on LPS-induced systemic inflammatory response syndrome [73]. TRPA1 mediates the LPS-induced inflammatory responses in primary human osteoarthritic fibroblast-like synoviocytes [74]. The role of TRPA1 as an LPS sensor is suggested to be evolutionarily conserved [75], that occurs via mechanical modifications of the plasma lipid membrane. Interestingly, *Escherichia coli* (*E. coli*) LPS seems to be more effective on TRPA1 than other types of endotoxins [76]. Although previous studies demonstrate TRPA1 activation by LPS and its implication in acute LPS-induced pain and neurogenic inflammation [5], the relative importance of TLR4 and TRPA1 activation by LPS in our pneumonitis model remains to be elucidated.

The protective role of TRPA1 in the LPS-induced acute inflammatory processes including bronchial hyperreactivity is supported by previous results of our group reporting similar protective actions of capsaicin-sensitive sensory nerves and the TRPV1 receptor in the same model [77,78]. The similar functions of TRPA1 and TRPV1 ion channels are not surprising, since they are often co-expressed and interact with each other on the peptidergic sensory nerves [1,79]. The TRPA1-mediated protective effect might be explained by the release of anti-inflammatory sensory neuropeptides from primary afferents, such as somatostatin, similarly to the mechanism described earlier for TRPV1 activation [34,77].

TRPA1 proved to be protective against inflammatory bronchial hyperresponsiveness potentially via smooth muscle relaxant neuropeptides released from the sensory nerves, despite its presence on bronchial smooth muscle cells [47], which might directly lead to bronchoconstriction. Furthermore, bronchodilator effects of TRPA1 activation via non-epithelial PGE_2 production was recently reported in allergic airway inflammation models [80]. Such mechanism might also be involved in our results. A recent study also demonstrated significantly increased airway hyperresponsiveness in *Trpv4* and *Trpa1/Trpv1* double knockout mice as well. The TRPV4 antagonist HC067047 administered to *Trpa1/Trpv1* double knockout animals further increased the Penh value [81] supporting the protective role of these TRP channels in the LPS-induced acute airway inflammation model.

TRPA1-deficiency did not significantly alter inflammatory cell numbers in the histopathological pictures, but significantly increased neutrophil- and macrophage-derived MPO activity, which is supported by TRPA1 expression on these cells [36,82]. The discrepancies between the histopathological semiquantitative scores and the MPO activity might be due to the different sensitivity of the functional and morphological assessments, however, it has also been described that MPO protein expression itself might not correlate strongly with MPO activity due to genetic polymorphism or endogenous inhibitors [83]. Consequently, increased ROS production might contribute to the increased bronchial hyperreactivity in the *Trpa1*-deleted mice. These results are supported by earlier data that TRPA1 activation by irritants evokes defensive functions in the airways [54].

Despite these protective functions of TRPA1 in the acute LPS-evoked pneumonitis model, TRPA1 activation is required for chronic CSE-evoked emphysema and respiratory deterioration, such as MV, TV, PIF and PEF decrease with a peak after 3 months.

These data are supported by findings, that 4-week CSE increases TRPA1 mRNA level in the nodose and jugular ganglia, positively correlating with the inflammatory cell infiltration in the BALF [84]. Moreover, cigarette smoke extract also increased the expression of TRPA1 in airway epithelial cells in a hypoxia-inducible factor-1α-mediated manner [17,85]. Mostly in vitro data using cigarette smoke extract are available about the role of TRPA1 in cigarette smoke-induced airway inflammation. Isolated bronchi experiments suggested that cigarette smoke extract, as well as its components (acrolein

and crotonaldehyde) caused Ca^{2+}-dependent CGRP- and SP-release from the capsaicin-sensitive nerve endings, and TRPA1 was involved in the cigarette smoke extract-induced tracheal plasma extravasation and bronchoconstriction [6]. Cigarette smoke-induced CGRP release in the trachea were predominantly mediated by TRPA1 rather than nicotinic receptors [9]. Cigarette smoke and acrolein released keratinocyte chemoattractant (CXCL1/KC, mouse analogue of IL-8), which was attenuated by TRPA1 antagonists and TRPA1-deficiency [47]. Furthermore, cigarette smoke extract-induced and TRPA1-mediated IL-8 release was shown to develop via NADPH-oxidase activation and the MAPKs/NFκB signaling pathway-related Ca^{2+} influx [17]. TRPA1 is involved in cigarette smoke extract-evoked alveolar and bronchial epithelial damage [49]. Nicotine directly activates the TRPA1 receptor [8,10], which might mediate bronchoconstriction [47]. Similarly, ROS and several lipid peroxidation products also stimulate TRPA1, which is likely to contribute to oxidative stress-evoked airway pathologies induced by CSE [7,17,55], such as emphysema, for which we provided the first data here.

The extent of perivascular/peribronchial oedema was the most severe after 1 month and gradually decreasing afterwards, and the inflammatory cell infiltration reached its maximum after 2 months of CSE in both groups, which is in agreement with our earlier findings in the same model [63]. TRPA1 deficiency did not result in significant changes of the cellular components of these chronic inflammatory processes, as shown by both the histopathological results and BALF analysis.

Since the activation of TRPA1 exerts protective effects in LPS-induced acute pneumonitis and subsequent bronchial hyperreactivity, our findings clearly support the concept that short-term activation of TRPA1 results in defensive effects presumably via sensory nerves and consequently released protective neuropeptides. However, permanent stimulation of the receptor under chronic inflammatory conditions of the airways results in complex regulatory functions due to the diverse localization of TRPA1 also on non-neural cells and its broad range of both exogenous and endogenous activators.

The genetic deletion of the receptor does not directly predict prophylactic or therapeutic potential of TRPA1 agonists or antagonists. However, the activation of TRPA1 by commonly inhaled substances, e.g., cinnamaldehyde or carvacrol [7] (components of cinnamon or thyme essential oils) could be beneficial against acute inflammatory changes of the lung, additionally considering their antimicrobial potentials against pathogens predominant in airway infections [86].

Therefore, further research is needed to determine TRPA1 potential as a pharmacological target in the lung.

4. Methods

4.1. Animals

Experiments were performed on male and female *Trpa1*$^{-/-}$ mice and their *Trpa1*$^{+/+}$ counterparts (8–10 weeks, 20–25 g). The original heterozygote *Trpa1*$^{+/-}$ breeding pairs were a generous gift of Pierangelo Geppetti (Firenze, Italy) [87]. The endotoxin-induced pneumonitis model was carried out on female animals, while in the cigarette smoke-induced bronchitis model mice of both sexes were used. Background strain of the gene-deleted animals was C57Bl/6, and the germline transmission of the mutated allele and excision of the selection cassette were verified by PCR analysis. Animals were bred and kept in the Laboratory Animal House of the Department of Pharmacology and Pharmacotherapy, University of Pécs, Pécs, Hungary at 24–25 °C, provided with standard chow and water *ad libitum* and maintained under a 12-h light–dark cycle.

4.2. Ethics

All experimental procedures were carried out according to the 40/2013 (II.14.) Government Regulation on Animal Protection, Consideration Decree of Scientific Procedures of Animal Experiments (243/1988) and Directive 2010/63/EU of the European Parliament. Studies were approved and a license was given by the Ethics Committee on Animal Research of University of Pécs, Pécs, Hungary according

to the Ethical Codex of Animal Experiments (licence No.: BA02/2000-35/2016, BA02/2000-26/2018). We addressed the ARRIVE guidelines for designing, performing and reporting the experiments wherever possible.

4.3. Endotoxin-Induced Acute Pneumonitis

Acute interstitial lung inflammation was evoked by intranasal (i.n.) administration of 60 µL, 167 µg/mL *E. coli* (serotype: O83) endotoxin (lipopolysaccharide, LPS) under light ether anaesthesia [77]. LPS was isolated and purified in the Department of Microbiology, University of Pécs, Pécs, Hungary [88]. Control animals received the same volume of sterile PBS.

Endotoxin is a component of the cell wall of Gram-negative bacteria, composed of a phosphoglycolipid (lipid A) covalently bound to a hydrophilic heteropolysaccharide part [89]. LPS—connected to the specific LPS binding protein (LBP)—is able to bind to Toll-like receptor 4 (TLR4)-CD14 glycoprotein complex expressed on macrophages and monocytes [90]. Via the p38-MAPK signaling pathway it induces the activation and accumulation of immune cells [91,92]. As a result, inflammatory cytokines and proinflammatory mediators (e.g., bradykinin, leukotrienes and prostaglandins) are released from the activated immune cells directly activating the sensory nerve endings [93]. Beside the activation of immune cells, LPS also elicits bronchial contraction in the lung causing enhanced airway resistance [94].

4.4. Cigarette Smoke-Induced Chronic Airway Inflammation

Chronic bronchitis was elicited by whole body cigarette smoke exposure for 4 months. Mice were exposed to cigarette smoke (3R4F Kentucky Research Cigarette; University of Kentucky, Lexington, KY, USA) twice daily, 10 times per week in a whole body smoke exposure chamber (Teague Enterprises, Woodland, CA, USA) for 30 min followed by a ventilation period of 30 min as described previously [63].

4.5. Investigation of Airway Function and Bronchial Responsiveness

Parameters of the airway function were measured in conscious, spontaneously breathing mice with the help of unrestrained whole-body plethysmography (Buxco Europe Ltd., Winchester, UK).

In the endotoxin-induced acute pneumonitis model, breathing frequency (f) and carbachol-induced airway reactivity were measured before and 24 h after intranasal PBS/LPS administration [95]. Bronchoconstriction was induced by increasing concentrations (5.5, 11 and 22 mM) of the muscarinic receptor agonist carbachol (50 µL/mouse), and the Penh (enhanced pause) value was determined. Penh is a complex calculated parameter ((expiratory time/relaxation time) − 1)/(max. expiratory flow/max. inspiratory flow), well correlating with bronchoconstriction and airway resistance measured in ventilated animals using invasive techniques [34].

Considering that cigarette smoke-induced chronic bronchitis model is a disease model with high translational relevance, we performed an extended analysis of the respiratory functions determining f, TV, MV, Ti, Te, RT, PIF, PEF and Penh before and at the end of every month of the 4-month-investigational period as described previously [63].

4.6. Cell Composition Analysis of the Bronchoalveolar Lavage Fluid (BALF)

In the cigarette smoke exposure model, mice were anaesthetised with ketamine and xylazine (100 mg/kg and 5 mg/kg, s.c., respectively) and the lungs were washed with 5 mL PBS. BALF was collected in centrifuge tubes (1000 rpm, 5 min) and the supernatants were removed. Cells were resuspended in staining buffer (0.1% NaN_3 and 0.1% BSA dissolved in 500 µL PBS), and 1 µL CD45 fluorescein-5-isothiocyanate (FITC) solution was given to the samples. After incubation of 30 min, 1 µL propidium-iodide was given to the samples and after centrifugation (1000 rpm, 5 min) the supernatant was removed again. Cells were resuspended in fixation buffer (3% formaldehyde dissolved in 700 µL PBS) and the cell profile of the samples was analysed with a CyFlow Space flow cytometer (Sysmex Partec, Münster, Germany) [96].

We previously showed that in the CSE model perivascular/peribronchial oedema developed in the 1st month, while in the 2nd and 3rd months inflammatory cell infiltration dominated the histopathological picture, which decreased by the 4th month accompanied by tissue destruction [63]. Based on these data, we investigated the amount of inflammatory cells in the BALF after the 2nd and 3rd months.

4.7. Histological Examination of the Lungs

In both models, lungs were removed following cervical dislocation in deep anaesthesia. The left lung was fixed in 4% formaldehyde and embedded in paraffin for histopathological processing. Sections were made with 5–7 μm microtome and stained with hematoxylin-eosin (HE). One section of the lungs of the endotoxin-treated mice was stained with periodic acid-Schiff (PAS) reagent in order to visualize mucus producing goblet cells. Semiquantitative evaluation of the histological alterations was performed by an expert pathologist blinded from the experimental design.

In the acute pneumonitis model, semiquantitative histopathological scoring of the lungs was performed based on the following parameters: perivascular oedema (0–3), accumulation of the perivascular and peribonchial neutrophil granulocytes (0–3), infiltration of activated macrophages and mononuclear cells into the alveolar space (0–2), as well as hyperplasia of the bronchiolar goblet cells (0–2) [97]. The composite inflammatory score (ranging between 0 and 10) was generated by addition of the individual histopathological parameters.

In the chronic COPD model, semiquantitative histopathological scoring of the lungs was established by our work group and performed on the basis of perivascular oedema, the accumulation of neutrophil granulocytes into the perivascular/peribronchial and interstitial space, as well as the perivascular/peribronchial and interstitial infiltration of macrophages and lymphocytes with scores ranging from 0–3 (0: intact, 0.5: focal mild, 1: diffuse mild, 1.5: focal moderate, 2: diffuse moderate, 2.5: focal severe, 3: diffuse severe).

Quantitative histopathological evaluation of emphysema was performed by the measurement of the mean linear intercept as described previously [98]. Briefly, air space enlargement was assessed by the measurement of the alveolar space or alveolar and ductal air space along parallel lines on approximately 400,000 μm^2 representative areas on each slide by The Case Viewer software (3DHISTECH, Budapest, Hungary).

4.8. Morphological Evaluation of the Lungs with In Vivo MicroCT Investigation

In the cigarette smoke exposure model, structural alterations, such as the LAA/TLV% characteristic to emphysema was also measured by in vivo microCT in a self-controlled manner, before, as well as 2 and 4 months after CSE exposure as described previously [63]. Briefly, mice were anaesthetized with pentobarbital (70 mg/kg) i.p. and their lungs were imaged by breath-gated tomography on a Skyscan 1176 high resolution microtomograph (Skyscan, Kontich, Belgium). Reconstruction and morphometric analysis were performed with the software provided by the manufacturer.

4.9. Determination of Myeloperoxidase (MPO) Activity from Lung Homogenates with Spectrophotometry

During the evolvement of endotoxin-induced acute pneumonitis, MPO enzyme is produced by the accumulated neutrophil granulocytes, monocytes and macrophages [99]. The MPO activity of the lung homogenates were measured by spectrophotometry using H_2O_2-3,3′,5,5′-tetramethyl-benzidine (TMB/H_2O_2) and compared to a standard MPO preparation as described earlier [98].

4.10. Statistical Analysis

Statistical analysis was performed by the GraphPad Prism v6 software (GraphPad Software, San Diego, CA, USA). Comparison of basal respiratory functions of intact wildtype and TRPA-deficient mice was performed by a Student's t-test for unpaired comparison. Parameters of the respiratory function in both the LPS and CSE study, as well as LAA/TLV%, mean linear intercept, and BALF

inflammatory cell counts were evaluated by two-way ANOVA followed by Tukey's post hoc test. MPO activity was analysed by one-way ANOVA followed by Bonferroni's post-test. Histopathological semiquantitative scores were evaluated by Kruskal–Wallis analysis followed by Dunn's post-test. In all cases $p < 0.05$ was accepted as significant.

Author Contributions: Conceptualization, Z.H. (Zsuzsanna Helyes), Z.H. (Zsófia Hajna), K.C., E.P.; funding acquisition, Z.H. (Zsuzsanna Helyes), E.P., investigation, Z.H. (Zsófia Hajna), K.C., Á.K., I.S.; formal analysis: Z.H. (Zsófia Hajna), K.C., L.K., T.K., methodology, Z.H. (Zsófia Hajna), K.C., Á.K., T.K., B.K., A.P., Z.H. (Zsuzsanna Helyes).; project administration, Z.H. (Zsófia Hajna), K.C., I.S.; resources, B.K., Z.H. (Zsuzsanna Helyes), E.P.; supervision, Z.H. (Zsuzsanna Helyes); visualization, Z.H. (Zsófia Hajna), K.C., A.P., T.K., L.K., writing—original draft, Z.H. (Zsófia Hajna), K.C., Z.H. (Zsuzsanna Helyes); writing—review and editing, Z.H. (Zsófia Hajna), K.C., Á.K., L.K., T.K., A.P., I.S., B.K., E.P., Z.H. (Zsuzsanna Helyes). All authors have read and approved the final manuscript.

Funding: Z.H. (Zsuzsanna Helyes) was supported by the Higher Education Institutional Excellence Program of the Ministry of Human Capacities in Hungary, 20765-3/2018/FEKUTSRTAT; PEPSYS: Complexity of Peptidergic Signalization and its Role in Systemic Diseases, GINOP-2.3.2-15-2016-00050; Human Resource Development Operational Program, EFOP-3.6.2-16-2017-00006 LIVE LONGER and EFOP-3.6.1-16-2016-00004; and Economic Development and Innovation Operational Program, GINOP-2.3.2-15-2016-00048 STAY ALIVE. K.C. was supported by the ÚNKP-19-3-III-PTE-211 New National Excellence Program of the Ministry of Human Capacities. Á.K. was supported by János Bolyai Research Scholarships of the Hungarian Academy of Sciences and ÚNKP-19-4 New National Excellence Program of the Ministry For Innovation And Technology.

Acknowledgments: The in vivo imaging experiments were performed in the Small Animal Imaging Core Facility of the Szentágothai Research Centre, University of Pécs, Hungary.

Conflicts of Interest: The authors declare no conflict of interest.

References

1. Nassenstein, C.; Kwong, K.; Taylor-Clark, T.; Kollarik, M.; MacGlashan, D.M.; Braun, A.; Undem, B.J. Expression and function of the ion channel TRPA1 in vagal afferent nerves innervating mouse lungs. *J. Physiol.* **2008**, *586*, 1595–1604. [CrossRef] [PubMed]
2. Zygmunt, P.M.; Högestätt, E.D. TRPA1. In *Mammalian Transient Receptor Potential (TRP) Cation Channels*; Nilius, B., Flockerzi, V., Eds.; Mammalian; Springer: Berlin/Heidelberg, Germany, 2014; ISBN 9783642542152.
3. Gaudet, R. A primer on ankyrin repeat function in TRP channels and beyond. *Mol. Biosyst.* **2008**, *4*, 372–379. [CrossRef] [PubMed]
4. Cordero-Morales, J.F.; Gracheva, E.O.; Julius, D. Cytoplasmic ankyrin repeats of transient receptor potential A1 (TRPA1) dictate sensitivity to thermal and chemical stimuli. *Proc. Natl. Acad. Sci. USA* **2011**, *108*, E1184–E1191. [CrossRef] [PubMed]
5. Meseguer, V.; Alpizar, Y.A.; Luis, E.; Tajada, S.; Denlinger, B.; Fajardo, O.; Manenschijn, J.-A.; Fernández-Pena, C.; Talavera, A.; Kichko, T.; et al. TRPA1 channels mediate acute neurogenic inflammation and pain produced by bacterial endotoxins. *Nat. Commun.* **2014**, *5*. [CrossRef] [PubMed]
6. Andrè, E.; Campi, B.; Materazzi, S.; Trevisani, M.; Amadesi, S.; Massi, D.; Creminon, C.; Vaksman, N.; Nassini, R.; Civelli, M.; et al. Cigarette smoke—Induced neurogenic inflammation is mediated by α,β-unsaturated aldehydes and the TRPA1 receptor in rodents. *J. Clin. Investig.* **2008**, *118*, 2574–2582. [CrossRef] [PubMed]
7. Bessac, B.F.; Jordt, S.-E. Breathtaking TRP Channels: TRPA1 and TRPV1 in Airway Chemosensation and Reflex Control. *Physiology* **2008**, *23*, 360–370. [CrossRef] [PubMed]
8. Chung, S.; Baumlin, N.; Dennis, J.S.; Moore, R.; Salathe, S.F.; Whitney, P.L.; Sabater, J.; Abraham, W.M.; Kim, M.D.; Salathe, M. Electronic cigarette vapor with nicotine causes airway mucociliary dysfunction preferentially via TRPA1 receptors. *Am. J. Respir. Crit. Care Med.* **2019**, *200*, 1134–1145. [CrossRef]
9. Kichko, T.I.; Kobal, G.; Reeh, P.W. Cigarette smoke has sensory effects through nicotinic and TRPA1 but not TRPV1 receptors on the isolated mouse trachea and larynx. *Am. J. Physiol. Lung Cell. Mol. Physiol.* **2015**, *309*, L812–L820. [CrossRef]
10. Talavera, K.; Gees, M.; Karashima, Y.; Meseguer, V.M.; Vanoirbeek, J.A.J.; Damann, N.; Everaerts, W.; Benoit, M.; Janssens, A.; Vennekens, R.; et al. Nicotine activates the chemosensory cation channel TRPA1. *Nat. Neurosci.* **2009**, *12*, 1293–1299. [CrossRef]

11. Shapiro, D.; Deering-Rice, C.E.; Romero, E.G.; Hughen, R.W.; Light, A.R.; Veranth, J.M.; Reilly, C.A. Activation of Transient Receptor Potential Ankyrin-1 (TRPA1) in Lung Cells by Wood Smoke Particulate Material. *Chem. Res. Toxicol.* **2013**, *26*, 750–758. [CrossRef]
12. Deering-Rice, C.E.; Memon, T.; Lu, Z.; Romero, E.G.; Cox, J.; Taylor-Clark, T.; Veranth, J.M.; Reilly, C.A. Differential Activation of TRPA1 by Diesel Exhaust Particles: Relationships between Chemical Composition, Potency, and Lung Toxicity. *Chem. Res. Toxicol.* **2019**, *32*, 1040–1050. [CrossRef] [PubMed]
13. Memon, T.A.; Nguyen, N.D.; Burrell, K.L.; Scott, A.F.; Almestica-Roberts, M.; Rapp, E.; Deering-Rice, C.E.; Reilly, C.A. Wood Smoke Particles Stimulate MUC5AC Overproduction by Human Bronchial Epithelial Cells through TRPA1 and EGFR Signaling. *Toxicol. Sci.* **2020**, *174*, 278–290. [CrossRef] [PubMed]
14. Trevisani, M.; Siemens, J.; Materazzi, S.; Bautista, D.M.; Nassini, R.; Campi, B.; Imamachi, N.; André, E.; Patacchini, R.; Cottrell, G.S.; et al. 4-Hydroxynonenal, an endogenous aldehyde, causes pain and neurogenic inflammation through activation of the irritant receptor TRPA1. *Proc. Natl. Acad. Sci. USA* **2007**, *104*, 13519–13524. [CrossRef] [PubMed]
15. Taylor-Clark, T.E.; McAlexander, M.A.; Nassenstein, C.; Sheardown, S.A.; Wilson, S.; Thornton, J.; Carr, M.J.; Undem, B.J. Relative contributions of TRPA1 and TRPV1 channels in the activation of vagal bronchopulmonary C-fibres by the endogenous autacoid 4-oxononenal. *J. Physiol.* **2008**, *14*, 3447–3459. [CrossRef]
16. Graepel, R.; Fernandes, E.S.; Aubdool, A.A.; Andersson, D.A.; Bevan, S.; Brain, S.D. 4-Oxo-2-nonenal (4-ONE): Evidence of Transient Receptor Potential Ankyrin 1-Dependent and -Independent Nociceptive and Vasoactive Responses In Vivo. *J. Pharmacol. Exp. Ther.* **2011**, *337*, 117–124. [CrossRef]
17. Lin, A.-H.; Liu, M.-H.; Ko, H.-K.; Perng, D.-W.; Lee, T.-S.; Kou, Y.R. Lung Epithelial TRPA1 Transduces the Extracellular ROS into Transcriptional Regulation of Lung Inflammation Induced by Cigarette Smoke: The Role of Influxed Ca2+. *Mediat. Inlfammation* **2015**, *2015*. [CrossRef]
18. Taylor-Clark, T.E.; Undem, B.J.; MacGlashan, D.W.; Ghatta, S.; Carr, M.J.; McAlexander, M.A. Prostaglandin-Induced Activation of Nociceptive Neurons via Direct Interaction with Transient Receptor Potential A1 (TRPA1). *Mol. Pharmacol.* **2008**, *73*, 274–281. [CrossRef]
19. Al-Shamlan, F.; El-Hashim, A.Z. Bradykinin sensitizes the cough reflex via a B2 receptor dependent activation of TRPV1 and TRPA1 channels through metabolites of cyclooxygenase and 12-lipoxygenase. *Respir. Res.* **2019**, *20*. [CrossRef]
20. Pozsgai, G.; Hajna, Z.; Bagoly, T.; Boros, M.; Kemény, Á.; Materazzi, S.; Nassini, R.; Helyes, Z.; Szolcsányi, J.; Pintér, E. The role of transient receptor potential ankyrin 1 (TRPA1) receptor activation in hydrogen-sulphide-induced CGRP-release and vasodilation. *Eur. J. Pharmacol.* **2012**, *689*, 56–64. [CrossRef]
21. Hajna, Z.; Sághy, É.; Payrits, M.; Aubdool, A.A.; Szőke, É.; Pozsgai, G.; Bátai, I.Z.; Nagy, L.; Filotás, D.; Helyes, Z.; et al. Capsaicin-Sensitive Sensory Nerves Mediate the Cellular and Microvascular Effects of H2S via TRPA1 Receptor Activation and Neuropeptide Release. *J. Mol. Med.* **2016**, *60*, 157–170. [CrossRef]
22. Bandell, M.; Story, G.M.; Hwang, S.W.; Viswanath, V.; Eid, S.R.; Petrus, M.J.; Earley, T.J.; Patapoutian, A. Noxious Cold Ion Channel TRPA1 Is Activated by Pungent Compounds and Bradykinin. *Neuron* **2004**, *41*, 849–857. [CrossRef]
23. Hinman, A.; Chuang, H.; Bautista, D.M.; Julius, D. TRP channel activation by reversible covalent modification. *Proc. Natl. Acad. Sci. USA* **2006**, *103*, 19564–19568. [CrossRef] [PubMed]
24. Macpherson, L.J.; Dubin, A.E.; Evans, M.J.; Marr, F.; Schultz, P.G.; Cravatt, B.F.; Patapoutian, A. Noxious compounds activate TRPA1 ion channels through covalent modification of cysteines. *Nature* **2007**, *445*, 541–545. [CrossRef]
25. Nilius, B.; Prenen, J.; Owsianik, G. Irritating channels: The case of TRPA1. *J. Physiol.* **2011**, *589*, 1543–1549. [CrossRef]
26. Chen, J.; Hackos, D.H. TRPA1 as a drug target—Promise and challenges. *Naunyn. Schmiedebergs. Arch. Pharmacol.* **2015**, *388*, 451–463. [CrossRef]
27. Grace, M.; Birrell, M.A.; Dubuis, E.; Maher, S.A.; Belvisi, M.G. Transient receptor potential channels mediate the tussive response to prostaglandin E2 and bradykinin. *Thorax* **2012**, *67*, 891–900. [CrossRef]
28. Wang, S.; Dai, Y.; Fukuoka, T.; Yamanaka, H.; Kobayashi, K.; Obata, K.; Cui, X.; Tominaga, M.; Noguchi, K. Phospholipase C and protein kinase A mediate bradykinin sensitization of TRPA1: A molecular mechanism of inflammatory pain. *Brain* **2008**, *131*, 1241–1251. [CrossRef]

29. Meents, J.E.; Fischer, M.J.M.; McNaughton, P.A. Sensitization of TRPA1 by Protein Kinase A. *PLoS ONE* **2017**, *12*, e0170097. [CrossRef]
30. Sun, H.; Meeker, S.; Undem, B.J. Role of TRP channels in Gq-coupled Protease-activated Receptor 1-mediated activation of Mouse Nodose Pulmonary C-fibers. *Am. J. Physiol. Lung Cell. Mol. Physiol.* **2020**, *318*, L192–L199. [CrossRef]
31. Kádková, A.; Synytsya, V.; Krusek, J.; Zímová, L.; Vlachová, V. Molecular Basis of TRPA1 Regulation in Nociceptive Neurons. A Review. *Physiol. Res.* **2017**, *66*, 425–439. [CrossRef]
32. Geppetti, P.; Nassini, R.; Materazzi, S.; Benemei, S. The concept of neurogenic inflammation. *BJU Int.* **2008**, *101*, 2–6. [CrossRef] [PubMed]
33. Szolcsányi, J. Capsaicin-sensitive sensory nerve terminals with local and systemic efferent functions: Facts and scopes of an unorthodox neuroregulatory mechanism. *Prog. Brain Res.* **1996**, *113*, 343–359. [PubMed]
34. Helyes, Z.; Pintér, E.; Sándor, K.; Elekes, K.; Bánvölgyi, Á.; Keszthelyi, D.; Szőke, É.; Tóth, D.M.; Sándor, Z.; Kereskai, L.; et al. Impaired defense mechanism against inflammation, hyperalgesia, and airway hyperreactivity in somatostatin 4 receptor gene-deleted mice. *Proc. Natl. Acad. Sci. USA* **2009**, *106*, 13088–13093. [CrossRef]
35. Fernandes, E.S.; Fernandes, M.A.; Keeble, J.E. The functions of TRPA1 and TRPV1: Moving away from sensory nerves. *Br. J. Pharmacol.* **2012**, *166*, 510–521. [CrossRef]
36. Kun, J.; Perkecz, A.; Knie, L.; Sétáló, G., Jr.; Tornóczki, T.; Pintér, E.; Bán, Á. TRPA1 receptor is upregulated in human oral lichen planus. *Oral. Dis.* **2017**, *23*, 189–198. [CrossRef]
37. Bertin, S.; Aoki-Nonaka, Y.; Lee, J.; de Jong, P.R.; Kim, P.; Han, T.; Yu, T.; To, K.; Takahashi, N.; Boland, B.S.; et al. The TRPA1 ion channel is expressed in CD4+ T cells and restrains T cell-mediated colitis through inhibition of TRPV1. *Gut* **2017**, *66*, 1584–1596. [CrossRef]
38. Sahoo, S.S.; Majhi, R.K.; Tiwari, A.; Acharya, T.; Kumar, P.S.; Saha, S.; Kumar, A.; Goswami, C.; Chattopadhyay, S. Transient receptor potential ankyrin1 channel is endogenously expressed in T cells and is involved in immune functions. *Biosci. Rep.* **2019**, *39*, 1–16. [CrossRef]
39. Atoyan, R.; Shnader, D.; Botchkareva, N. Non-Neuronal Expression of Transient Receptor Potential Type A1 (TRPA1) in Human Skin. *J. Invest. Dermatol.* **2009**, *129*, 2312–2315. [CrossRef]
40. Kemény, Á.; Kodji, X.; Horváth, S.; Komlódi, R.; Szőke, É.; Sándor, Z.; Perkecz, A.; Gyömörei, C.; Sétáló, G.; Kelemen, B.; et al. TRPA1 acts in a protective manner in imiquimod-induced psoriasiform dermatitis in mice. *J. Investig. Dermatol.* **2018**, *138*, 1774–1784. [CrossRef]
41. Streng, T.; Axelsson, H.E.; Hedlund, P.; Andersson, D.A.; Jordt, S.-E.; Bevan, S.; Andersson, K.-E.; Högestätt, E.D.; Zygmunt, P.M. Distribution and Function of the Hydrogen Sulfide—Sensitive TRPA1 Ion Channel in Rat Urinary Bladder. *Eur. Urol.* **2008**, *53*, 391–400. [CrossRef]
42. Earley, S.; Gonzales, A.L.; Crnich, R. Endithelium-Dependent Cerebral Artery Dilation Mediated by TRPA1 and Ca2+-Activated K+ Channels. *Circ. Res.* **2009**, *104*, 987–994. [CrossRef]
43. Nummenmaa, E.; Hämäläinen, M.; Moilanen, L.J.; Paukkeri, E.-L.; Nieminen, R.M.; Moilanen, T.; Vuolteenaho, K.; Moilanen, E. Transient receptor potential ankyrin 1 (TRPA1) is functionally expressed in primary human osteoarthritic chondrocytes. *Arthritis Res. Ther.* **2016**, *18*, 185. [CrossRef]
44. Jaquemar, D.; Schenker, T.; Trueb, B. An Ankyrin-like Protein with Transmembrane Domains Is Specifically Lost after Oncogenic Transformation of Human Fibroblasts. *J. Biol. Chem.* **1999**, *274*, 7325–7333. [CrossRef]
45. Stokes, A.; Wakano, C.; Koblan-Huberson, M.; Adra, C.N.; Fleig, A.; Turner, H. TRPA1 is a substrate for de-ubiquitination by the tumor suppressor CYLD. *Cell. Signal.* **2006**, *18*, 1584–1594. [CrossRef]
46. Mukhopadhyay, I.; Kulkarni, A.; Khairatkar-Joshi, N. Blocking TRPA1 in Respiratory Disorders: Does It Hold a Promise? *Pharmaceuticals* **2016**, *9*, 70. [CrossRef]
47. Nassini, R.; Pedretti, P.; Moretto, N.; Fusi, C.; Carnini, C.; Facchinetti, F.; Viscomi, A.R.; Pisano, A.R.; Stokesberry, S.; Brunmark, C.; et al. Transient Receptor Potential Ankyrin 1 Channel Localized to Non-Neuronal Airway Cells Promotes Non-Neurogenic Inflammation. *PLoS ONE* **2012**, *7*, e42454. [CrossRef]
48. Kannler, M.; Lüling, R.; Yildirim, A.Ö.; Gudermann, T.; Steinritz, D.; Dietrich, A. TRPA1 channels: Expression in non-neuronal murine lung tissues and dispensability for hyperoxia-induced alveolar epithelial hyperplasia. *Pflügers Arch. Eur. J. Physiol.* **2018**, *470*, 1231–1241. [CrossRef]
49. Wang, M.; Zhang, Y.; Xu, M.; Zhang, H.; Chen, Y.; Fan, K.; Adcock, I.M.; Li, F. Free Radical Biology and Medicine Roles of TRPA1 and TRPV1 in cigarette smoke -induced airway epithelial cell injury model. *Free Radic. Biol. Med.* **2019**, *134*, 229–238. [CrossRef]

50. Yap, M.J.G.; Ueda, T.; Takeda, N.; Fukumitsu, K.; Fukuda, S.; Uemura, T.; Tajiri, T.; Ohkubo, H.; Maeno, K.; Ito, Y.; et al. Cytokine An inflammatory stimulus sensitizes TRPA1 channel to increase cytokine release in human lung fibroblasts. *Cytokine* **2020**, *129*, 155027. [CrossRef]
51. Nilius, B.; Appendino, G.; Owsianik, G. The transient receptor potential channel TRPA1: From gene to pathophysiology. *Pflügers Arch. Eur. J. Physiol.* **2012**, *464*, 425–458. [CrossRef]
52. López-Requena, A.; Boonen, B.; van Greven, L.; Hellings, P.W.; Alpizar, Y.A.; Talavera, K. Roles of Neuronal TRP Channels in Neuroimmune Interactions. In *Neurobiology of TRP Channels*; Emir, T.L.R., Ed.; CRC Press/Taylor & Francis: Boca Raton, FL, USA, 2017.
53. Talavera, K.; Startek, J.B.; Alvarez-Collazo, J.; Boonen, B.; Alpizar, Y.A.; Sanchez, A.; Naert, R.; Nilius, B. Mammalian Transient Receptor Potential TRPA1 Channels: From Structure to Disease. *Physiol. Rev.* **2020**, *100*, 725–803. [CrossRef]
54. Chen, J.; McGaraughty, S.; Kym, P. TRPA1 in drug discovery. In *TRP Channels in Drug Discovery*; Szallasi, A., Bíró, T., Eds.; Humana Press, Springer: Totowa, NJ, USA, 2012; pp. 43–59.
55. Viana, F. TRPA1 channels: Molecular sentinels of cellular stress and tissue damage. *J. Physiol.* **2016**, *594*, 4151–4169. [CrossRef]
56. Grace, M.S.; Baxter, M.; Dubuis, E.; Birrell, M.A.; Belvisi, M.G. Transient receptor potential (TRP) channels in the airway: Role in airway disease. *Br. J. Pharmacol.* **2014**, *171*, 2593–2607. [CrossRef]
57. Banner, H.K.; Igney, F.; Poll, C. TRP channels: Emerging targets for respiratory disease. *Pharmacol. Ther.* **2011**, *130*, 371–384. [CrossRef]
58. Yang, H.; Li, S. Transient Receptor Potential Ankyrin 1 (TRPA1) Channel and Neurogenic Inflammation in Pathogenesis of Asthma. *Med. Sci. Monit.* **2016**, *22*, 2917–2923. [CrossRef]
59. Bonvini, S.J.; Belvisi, M.G. Cough and airway disease: The role of ion channels. *Pulm. Pharmacol. Ther.* **2017**, *47*, 21–28. [CrossRef]
60. Wallace, H. Airway Pathogenesis Is Linked to TRP Channels. In *Neurobiology of TRP Channels*; Emir, T.L.R., Ed.; CRC Press/Taylor & Francis: Boca Raton, FL, USA, 2017.
61. Prandini, P.; De Logu, F.; Fusi, C.; Provezza, L.; Nassini, R.; Montagner, G.; Materazzi, S.; Munari, S.; Gilioli, E.; Bezzerri, V.; et al. Transient Receptor Potential Ankyrin 1 Channels Modulate Inflammatory Response in Respiratory Cells from Patients with Cystic Fibrosis. *Am. J. Respir. Cell Mol. Biol.* **2016**, *55*, 645–656. [CrossRef]
62. Dietrich, A. Modulators of Transient Receptor Potential (TRP) Channels as Therapeutic Options in Lung Disease. *Pharmaceuticals* **2019**, *12*, 23. [CrossRef]
63. Kemény, Á.; Csekő, K.; Szitter, I.; Varga, Z.V.; Bencsik, P.; Kiss, K.; Halmosi, R.; Deres, L.; Erős, K.; Perkecz, A.; et al. Integrative characterization of chronic cigarette smoke-induced cardiopulmonary comorbidities in a mouse model. *Environ. Pollut.* **2017**, *229*, 746–759. [CrossRef]
64. Caceres, A.I.; Brackmann, M.; Elia, M.D.; Bessac, B.F.; del Camino, D.; D'Amours, M.; Witek, J.S.; Fanger, C.M.; Chong, J.A.; Hayward, N.J.; et al. A sensory neuronal ion channel essential for airway inflammation and hyperreactivity in asthma. *Proc. Natl. Acad. Sci. USA* **2009**, *106*, 9099–9104. [CrossRef]
65. Raemdonck, K.; de Alba, J.; Birrell, M.A.; Grace, M.; Maher, S.A.; Irvin, C.G.; Fozard, J.R.; O'Byrne, P.M.; Belvisi, M.G. A role for sensory nerves in the late asthmatic response. *Thorax* **2012**, *67*, 19–25. [CrossRef] [PubMed]
66. Geppetti, P.; Patacchini, R.; Nassini, R.; Materazzi, S. Cough: The Emerging Role of the TRPA1 Channel. *Lung* **2010**, *188*, S63–S68. [CrossRef] [PubMed]
67. Nassini, R.; Materazzi, S.; De Siena, G.; De Cesaris, F.; Geppetti, P. Transient receptor potential channels as novel drug targets in respiratory diseases. *Curr. Opin. Investig. Drugs* **2010**, *11*, 535–542.
68. Mazzone, S.B.; Undem, B.J. Vagal afferent innervation of the airways in health and disease. *Physiol. Rev.* **2016**, *96*, 975–1024. [CrossRef]
69. Undem, B.J.; Kollarik, M. The role of vagal afferent nerves in chronic obstructive pulmonary disease. *Proc. Am. Thorac. Soc.* **2005**, *2*, 355–360. [CrossRef]
70. Canning, B.J. Afferent nerves regulating the cough reflex: Mechanisms and Mediators of Cough in Disease. *Otolaryngol. Clin. N. Am.* **2010**, *43*, 15–25. [CrossRef]
71. Boonen, B.; Alpizar, Y.A.; Meseguer, V.M.; Talavera, K. TRP Channels as Sensors of Bacterial Endotoxins. *Toxins (Basel)* **2018**, *10*, 326. [CrossRef]

72. Mazgaeen, L.; Gurung, P. Recent Advances in Lipopolysaccharide Recognition Systems. *Int. J. Mol. Sci.* **2020**, *21*, 379.
73. Mendes, S.J.F.; Sousa, F.I.A.B.; Pereira, D.M.S.; Ferro, T.A.F.; Pereira, I.C.P.; Silva, B.L.R.; Pinheiro, A.J.M.C.R.; Mouchrek, A.Q.S.; Monteiro-Neto, V.; Costa, S.K.P.; et al. Cinnamaldehyde modulates LPS-induced systemic inflammatory response syndrome through TRPA1-dependent and independent mechanisms. *Int. Immunopharmacol.* **2016**, *34*, 60–70. [CrossRef]
74. Yin, S.; Wang, P.; Xing, R.; Zhao, L.; Li, X.; Zhang, L.; Xiao, Y. Transient Receptor Potential Ankyrin 1 (TRPA1) Mediates Lipopolysaccharide (LPS)-Induced Inflammatory Responses in Primary Human Osteoarthritic Fibroblast-Like Synoviocytes. *Inflammation* **2018**, *41*, 700–709. [CrossRef]
75. Soldano, A.; Alpizar, Y.A.; Boonen, B.; Franco, L.; López-Requena, A.; Liu, G.; Mora, N.; Yaksi, E.; Voets, T.; Vennekens, R.; et al. Gustatory-mediated avoidance of bacterial lipopolysaccharides via TRPA1 activation in Drosophila. *Elife* **2016**, *5*, e13133. [CrossRef]
76. Startek, J.B.; Talavera, K.; Voets, T.; Alpizar, Y.A. Differential interactions of bacterial lipopolysaccharides with lipid membranes: Implications for TRPA1-mediated chemosensation. *Sci. Rep.* **2018**, *8*. [CrossRef]
77. Elekes, K.; Helyes, Z.; Németh, J.; Sándor, K.; Pozsgai, G.; Kereskai, L.; Börzsei, R.; Pintér, E.; Szabó, Á.; Szolcsányi, J. Role of capsaicin-sensitive afferents and sensory neuropeptides in endotoxin-induced airway inflammation and consequent bronchial hyperreactivity in the mouse. *Regul. Pept.* **2007**, *141*, 44–54. [CrossRef]
78. Helyes, Z.; Elekes, K.; Németh, J.; Pozsgai, G.; Sándor, K.; Kereskai, L.; Börzsei, R.; Pintér, E.; Szabó, Á.; Szolcsányi, J. Role of transient receptor potential vanilloid 1 receptors in endotoxin-induced airway inflammation in the mouse. *Am. J. Physiol. Lung Cell. Mol. Physiol.* **2007**, *292*, 1173–1181. [CrossRef]
79. Lee, L.-Y.; Hsu, C.-C.; Lin, Y.-J.; Lin, R.-L.; Khosravi, M. Interaction between TRPA1 and TRPV1: Synergy on pulmonary sensory nerves. *Pulm. Pharmacol. Ther.* **2015**, *35*, 87–93. [CrossRef]
80. Marsh, B.J.; Fryer, A.D.; Jacoby, D.B.; Drake, M.G. TRPA1 causes rapid bronchodilation via non-epithelial PGE2. *Am. J. Physiol. Cell. Mol. Physiol.* **2020**, *318*, L943–L952. [CrossRef]
81. Alpizar, Y.A.; Boonen, B.; Sanchez, A.; Jung, C.; López-Requena, A.; Naert, R.; Steelant, B.; Luyts, K.; Plata, C.; De Vooght, V.; et al. TRPV4 activation triggers protective responses to bacterial lipopolysaccharides in airway epithelial cells. *Nat. Commun.* **2017**, *8*, 1059. [CrossRef]
82. Chao, L.K.; Hua, K.-F.; Hsu, H.-Y.; Cheng, S.-S.; Lin, I.-F.; Chen, C.-J.; Chen, S.-T.; Chang, S.-T. Cinnamaldehyde inhibits pro-inflammatory cytokines secretion from monocytes/macrophages through suppression of intracellular signaling. *Food Chem. Toxicol.* **2008**, *46*, 220–231. [CrossRef]
83. Pulli, B.; Ali, M.; Forghani, R.; Schob, S.; Hsieh, K.L.C.; Wojtkiewicz, G.; Linnoila, J.J.; Chen, J.W. Measuring Myeloperoxidase Activity in Biological Samples. *PLoS ONE* **2013**, *8*, e67976. [CrossRef]
84. Dupont, L.L.; Alpizar, Y.A.; Brusselle, G.G.; Bracke, K.R.; K, T.; Joos, G.F.; Maes, T. Expression of transient receptor potential (TRP) channels in a murine model of cigarette smoke exposure. In Proceedings of the C34 Insights into COPD Pathogenesis from Pre-Clinical Studies, San Diego, CA, USA, 16–21 May 2014.
85. Nie, Y.; Huang, C.; Zhong, S.; Wortley, M.A.; Luo, Y.; Luo, W.; Xie, Y.; Lai, K.; Zhong, N. Cigarette smoke extract (CSE) induces transient receptor potential ankyrin 1 (TRPA1) expression via activation of HIF1αin A549 cells. *Free Radic. Biol. Med.* **2016**, *99*, 498–507. [CrossRef]
86. Ács, K.; Bencsik, T.; Böszörményi, A.; Kocsis, B.; Horváth, G. Essential Oils and Their Vapors as Potential Antibacterial Agents Against Respiratory Tract Pathogens. *Nat. Pord. Commun.* **2016**, *11*, 1709–1712. [CrossRef]
87. Bautista, D.M.; Jordt, S.-E.; Nikai, T.; Tsuruda, P.R.; Read, A.J.; Poblete, J.; Yamoah, E.N.; Basbaum, A.I.; Julius, D. TRPA1 Mediates the Inflammatory Actions of Environmental Irritants and Proalgesic Agents. *Cells* **2006**, *124*, 1269–1282. [CrossRef]
88. Westphal, O.; Jahn, K. Bacterial lipopolysaccharides: Extraction with phenolwater and further applications of the procedure. In *Methods in Carbohydrate Chemistry*; Whistler, R.L., Ed.; Academic Press: New York, NY, USA, 1965; pp. 83–91.
89. Rietschel, E.T.; Kirikae, T.; Schade, F.U.; Mamai, U.; Günter, S.; Loppnow, H.; Ulmer, A.J.; Zähringer, U.; Seydel, U.; Di Padova, F.; et al. Bacterial endotoxin: Molecular rekationships of sturcutre to activity and function. *FASEB J.* **1994**, *8*, 217–225. [CrossRef]

90. Poltorak, A.; He, X.; Smirnova, I.; Liu, M.-Y.; Van Huffel, C.; Du, X.; Birdwell, D.; Alejos, E.; Silva, M.; Galanos, C.; et al. Defective LPS Signaling in C3H/HeJ and C57BL/10ScCr Mice: Mutations in Tlr4 Gene. *Science* **1998**, *282*, 2085–2088. [CrossRef]
91. Haddad, E.-B.; Birrell, M.; McCluskie, K.; Ling, A.; Webber, S.E.; Foster, M.L.; Belvisi, M.G. Role of p38 MAP kinase in LPS-induced airway inflammation in the rat. *Br. J. Pharmacol.* **2001**, *132*, 1715–1724. [CrossRef]
92. Togbe, D.; Schnyder-Candrian, S.; Schnyder, B.; Doz, E.; Noulin, N.; Janot, L.; Secher, T.; Gasse, P.; Lima, C.; Coelho, F.R.; et al. Toll-like receptor and tumour necrosis factor dependent endotoxin-induced acute lung injury. *Int. J. Exp. Path.* **2007**, *88*, 387–391. [CrossRef]
93. Helyes, Z.; Hajna, Z. Endotoxin-induced airway inflammation and asthma models. In *TRP Channels in Drug Discovery*; Szallasi, A., Bíró, T., Eds.; Humana Press: Totowa, NJ, USA, 2012; pp. 301–342. ISBN 978-1-62703-076-2.
94. Lefort, J.; Motreff, L.; Vargaftig, B.B. Airway Administration of Escherichia coli Endotoxin to Mice Induces Glucocorticosteroid-Resistant Bronchoconstriction and Vasopermeation. *Am. J. Respir. Cell Mol. Biol.* **2001**, *24*, 345–351. [CrossRef]
95. Hajna, Z.; Borbély, É.; Kemény, Á.; Botz, B.; Kereskai, L.; Szolcsányi, J.; Pintér, E.; Paige, C.J.; Berger, A.; Helyes, Z. Hemokinin-1 is an important mediator of endotoxin-induced acute airway inflammation in the mouse. *Peptides* **2015**, *64*, 1–7. [CrossRef]
96. Ma, W.; Cui, W.; Lin, Q. Improved immnunophenotyping of lymphocytes in bronchoalveolar lavage fluid (BALF) by flow cytometry. *Clin. Chim. Acta* **2001**, *313*, 133–138. [CrossRef]
97. Zeldin, D.C.; Wohlford-Lenane, C.; Chulada, P.; Bradbury, J.A.; Scarborough, P.E.; Roggli, V.; Langenbach, R.; Schwartz, D.A. Airway Inflammation and Responsiveness in Prostaglandin H Synthase – Deficient Mice Exposed to Bacterial Lipopolysaccharide. *Am. J. Respir. Cell Mol. Biol.* **2001**, *25*, 457–465. [CrossRef]
98. Helyes, Z.; Kemény, Á.; Csekő, K.; Szőke, É.; Elekes, K.; Mester, M.; Sándor, K.; Perkecz, A.; Kereskai, L.; Márk, L.; et al. Marijuana smoke induces severe pulmonary hyperresponsiveness, inflammation, and emphysema in a predictive mouse model not via CB1 receptor activation. *Am. J. Physiol. Lung Cell. Mol. Physiol.* **2017**, *313*, L267–L277. [CrossRef] [PubMed]
99. Rodrigues, M.R.; Rodriguez, D.; Russo, M.; Campa, A. Macrophage Activation Includes High Intracellular Myeloperoxidase Activity. *Biochem. Biophys. Res. Commun.* **2002**, *292*, 869–873. [CrossRef] [PubMed]

pharmaceuticals

MDPI

Review

Role of TRPV1 and TRPA1 Ion Channels in Inflammatory Bowel Diseases: Potential Therapeutic Targets?

Kata Csekő [1,†], Bram Beckers [2,3,†], Daniel Keszthelyi [2,3] and Zsuzsanna Helyes [1,4,*]

1 Department of Pharmacology and Pharmacotherapy, Medical School and Molecular Pharmacology Research Group, Szentágothai Research Centre, University of Pécs, H-7624 Pécs, Hungary; csekoe.kata@gmail.com
2 Division of Gastroenterology-Hepatology, Department of Internal Medicine, Maastricht University Medical Center (MUMC+), 6202 AZ Maastricht, The Netherlands; ab.beckers@maastrichtuniversity.nl (B.B.); daniel.keszthelyi@maastrichtuniversity.nl (D.K.)
3 NUTRIM, School of Nutrition and Translational Research in Metabolism, Maastricht University, 6202 AZ Maastricht, The Netherlands
4 PharmInVivo Ltd., H-7629 Pécs, Hungary
* Correspondence: zsuzsanna.helyes@aok.pte.hu; Tel.: +36-72-536001/35591, 29043
† The authors contributed equally to the present work.

Received: 11 March 2019; Accepted: 27 March 2019; Published: 30 March 2019

Abstract: Inflammatory bowel diseases (IBD) have long been recognized to be accompanied by pain resulting in high morbidity. Transient receptor potential vanilloid 1 (TRPV1) and ankyrin 1 (TRPA1) ion channels located predominantly on the capsaicin-sensitive sensory neurons play a complex role in hyperalgesia and neurogenic inflammation. This review provides an overview of their expression and role in intestinal inflammation, in particular colitis, that appears to be virtually inconsistent based on the thorough investigations of the last twenty years. However, preclinical results with pharmacological interventions, as well as scarcely available human studies, more convincingly point out the potential therapeutic value of TRPV1 and TRPA1 antagonists in colitis and visceral hypersensitivity providing future therapeutical perspectives through a complex, unique mechanism of action for drug development in IBD.

Keywords: IDB; Crohn's disease; ulcerative colitis; TRPV1; TRPA1; human studies; animal studies; colitis models

1. Introduction

Inflammatory bowel disease (IBD) is a group of chronic relapsing and remitting inflammatory disorders of the bowel [1,2]. The two major groups of IBD are Crohn's disease (CD) and ulcerative colitis (UC), each having its own disease characteristics. The cardinal symptom in both disorders however, is abdominal pain, which often causes significant morbidity. Transient receptor potential vanilloid 1 (TRPV1) and ankyrin 1 (TRPA1) ion channels located predominantly on the capsaicin-sensitive sensory neurons play a complex role in hyperalgesia and neurogenic inflammation, and although their role in colitis is seemingly contradictory, there is a growing evidence on their involvement in IBD. The aim of this review is therefore to provide an overview of their expression and role in intestinal inflammation, in particular colitis.

CD is characterized by lesions affecting the entire gastrointestinal tract, UC per definition is limited to the colon. In addition, whereas inflammation is usually confined to the mucosa in UC, it often extends beyond the muscular layers in CD (i.e., transmural inflammation). Microscopically, one can sometimes identify characteristic differences, with non-caseating granulomas present in CD

and crypt abscesses in UC. Even clinical differences exist, as bloody stools are commonly seen in UC but far less often in CD. On the other hand, perianal disease (including fistulas and perianal abscesses) is more suggestive for CD than UC. Other symptoms are encountered in both UC and CD, including malaise, fatigue, diarrhoea and loss of appetite.

As mentioned above, disease activity varies during the course of the disorder, meaning that both the extent of inflammation and patient symptoms change over time. In order to monitor disease activity, both clinical and biochemical assessments are used, as well as endoscopic follow-up. Currently commonly used biomarker is fecal calprotectin (a non-invasive inflammatory marker that correlates well with disease activity in both UC and CD) [3]. No other biomarkers have yet been established as an instrument to monitor disease activity in clinical practice.

Although biochemical/endoscopic signs of disease activity are important to monitor, it should be noted that IBD patients often report symptoms during clinical and biochemical remission. These symptoms may include abdominal pain, bloating, or a feeling of incomplete rectal evacuation, accompanied by a disturbed bowel pattern. Since these symptoms are compatible with irritable bowel syndrome, they are often referred to as "IBS-like". In clinical practice, treatment of these IBS-like symptoms in IBD patients remains particularly challenging. Increasing understanding of the biological and molecular background of these phenomena can therefore potentially contribute to the development of novel treatment paradigms.

2. Inflammatory Bowel Diseases (IBD) and Related Pain

Inflammatory states have long been recognized to be accompanied by pain, as captured by the early Latin definition of inflammation (*calor, rubor, tumor* and *dolor*) [4]. In line with this definition, abdominal pain is a cardinal symptom of IBD [5]. Inflammation is likely the primary cause of abdominal pain in active IBD and one of the main suspects in the pathophysiology of ongoing complaints during remission, although the latter is still a subject of discussion [6]. Over 30% of UC patients in remission and almost double this percentage in quiescent CD patients have IBS-like symptoms [7]. On the basis of pain symptoms, one could expect visceral hypersensitivity to be present in active IBD and in symptomatic quiescent IBD patients. Already in the late seventies, Farthing and colleagues studied sensory responses to rectal balloon distensions in patients with ulcerative colitis, as compared to healthy controls [8]. Not surprisingly, it was demonstrated that patients with active ulcerative colitis tolerated a far smaller balloon volume than healthy controls. Similar findings were later reported by two other research groups [9,10]. Moreover, Rao and co-workers showed that hyperalgesia largely subsided upon remission. Finally, Hoboken and colleagues observed rectal hypersensitivity in UC patients in remission that reported IBS-like symptoms. However, these IBS-like symptoms do not appear to be associated with initial extent of the disease [7]. Moreover, no differences have been found in fecal calprotectin between UC patients in remission with or without IBS-like symptoms [11,12]. It is therefore more likely that the acute inflammatory phase induced lasting changes in visceral nociception in these patients, rather than low-grade mucosal inflammation causing ongoing symptoms during remission.

Paradoxically, two more recent studies reported similar or even higher rectal discomfort thresholds in IBD patients (either active disease or in remission) as compared to healthy controls [13,14]. However, important differences with the above mentioned studies should be kept in mind when interpreting these results. First, Bernstein and co-workers studied CD patients with isolated ileal involvement only, with balloon distensions consequently being applied to non-inflamed tissue. The observed higher rectal discomfort thresholds in CD patients during a ramp distension protocol would therefore more likely represent a form of central compensation due to a chronic inflammatory state and subsequent nociceptive signaling, rather than an effect at the peripheral level. The same research group conducted a similar study in UC patients. Using a threshold tracking paradigm, which is considered a non-biased distension protocol as the direction of each step depends on the patient's response during the previous distension [15], it was demonstrated that UC patients had similar rectal discomfort thresholds as

healthy volunteers. It should be noted, however, that UC patients in this study were either in remission or were reported to have only mild disease activity, with most patients being asymptomatic. Results therefore do not necessarily contradict the earlier balloon distension studies, in which patients often had significant disease activity.

3. Transient Receptor Potential Vanilloid 1 and Ankyrin 1 Pain Sensing Ion Channels

Transient receptor potential (TRP) ion channels comprise more than 30 structurally related ion channels, divided into the TRPC (Canonical), the TRPV (Vanilloid), the TRPM (Melastatin), the TRPP (Polycystin), the TRPML (Mucolipin), the TRPA (Ankyrin) and the TRPN (NOMPC) subfamilies based on their sequence homology [16]. Most of them are non-selective cation channels, however, they exhibit differences in permeability and selectivity [17]. These ion channels are tetramers composed of six transmembrane domains, with a pore formed by the hydrophobic region between the fifth and sixth segments. They can assemble as homo- or heterotetramers to form functional units [18]. The physiological role of TRP channels ranges from store-operated calcium channels to thermo-, mechano- and chemosensors.

The most investigated members of the family in relation to gastrointestinal inflammation include vanilloid 1 (TRPV1), ankyrin 1 (TRPA1). They are located predominantly on the capsaicin-sensitive sensory neurons, but several non-neural expressions have recently been described that drew great attention to this research area [19]. In general, they are activated by a variety of exogenous chemicals and endogenous mediators making them important regulatory structures in inflammatory and pain processes. Here we focus on TRPV1 and TRPA1, since there are many experimental and clinical results describing their expression and importance in the gastrointestinal tract most importantly in the colon.

TRPV1 and TRPA1 are polymodal nociceptors playing an important role in thermo- mechanical- and chemo-sensation, and play a complex role in hyperalgesia and neurogenic inflammation. Their endogenous activators are often produced during inflammation, e.g., lipoxygenase products, the acidified pH of the inflamed tissue, and the gastrointestinal mucosa is frequently exposed to their exogenous agonists, such as capsaicin, allyl isothiocyanate, allicin etc. ingested by food. Furthermore, TRPV1 and TRPA1 are capable of functional interaction, such as heterologous desensitization [20], since the majority of TRPA1 expressing nerve fibers co-express TRPV1 [21]. Both ion channels can be sensitized by a variety of other mechanisms, such as prostaglandins, bradykinin and proteases, e.g., cathepsin expressed by immune cells, via the protease-activated receptor 2 (PAR2) present on both capsaicin-sensitive nerve endings and the immune cells themselves [22,23].

TRPV1 and TRPA1 in IBD Patients

Putative evidence points toward sensitization and even activation of TRPV1 by various inflammatory mediators, as indicated by the multiplicity of animal studies reported below. In vitro studies using human embryonic kidney cells (HEK293 cells) transfected with rat TRPV1 cDNA have reported TRPV1 sensitization by various mediators of inflammation as well, including prostaglandin E2 and prostaglandin I2, bradykinin, nerve growth factor and the chemokine CCL3 [24–27]. Moreover, in a study with rectal biopsy material from healthy volunteers, pre-incubation with histamine was shown to potentiate TRPV1 responses. Inflammation associated tissue acidification would furthermore appear to be an obvious route for TRPV1 activation [28]. Indeed, intradermal and intramuscular low pH injections in healthy volunteers were shown to elicit moderate pain responses, which were potentiated by the injection of prostaglandin E2 [29]. Similarly, Jones and colleagues demonstrated that topical application of capsaicin potentiated pain responses to iontophoresis of protons [30]. It should be noted, however, that desensitization after repeated topical capsaicin application did not reduce acid-induced pain responses, suggesting that other receptors are involved as well. Nonetheless sufficient data indicates TRPV1 is sensitized in inflammatory conditions, thus potentially resulting in hyperalgesia and abdominal pain in IBD.

Although TRPV1 appears to be sensitized by inflammatory mediators, studies on the expression of TRPV1 in inflamed human intestine, and in particular colon tissue have yielded contradictory results (Tables 1 and 2). Yiangou and co-workers previously investigated TRPV1 immunoreactivity in colonic tissue samples from IBD patients who underwent a colectomy due to refractory disease, using tissue samples obtained from resections due to non-obstructing carcinoma as controls [31]. It was demonstrated that TRPV1 immunoreactivity was greatly increased in the colonic nerve fibers of patients with IBD as compared to controls. These findings were recently corroborated by a study with samples from 60 IBD patients (30 patients with UC and 30 patients with CD) [32]. Whereas Yiangou observed increased expression in the submucosa only, Luo and colleagues reported increased TRPV1 expression in both the mucosa and infiltrating inflammatory cells. On the other hand, we observed decreased levels of TRPV1 mRNA in biopsy material from patients with active and inactive CD and UC as compared to healthy controls [33]. In line with our findings, Rizopoulos and colleagues very recently reported decreased TRPV1 expression in mucosal biopsy material from UC patients, as compared to colonic resections from non-IBD patients [34]. Importantly, TRPV1 expression does not appear to be correlated with disease activity, arguing against a role for the extent of inflammation. Regardless of the direction of regulation, inflammation induced changes in TRPV1 expression are likely reversible. Akbar and co-workers found no differences in TRPV1-immunoreactivity in rectosigmoid biopsies when comparing samples from asymptomatic quiescent IBD patients and healthy volunteers, but did find increased TRPV1 expression in quiescent IBD patients with abdominal pain [35]. Similarly, we did not observe significant differences in TRPV1 transcription in sigmoid colonic mucosal samples from (primarily asymptomatic) quiescent UC patients, as compared to healthy controls [36].

Table 1. Alterations in TRPV1 and TRPA1 transcription/expression in Crohn's disease (CD) patients with fold-changes where available. (IHC: immunohistochemistry, IF: immunofluorescence).

Disease Activity	Ion Channel	Sampling Method/Location	Methods	Results; Number of Patients	Relation to Abdominal Complaints and/or Disease severity	Ref
Active CD	TRPV1	Resection (colectomy)	IHC (computerized image analysis)	upregulated in submucosa; $n = 6$	Not reported	[31]
		Colon biopsy–affected and non-affected regions	IHC (computerized image analysis)	upregulated in mucosa and infiltrating inflammatory cells; $n = 30$	No significant correlation between disease severity and TRPV1 expression	[32]
		Distal colon biopsy	IHC, qPCR	downregulated mRNA n = not reported	Not reported	[33]
		Colon biopsy	IF	downregulated mRNA $n = 6$	Not reported	[37]
	TRPA1	Distal colon biopsy	IHC, qPCR	upregulated mRNA n = not reported	Not reported	[33]
		Colon biopsy	IF	upregulated mRNA $n = 7$	Not reported	[37]
CD in remission	TRPV1	Distal colon biopsy	IHC, qPCR	downregulated mRNA n = not reported	Not reported	[33]
		Rectosigmoid biopsy	IHC	upregulated in symptomatic quiescent patients; 3.9-fold increase in median number of TRPV1-immunoreactive fibers (CD and UC combined) $n = 9$	Significant correlation between TRPV1 expression and abdominal pain score	[35]
CD – disease activity unknown	TRPA1	Surgical samples of fibrotic regions (colon)	IHC	Denser immunoreactivity in mucosal and submucosal layers $n = 3$	Not reported	[38]
		Biopsy from fibrotic regions (colon)	IHC, RT-PCR	upregulated mRNA and protein levels $n = 8$	Not reported	[39]

Table 2. Alterations in TRPV1 and TRPA1 transcription/expression in ulcerative colitis (UC) patients with fold-changes where available.

Disease Activity	Ion Channel	Sampling Method/Location	Methods	Results; Number of Patients	Relation to Abdominal Complaints and/or Disease Severity	Ref
Active UC	TRPV1	Resection (colectomy)	IHC (computerized image analysis)	upregulated in submucosa $n = 3$	Not reported	[31]
		Colon biopsy–affected and non-affected regions	IHC (computerized image analysis)	upregulated in mucosa and infiltrating inflammatory cells; $n = 30$	No significant correlation between disease severity and TRPV1 expression	[32]
		Distal colon biopsy	IHC, qPCR	downregulated mRNA	Not reported	[33]
		Colon biopsy	IHC (manual counting by two observers)	downregulated protein $n = 26$	No significant correlation between clinical features and TRPV1 expression	[34]
UC in remission	TRPV1	Distal colon biopsy	IHC, qPCR	downregulated mRNA	Not reported	[33]
		Colon biopsy	IHC (manual counting by two observers)	downregulated protein $n = 24$	No significant correlation between clinical features and TRPV1 expression	[34]
		Rectosigmoid biopsy	IHC	upregulated in patients with IBS-like symptoms; 3.9-fold increase in median number of TRPV1-immunoreactive fibers (CD and UC combined) $n = 11$	Significant correlation between TRPV1 expression and abdominal pain score	[35]
		Rectosigmoid biopsy	qPCR	No significant difference in mRNA levels between asymptomatic patients and healthy controls $n = 34$	Not reported	[36]

There are few data regarding the expression and function of TRPA1 in IBD patients. However, results appear to be less contradictory than with TRPV1 (Tables 1 and 2). In our study with biopsy material from patients with active and inactive CD and UC, we found a significant TRPA1 mRNA upregulation. Similarly, Bertin and co-workers found TRPA1 to be upregulated in patients with active UC and CD, although the difference was non-significant because of small sample size (n = 13). Triple immunofluorescence staining for TRPV1, TRPA1 and CD4 demonstrated that infiltrating CD4+ T cells were also positive for TRPV1 and TRPA1 [37]. Moreover, a significantly higher number of these cells was found in the colonic tissue samples of both UC and CD patients. Two other studies also reported increased TRPA1 expression in stenotic regions in the colon of CD patients, in samples obtained surgically and endoscopically. These studies suggested TRPA1 to be anti-fibrotic. Using a culture medium containing normal human intestinal myofibroblasts (InMyoFibs), it was demonstrated that adding type I collagen to the medium enhanced TRPA1 expression [38]. When fibrosis was elicited by transforming growth factor β1, knockdown of TRPA1 with siRNA resulted in enhanced fibrogenic effects [38].

4. Animal Models of IBD

Unfortunately ideal IBD models with real translational value do not exist in animals, because they cannot completely mimic the complexity of the multifactorial psychosomatic disease. Moreover, as colitis models usually involve short-term administration of an irritating substance, these rather represent acute inflammation. This is a significant limitation of these models in the context of their representation of IBD, which is a chronic disease. In addition to the duration of administration, the type of irritating substance being used determines the characteristics of the model. The fact that model specifics can influence the results should be taken into consideration in their interpretation. We have to rely on well-established and characterized mechanism models exhibiting most autoimmune and inflammatory components of the human disease [40]. Since human studies revealed a potential role of TRPA1 and TRPV1 receptors in the pathogenesis of IBD, but only expression changes could be detected in the human samples, preclinical tests are essential to have a better insight into the pathogenesis of IBD, investigate functional alterations including the role of these ion channels, as well as perform pharmacological interventions.

Besides chemical induction and bacterial infection (with *Salmonella typhimurium* and *Salmonella dublin* or invasive-adherent *Escherichia coli*) several transgenic and knockout strains have been developed in order to investigate the specific pathophysiologic alterations in IBD.

Administration of 1%–5% dextran sulfate sodium (DSS) in the drinking water of animals is a widely used method of chemically-induced colitis by disrupting the tight junctions between the intestinal epithelial cells and inducing inflammation through exposing the lamina propria to bacterial and other toxins, infective agents and antigens [41]. The consequent inflammatory cascade with a characteristic symptomatology (bloody diarrhea, weight loss and histopathology with inflammation limited to the mucosa, as well as cytokine profile) is considered to model UC with several limitations such as great variability between the experimental paradigms including concentration, molecular weight and sulphate content of DSS, intestinal flora, strain differences, administration protocol and timing, as well as the endpoints [42].

Further UC-related rodent models include the intrarectal administration of oxazolone and acetic acid. Oxazolone induces a characteristic T helper 2 (Th2) predominant immune response associated with epithelial cell loss in the colon, acetic acid administration evokes direct chemical damage (erosions, ulcerations accompanied by crypt abnormalities) in the distal colon.

In contrast to these UC-like models, trinitrobenzene or dinitrobenzene sulfonic acid (TNBS/DNBS) colitis is associated with profound transmural infiltration of inflammatory cells and Th1-mediated immune response, thus resembling more to CD [43].

For the investigation of T-cell-mediated pathogenesis of colitis, IL-7 overexpressing and T-cell receptor α chain (*TCRα*) deficient (knockout: KO) mice are used in acute and chronic models, respectively, associated with neutrophilic and lymphocytic infiltration [44,45]. Other mouse strains developing spontaneous colitis include Wiskott-Aldrich syndrome protein (*WASP*) KO mice with characteristically elevated levels of Th2 cytokines [46]. Meanwhile, 25% of mice lacking the multidrug resistance 1a gene (*Mdr1α* KO) also show similar symptoms due to a decreased production of IL-10 and functional Treg cells [47]. Furthermore, *IL-2* KO, as well as guanine nucleotide-binding protein subunit α-2 (*Gαi2*) KO mice exhibit UC-like phenotype with crypt abscess formations and ulcerations [48,49].

4.1. Expression of TRPV1 and TRPA1 in Animal Colon

In the gastrointestinal tract TRPV1 is often co-expressed with TRPA1 in capsaicin-sensitive extrinsic sensory nerves, especially in the primary sensory neurons of the dorsal root ganglia. The density of these TRPV1 positive fibers increase from proximal to distal regions of the colon in mice [50]. Furthermore, during DSS colitis the proportion of DRG neurons expressing TRPV1, and their relative TRPV1 mRNA levels increase with a subsequently elevated release of sensory neuropeptides, such as calcitonin gene-related peptide (CGRP) and substance P (SP) [51]. Although the role of TRP-expressing afferents in inflammation is undisputable, there is growing evidence on the expression of TRPV1 and TRPA1 in intrinsic sensory neurons of the myenteric and submucosal plexuses [33,50,52,53] as well as on the surface epithelial cells of colonic mucosa [33,53,54]. The importance of sensory-immune interactions in colonic inflammation is also supported by the expression of TRPV1 and TRPA1 on inflammatory cells like mucosal macrophages, as well as CD4+ T cells [33,37,55] (Tables 3 and 4).

Table 3. mRNA expression of TRPV1 and TRPA1 in the animal colon (ISH: in situ hybridization).

mRNA	Location	Method	Model, Animal Species/Strain	Ref
TRPV1	isolated crypts, submucosal and muscle layers of distal, middle and proximal colon	qPCR	intact male Wistar rats	[54]
	upregulated in colonic DRG to the distal colon in DSS-colitis		2.5% DSS-treated C57BL/6 mice	[51]
	unaltered in distal colon, cell type not specified		DSS colitis - male C57BL/6 mice	[33]
	CD4+ T cells		primary cell culture from C57BL/6 spleen	[55]
TRPA1	muscularis externa and mucosa of duodenum, ileum and colon; cell type not specified		intact C57BL/6 mice	[53]
	surface epithelium of middle colon	ISH	intact male Wistar rats	[54]
	isolated crypts, submucosal and muscle layers of distal, middle and proximal colon	qPCR	intact male Wistar rats	[54]
	upregulated in distal colon, cell type not specified		DSS colitis - male C57BL/6 mice	[33]

Table 4. Protein expression of TRPV1 and TRPA1 in the animal colon (IHC: immunohistochemistry).

Protein	Location	Method	Model, Animal Species/Strain	Ref
TRPV1	intrinsic sensory neurons of the myenteric plexus-longitudinal muscle of ileum and colon	IHC	intact Sprague-Dawley rats and Dunkin-Hartley guinea pigs of both sexes	[52]
	mucosa, submucosal layers, myenteric plexus and mucosal layer of rectum, distal, transverse and proximal colon		male ddY mice	[50]
	immunopositive neuron fiber density is higher in the distal than the proximal colon		intact and 2.5% DSS-treated C57BL/6 mice colon	[51]
	enteric ganglia, epithelial cells of the distal colon, myenteric and submucosal plexuses, mucosal macrophages, leukocytes		male C57BL/6 mice	[33]
	membrane of resting CD4+ T cells	immunoblotting, flow cytometry, confocal microscopy	primary cell culture from C57BL/6 spleen	[55]
TRPA1	distal colonic epithelial cells, myenteric and submucosal plexuses, interstitial macrophages	IHC	male C57BL/6 mice	[33]
	myenteric and submucosal ganglia; surface epithelial cells of small and large intestines		intact C57BL/6 mice	[53]
	surface epithelium of middle colon		intact male Wistar rats	[54]
	membrane of resting CD4+ T cells	IHC, confocal microscopy	primary cell culture from C57BL/6 spleen	[37]

4.2. Role of TRP Channels in Animal Models of Colitis

The role of TRP channels, in particular TRPV1 and TRPA1 is virtually contradictory in the pathogenesis of IBD. Several studies have been focused on elucidating the mechanism by which these channels might mediate pro-inflammatory and/or anti-inflammatory effects (Table 5).

Table 5. Role of TRPV1 and TRPA1 in animal models of colitis (*Trpv1*$^{-/-}$, *Trpa1*$^{-/-}$ gene deleted mice were bred on C57BL/6 background).

Approaches	Results	Animal Strain/Species	Model	Ref
TRPV1 antagonist	*reduces* colitis severity	Sprague-Dawley rats	5% DSS + capsazepine	[56]
		female BALB/c mice	5% DSS + capsazepine/JNJ 10185734	[57]
		Sprague-Dawley rats	TNBS + capsazepine	[58]
		female Wistar rats	TNBS + BCTC	[59]
		IL10$^{-/-}$ *Trpv1*$^{-/-}$ mice	*IL10*$^{-/-}$ -induced spontaneous colitis + SB366791	[55]
TRPV1 agonist	*attenuates* colitis/visceral hyperalgesia	male Sprague-Dawley rats	TNBS + capsaicin	[60]
		male BALB/c mice	DNBS + curcumin	[61]
		male Sprague-Dawley rats	5% DSS + curcumin	[62]
TRPV1 gene deletion	*decreases* colitis	*female Trpv1*$^{-/-}$ mice	2% DSS	[63]
		IL10$^{-/-}$ *Trpv1*$^{-/-}$ mice	*IL10*$^{-/-}$-induced spontaneous colitis	[55]
		male *Trpv1*$^{-/-}$ mice	2% DSS	[64]
	aggravates colitis	*female Trpv1*$^{-/-}$ mice	DNBS	[65]
	does not affect colitis severity	*female Trpv1*$^{-/-}$ mice	5% DSS	[63]
		Trpv1$^{-/-}$ mice	TNBS	[66]
		Trpv1$^{-/-}$ mice	2.5% DSS	[67]
	protects against chronic pain during recovery	*Trpv1*$^{-/-}$ mice	2.5% DSS	[67]
	decreases CD4+ T cell activation and cytokine production	*IL10*$^{-/-}$ *Trpv1*$^{-/-}$ mice	*IL10*$^{-/-}$-induced spontaneous colitis	[55]
TRPA1 antagonist	*reduces* colitis severity	C57BL/6 mice	TNBS + HC-030031; DSS + HC-030031	[66]
	reverses visceromotor response	female Wistar rats	TNBS/ethanol + TCS-5861528	[59]
TRPA1 gene deletion	*decreases* colitis	Trpa1$^{-/-}$ mice	TNBS, 2% DSS	[66]
		male *Trpa1*$^{-/-}$ mice	2% DSS	[64]
	aggravates colitis	*male Trpa1*$^{-/-}$ mice	2% DSS	[33]
		IL10$^{-/-}$ *Trpa1*$^{-/-}$ mice	*IL10*$^{-/-}$-induced spontaneous colitis	[37]
	increases TRPV1 channel activity in CD4+ T cells, *increases* CD4+ T cell activation and proinflammatory cytokine production	*IL10*$^{-/-}$ *Trpa1*$^{-/-}$ mice	*IL10*$^{-/-}$-induced spontaneous colitis	[37]
Capsaicin-induced sensory desensitization	*aggravates* colitis	female BALB/c mice	oxazolone	[68]
		male *Trpv1*$^{-/-}$, *Trpa1*$^{-/-}$ mice	2% DSS	[64]
	alleviates colitis	Sprague-Dawley rats	5% DSS	[56]
RTX-denervation	*alleviates* colitis	C57BL/6 mice	TNBS, 2% DSS	[66]

Goso and co-workers provided the first evidence for a protective role of TRPV1-expressing peptidergic sensory nerves via the release of the protective neurotransmitter CGRP upon acute

co-administration of capsaicin in a TNBS-induced colitis model [60]. Administration of TRPV1 agonists, resiniferatoxin (RTX) or high dose capsaicin, induces a sustained functional denervation of TRPV1-expressing extrinsic neurons, thus it provides a method in animal models for the investigation of these sensory afferents and the released neurotransmitters. The results of this chemical desensitization are not coherent, since pro-inflammatory and protective roles have also been described. Neonatal capsaicin desensitization, as well as the administration of the TRPV1 antagonist capsazepine have been reported to significantly attenuate macroscopic damage score, myeloperoxidase (MPO) activity increase (peroxidase enzyme released from neutrophil granulocytes in the inflamed tissues) and inflammatory histopathological alterations compared to normal DSS-treated rats attributing the colitogenic effect to SP released from the nerve terminals of TRPV1-expressing sensory fibers [56]. Meanwhile, Utsumi and co-workers found opposing results in the same model after adult treatment by high doses of capsaicin, which exacerbated colitis and reduced the inflammation-induced upregulation of both SP- and CGRP-positive fibers [64]. However, they described that TRPV1 and TRPA1 gene deletion decreased colitis severity and the upregulation of SP-positive nerve fibers without influencing protective CGRP-positive nerves. Similarly, neonatal capsaicin denervation resulted in more severe colitis in the oxazolon-induced model, but exacerbation was not accompanied by changes in the expression and distribution of CGRP- and SP-immunoreactive nerves in the colon [68]. These virtually contradictory pro- and anti-inflammatory effects of neuropeptides released from the TRPV1/A1-expressing fibers during chemically-induced colitis were further investigated in the TNBS model, where abrogated CGRP release in the isolated colon preparations and dorsal root ganglia were observed in *Trpa1*, but not in *Trpv1* gene-deficient mice. They showed that this mechanism is mediated via the sustained sensitization of TRPA1 by TNBS covalently binding to the cysteine and lysine residues in the cytoplasmic N-terminus of the receptor protein. TNBS induces similar severe acute colitis in wildtype and *Trpv1*$^{-/-}$, but reduced inflammation in *Trpa1*$^{-/-}$ mice or wildtype animals treated with the TRPA1 antagonist HC-030031. Sensory denervation, as well as *SP* gene-deletion abolished both TNBS and DSS-induced colitis, while in *CGRP*-deficient mice TNBS induced a more severe colitis further supporting the opposing actions of the sensory neuropeptides released from the same nerve terminals [51,66]. *Trpv1*-deficiency did not affect disease severity, only prevented chronic pain development during the recovery phase of DSS-induced colitis [67]. However, this result was challenged by other studies demonstrating the pathogenic role of TRPV1 by gene-deleted mice exhibiting less severe DSS-induced colitis, concluding that inflammatory mediators activate the TRPV1 receptor and induce neurogenic inflammatory components by releasing SP, neurotensin, vasoactive intestinal polypeptide and galanin [64,69]. Meanwhile, Massa and co-workers found more severe DNBS-induced colitis in *Trpv1*$^{-/-}$ mice, suggesting a protective role of TRPV1 [65]. Bertin and co-workers proposed non-neuronal TRPV1 and TRPA1-mediated proinflammatory mechanisms in colitis. They showed that both channels are present on mouse and human CD4+ T cells and play an important regulatory role in their activation and the production of proinflammatory cytokines, such as interferon- γ (IFN-γ), interleukin-2 (IL-2), IL-10 and tumor necrosis factor α (TNFα). In a spontaneous *IL10*$^{-/-}$ colitis model both genetic deletion and pharmacologic inhibition of TRPV1 resulted in attenuated inflammation. They provided clear experimental evidence in a T cell adoptive transfer model that TRPV1-expressing CD4+ T cells are involved in colitis pathogenesis [55]. In the same experimental paradigm TRPA1 was described to exert protective actions by restraining TRPV1 activity on these immune cells, thus controlling their activation and inflammatory functions [37]. The protective role of TRPA1 was also supported by TRPA1-mediated downregulation of proinflammatory neuropeptides SP, neurokinins A, B (NKA, NKB) and NK1 receptor, as well as cytokines and chemokines like TNFα, IL-1β, monokine induced by gamma interferon (MIG) and monocyte chemotactic protein-1 (MCP-1) [33].

Pharmacological interventions with curcumin had anti-inflammatory and anti-hyperalgesic effects in colitis models [61,62]. Although in these studies curcumin was interpreted and discussed as a TRPV1 agonist, it is important to note that curcumin is a non-selective compound having a typical pleiotropic effect including direct antioxidant activity, anticancer and antimicrobial properties mediated

by a wide range of targets, even the TRPA1 receptor [70–72]. Considering that TRPA1 is almost exclusively expressed in TRPV1-positive neurons and both channels are known to interact [20,21], cross-desensitization could have a role in the actions of curcumin. Furthermore, curcumin was also described as a TRPV1 antagonist, because it inhibited capsaicin-evoked potentials [73]. In a clinical study, curcumin was reported to significantly reduce relapse rate in UC patients not via the activation, but the inhibition of TRPV1 either directly or by ways of cross-desensitization of TRPA1 [74]. However, we should be cautious when drawing conclusions regarding TRPV1 involvement based on the results of curcumin administration.

Cannabinoids have also shown beneficial effects in animal colitis models [65,75]. Changes in the endocannabinoid system during intestinal inflammation have been described and TRPV1-associated effects could be involved in the anti-inflammatory effects of cannabinoids [75–77]. More than two-fold increase of anandamide also acting as a TRPV1 agonist was described in the human UC biopsy samples [75]. A single oral dose of the endocannabinoid palmitoylethanolamide (PEA) was shown to increase 2-arachidonoylglycerol (2-AG) blood levels in human volunteers [78]. In HEK-293 cells transfected with human recombinant TRPV1, PEA significantly enhanced 2-AG induced activation and desensitization of TRPV1. It was therefore speculated that 2-AG is responsible for the protective effect of PEA during an induced inflammatory response [79]. In a study using colonic explants of six quiescent IBD patients, it was demonstrated that treatment with PEA and cannabidiol (CBD) suppressed secretion of inflammatory mediators in explants exposed to inflammatory cytokines that was counteracted by the TRPV1 antagonist [77].

Other TRPV1 and TRPA1 antagonists also showed mainly protective actions. TRPV1 blockade by the non-selective antagonist capsazepine, JNJ 10185734, BCTC and SB366791 in various models of colitis exerted anti-inflammatory actions supporting the pathogenic role of TRPV1 in experimental IBD [55–59]. Moreover, both intraperitoneal and intrathecal administrations of TRPV1 and TRPA1 antagonists exerted analgesic actions in rat colitis models highlighting central nervous system mechanisms [59].

5. Conclusions, Drug Developmental Perspectives

TRPV1 and TRPA1 expression, and experimental data regarding its role in colitis appears to be virtually inconsistent. Activation of these receptors on sensory nerve terminals mediates neurogenic inflammation via the release of SP and CGRP, resulting in increased vascular permeability, plasma protein extravasation and inflammatory cell activation. Meanwhile, anti-inflammatory sensory neuropeptides, such as somatostatin and opioid peptides released simultaneously from the same nerve ending exert anti-inflammatory and analgesic actions both locally and systemically through getting into the circulation. Furthermore, these ion channels on vascular smooth muscle and inflammatory cells such as macrophages and T helper cells mediate both pro- and anti-inflammatory functions. Therefore, the overall role of TRPV1 and TRPA1 in experimental colitis is dependent on (1) the diversity of the expression of these ion channels on sensory nerves, immune cells, epithelial cells and vascular smooth muscle cells [19], (2) the consequent activation-induced release of broad range of pro- and anti-inflammatory mediators including sensory neuropeptides and cytokines exerting divergent mechanisms, (3) the complex interactions of the co-expressed TRPV1 and TRPA1 receptors (Figure 1), (4) differences of the experimental models, protocols and paradigms (species, strain, concentration and composition of the chemicals, duration, intensity, complex mechanisms of the injury), as well as several limitations of the models [42].

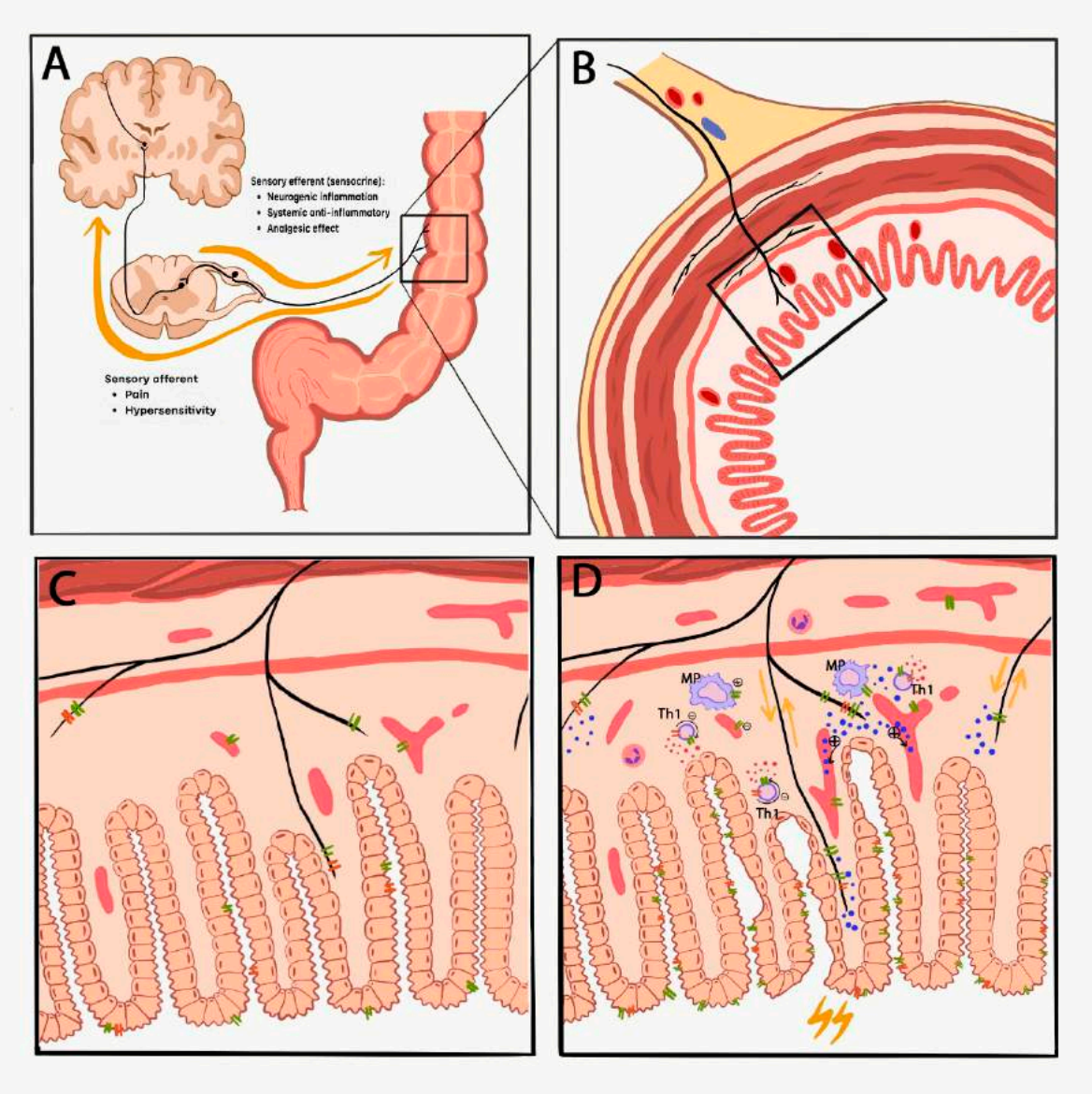

Figure 1. The complex interactions of TRPV1 and TRPA1 and their virtually contradictory role in colitis. Panel A demonstrates the afferent and efferent (sensocrine) functions (yellow arrows) of the capsaicin-sensitive sensory nerve fibers. Panel C (without inflammation) and D (during inflammation) depict an enlarged schematic section of the colon cross section (panel B) focusing on the expression and interaction of TRPV1 (green double lines) and TRPA1 (orange double lines) in the colon mucosa. Neurogenic inflammation is mediated via the release of SP and CGRP (blue dots represent neurotransmitters, such as SP, CGRP and somatostatin), resulting in increased vascular permeability, plasma protein extravasation and inflammatory cell activation. Meanwhile, anti-inflammatory sensory neuropeptides, such as somatostatin and opioid peptides released simultaneously from the same nerve ending exert anti-inflammatory and analgesic actions both locally and systemically through getting into the circulation. Furthermore, these ion channels on vascular smooth muscle and inflammatory cell such as macrophages (MP) and T helper cells (Th1) mediate both pro- (+) and anti-inflammatory (-) effects by regulating the release of cytokines (IFN-γ, IL-2, IL-10, TNFα are represented as red dots).

However, preclinical results with pharmacological interventions, as well as scarcely available human studies, more convincingly point out the potential therapeutic value of TRPV1 and TRPA1 antagonists in colitis and visceral hypersensitivity providing future therapeutical perspectives for small molecule candidates. The first generation TRPV1 compounds thoroughly investigated in a broad range

of clinical trials as novel analgesic and anti-inflammmatory drugs interfered with thermoregulation, elicited severe hyperthermia [80,81] and raised heat pain thresholds with consequently increased burn risk [82,83]. Therefore, they could not be registered for the clinical practice. Second generation new drugs with different inhibition sites on the TRPV1 and/or TRPA1 antagonists without the hyperthermic side effect could provide solutions to these problems [84]. Their clinical efficacies are currently intensively investigated, but they could open new perspectives through a complex, unique mechanism of action for drug development in IBD [85,86].

Author Contributions: K.C. and B.B. contributed equally to the present work. B.B. and D.K. focused on literature search regarding human data, K.C. and Z.H. reviewed animal studies. K.C. and B.B. prepared the tables, K.C. made the figure with the assistance of Z.H. and D.K. K.C., B.B., D.K. and Z.H. substantially contributed to the writing of the manuscript and interpreting the data. All authors read and approved the final manuscript.

Funding: Z.H. was supported by the Higher Education Institutional Excellence Program of the Ministry of Human Capacities in Hungary, 20765-3/2018/FEKUTSRTAT; PEPSYS: Complexity of Peptidergic Signalization and its Role in Systemic Diseases, GINOP-2.3.2-15-2016-00050; Human Resource Development Operational Program, EFOP-3.6.2-16-2017-00006 LIVE LONGER; and Economic Development and Innovation Operational Program, GINOP-2.3.2-15-2016-00048 STAY ALIVE; K.C. was supported by the ÚNKP-18-3-IV-PTE-143 New National Excellence Program of the Ministry of Human Capacities.

Conflicts of Interest: D.K. has received research funding from Grünenthal GmbH, Willpharma BV and Allergan, Ltd. D.K. has served as a scientific advisor for Biocodex Benelux and Bayer GmnH. The other authors declare no conflict of interest.

References

1. Torres, J.; Mehandru, S.; Colombel, J.-F.; Peyrin-Biroulet, L. Crohn's Disease. *Lancet* **2017**, *389*, 1741–1755. [CrossRef]
2. Ungaro, R.; Mehandru, S.; Allen, P.B.; Peyrin-Biroulet, L.; Colombel, J.-F. Ulcerative Colitis. *Lancet* **2017**, *389*, 1756–1770. [CrossRef]
3. Bourgonje, A.R.; von Martels, J.Z.H.; de Vos, P.; Faber, K.N.; Dijkstra, G. Increased Fecal Calprotectin Levels in Crohn's Disease Correlate with Elevated Serum Th1- and Th17-Associated Cytokines. *PLoS ONE* **2018**, *13*, e0193202. [CrossRef]
4. Kidd, B.L.; Urban, L.A. Mechanisms of Inflammatory Pain. *Br. J. Anaesth.* **2001**, *87*, 3–11. [CrossRef] [PubMed]
5. Bielefeldt, K.; Davis, B.; Binion, D.G. Pain and Inflammatory Bowel Disease. *Inflamm. Bowel Dis.* **2011**, *15*, 778–788. [CrossRef]
6. Beckers, A.B.; Weerts, Z.Z.R.M.; Helyes, Z.; Masclee, A.A.M.; Keszthelyi, D. Review Article: Transient Receptor Potential Channels as Possible Therapeutic Targets in Irritable Bowel Syndrome. *Aliment. Pharmacol. Ther.* **2017**, *46*, 938–952. [CrossRef]
7. Simren, M.; Axelsson, J.; Gillberg, R.; Abrahamsson, H.; Svedlund, J.; Björnsson, E.S. Quality of Life in Inflammatory Bowel Disease in Remission: The Impact of IBS-Like Symptoms and Associated Psychological Factors. *Am. J. Gastroenterol.* **2002**, *97*, 389–396. [CrossRef]
8. Farthing, M.J.G.; Lennard-Jones, J.E. Sensibility of the Rectum to Distension and the Anorectal Distension Reflex in Ulcerative Colitis. *Gut* **1978**, *19*, 64–69. [CrossRef]
9. Rao, S.S.C.; Read, N.W.; Davison, P.A.; Bannister, J.J.; Holdsworth, C.D. Anorectal Sensitivity and Responses to Rectal Distention in Patients with Ulcerative Colitis. *Gastroenterology* **1987**, *93*, 1270–1275. [CrossRef]
10. Loening-Baucke, V.; Metcalf, A.M.; Shirazi, S. Anorectal Manometry in Active and Quiescent Ulcerative Colitis. *Am. J. Gastroenterol.* **1989**, *84*, 892–897.
11. van Hoboken, E.A.; Thijssen, A.Y.; Verhaaren, R.; van der Veek, P.P.J.; Prins, F.A.; Verspaget, H.W.; Masclee, A.A.M. Symptoms in Patients with Ulcerative Colitis in Remission Are Associated with Visceral Hypersensitivity and Mast Cell Activity. *Scand. J. Gastroenterol.* **2011**, *46*, 981–987. [CrossRef]
12. Keszthelyi, D.; Jonkers, D.M.; Hamer, H.M.; Masclee, A.A.M. Letter: The Role of Sub-Clinical Inflammation and TRPV1 in the in Ulcerative Colitis in Remission. *Aliment. Pharmacol. Ther.* **2013**, *38*, 559–562. [CrossRef] [PubMed]

13. Bernstein, C.N.; Niazi, N.; Robert, M.; Mertz, H.; Kodner, A.; Munakata, J.; Naliboff, B.; Mayer, E.A. Rectal Afferent Function in Patients with Inflammatory and Functional Intestinal Disorders. *Pain* **1996**, *66*, 151–161. [CrossRef]
14. Chang, L.; Munakata, J.; Mayer, E.A.; Schmulson, M.J.; Johnson, T.D.; Bernstein, C.N.; Saba, L.; Naliboff, B.; Anton, P.A.; Matin, K. Perceptual Responses in Patients with Inflammatory and Functional Bowel Disease. *Gut* **2000**, *47*, 497–505. [CrossRef] [PubMed]
15. Whitehead, W.E.; Delvaux, M. Standardization of Barostat Procedures for Testing Smooth Muscle Tone and Sensory Thresholds in the Gastrointestinal Tract. *Dig. Dis. Sci.* **1997**, *42*, 223–241. [CrossRef] [PubMed]
16. Pedersen, F.S.; Owsianik, G.; Nilius, B. TRP Channels: An Overview. *Cell Calcium* **2005**, *38*, 233–252. [CrossRef] [PubMed]
17. Abramowitz, J.; Yildirim, E.; Birnbaumer, L. The TRPC Family of Ion Channels: Relation to the TRP Superfamily and Role in Receptor- and Store-Operated Calcium Entry. In *TRP Ion Channel Function in Sensory Transduction and Cellular Signaling Cascades*; Liedtke, W.B., Heller, S., Eds.; CRC Press: Boca Raton, FL, USA, 2007; Chapter 1.
18. Latorre, R.; Zaelzer, C.; Brauchi, S. Structure-Functional Intimacies of Transient Receptor Potential Channels. *Q. Rev. Biophys.* **2009**, *42*, 201–246. [CrossRef]
19. Fernandes, E.S.; Fernandes, M.A.; Keeble, J.E. The Functions of TRPA1 and TRPV1: Moving Away from Sensory Nerves. *Br. J. Pharmacol.* **2012**, *166*, 510–521. [CrossRef]
20. Ruparel, N.B.; Patwardhan, A.M.; Akopian, A.N.; Hargreaves, K.M. Homologous and Heterologous Desensitization of Capsaicin and Mustard Oil Responses Utilize Different Cellular Pathways in Nociceptors. *Pain* **2008**, *135*, 271–279. [CrossRef] [PubMed]
21. Story, G.M.; Peier, A.M.; Reeve, A.J.; Eid, S.R.; Mosbacher, J.; Hricik, T.R.; Earley, T.J.; Hergarden, A.C.; Andersson, D.A.; Hwang, S.W.; et al. ANKTM1, a TRP-like Channel Expressed in Nociceptive Neurons, Is Activated by Cold Temperatures. *Cell* **2003**, *112*, 819–829. [CrossRef]
22. Amadesi, S.; Nie, J.; Vergnolle, N.; Cottrell, G.S.; Grady, E.F.; Trevisani, M.; Manni, C.; Geppetti, P.; McRoberts, J.A.; Ennes, H.; et al. Protease-Activated Receptor 2 Sensitizes the Capsaicin Receptor Transient Receptor Potential Vanilloid Receptor 1 to Induce Hyperalgesia. *J. Neurosci.* **2004**, *24*, 4300–4312. [CrossRef]
23. Cattaruzza, F.; Lyo, V.; Jones, E.; Pham, D.; Hawkins, J.; Kirkwood, K.; Valdez-Morales, E.; Ibeakanma, C.; Vanner, S.J.; Bogyo, M.; et al. Cathepsin S Is Activated During Colitis and Causes Visceral Hyperalgesia by a PAR2-Dependent Mechanism in Mice. *Gastroenterology* **2011**, *141*, 1864–1874.el–3. [CrossRef] [PubMed]
24. Shin, J.; Cho, H.; Hwang, S.W.; Jung, J.; Shin, C.Y.; Lee, S.; Kim, S.H.; Lee, M.G.; Choi, Y.H.; Kim, J.; et al. Bradykinin-12-Lipoxygenase-VR1 Signaling Pathway for Inflammatory Hyperalgesia. *Proc. Natl. Acad. Sci. USA* **2002**, *99*, 10150–10155. [CrossRef] [PubMed]
25. Zhang, X.; Huang, J.; Mcnaughton, P.A. NGF Rapidly Increases Membrane Expression of TRPV1 Heat-Gated Ion Channels. *EMBO J.* **2005**, *24*, 4211–4223. [CrossRef]
26. Zhang, N.; Inan, S.; Cowan, A.; Sun, R.; Wang, J.M.; Rogers, T.J.; Caterina, M.; Oppenheim, J.J. A Proinflammatory Chemokine, CCL3, Sensitizes the Heat- and Capsaicin-Gated Ion Channel TRPV1. *Proc. Natl. Acad. Sci. USA* **2005**, *102*, 4536–4541. [CrossRef] [PubMed]
27. Moriyama, T.; Higashi, T.; Togashi, K.; Iida, T.; Segi, E.; Sugimoto, Y.; Tominaga, T.; Narumiya, S.; Tominaga, M. Sensitization of TRPV1 by EP 1 and IP Reveals Peripheral Nociceptive Mechanism of Prostaglandins. *Mol. Pain* **2005**, *13*, 1–13. [CrossRef]
28. Okajima, F. Regulation of Inflammation by Extracellular Acidification and Proton-Sensing GPCRs. *Cell. Signal.* **2013**, *25*, 2263–2271. [CrossRef] [PubMed]
29. Rukwied, R.; Chizh, B.A.; Lorenz, U.; Obreja, O.; Margarit, S.; Schley, M.; Schmelz, M. Potentiation of Nociceptive Responses to Low PH Injections in Humans by Prostaglandin E2. *J. Pain* **2019**, *8*, 443–451. [CrossRef]
30. Jones, N.G.; Slater, R.; Cadiou, H.; Mcnaughton, P.; Mcmahon, S.B. Acid-Induced Pain and Its Modulation in Humans. *J. Neurosci.* **2004**, *24*, 10974–10979. [CrossRef]
31. Yiangou, Y.; Facer, P.; Dyer, N.H.C.; Chan, C.L.H.; Knowles, C.; Williams, N.S.; Anand, P. Vanilloid Receptor 1 Immunoreactivity in Inflamed Human Bowel. *Lancet* **2001**, *357*, 1338–1339. [CrossRef]
32. Luo, C.; Wang, Z.; Mu, J.; Zhu, M.; Zhen, Y.; Zhang, H. Upregulation of the Transient Receptor Potential Vanilloid 1 in Colonic Epithelium of Patients with Active Inflammatory Bowel Disease. *Int. J. Clin. Exp. Pathol.* **2017**, *10*, 11335–11344.

33. Kun, J.; Szitter, I.; Kemény, Á.; Perkecz, A.; Kereskai, L.; Pohóczky, K.; Vincze, Á.; Szabó, I.; Szolcsányi, J.; Pintér, E.; Helyes, Z. Upregulation of the Transient Receptor Potential Ankyrin 1 Ion Channel in the Inflamed Human and Mouse Colon and Its Protective Roles. *PLoS ONE* **2014**, *9*, e108164. [CrossRef] [PubMed]
34. Rizopoulos, T.; Papadaki-Petrou, H.; Assimakopoulou, M. Expression Profiling of the Transient Receptor Potential Vanilloid (TRPV) Channels 1, 2, 3 and 4 in Mucosal Epithelium of Human Ulcerative Colitis. *Cells* **2018**, *7*, 61. [CrossRef] [PubMed]
35. Akbar, A.; Yiangou, Y.; Facer, P.; Brydon, W.G.; Walters, J.R.F.; Anand, P.; Ghosh, S. Expression of the TRPV1 Receptor Differs in Quiescent Inflammatory Bowel Disease with or without Abdominal Pain. *Gut* **2010**, *59*, 767–774. [CrossRef] [PubMed]
36. Keszthelyi, D.; Troost, F.J.; Jonkers, D.M.; Helyes, Z.; Hamer, H.M.; Ludidi, S.; Vanhoutvin, S.; Venema, K.; Dekker, J.; Szolcsányi, J.; et al. Alterations in Mucosal Neuropeptides in Patients with Irritable Bowel Syndrome and Ulcerative Colitis in Remission: A Role in Pain Symptom Generation? *Eur. J. Pain* **2013**, *17*, 1299–1306. [CrossRef] [PubMed]
37. Bertin, S.; Aoki-Nonaka, Y.; Lee, J.; de Jong, P.R.; Kim, P.; Han, T.; Yu, T.; To, K.; Takahashi, N.; Boland, B.S.; et al. The TRPA1 Ion Channel Is Expressed in CD4+ T Cells and Restrains T Cell-Mediated Colitis through Inhibition of TRPV1. *Gut* **2017**, *66*, 1584–1596. [CrossRef] [PubMed]
38. Hiraishi, K.; Kurahara, L.-H.; Sumiyoshi, M.; Hu, Y.; Koga, K.; Onitsuka, M.; Kojima, D.; Yue, L.; Takedatsu, H.; Jian, Y.-W.; et al. Daikenchuto (Da-Jian-Zhong-Tang) Ameliorates Intestinal Fibrosis by Activating Myofibroblast Transient Receptor Potential Ankyrin 1 Channel. *World J. Gastroenterol.* **2018**, *24*, 4036–4053. [CrossRef]
39. Kurahara, L.H.; Hiraishi, K.; Hu, Y.; Koga, K.; Onitsuka, M.; Doi, M.; Aoyagi, K.; Takedatsu, H.; Kojima, D.; Fujihara, Y.; et al. Activation of Myofibroblast TRPA1 by Steroids and Pirfenidone Ameliorates Fibrosis in Experimental Crohn's Disease. *Cell. Mol. Gastroenterol. Hepatol.* **2018**, *5*, 299–318. [CrossRef]
40. Valatas, V.; Bamias, G.; Kolios, G. Experimental Colitis Models: Insights into the Pathogenesis of in Fl Ammatory Bowel Disease and Translational Issues. *Eur. J. Pharmacol.* **2015**, *759*, 253–264. [CrossRef]
41. Low, D.; Nguyen, D.D.; Mizoguchi, E. Animal Models of Ulcerative Colitis and Their Application in Drug Research. *Drug Des. Dev. Ther.* **2013**, *7*, 1341–1357.
42. Perse, M.; Cerar, A. Dextran Sodium Sulphate Colitis Mouse Model: Traps and Tricks. *J. Biomed. Biotechnol.* **2012**, 718617.
43. Kawada, M.; Arihiro, A.; Mizoguchi, E. Insights from Advances in Research of Chemically Induced Experimental Models of Human Inflammatory Bowel Disease. *World J. Gastroenterol.* **2007**, *13*, 5581–5593. [CrossRef] [PubMed]
44. Watanabe, M.; Ueno, Y.; Yajima, T.; Okamoto, S.; Hayashi, T.; Yamazaki, M.; Iwao, Y.; Ishii, H.; Habu, S.; Uehira, M.; et al. Interleukin 7 Transgenic Mice Develop Chronic Colitis with Decreased Interleukin 7 Protein Accumulation in the Colonic Mucosa. *J. Exp. Med.* **1998**, *187*, 389–402. [CrossRef] [PubMed]
45. Mombaerts, P.; Mizoguchi, E.; Grusby, M.J.; Glimcher, L.H.; Bhan, A.K.; Tonegawa, S. Spontaneous Development of Inflammatory Bowel Disease in T Cell Receptor Mutant Mice. *Cell* **1993**, *75*, 275–282. [CrossRef]
46. Nguyen, D.D.; Maillard, M.H.; Cotta-de-Almeida, V.; Mizoguchi, E.; Klein, C.; Fuss, I.; Nagler, C.; Mizoguchi, A.; Bhan, A.K.; Snapper, S.B. Lymphocyte-Dependent and Th2 Cytokine-Associated Colitis in Mice Deficient in Wiskott-Aldrich Syndrome Protein. *Gastroenterology* **2007**, *133*, 1188–1197. [CrossRef]
47. Panwala, C.M.; Jones, J.C.; Viney, J.L. A Novel Model of Inflammatory Bowel Disease: Mice Deficient for the Multiple Drug Resistance Gene, Mdr1a, Spontaneously Develop Colitis. *J. Immunol.* **1998**, *161*, 5733–5744.
48. Sadlack, B.; Merz, H.; Schorle, H.; Schimpl, A.; Feller, A.C.; Horak, I. Ulcerative Colitis-like Disease in Mice with a Disrupted Interleukin-2 Gene. *Cell* **1993**, *75*, 253–261. [CrossRef]
49. Rudolph, U.; Finegold, M.J.; Rich, S.S.; Harriman, G.R.; Srinivasan, Y.; Brabet, P.; Boulay, G.; Bradley, A.; Birnbaumer, L. Ulcerative Colitis and Adenocarcinoma of the Colon in Gαi2-Deficient Mice. *Nat. Genet.* **1995**, *10*, 143–150. [CrossRef] [PubMed]
50. Matsumoto, K.; Kurosawa, E.; Terui, H.; Hosoya, T.; Tashima, K.; Murayama, T.; Priestley, J.V.; Horie, S. Localization of TRPV1 and Contractile Effect of Capsaicin in Mouse Large Intestine: High Abundance and Sensitivity in Rectum and Distal Colon. *Am. J. Physiol. Gastrointest. Liver Physiol.* **2009**, *297*, 348–360. [CrossRef] [PubMed]

51. Engel, M.A.; Khalil, M.; Mueller-Tribbensee, S.M.; Becker, C.; Neuhuber, W.L.; Neurath, M.F.; Reeh, P.W. The Proximodistal Aggravation of Colitis Depends on Substance P Released from TRPV1-Expressing Sensory Neurons. *J. Gastroenterol.* **2012**, *47*, 256–265. [CrossRef] [PubMed]
52. Anavi-Goffer, S.; Mckay, N.G.; Ashford, M.L.J.; Coutts, A.A. Vanilloid Receptor Type 1-Immunoreactivity Is Expressed by Intrinsic Afferent Neurones in the Guinea-Pig Myenteric Plexus. *Neurosci. Lett.* **2002**, *319*, 53–57. [CrossRef]
53. Poole, D.P.; Pelayo, J.C.; Cattaruzza, F.; Kuo, Y.-M.; Gai, G.; Chiu, J.V.; Bron, R.; Furness, J.B.; Grady, E.F.; Bunnett, N.W. Transient Receptor Potential Ankyrin 1 Is Expressed by Inhibitory Motoneurons of the Mouse Intestine. *Gastroenterology* **2011**, *141*, 565–575. [CrossRef] [PubMed]
54. Kaji, I.; Yasuoka, Y.; Karaki, S.; Kuwahara, A. Activation of TRPA1 by Luminal Stimuli Induces EP 4-Mediated Anion Secretion in Human and Rat Colon. *Am. J. Physiol. Gastrointest. Liver Physiol.* **2011**, *302*, 690–701. [CrossRef]
55. Bertin, S.; Aoki-Nonaka, Y.; de Jong, P.R.; Nohara, L.L.; Xu, H.; Stanwood, S.R.; Srikanth, S.; Lee, J.; To, K.; Abramson, L.; et al. The Ion Channel TRPV1 Regulates the Activation and Proinflammatory Properties of CD4+ T Cells. *Nat. Immunol.* **2014**, *15*, 1055–1063. [CrossRef] [PubMed]
56. Kihara, N.; de la Fuente, S.G.; Fujino, K.; Takahashi, T.; Pappas, T.N.; Mantyh, C.R. Vanilloid Receptor-1 Containing Primary Sensory Neurones Mediate Dextran Sulphate Sodium Induced Colitis in Rats. *Gut* **2003**, *52*, 713–719. [CrossRef]
57. Kimball, E.S.; Wallace, N.H.; Schneider, C.R.; D'Andrea, M.R.; Hornby, P.J. Vanilloid Receptor 1 Antagonists Attenuate Disease Severity in Dextran Sulphate Sodium-Induced Colitis in Mice. *Neurogastroenterol. Motil.* **2004**, *16*, 811–818. [CrossRef]
58. Fujino, K.; Takami, Y.; de la Fuente, S.G.; Ludwig, K.A.; Mantyh, C.R. Inhibition of the Vanilloid Receptor Subtype-1 Attenuates TNBS-Colitis. *J. Gastrointest. Surg.* **2004**, *7*, 842–848. [CrossRef] [PubMed]
59. Vermeulen, W.; De Man, J.; De Schepper, H.U.; Bult, H.; Moreels, T.G.; Pelckmans, P.A.; De Winter, B.Y. Role of TRPV1 and TRPA1 in Visceral Hypersensitivity to Colorectal Distension during Experimental Colitis in Rats. *Eur. J. Pharmacol.* **2013**, *698*, 404–412. [CrossRef] [PubMed]
60. Goso, C.; Evangelista, S.; Tramontana, M.; Manzini, S.; Blumberg, P.M.; Szallasi, A. Topical Capsaicin Administration Protects against Trinitrobenzene Sulfonic Acid-Induced Colitis in the Rat. *Eur. J. Pharmacol.* **1993**, *249*, 185–190. [CrossRef]
61. Martelli, L.; Ragazzi, E.; Di Mario, F.; Martelli, M.; Castagliuolo, I.; Dal Maschio, M.; Palu, G.; Maschietto, M.; Scorzeto, M.; Vassanelli, S.; et al. A Potential Role for the Vanilloid Receptor TRPV1 in the Therapeutic Effect of Curcumin in Dinitrobenzene Sulphonic Acid-Induced Colitis in Mice. *Neurogastroenterol. Motil.* **2007**, *19*, 668–674. [CrossRef]
62. Yang, M.; Wang, J.; Yang, C.; Han, H.; Rong, W.; Zhang, G. Oral Administration of Curcumin Attenuates Visceral Hyperalgesia through Inhibiting Phosphorylation of TRPV1 in Rat Model of Ulcerative Colitis. *Mol. Pain* **2017**, *13*, 1744806917726416. [CrossRef]
63. Szitter, I.; Pozsgai, G.; Sandor, K.; Elekes, K.; Kemeny, A.; Perkecz, A.; Szolcsanyi, J.; Helyes, Z.; Pinter, E. The Role of Transient Receptor Potential Vanilloid 1 (Trpv1) Receptors in Dextran Sulfate-Induced Colitis in Mice. *J. Mol. Neurosci.* **2010**, *42*, 80–88. [CrossRef] [PubMed]
64. Utsumi, D.; Matsumoto, K.; Tsukahara, T.; Amagase, K.; Tominaga, M.; Kato, S. Transient Receptor Potential Vanilloid 1 and Transient Receptor Potential Ankyrin 1 Contribute to the Progression of Colonic Inflammation in Dextran Sulfate Sodium-Induced Colitis in Mice: Links to Calcitonin Gene-Related Peptide and Substance P. *J. Pharmacol. Sci.* **2018**, *136*, 121–132. [CrossRef]
65. Massa, F.; Sibaev, A.; Marsicano, G.; Blaudzun, H.; Storr, M.; Lutz, B. Vanilloid Receptor (TRPV1)-Deficient Mice Show Increased Susceptibility to Dinitrobenzene Sulfonic Acid Induced Colitis. *J. Mol. Med.* **2006**, *84*, 142–146. [CrossRef]
66. Engel, M.A.; Leffler, A.; Niedermirtl, F.; Babes, A.; Mueller-Tribbensee, S.M.; Khalil, M.; Siklosi, N.; Nau, C.; Ivanovic-Burmazovic, I.; Neuhuber, W.L.; et al. TRPA1 and Substance P Mediate Colitis in Mice. *Gastroenterology* **2011**, *141*, 1346–1358. [CrossRef]
67. Lapointe, T.K.; Basso, L.; Iftinca, M.C.; Flynn, R.; Chapman, K.; Dietrich, G.; Vergnolle, N.; Altier, C. TRPV1 Sensitization Mediates Postinflammatory Visceral Pain Following Acute Colitis. *Am. J. Physiol. Gastrointest. Liver Physiol.* **2015**, *309*, 87–99. [CrossRef]

68. Lee, J.; Yamamoto, T.; Kuramoto, H.; Kadowaki, M. TRPV1 Expressing Extrinsic Primary Sensory Neurons Play a Protective Role in Mouse Oxazolone-Induced Colitis. *Auton. Neurosci. Basic Clin.* **2012**, *166*, 72–76. [CrossRef]
69. Szitter, I.; Pintér, E.; Perkecz, A.; Kemény, Á.; Kun, J.; Kereskai, L.; Pietra, C.; Quinn, J.P.; Zimmer, A.; Berger, A.; Paige, C.J.; et al. Role of Neurokinin 1 Receptors in Dextran Sulfate-Induced Colitis: Studies with Gene-Deleted Mice and the Selective Receptor Antagonist Netupitant. *Inflamm. Res.* **2014**, *63*, 399–409. [CrossRef]
70. Nalli, M.; Ortar, G.; Moriello, A.S.; Marzo, V.D.; Petrocellis, L.D. Effects of Curcumin and Curcumin Analogues on TRP Channels. *Fitoterapia* **2017**, *122*, 126–131. [CrossRef]
71. Leamy, A.W.; Shukla, P.; Mcalexander, M.A.; Carr, M.J.; Ghatta, S. Crucumin ((E,E)-1,7-Bis(4-Hydroxy-3-Methoxyphenyl)-1,6-Heptadiene-3,5-Dione) Activates and Desensitizes the Nociceptor Ion Channel TRPA1. *Neurosci. Lett.* **2011**, *503*, 157–162. [CrossRef]
72. Larmonier, C.B.; Midura-Kiela, M.T.; Ramalingam, R.; Laubitz, D.; Janikashvili, N.; Larmonier, N.; Ghishan, F.K.; Kiela, P.R. Modulation of Neutrophil Motility by Curcumin: Implications for Inflammatory Bowel Disease. *Inflamm. Bowel Dis.* **2011**, *17*, 503–515. [CrossRef]
73. Zhi, L.; Dong, L.; Kong, D.; Sun, B.; Sun, Q.; Grundy, D.; Zhang, G.; Rong, W. Curcumin Acts via Transient Receptor Potential Vanilloid-1 Receptors to Inhibit Gut Nociception and Reverses Visceral Hyperalgesia. *Neurogastroenterol. Motil.* **2013**, *25*, 429–440. [CrossRef] [PubMed]
74. Hanai, H.; Iida, T.; Takeuchi, K.; Watanabe, F.; Maruyama, Y.; Andoh, A.; Tsujikawa, T.; Fujiyama, Y.; Mitsuyama, K.; Sata, M.; et al. Curcumin Maintenance Therapy for Ulcerative Colitis: Randomized, Multicenter, Double-Blind, Placebo-Controlled Trial. *Clin. Gastroenterol. Hepatol.* **2006**, *4*, 1502–1506. [CrossRef] [PubMed]
75. D'Argenio, G.; Valenti, M.; Scaglione, G.; Cosenza, V.; Sorrentini, I.; Di Marzo, V. Up-Regulation of Anandamide Levels as an Endogenous Mechanism and a Pharmacological Strategy to Limit Colon Inflammation. *FASEB J.* **2006**, *20*, 568–570. [CrossRef] [PubMed]
76. Hasenoehrl, C.; Taschler, U.; Storr, M.; Schicho, R. The Gastrointestinal Tract—A Central Organ of Cannabinoid Signaling in Health and Disease. *Neurogastroenterol. Motil.* **2016**, *28*, 1765–1780. [CrossRef] [PubMed]
77. Couch, D.G.; Tasker, C.; Theophilidou, E.; Lund, J.N.; O'Sullivan, S.E. Cannabidiol and Palmitoylethanolamide Are Anti-Inflammatory in the Acutely Inflamed Human Colon. *Clin. Sci.* **2017**, *131*, 2611–2626. [CrossRef]
78. Petrosino, S.; Moriello, A.S.; Cerrato, S.; Fusco, M.; Puigdemont, A.; De Petrocellis, L.; Di Marzo, V. The Anti-Inflammatory Mediator Palmitoylethanolamide Enhances the Levels of 2-Arachidonoyl-Glycerol and Potentiates Its Actions at TRPV1 Cation Channels. *Br. J. Pharmacol.* **2016**, *173*, 1154–1162. [CrossRef]
79. Petrosino, S.; Cristino, L.; Karsak, M.; Gaffal, E.; Ueda, N.; Tüting, T.; Bisogno, T.; De Filippis, D.; D'Amico, A.; Saturnino, C.; et al. Protective Role of Palmitoylethanolamide in Contact Allergic Dermatitis. *Exp. Allergy Immunol.* **2010**, *65*, 698–711. [CrossRef]
80. Swanson, D.M.; Dubin, A.E.; Shah, C.; Nasser, N.; Chang, L.; Dax, S.L.; Jetter, M.; Breitenbucher, J.G.; Liu, C.; Mazur, C.; et al. Identification and Biological Evaluation of 4-(3-Trifluoromethylpyridin-2-Yl)Piperazine-1-Carboxylic Acid (5-Trifluoromethylpyridin-2-Yl) Amide, a High Affinity TRPV1 (VR1) Vanilloid Receptor Antagonist. *J. Med. Chem.* **2005**, *48*, 1857–1872. [CrossRef]
81. Steiner, A.A.; Turek, V.F.; Almeida, M.C.; Burmeister, J.J.; Oliveira, D.L.; Roberts, J.L.; Bannon, A.W.; Norman, M.H.; Louis, J.; Treanor, J.J.S.; et al. Nonthermal Activation of Transient Receptor Potential Vanilloid-1 Channels in Abdominal Viscera Tonically Inhibits Autonomic Cold-Defense Effectors. *J. Neurosci.* **2007**, *27*, 7459–7468. [CrossRef]
82. Arendt-Nielsen, L.; Harris, S.; Whiteside, G.T.; Hummel, M.; Knappenberger, T.; O'Keefe, S.; Kapil, R.; Kyle, D. A Randomized, Double-Blind, Positive-Controlled, 3-Way Cross-over Human Experimental Pain Study of a Trpv1 Antagonist (V116517) in Healthy Volunteers and Comparison with Preclinical Profile. *Pain* **2016**, *157*, 2057–2067. [CrossRef] [PubMed]
83. Gavva, N.R.; Treanor, J.J.S.; Garami, A.; Fang, L.; Surapaneni, S.; Akrami, A.; Alvarez, F.; Bak, A.; Darling, M.; Gore, A.; et al. Pharmacological Blockade of the Vanilloid Receptor TRPV1 Elicits Marked Hyperthermia in Humans. *Pain* **2008**, *136*, 202–210. [CrossRef] [PubMed]

84. Chen, J.; Hackos, D.H. TRPA1 as a Drug Target—Promise and Challenges. *Naunyn-Schmiedeberg's Arch. Pharmacol.* **2015**, *388*, 451–463. [CrossRef] [PubMed]
85. Chiche, D.; Brown, W.; Walker, P. NEO6860, a Novel Modality Selective TRPV1 Antagonist: Results from a Phase I, Double-Blind, Placebo-Controlled Study in Healthy Subjects. *J. Pain* **2016**, *17*, S79. [CrossRef]
86. Kaneko, Y.; Szallasi, A. Transient Receptor Potential (TRP) Channels: A Clinical Perspective. *Br. J. Pharmacol.* **2013**, *171*, 2474–2507. [CrossRef]

International Journal of
Molecular Sciences

MDPI

Article

Upregulation of the TRPA1 Ion Channel in the Gastric Mucosa after Iodoacetamide-Induced Gastritis in Rats: A Potential New Therapeutic Target

Kata Csekő [1,2,*], Dániel Pécsi [3,4], Béla Kajtár [5], Ivett Hegedűs [5], Alexander Bollenbach [6], Dimitrios Tsikas [6], Imre László Szabó [4], Sándor Szabó [7,8,†] and Zsuzsanna Helyes [1,2,9,†]

1 Department of Pharmacology and Pharmacotherapy, Medical School, University of Pécs, H-7624 Pécs, Hungary; zsuzsanna.helyes@aok.pte.hu
2 Szentagothai Research Centre, University of Pécs, H-7624 Pécs, Hungary
3 Institute for Translational Medicine, Medical School, University of Pécs, H-7624 Pécs, Hungary; daniel.pecsi@aok.pte.hu
4 1st Department of Medicine, Medical School, University of Pécs, H-7624 Pécs, Hungary; szaboimi@yahoo.com
5 Department of Pathology, Medical School, University of Pécs, H-7624 Pécs, Hungary; belakajtar@yahoo.com (B.K.); hegiv@citromail.hu (I.H.)
6 Hannover Medical School, Institute of Toxicology, Core Unit Proteomics, 30625 Hannover, Germany; bollenbach.alexander@mh-hannover.de (A.B.); tsikas.dimitros@mh-hannover.de (D.T.)
7 School of Medicine, University of California, Irvine, CA 92697, USA; sszabo@auhs.edu
8 Department of Pharmaceutical Science, American University of Health Sciences, Signal Hill, CA 90755, USA
9 PharmInVivo Ltd., H-7629 Pécs, Hungary
* Correspondence: csekoe.kata@gmail.com; Tel.: +36-72-536-001 (ext. 35386); Fax: +36-72-536-218
† These authors contributed equally to this work.

Received: 7 June 2020; Accepted: 28 July 2020; Published: 5 August 2020

Abstract: Acute gastritis is often untreatable by acid secretion-inhibiting drugs. Understanding the protective mechanisms including the role of Transient Receptor Potential Ankyrin1 (TRPA1) and Vanilloid1 (TRPV1) channels localized on capsaicin-sensitive afferents and non-neuronal structures might identify novel therapeutic approaches. Therefore, we characterized a translational gastritis model using iodoacetamide (IAA) and investigated TRPA1/V1 expressions. Wistar rats and CD1, C57Bl/6J mice were exposed to IAA-containing (0.05, 0.1, 0.2, 0.3, 0.5%) drinking water for 7 or 14 days. Body weight and water consumption were recorded daily. Macroscopic lesions were scored, qualitative histopathologic investigation was performed, TRPA1/V1 immunopositivity and mRNA expressions were measured. IAA induced a concentration-dependent weight loss and reduced water intake in both species. Hyperemia, submucosal edema, inflammatory infiltration and hemorrhagic erosions developed after 7 days, while ulcers after 14 days in rats. *Trpa1* mRNA/protein expressions were upregulated at both timepoints. Meanwhile, TRPV1 immunopositivity was upregulated in the gastric corpus after 0.05% IAA ingestion, but downregulated after 0.2%, whereas *Trpv1* mRNA did not change. Interestingly, no macroscopic/microscopic changes were observed in mice. These are the first data for the concentration- and duration-dependent changes in the IAA-induced gastritis in rats accompanied by TRPA1 upregulation, therefore, its therapeutic potential in gastritis should further be investigated.

Keywords: TRPA1; TRV1; gastritis; inflammation; erosion; rodent

1. Introduction

Gastric mucosal injury can be exhibited by various forms of macroscopic and histopathological alterations, such as diffuse hyperemia, inflammation, erosion, or even hemorrhagic ulcerations. Several attempts have been made to classify the different types of gastritis, but it is difficult due to the complexity of its pathophysiological mechanisms [1]. There is often no correlation between the symptoms and the macroscopic lesions or histopathological changes [2]. Based on its localization, the injury can be diffuse, antrum- or corpus-predominant, or even multifocal. Regarding the duration, we can differentiate between acute or chronic forms [3]. However, the etiology of the condition is at least as important.

Several drugs may alleviate the gastric lesions induced by chemical factors such as the non-steroidal anti-inflammatory drugs (NSAID), alcohol or bile reflux, *Helicobacter pylori* infection or irradiation [4]. The gold standard treatment is often limited to acid secretion inhibitors, such as proton pump inhibitors or histamine H2 receptor antagonists, since enhancing cytoprotective mechanisms is challenging [5]. The gastroprotective effect of capsaicin-sensitive peptidergic sensory neurons innervating the gastric mucosa has long been investigated by our group [6–8].

Recently special focus has been directed towards the Transient Receptor Potential Vanilloid 1 (TRPV1, "capsaicin receptor") and Ankyrin 1 (TRPA1) ion channels located and often co-expressed mainly on these sensory fibers, which are identified as novel anti-inflammatory, analgesic and gastroprotective targets. These polymodal nociceptors play an important role in thermo-, mechanical- and chemo-sensation, as well as neurogenic inflammation and hyperalgesia [9–12]. Besides the exogenous agents, especially spices, like capsaicin (the pungent agent of chili pepper), cinnamaldehyde, allyl isothiocyanate (mustard oil) and allicin, they are activated by several endogenous agents as lipoxygenase products, bradykinin, and protons produced in the inflammatory tissues [10,12,13]. Their activation leads to the release of pro-inflammatory neuropeptides, such as calcitonin gene-related peptide (CGRP) and substance P (SP) resulting in vasodilation, plasma protein extravasation and inflammatory cell activation (neurogenic inflammation) [14,15]. Meanwhile, anti-inflammatory, analgesic and cytoprotective mediators—most importantly somatostatin—are also released from the same nerve ending, which inhibit inflammation and tissue damage both locally and systemically [8,16].

TRPV1 is also present on several non-neuronal structures in the gastrointestinal tract, such as the gastrin-secreting parietal and gastric epithelial cells, as well as the esophageal, small intestinal and colonic epithelial cells [17,18]. TRPA1 is less extensively studied, but its expression was described in isolated crypts and epithelial cells of the colon, as well as small intestinal neuroendocrine cells [18–20]. Moreover, both receptors were reported on $CD4^+$ T cells emphasizing their role in sensory-immune interactions [21,22].

The role of TRPV1 in gastrointestinal mucosal defense mechanisms is virtually controversial. Studies with *Trpv1* and *Trpa1* gene-deficient mice show contradictory data about their roles in colitis, most likely depending on the key pathomechanisms of the different colitis models [23]. *Trpa1* and *Trpv1* gene deletion decreased dextran sulfate sodium (DSS)-induced colitis severity [24], as well as $Il10^{-/-}$-induced spontaneous colitis in *Trpv1*-deficient mice [21], whereas *Trpv1*-deficient mice exhibited more severe colitis in the dinitrobenzene sulfonic acid (DNBS)-induced model [25]. The protective role of TRPA1 has also been described in the $Il10^{-/-}$-induced spontaneous colitis model [22]. Low dose of the TRPV1 activator capsaicin is protective against the alcohol- and indomethacin-induced gastric mucosal injury [26], it reduces basal gastric acid secretion and enhances gastric emptying [27]. In contrast to TRPV1, little is known about the expression changes and role of TRPA1 in the stomach [28].

Animal models are important for the molecular investigation of gastric injury, since these models may reveal very early biochemical and molecular alterations, much before microscopic or macroscopic lesions can be seen. Good models should have translational relevance. However, in virtually all animal models of gastric injury (e.g., NSAID-, stress-induced) the lesions are well circumscribed (i.e., superficial erosions and/or deep ulcers). Gastritis in humans, on the other hand, is a diffuse inflammatory damage involving all or most parts of the stomach [1]. Iodoacetamide (IAA) is a water soluble sulfhydryl

alkylating chemical, which, by depleting sulfhydryl groups, including the protective antioxidant glutathione (GSH) in the gastric mucosa, allows reactive oxygen species production and oxidative tissue damage [29]. The reduced GSH plays an essential role in maintaining mucosal integrity [30]. Nitric oxide synthase (NOS) also contributes to mucosal protection via the production of nitric oxide (NO), which increases mucosal blood flow like other gastroprotective compounds [31,32]. IAA may interfere with NOS activity, thus also affecting gastric mucosal integrity. Reactive oxygen species react with various cell components including cell membrane, mitochondria and DNA, potentially leading to cell death/necrosis, which triggers neutrophil recruitment [33,34].

Therefore, our aim was to characterize a translationally relevant gastritis model using the irreversible sulfhydryl-group blocker IAA and to investigate the expression changes of TRPA1 and TRPV1 in this model.

2. Results

2.1. Macroscopic Evaluation of Rat Gastric Mucosa

Gastritis was induced by the administration of 0.05%, 0.1% or 0.2% IAA solution in the drinking water of Wistar rats, littermates drinking IAA-free tap water served as control animals. Rats were euthanized at days 7 and 14, their stomachs were harvested and opened along the greater curvature.

Extensive hyperemia, mucosal hemorrhage and several erosions or superficial ulcers were observed at both timepoints in all three examined concentrations. Semi-quantitative analysis showed significant hyperemic areas and erosions in both 0.05% and 0.2% IAA-treated groups at day 7 compared to the controls. At day 14, lesions, especially the extent of the hyperemic area in the 0.1% and 0.2% IAA-treated groups were significantly greater. Macroscopic changes showed no significant difference either by the increasing concentrations of ingested IAA or by time; however, ulcerations were more pronounced after 14 days of IAA-drinking (Figures 1 and 2).

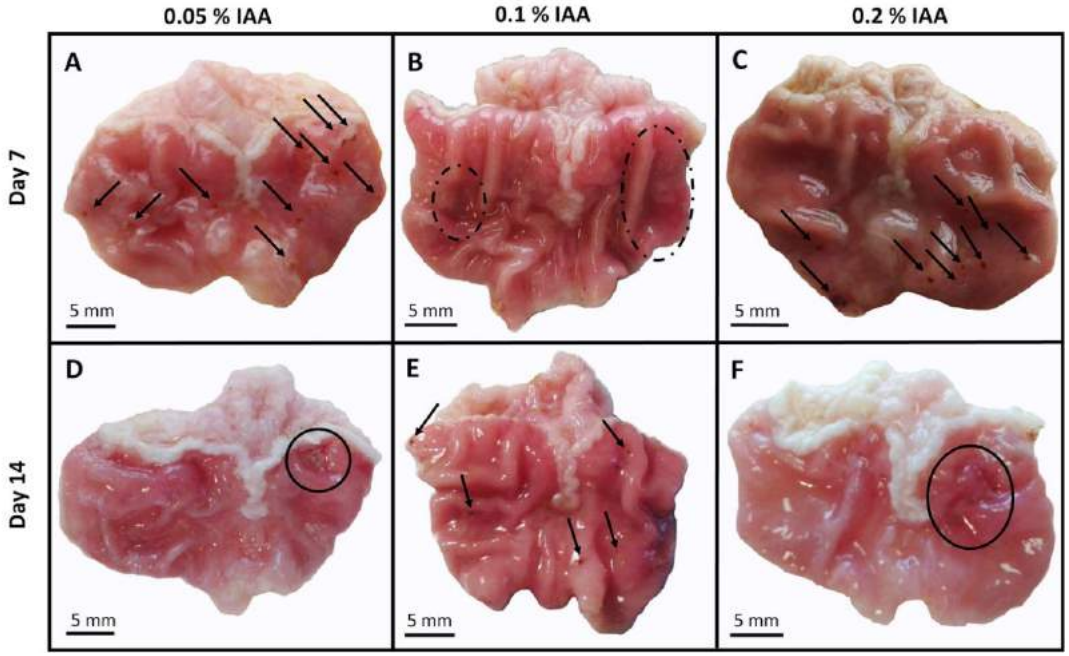

Figure 1. Macroscopic pictures of iodoacetamide-induced (IAA) gastric mucosal inflammation. Representative photos of gastric mucosa of Wistar rats receiving (**A**) 0.05%, (**B**) 0.1%, (**C**) 0.2% IAA for 7 and (**D**–**F**) for 14 days, respectively. After 7 days, diffuse hyperemia (dashed circles) and several superficial mucosal erosions (black arrows) developed, while by the end of the 14-day-long protocol, chronic ulcers were also observable in some animals (circles on panel (**D**,**F**)).

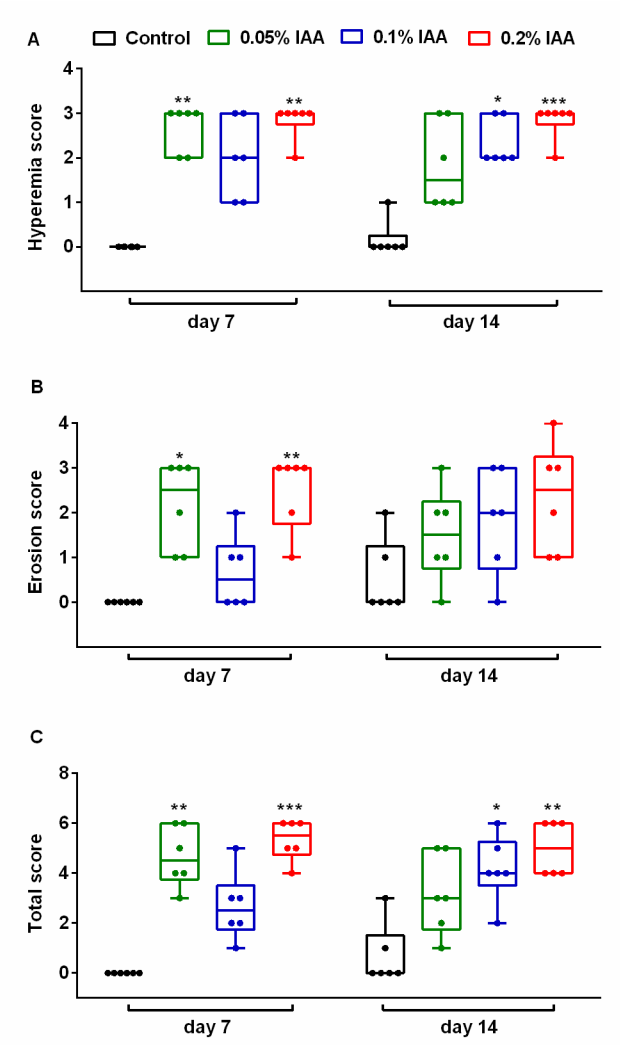

Figure 2. Semi-quantitative macroscopic evaluation of gastric mucosa in Wistar rats. Macroscopic findings, such as (**A**) hyperemia, (**B**) superficial erosions/ulcers and (**C**) total score were evaluated semi-quantitatively. 0.05% IAA induced significant lesions after 7 days, which were less pronounced after 14 days, whereas in the 0.1% IAA-treated group, the peak in macroscopic changes was observed after 14 days. 0.2% IAA induced hyperemia, and erosions developed at both timepoints, although there was no significant difference in macroscopic picture by IAA concentrations. Box plots represent minimum, first quartile, median, third quartile, and maximum values with individual data plots; $n = 6$/group. (Kruskal–Wallis followed by Dunn's multiple comparison test to observe intergroup differences at given timepoints, * $p < 0.05$, ** $p < 0.005$, *** $p < 0.001$ vs. control group; Mann–Whitney test was performed to analyze intragroup differences by time—not significant).

2.2. Microscopic Alterations in the Inflamed Rat Gastric Mucosa

Seven days of IAA treatment resulted in submucosal widening due to massive edema. In higher concentrations, extensive inflammatory cell infiltration was also observed. After 14 days, focal epithelial cell sloughing/erosions, and in some areas, almost total mucosal necrosis involving the muscularis mucosae were seen, admixed with acute and chronic inflammatory cells, both in the mucosa and the submucosa (Figure 3).

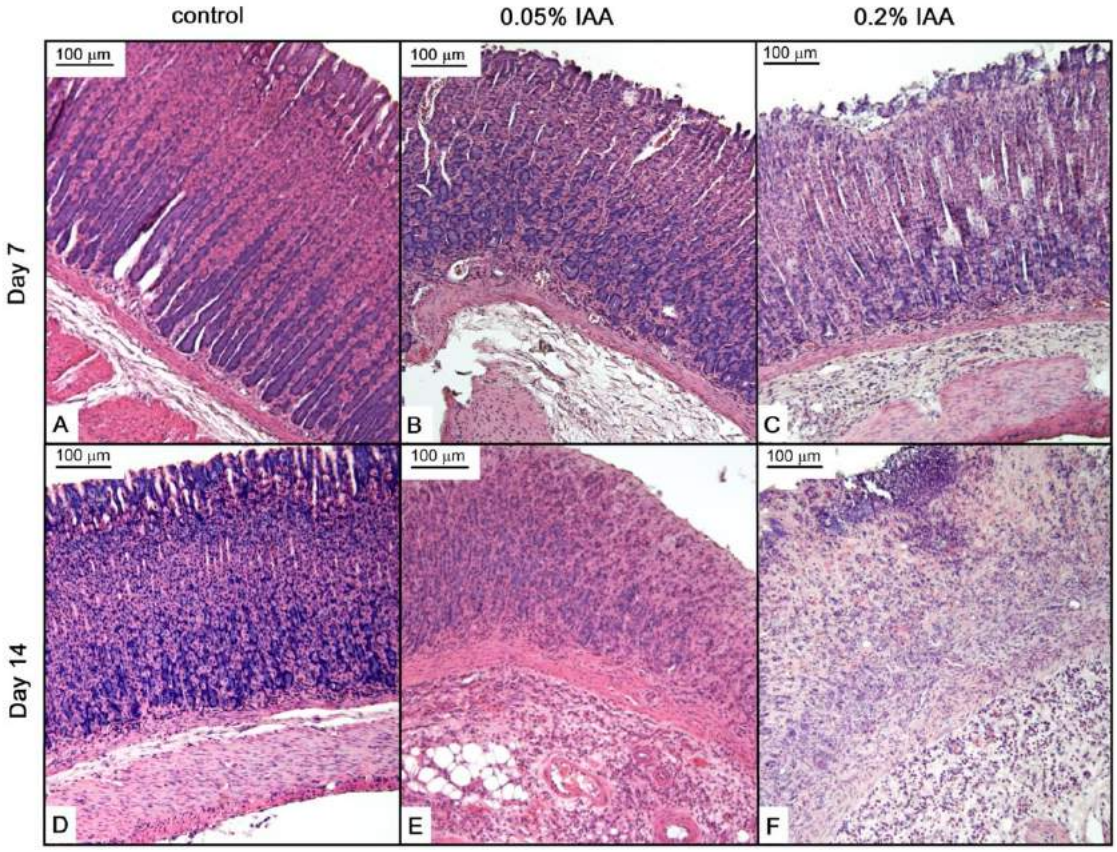

Figure 3. IAA treatment induced microscopic alterations in Wistar rat gastric mucosa. Representative HE-stained microscopic pictures of (**A**), (**D**) control; (**B**,**E**) 0.05% IAA-treated, and (**C**,**F**) 0.2% IAA-treated rat gastric mucosa at days 7 and 14, respectively.

2.3. Weight Change and Water Consumption

In Wistar rats, IAA induced a concentration-dependent weight change. Similarly to vehicle-treated animals, low concentration (0.05%) of IAA resulted in ~15% weight gain by the end of the 14-day experiment. Meanwhile, 0.1% and 0.2% IAA induced a concentration-dependent, gradual weight loss with a maximum of 13.4 ± 1.2% and 32.5 ± 3.3%, respectively (Figure 4A). The total water consumption of the 0.05% and the 0.1% IAA-treated groups was halved compared to the control group, and it was even more decreased to around 9 mL daily in the case of 0.2% concentration (Figure 4B).

2.4. GSH Concentration of the Rat Stomach Tissue

The GSH content of the rat gastric mucosa was measured to be (mean ± standard deviation) 3.64 ± 1.91 nmol/mg protein in the control group, 5.82 ± 3.94 nmol/mg protein in the group receiving 0.1% IAA for 7 days, and 5.71 ± 2.07 nmol/mg protein in the group receiving 0.1% IAA for 14 days (data not shown). There were no statistically significant differences between the groups ($p = 0.343$, one-way ANOVA). The content of free GSH measured by us has also been reported by other groups for gastric mucosa in rats [35].

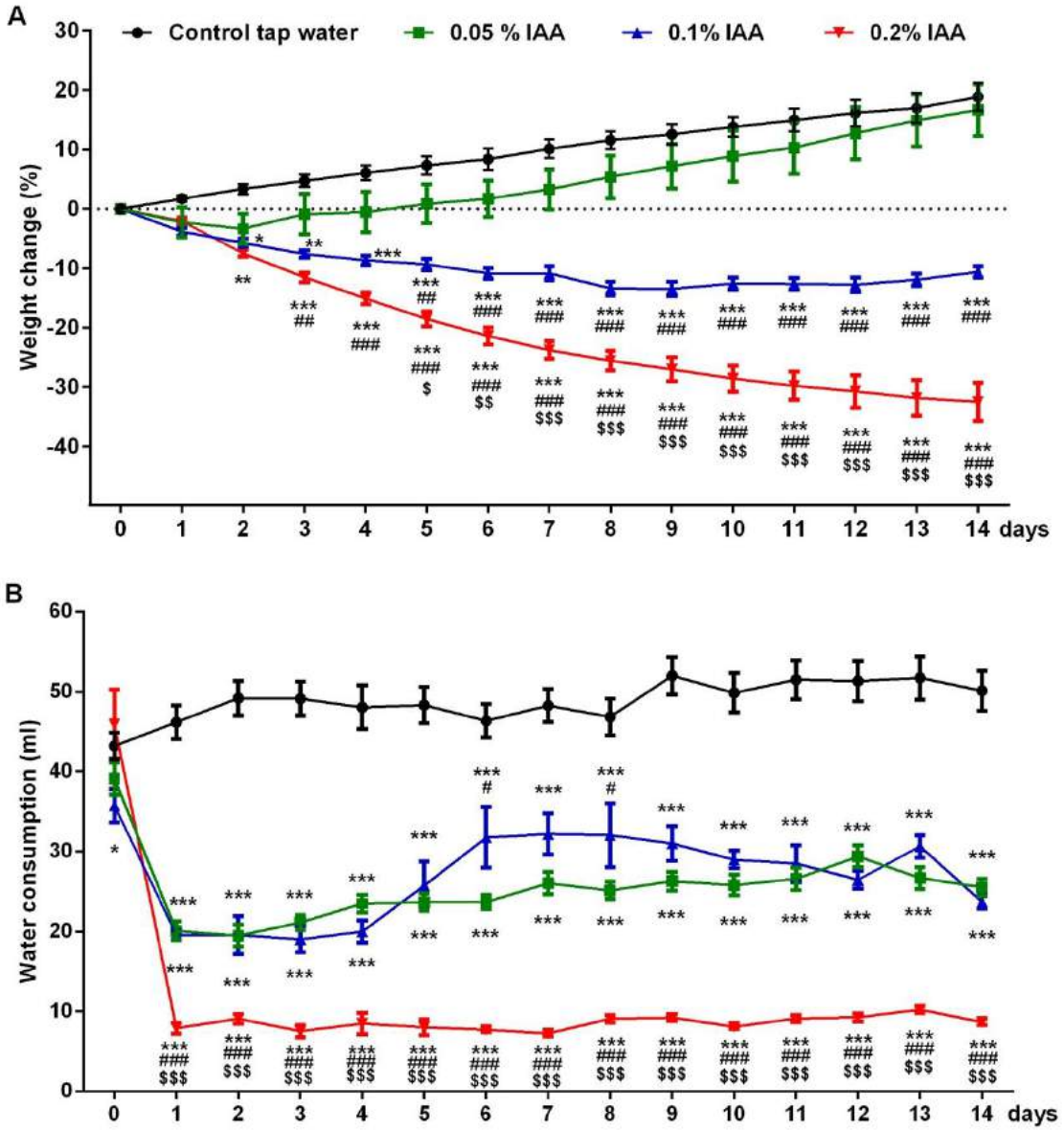

Figure 4. IAA-induced body weight change and water intake in Wistar rats. (**A**) IAA administration resulted in a dose-dependent weight loss and (**B**) reduced water intake in Wistar rats. Data are shown as means ± SEM; n = 6/group (repeated measures two-way ANOVA followed by Bonferroni's modified t-test; * $p < 0.05$, ** $p < 0.005$, *** $p < 0.001$ vs. control group; # $p < 0.05$ ## $p < 0.005$ ### $p < 0.001$ vs. 0.05% IAA group; $ $p < 0.05$ $$ $p < 0.05$ $$$ $p < 0.001$ vs. 0.1% IAA group).

N-acetylcysteine ethyl ester (NACET) is a useful reagent to reduce disulfides to their sulfhydryl compounds. Previously, we have shown that NACET is useful for the measurement of tGSH [36]. IAA treatment increased tGSH (based on the peak area in mAU of the GSH peak) numerically, but not significantly in the rat gastric mucosa: 2.55 ± 0.85 in the control group; 3.15 ± 1.21 in the group treated with 0.1% IAA for 7 days; and 3.25 ± 0.82 in the group treated with 0.1% IAA for 14 days (Figure 5B). tGluCys increased significantly (between one week and two weeks: 5.78 ± 0.18; 5.97 ± 0.23; 6.18 ± 0.20, respectively) (Figure 5A). These changes resulted in a decrease in the tGluCys/tGSH molar ratio, which was not significant: 2.43 ± 0.72; 2.13 ± 0.77; 1.98 ± 0.39, respectively (data not shown).

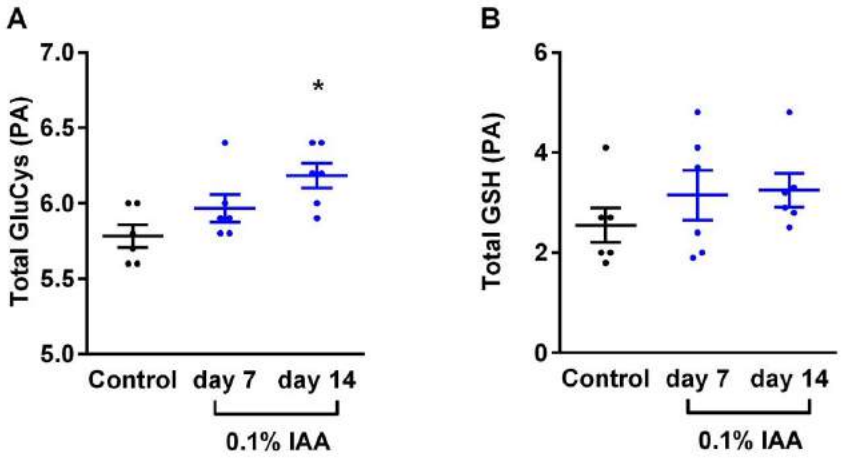

Figure 5. (**A**) Total glutathione (GSH) and (**B**) Total GSH (tGSH) γ-glutamyl-cysteine levels of the rat gastric mucosa measured by HPLC analysis. Data are shown as mean ± SEM; n = 6/group (ordinary one-way ANOVA; * $p < 0.05$).

2.5. Quantification of TRPA1 and TRPV1 Immunopositivity

Mild TRPA1 and strong TRPV1 immunopositivity was detected on the epithelial cells in the intact control samples. Quantification, as shown by the ratio of immunopositive cells, revealed a significant upregulation of TRPA1 after both 0.05% and 0.2% IAA administration by day 14 in both the antrum and corpus epithelial cells. Although TRPV1 immunopositivity also increased in the corpus, but did not change in the antrum in the case of 0.05% IAA, it significantly decreased in both localizations after 0.2% IAA treatment (Figure 6).

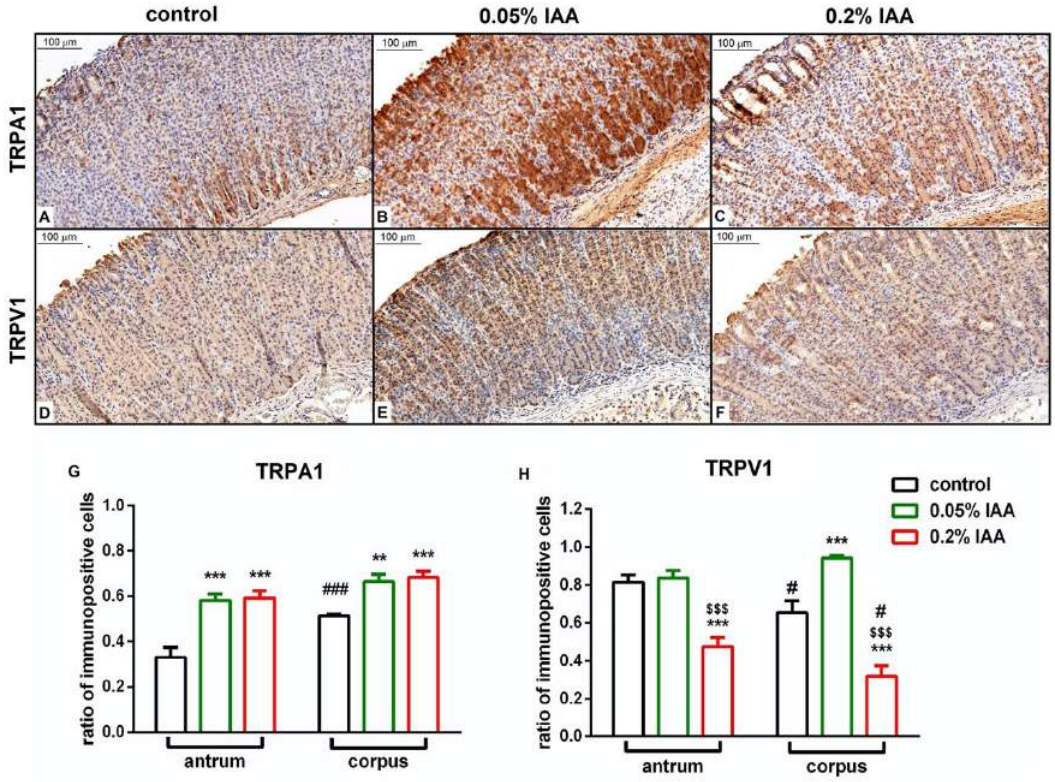

Figure 6. Quantitative analysis of TRPA1 and TRPV1 immunohistochemistry. Representative pictures of (**A**–**C**) TRPA1 (antrum) and (**D**–**F**) TRPV1 (corpus) immunohistochemistry of rat gastric mucosa (**A**,**D**) under control conditions, and 14 days after (**B**,**E**) 0.05% IAA, and (**C**,**F**) 0.2% IAA treatment. Panel (**G**,**H**)

demonstrates the quantitative histopathological analysis of TRPA1 and TRPV1 immunohistochemistry, respectively, calculated by the ratio of immunopositive cells/total cell number. Data are shown as means ± SEM; $n = 6$ animals/group, 10 fields of vision/slide/animal; ordinary two-way ANOVA followed by Dunn's multiple comparisons test ** $p < 0.005$, *** $p < 0.001$ vs. control group; $$$ $p < 0.001$ vs. 0.05% IAA-treated group; # $p < 0.05$, ### $p < 0.001$ vs. respective antrum samples.

2.6. *Trpa1, Trpv1* Relative Gene Expression Changes in the Inflamed Rat Stomach

In agreement with the TRPA1 protein expression, *Trpa1* mRNA was significantly upregulated in both 0.05% and 0.2% IAA-treated groups after 7 and 14 days as well, however, there was no detectable alteration in *Trpv1* relative gene expression either by time, dose or localization (Figure 7).

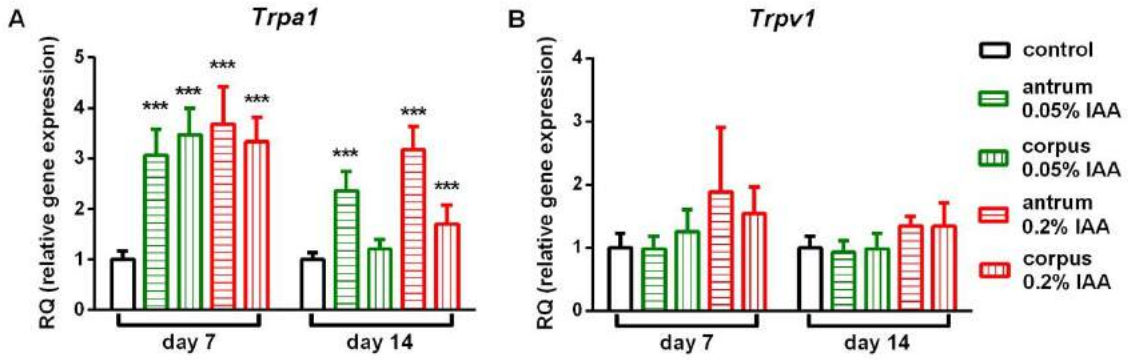

Figure 7. Relative gene expression of *Trpa1* and *Trpv1*. mRNA levels of (**A**) *Trpa1* were significantly upregulated after 0.05% and 0.2% IAA treatment, whereas (**B**) *Trpv1* gene expression did not show significant alterations either by time, concentration or localization. Data are shown as means ± SEM; $n = 6$/group; Student's unpaired *t*-probe *** $p < 0.001$ vs. control group.

2.7. *IAA-Induced Alterations in Mice*

CD1 and C57Bl/6J mice were administered 0.1%, 0.3%, or 0.5% IAA solution in the drinking water for 7 or 14 days; littermates drinking IAA-free tap water served as control animals.

In CD1 mice, we observed an IAA dose-dependent continuous, gradual weight loss; in the 0.3% and 0.5% IAA-treated groups, weight reduction was so severe at the end of the 7-day-long protocol, that a 14-day-long protocol could not be performed due to the ethical considerations of humane endpoints (Figure 8A,C). Although water intake was significantly reduced in all IAA-treated groups, it showed no concentration-dependence, and could not explain the remarkable dose-dependent weight loss of these animals.

C57Bl/6J mice proved to be more resistant to 0.3% IAA, which induced ~14% weight loss after 7 days, half as much as the same concentration in CD1 mice (~28%). Interestingly, adding 2% sucrose to 0.3% IAA significantly reduced both the fluid intake, as well as the weight (~21%) of C57Bl/6J mice compared to the 0.3% IAA-drinking group (Figure 8B,D).

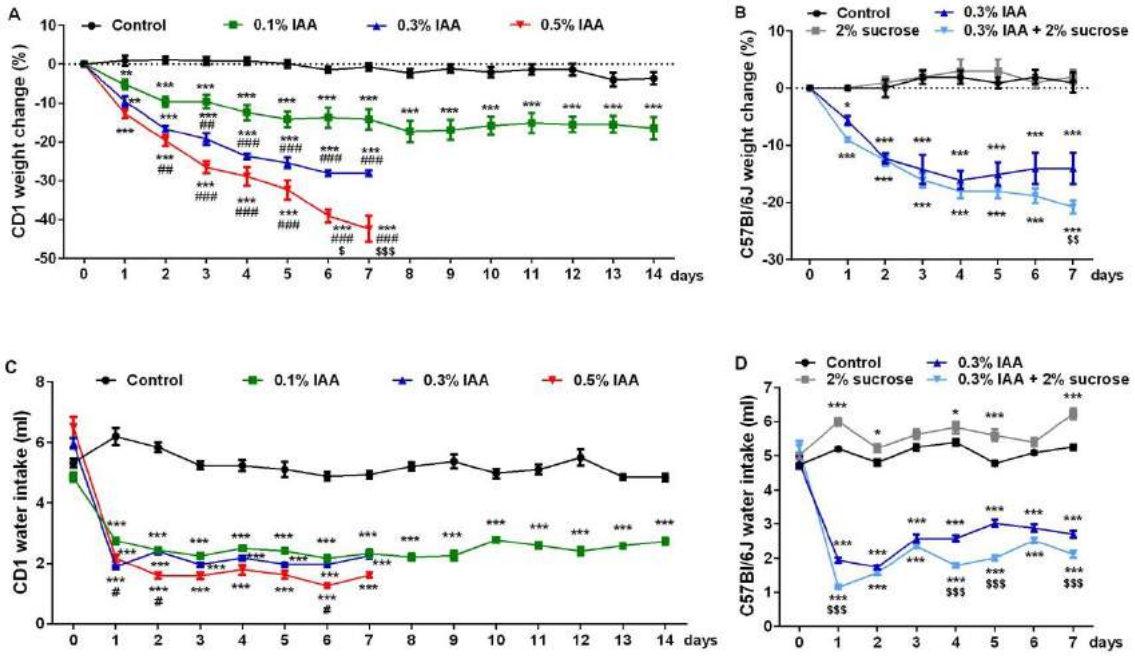

Figure 8. IAA-induced weight change and water intake in mice. IAA administration resulted in (**A**,**B**) a dose-dependent weight loss and (**C**,**D**) significantly reduced water intake in both CD1 and C57Bl/6J mice, respectively. Data are shown as means ± SEM; n = 6/group (repeated-measures ANOVA followed by Bonferroni's modified t-test; * $p < 0.05$, ** $p < 0.005$, *** $p < 0.0005$ vs. control group; # $p < 0.05$, ## $p < 0.005$, ### $p < 0.0005$ vs. 0.1% IAA group, \$ $p < 0.05$, \$\$ $p < 0.005$, \$\$\$ $p < 0.0005$ vs. 0.3% IAA group).

Surprisingly, in contrast to Wistar rats, where we observed similar body weight change and decreased water intake, no macroscopic lesions or microscopic alterations were present in either of the mouse groups drinking IAA (Table 1).

Table 1. Summary of IAA administration-induced alterations in mice.

Strain	IAA Conc.	Duration	Weight Loss	Water Intake	Macroscopic and Microscopic Picture
CD1	0.1%	14 days	~17%	↓	negative
CD1	0.1%	7 days	~14%	↓	negative
CD1	0.3%	7 days	~28%	↓	negative
CD1	0.5%	7 days	~42%	↓↓	negative
C57Bl/6J	0.3%	7 days	~14%	↓	negative
C57Bl/6J	0.3% + 2% sucrose	7 days	~21%	↓↓	negative

3. Discussion

This is the first comprehensive and comparative acute and chronic diffuse gastritis model study, in which IAA-induced concentration- and duration-dependent changes were described in Wistar rats. IAA induced concentration-dependent weight loss and gastric erosions already after 7-day ingestion of IAA in drinking water accompanied by massive submucosal edema and extensive infiltration by acute and chronic inflammatory cells, and subsequently, hemorrhagic erosions. After 14 days, ulcers were observed as deep necrosis involving the muscularis mucosae, which was more severe and more extensive in rats with high (0.2%) IAA concentration in their drinking water.

IAA is a sulfhydryl alkylating agent, which inhibits free radical scavenging by depleting reduced GSH, thus inducing gastric injury [29]. However, although this mechanism of action is the state of the art, GSH concentrations are rarely measured directly in the stomach mucosa. In our present

study, we did not find GSH reduction in response to IAA application. This might be due to the fact that we measured it after 7 or 14 days of IAA ingestion when the lesions were already fully developed or started to heal. Furthermore, we used the whole stomach tissue, not only the mucosa. Nevertheless, the small, but significant increase in tGluCys also supports the onset of the healing phase with the elevation of oxidative stress and/or GSH synthesis enzyme activity. IAA-induced rapid GSH depletion was demonstrated in cultured Wistar rat astrocytes [37], rat hepatocytes [38,39], and in human erythrocytes as well [39]. GSH content from in vivo experiments are highly influenced by the complex inflammatory/oxidative/antioxidant regulatory system of the animal, as well as the differences in sampling protocols. In an IAA-induced gastritis model, 0.1% IAA induced a robust, almost 4-fold increase in gastric mucosal GSH after one week, whereas in the same experimental paradigm, an approximately 50% decrease was measured after two weeks of IAA administration [40]. The robust GSH increase was accompanied by a similarly elevated MPO activity, which is a reliable indicator of inflammatory cell infiltration/activation, suggesting that at the time of lesion formation, the fine regulation is also activated to counteract the imbalance of the aggressive/defensive factors. Similar rebound GSH increase was reported on alveolar epithelial cells [41], where genes involved in GSH synthesis, such as γ-glutamylcysteine transpeptidase, and activator protein-1 (AP-1) were upregulated as an adaptive mechanism.

Only a few studies have used the IAA gastritis model, but with different paradigms: 1) various durations (5 days–25 weeks) [42–45], 2) rats weighing 100–500 g [43,46], 3) different strains [42,44,46], 4) different IAA concentrations [33,44,45,47], 5) routes of administration, even with additional sucrose in drinking water [33,34,44,47]. Therefore, the comparison of the outcomes and conclusions of these different studies is not easy, but they are consistent in myeloperoxidase (MPO) elevation and macroscopic/microscopic alterations characteristic to diffuse gastritis with hemorrhages. We did not observe significant changes in the severity of lesions regarding hyperemia and erosions between 7 and 14 administration days in agreement with the literature [34], although ulcer formation was more pronounced after 14 days.

In this well-characterized gastric erosion/ulcer inflammatory model, our major finding is that both 0.05% and 0.2% IAA ingestion induced *Trpa1*, but not *Trpv1* mRNA upregulation in the rat antrum and corpus after 7 days—that remained elevated by the end of the 14-day period.

Most activators of the TRPA1 channel are structurally diverse molecules, which suggests that their effect is not exerted based on the conventional lock-and-key principle. They act as reactive electrophile compounds (allylisothiocyanate, cinnamaldehyde) inducing covalent reversible modifications of the cytoplasmic N terminal of the receptor [48,49]. IAA being a cysteine-modifying alkylating compound is able to bind covalently to the reactive cytoplasmic cysteine residues, thus inducing TRPA1 activation as demonstrated in HEK cell culture by Ca^{2+} imaging [48]. However, TRPA1 upregulation in our experiments is not explained simply by direct IAA-evoked receptor activation or desensitization, since prolonged administration of IAA to human TRPA1-expressing cells was described not to induce receptor desensitization [50]. Moreover, IAA acts as a partial TRPA1 agonist, since after its continuous administration, a subsequently applied other agonists (*para*-benzoquinone) that induce rapid desensitization by itself further increased TRPA1-mediated Ca^{2+} current [50]. Therefore, IAA-induced TRPA1 expression increase in the stomach is more likely due to the inflammatory cascade, which is further supported by its upregulation in water immersion restraint, stress-induced acute gastric mucosal ulcerations in rats [51].

There are no data on the expression and function of the TRPA1 channel in gastritis and only little information is available on TRPV1. The distribution of TRPV1 immunopositivity was reported to be increased in chronic gastritis biopsies, however, in that study, control samples were collected from patients with functional dyspepsia [52]. Their investigation is more thorough in inflammatory bowel disease, their expression changes and the role are virtually controversial, but the overall function is likely to be protective [23].

TRPV1/A1 expression on capsaicin-sensitive peptidergic nerve endings and non-neural cells, such as gastric epithelial and inflammatory cells [18,19,21,22], also shown by our present results detecting TRPA1 mRNA in the stomach, make the interpretation of their roles much more complex. Several endogenous inflammatory mediators activating TRPV1 (protons, lipoxygenase products) are produced during the IAA-induced inflammatory reaction, which might also influence TRPA1 function and expression since their interactions have been described [22,53,54].

The role of capsaicin-sensitive sensory nerves in IAA-induced gastritis has been investigated by defunctionalizing these neurons with high doses of capsaicin [47]. The role of these peptidergic afferents depends on the experimental paradigm and the consequent pathophysiological mechanisms—they can both inhibit (e.g., ethanol-induced gastritis) or aggravate the inflammation presumably via SP and CGRP release (e.g., IAA-induced gastritis), underlining the role of neurogenic component in inflammation [47]. The role of TRPA1 and TRPV1 in gastritis might also be attributed to the mediation of inflammatory visceral hyperalgesia and abdominal pain. IAA was shown to significantly increase Na^+ current in the dorsal root ganglia of T9 and T10 afferent neurons [55], and enhanced visceromotor responses primarily by increased activity of the splanchnic nerves [46].

Surprisingly, mice (both CD1 and C57Bl/6J strains) proved to be resistant to all applied concentrations of IAA, even higher than the most damaging one in the rat. Although they also exhibited concentration-dependent weight loss similar to the rat, no macroscopic or microscopic changes have been found in the stomach. The few studies coming from one group point out the lack of IAA-induced macroscopic lesions in mice supporting our present results, but describe a mixed inflammatory infiltration, characteristic to mild gastritis [56]. Interestingly, most of these studies showed that after an initial weight loss, mice recovered by the third day of administration, although their water intake was reduced by approximately 50% throughout the study [57–59]. This is also in agreement with our observation, that body weight loss cannot be explained solely by less drinking in IAA-treated animals. The concentration-dependent reduction in fluid consumption suggests an oral aversion that might be due to the potential gastro-irritating effect of the colorless, odorless IAA solution.

Since TRPA1 is activated by IAA, it raises the question whether the known species differences in sequence homology, as well as its selectivity to a range of ligands, might contribute to the observed species differences in the IAA model. As discussed above, IAA contains a highly reactive electrophilic moiety lacking structural selectivity, that forms alklylation adducts by binding to the cysteine residues on the N-terminal of TRPA1 [49], which might potentially lead to its activation [48]. Therefore, it is more likely, that species differences in the IAA-induced diffuse gastritis model is not due to the heterogeneity in TRPA1 ion channel sequence, and that TRPA1 upregulation is rather a consequence of tissue injury. Determining resistance mechanisms was beyond the scope of our study; however, it might provide valuable information on gastroprotective mechanisms yet not fully known. As a general limitation of all immunohistochemical techniques, TRPA1- and TRPV1-like immunopositivity determined on the histopathological sections in our study might not provide direct evidence for the receptor protein expression. However, (i) the parallel receptor mRNA changes, (ii) the positive control with dorsal root ganglia samples, (iii) the lack of immunopositivity with the blocking peptides provided by the producers, (iv) as well as the extensive use of both antibodies in the literature [60,61] and in our earlier studies [18,62,63] suggest the reliability and validity of our IHC results supporting our conclusion.

Here, we show the first results on the upregulation of the TRPA1 ion channel in a well-characterized translational gastric injury model in correlation with duration-dependent macroscopic and microscopic lesions. These data will provide a good basis for evaluating the effect of TRPA1-targeting pharmacological interventions on the different components of the gastric injury.

4. Materials and Methods

4.1. Animals and Ethics

Experiments were performed on 8-week-old male CD1 and C57Bl/6J mice weighing 18–25 g and Wistar rats weighing 180–220 g at the beginning of the study; each group consisted of 6 animals. Animals were bred and kept in the Laboratory Animal House of the Department of Pharmacology and Pharmacotherapy, University of Pécs, at 24–25 °C, provided with standard rodent chow and water ad libitum, maintained under 12 h light-dark cycle. All procedures were carried out according to the 40/2013 (II.14.) Government Regulation on Animal Protection and Consideration Decree of Scientific Procedures of Animal Experiments and Directive 2010/63/EU of the European Parliament. They were approved by the Ethics Committee on Animal Research of University of Pécs according to the Ethical Codex of Animal Experiments (license no.: BA02/2000-20/2019, 27 June 2019).

4.2. Experimental Protocol

Gastritis was induced by the administration of IAA (Sigma-Aldrich Inc., Darmstadt, Germany) to the drinking water. Since IAA is light-sensitive, IAA-containing drinking water was prepared freshly every day by dissolving 0.1, 0.2, 0.4, 0.6 or 1 g IAA in 200 mL tap water (0.05%, 0.1%, 0.2%, 0.3% and 0.5% concentration, respectively) for 7 or 14 days consecutively, depending on the experimental paradigm.

4.3. Study in Rats

Rats were randomized into 8 groups of 6 animals in each, and received 0.05%, 0.1% or 0.2% IAA solution in the drinking water for 7 or 14 days consecutively. Littermates drinking IAA-free tap water served as control animals (Figure 9).

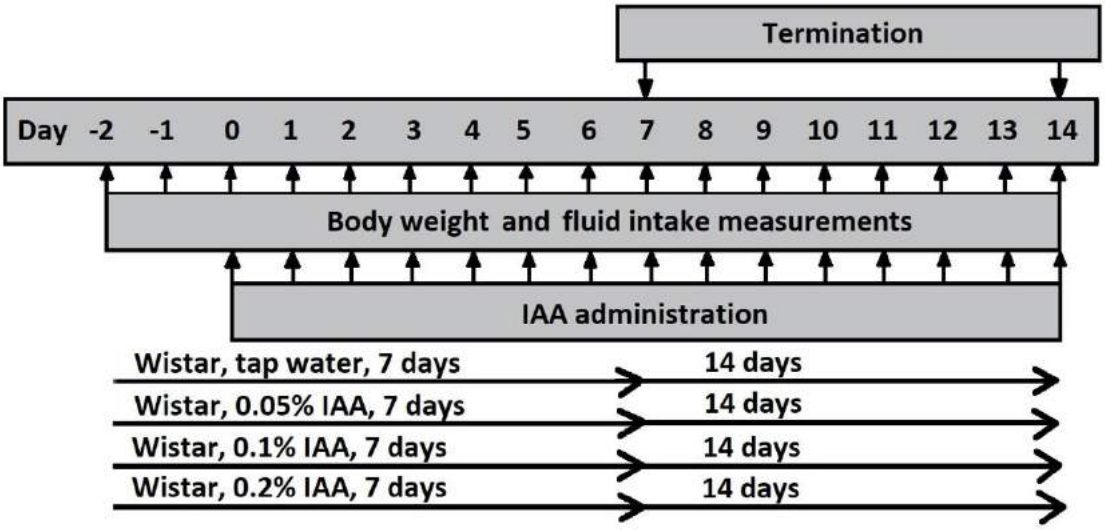

Figure 9. Experimental design of IAA gastritis with Wistar rats. Male Wistar rats were divided into 8 groups according to the duration of the protocol (7 days or 14 days) and concentration (0.05%, 0.1% or 0.2%) of IAA dissolved in drinking water. Control rats received tap water. Body weight and fluid intake were monitored daily throughout the experiment. At the end of the protocol, rats were euthanized and their stomachs were excised for macroscopic, microscopic evaluation and further molecular biological assessment.

4.4. Study in Mice

In the first mouse study, CD1 mice were randomized into 4 groups: mice receiving 0.1% IAA for 7 and 14 days, with the respective control groups. Based on the negative results of this study, CD1 mice were randomized in 3 groups receiving 0.3% and 0.5% IAA for 7 days; the control group drank tap

water. To investigate interstrain differences, C57Bl/6J mice were randomized into 4 groups receiving (1) 0.3% IAA-containing drinking water, (2) 0.3% IAA-containing drinking water, which also contained 2% sucrose, (3) a control group drinking tap water, and (4) a second control group receiving 2% sucrose dissolved in tap water (Figure 10).

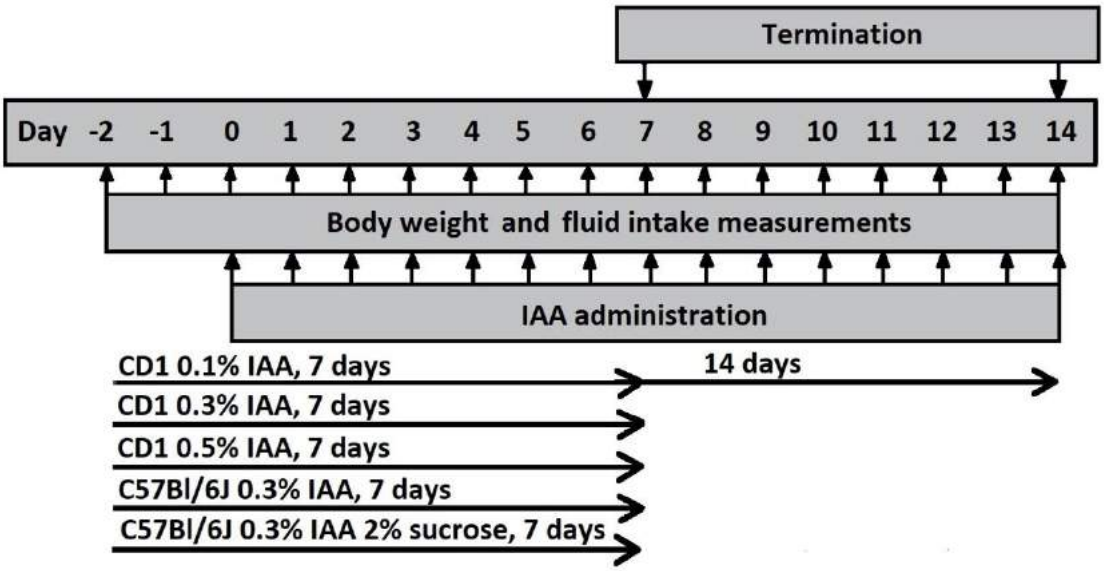

Figure 10. Experimental design of IAA gastritis with CD1 and C57Bl/6J mice. Male CD1 and C57Bl/6J mice were divided into groups receiving various concentrations (0.1%, 0.3% and 0.5%) of IAA dissolved in drinking water. Control mice received tap water. Body weight and fluid intake were monitored daily throughout the experiment. At the end of the protocol, mice were euthanized and their stomachs were excised for macroscopic and microscopic evaluation.

Fluid intake and body weight were measured daily in each study. At the end of the study, animals were euthanized under ketamine (120 mg/kg ip.; Calypsol, Gedeon Richter Plc., Budapest, Hungary) and xylazine (6 mg/kg ip.; Sedaxylan, Eurovet Animal Health B.V., Bladel, The Netherlands) anesthesia. The stomach was excised, opened along the greater curvature and rinsed with room temperature saline. After photo documentation of the macroscopic lesions, the stomach was cut in four sections: antrum and corpus specimens were fixed in 6% formaline and 5 μm sections were stained with hematoxylin and eosin (H&E) for histopathologic and immunohistochemical evaluation. Other antral and corpus samples were snap-frozen for molecular biologic assessments.

4.5. Macroscopic and Microscopic Evaluations of IAA-Induced Gastric Lesions

The extent and severity of the macroscopic lesions were evaluated by a semiquantitative scoring system based on the extent of hyperemia (0: none; 1: <25%, 2: 25–50%; 3: >50% of the total gastric mucosa) and the number of erosions/ulcerations (0: none; 1: 1–2; 2: 3–4; 3: ≥5). Excised gastric samples were paraformaldehyde-fixed (4%) and embedded in paraffin, 5 μm sections were cut and stained with H&E for further qualitative histological analysis, i.e., the assessment of the extent of lesions, submucosal infiltration and capillarization.

4.6. GSH Measurement

Total GSH (tGSH) and total γ-glutamyl-cysteine (tGluCys) were measured in gastric mucosa specimens by a specific HPLC method with RP 18 NUCLEOSHELL HPLC columns (Macherey-Nagel, Düren, Germany) after incubation with *N*-acetylcysteine ethyl ester (for detailed methodological description see (Supplementary Material (Figure S1)).

4.7. TRPV1 and TRPA1 Immunohistochemistry and Scoring

For antigen recovery, the paraformaldehyde-fixed and paraffin-embedded tissue samples were deparaffinized, rehydrated and incubated in acidic citrate buffer (pH 6) in a microwave oven. Endogenous peroxidase activity was quenched 3% hydrogen peroxide. The sections were washed and incubated in blocking solution, then treated with a 1:1000 dilution of rabbit polyclonal anti-TRPA1 (ab68848; Abcam, Cambridge, UK) and anti-TRPV1 (GP14100; Neuromics, Edina, MN, USA) antibodies. Slides were incubated with anti-rabbit secondary antibody conjugated with HRP (DakoCytomation, Carpinteria, CA, USA) with the EnVision system. The reaction was visualized by 0.01% hydrogen peroxide containing 3,3-diaminobenzidine tetrachloride, and histological counterstaining was performed with hematoxylin [64]. Quantitative assessment of TRPA1 and TRPV1 immunopositivity was performed based on the % ratio of the immunopositive cells on 10 fields of vision/slide/animal by an expert pathologist blinded to the study. Pannoramic Digital Slide Scanner with CaseViewer software (3DHISTECH Ltd., Budapest, Hungary) was used for both the evaluation and taking the representative photos of the slides. Incubating untreated rat gastric mucosa with Tris-buffered saline instead of the primary antibodies served as the negative control, while sections of rat dorsal root ganglia expressing TRPA1 and TRPV1 abundantly were used as positive controls. Antibody selectivity was validated by the lack of immunopositivity after the respective blocking peptides (ab150297 for TRPA1; Abcam, Cambridge, UK and P14100 for TRPV1; Neuromics, Edina, MN, USA) and was also based on literature data [65].

4.8. Determination of Trpv1 and Trpa1 Relative Gene Expression

Total RNA was purified by TRI Reagent (Molecular Research Center Inc., Cincinnati, OH, USA) with Direct-Zol RNA MiniPrep isolation kit (Zymo Research, Irvine, CA, USA) following the manufacturer's protocol. The quantity and purity of RNA samples were assessed by NanoDrop ND-1000 spectrophotometer (NanoDrop Technologies Inc., Wilmington, DE, USA) and then treated with deoxyribonuclease I enzyme (Zymo Research, Irvine, CA, USA). Purified total RNA (100 ng) was reverse transcribed with Maxima First Strand cDNA Synthesis Kit (Thermo Fisher Scientific, Waltham, MA, USA) according to the manufacturer's instructions. Real-time qPCR was conducted on a Stratagene Mx3000P qPCRSystem (Agilent Technologies, Santa Clara, CA, USA) using Luminaris HiGreen LowROX qPCR Master Mix (Thermo Fisher Scientific, Waltham, MA, USA) to amplify transcripts. The following primer pairs were used: the reference gene glyceraldehyde 3-phosphate dehydrogenase (*Gapdh*) (NM_017008.4) (sense): 5′-TGCACCACCAACTGCTTAGC-3′ and (antisense): 5′-GGCATGGACTGTGGTCATGAG-3′; *Trpv1* (NM_031982.1) (sense): 5′-AATACACCATCGCTCTGCT-3′ and (antisense): 5′-CAATGTGCAGTGCTGTCTGG-3′; *Trpa1* (NM_207608.1) (sense): 5′-ATCCAAATAGACCCAGGCACG-3′ and (antisense): 5′-CAAGCATGTGTCAATGTTTGGTACT-3′. Primers with similar efficiencies were used. In order to verify primer specificity, dissociation curve analyses were performed. All reactions were measured in triplicates, and the geometric mean of their Ct values were calculated. The determination of relative messenger RNA (mRNA) expression levels was performed according to the comparative DDCt method using samples of control animals as calibrator.

4.9. Statistical Analysis

Statistical analysis was performed by using GraphPad Prism v6 software. Values for all measurements are expressed as means ± SEM of $n = 6$ animals in each group. Evaluation of body weight change and fluid intake was performed by repeated-measures ANOVA followed by Bonferroni's modified *t*-test. Semiquantitative macroscopic scoring was analyzed by the non-parametric Kruskal–Wallis method followed by Dunn's multiple comparison test to observe intergroup differences at given timepoints, while Mann–Whitney test was performed to analyze intragroup differences by time. GSH measurements were analyzed by one-way ANOVA, while TRPA1 and TRPV1 immunopositivities were evaluated by ordinary

two-way ANOVA followed by Dunn's multiple comparisons test. qPCR measurements were evaluated by Student's unpaired *t*-test.

Supplementary Materials: Supplementary materials can be found at http://www.mdpi.com/1422-0067/21/16/5591/s1. Methods. GSH measurements. GSH results measured by GC-MS. Figure S1. Peak area ratio (PAR) of m/z 269/272 for pyroglutamate (pGlu) (A), of m/z 301/307 for glutamate (Glu) (B) and Glu-to-pGlu ratio (C) measured by GC-MS in intact and 0.1% IAA-treated stomach samples. Data are shown as mean ± SEM; $n = 6$/group (ordinary one-way ANOVA; * $p < 0.05$) [36,66–68].

Author Contributions: Conceptualization, Z.H., S.S. and I.L.S.; investigation, K.C., D.P., B.K., D.T. and I.H.; formal analysis, K.C., D.P. and D.T.; methodology, K.C, A.B., S.S. and Z.H.; project administration, K.C.; resources, Z.H., A.B. and D.T.; supervision, Z.H., S.S. and I.L.S.; visualization, K.C., D.P., B.K. and Z.H.; writing—original draft, Z.H. and K.C.; writing—review and editing, K.C., D.P., B.K., I.H., A.B., D.T., I.L.S., S.S. and Z.H. All authors have read and approved the final manuscript.

Funding: This work was supported by 20765-3/2018/FEKUTSRTAT, Higher Education Institutional Excellence Program of the Ministry of Human Capacities in Hungary; EFOP-3.6.2-16-2017-00006 LIVE LONGER, Human Resource Development Operational Program; EFOP-3.6.2-16-2017-00008, The role of neuro-inflammation in neurodegeneration: from molecules to clinics and GINOP-2.3.2-15-2016-00048 STAY ALIVE, Economic Development and Innovation Operational Program. K.C. was supported by the Richter Gedeon Talentum Foundation and ÚNKP-19-3-III-PTE-211 New National Excellence Program of the Ministry of Human Capacities.

Conflicts of Interest: The authors declare no conflict of interest.

References

1. Szabo, I.L.; Cseko, K.; Czimmer, J.; Mozsik, G. *Diagnosis of Gastritis—Review from Early Pathological Evaluation to Present Day Management*; Mozsik, G., Ed.; InTech Open Access Publisher: Rijeka, Yugoslavia, 2013; pp. 3–20.
2. Lu, C.L.; Chang, S.S.; Wang, S.S.; Chang, F.Y.; Lee, S.D. Silent peptic ulcer disease: Frequency, factors leading to "silence," and implications regarding the pathogenesis of visceral symptoms. *Gastrointest. Endosc.* **2004**, *60*, 34–38. [CrossRef]
3. Appelman, H.D. Gastritis: Terminology, Etiology, and Clinicopathological Correlations: Another Biased View. *Hum. Pathol.* **1994**, *25*, 1006–1019. [CrossRef]
4. McColl, K.E.L. Helicobacter pylori-Negative Nonsteroidal Anti-Inflammatory Drug-Negative Ulcer. *Gastroenterol. Clin. N. Am.* **2009**, *38*, 353–361. [CrossRef] [PubMed]
5. Kavitt, R.T.; Lipowska, A.M.; Anyane-Yeboa, A.; Gralnek, I.M. Diagnosis and Treatment of Peptic Ulcer Disease. *Am. J. Med.* **2019**, *132*, 447–456. [CrossRef]
6. Szolcsanyi, J.; Barthó, L. Impaired defense mechanism to peptic ulcer in the capsaicin-desensitized rat. In *Gastrointestinal Defense Mechanism*; Mózsik, G., Hanninen, O., Jávor, T., Eds.; Akadémiai Kiadó-Pergamon Press: Budapest, Hungary, 1981; pp. 39–51.
7. Abdel-Salam, O.M.E.; Debreceni, A.; Mózsik, G.; Szolcsányi, J. Capsaicin-sensitive afferent sensory nerves in modulating gastric mucosal defense against noxious agents. *J. Physiol. Paris* **1999**, *93*, 443–454. [CrossRef]
8. Szolcsányi, J.; Barthó, L. Capsaicin-sensitive afferents and their role in gastroprotection: An update. *J. Physiol. Paris* **2001**, *95*, 181–188. [CrossRef]
9. Geppetti, P.; Nassini, R.; Materazzi, S.; Benemei, S. The concept of neurogenic inflammation. *BJU Int.* **2008**, *101*, 2–6. [CrossRef]
10. Talavera, K.; Startek, J.B.; Alvarez-Collazo, J.; Boonen, B.; Alpizar, Y.A.; Sanchez, A.; Naert, R.; Nilius, B. Mammalian Transient Receptor Potential TRPA1 Channels: From Structure to Disease. *Physiol. Rev.* **2020**, *100*, 725–803. [CrossRef]
11. Giorgi, S.; Nikolaeva-Koleva, M.; Alarcón-Alarcón, D.; Butrón, L.; González-Rodríguez, S. Is TRPA1 burning down TRPV1 as druggable target for the treatment of chronic pain? *Int. J. Mol. Sci.* **2019**, *20*, 2906. [CrossRef]
12. Caterina, M.J.; Park, U. TRPV1: A Polymodal Sensor in the Nociceptor Terminal. *Curr. Top. Membr.* **2006**, *57*, 113–150. [CrossRef]
13. Viana, F. TRPA1 channels: Molecular sentinels of cellular stress and tissue damage. *J. Physiol.* **2016**, *594*, 4151–4169. [CrossRef] [PubMed]
14. Szolcsányi, J.; Helyes, Z.; Oroszi, G.; Németh, J.; Pintér, E. Release of somatostatin and its role in the mediation of the anti-inflammatory effect induced by antidromic stimulation of sensory fibres of rat sciatic nerve. *Br. J. Pharmacol.* **1998**, *123*, 936–942. [CrossRef] [PubMed]

15. Szolcsányi, J. Forty years in capsaicin research for sensory pharmacology and physiology. *Neuropeptides* **2004**, *38*, 377–384. [CrossRef] [PubMed]
16. Sgouros, S.N.; Bergele, C.; Viazis, N.; Avgerinos, A. Somatostatin and its analogues in peptic ulcer bleeding: Facts and pathophysiological aspects. *Dig. Liver Dis.* **2006**, *38*, 143–148. [CrossRef]
17. Faussone-Pellegrini, M.S.; Taddei, A.; Bizzoco, E.; Lazzeri, M.; Vannucchi, M.G.; Bechi, P. Distribution of the vanilloid (capsaicin) receptor type 1 in the human stomach. *Histochem. Cell Biol.* **2005**, *124*, 61–68. [CrossRef]
18. Kun, J.; Szitter, I.; Kemény, Á.; Perkecz, A.; Kereskai, L.; Pohóczky, K.; Vincze, Á.; Gódi, S.; Szabó, I.; Szolcsányi, J.; et al. Upregulation of the transient receptor potential ankyrin 1 ion channel in the inflamed human and mouse colon and its protective roles. *PLoS ONE* **2014**, *9*, e108164. [CrossRef]
19. Poole, D.P.; Pelayo, J.C.; Cattaruzza, F.; Kuo, Y.; Gai, G.; Chiu, J.V.; Bron, R.; Furness, J.B.; Grady, E.F.; Bunnett, N.W. Transient receptor potential ankyrin 1 is expressed by inhibitory motoneurons of the mouse intestine. *Gastroenterology* **2011**, *141*, 565–575. [CrossRef]
20. Kaji, I.; Yasuoka, Y.; Karaki, S.; Kuwahara, A. Activation of TRPA1 by luminal stimuli induces EP 4-mediated anion secretion in human and rat colon. *Am. J. Physiol. Gastrointest. Liver Physiol.* **2019**, 690–701. [CrossRef]
21. Bertin, S.; Aoki-Nonaka, Y.; De Jong, P.R.; Nohara, L.L.; Xu, H.; Stanwood, S.R.; Srikanth, S.; Lee, J.; To, K.; Abramson, L.; et al. The ion channel TRPV1 regulates the activation and proinflammatory properties of CD4+ T cells. *Nat. Immunol.* **2014**, *15*, 1055–1063. [CrossRef]
22. Bertin, S.; Aoki-Nonaka, Y.; Lee, J.; de Jong, P.R.; Kim, P.; Han, T.; Yu, T.; To, K.; Takahashi, N.; Boland, B.S.; et al. The TRPA1 ion channel is expressed in CD4+ T cells and restrains T cell-mediated colitis through inhibition of TRPV1. *Gut* **2017**, *66*, 1584–1596. [CrossRef]
23. Csekő, K.; Beckers, B.; Keszthelyi, D.; Helyes, Z. Role of TRPV1 and TRPA1 Ion Channels in Inflammatory Bowel Diseases: Potential Therapeutic Targets? *Pharmaceuticals* **2019**, *12*, 48. [CrossRef] [PubMed]
24. Utsumi, D.; Matsumoto, K.; Tsukahara, T.; Amagase, K.; Tominaga, M.; Kato, S. Transient receptor potential vanilloid 1 and transient receptor potential ankyrin 1 contribute to the progression of colonic inflammation in dextran sulfate sodium-induced colitis in mice: Links to calcitonin gene-related peptide and substance P. *J. Pharmacol. Sci.* **2018**, *136*, 121–132. [CrossRef] [PubMed]
25. Massa, F.; Sibaev, A.; Marsicano, G.; Blaudzun, H.; Storr, M.; Lutz, B. Vanilloid receptor (TRPV1)-deficient mice show increased susceptibility to dinitrobenzene sulfonic acid induced colitis. *J. Mol. Med.* **2006**, *84*, 142–146. [CrossRef] [PubMed]
26. Mózsik, G.; Szolcsányi, J.; Rácz, I. Gastroprotection induced by capsaicin in healthy human subjects. *World J. Gastroenterol.* **2005**, *11*, 5180–5184. [CrossRef] [PubMed]
27. Mózsik, G. *Capsaicin as New orally Applicable Gastroprotective and Therapeutic Drug Alone or in Combination with Nonsteroidal Anti-Inflammatory Drugs in Healthy Human Subjects and in Patients*; Abdel-Salam, O.M.E., Ed.; Springer: Basel, Switzerland, 2014; Volume 68, ISBN 9783034808279.
28. Yu, X.; Yu, M.; Liu, Y.; Yu, S. TRP channel functions in the gastrointestinal tract. *Semin. Immunopathol.* **2015**, *38*, 385–396. [CrossRef] [PubMed]
29. Szabo, S.; Trier, J.S.; Brown, A.; Schnoor, J. Sulfhydryl blockers induce severe inflammatory gastritis in the rat. *Gastroenterology* **1984**, *86*, 1271.
30. Szabo, S.; Trier, J.S.; Frankel, P.W. Sulfhydryl compounds may mediate gastric cytoprotection. *Science* **1981**, *214*, 200–202. [CrossRef]
31. Pihan, G.; Majzoubi, D.; Haudenschild, C.; Trier, J.S.; Szabo, S. Early microcirculatory stasis in acute gastric mucosal injury in the rat and prevention by 16,16-dimethyl prostaglandin E2 or sodium thiosulfate. *Gastroenterology* **1986**, *91*, 1415–1426. [CrossRef]
32. Szabo, S.; Brown, A. Prevention of ethanol-induced vascular injury and gastric mucosal lesions by sucralfate and its components: Possible role of endogenous sulfhydryls. *Proc. Soc. Expl. Biol. Med.* **1987**, *185*, 493–497. [CrossRef]
33. Lee, S.E.; Song, H.J.; Park, S.Y.; Nam, Y.; Min, C.H.; Lee, D.Y.; Jeong, J.Y.; Ha, H.S.; Kim, H.-J.; Whang, W.K.; et al. Effect of ECQ on iodoacetamide-induced chronic gastritis in rats. *Korean J. Physiol. Pharmacol.* **2013**, *17*, 469–477. [CrossRef]
34. Karmeli, F.; Okon, E.; Rachmilewitz, D. Sulphydryl blocker induced gastric damage is ameliorated by scavenging of free radicals. *Gut* **1996**, *38*, 826–831. [CrossRef] [PubMed]

35. Pastoris, O.; Verri, M.; Boschi, F.; Kastsiuchenka, O.; Balestra, B.; Pace, F.; Tonini, M.; Natale, G. Effects of esomeprazole on glutathione levels and mitochondrial oxidative phosphorylation in the gastric mucosa of rats treated with indomethacin. *Naunyn. Schmiedebergs. Arch. Pharmacol.* **2008**, *378*, 421–429. [CrossRef] [PubMed]
36. Michaelsen, J.T.; Dehnert, S.; Giustarini, D.; Beckmann, B.; Tsikas, D. HPLC analysis of human erythrocytic glutathione forms using OPA and N-acetyl-cysteine ethyl ester: Evidence for nitrite-induced GSH oxidation to GSSG. *J. Chromatogr. B* **2009**, *877*, 3405–3417. [CrossRef] [PubMed]
37. Schmidt, M.M.; Dringen, R. Differential effects of iodoacetamide and iodoacetate on glycolysis and glutathione metabolism of cultured astrocytes. *Front. Neuroenergetics* **2009**, *1*, 1–10. [CrossRef]
38. Mitchell, D.B.; Acosta, D.; Bruckner, J.V. Role of glutathione depletion in the cytotoxicity of acetaminophen in a primary culture system of rat hepatocytes. *Toxicology* **1985**, *37*, 127–146. [CrossRef]
39. Palmen, N.G.M.; Evelo, C.T.A. Glutathione depletion in human erythrocytes and rat liver: A study on the interplay between bioactivation and inactivation functions of liver and blood. *Toxicol. Vitr.* **1996**, *10*, 273–281. [CrossRef]
40. Elseweidy, M.M.; Younis, N.N.; Amin, R.S.; Abdallah, F.R.; Fathy, A.M.; Yousif, Z.A. Effect of some natural products either alone or in combination on gastritis induced in experimental rats. *Dig. Dis. Sci.* **2008**, *53*, 1774–1784. [CrossRef]
41. Rahman, I.; Antonicelli, F.; MacNee, W. Molecular mechanism of the regulation of glutathione synthesis by tumour necrosis factor-a and dexamethasone in human alveolar epithelial cells. *J. Biol. Chem.* **1999**, *274*, 5088–5096. [CrossRef]
42. Yasin, R.; Leese, C.L. The production of chronic gastritis and ulceration in the glandular stomach of rats by iodoacetamide (IAM). *Eur. J. Cancer* **1970**, *6*, 425–432. [CrossRef]
43. Dial, E.J.; Hall, L.R.; Romero, J.J.; Lichtenberger, L.M. Rats with gastritis have increased sensitivity to the gastrin stimulatory effects of luminal ammonia. *Gastroenterology* **1996**, *110*, 801–808. [CrossRef]
44. Barnett, K.; Bell, C.J.; McKnight, W.; Dicay, M.; Sharkey, K.A.; Wallace, J.L. Role of cyclooxygenase-2 in modulating gastric acid secretion in the normal and inflamed rat stomach. *Am. J. Physiol. Gastrointest. Liver Physiol.* **2000**, *279*, 1292–1297. [CrossRef] [PubMed]
45. Lalich, J.J. Iodoacetamide induced gastric ulcers in rats. *Proc. Soc. Expl. Biol. Med.* **1962**, *109*, 905–908. [CrossRef] [PubMed]
46. Ozaki, N.; Bielefeldt, K.; Sengupta, J.N.; Gebhart, G.F. Models of gastric hyperalgesia in the rat. *Am. J. Physiol. Gastrointest. Liver Physiol.* **2002**, *283*, 666–676. [CrossRef] [PubMed]
47. Larauche, M.; Anton, P.M.; Peiro, G.; Eutamène, H.; Buéno, L.; Fioramonti, J. Role of capsaicin-sensitive afferent nerves in different models of gastric inflammation in rats. *Auton. Neurosci. Basic Clin.* **2004**, *110*, 89–97. [CrossRef] [PubMed]
48. Macpherson, L.J.; Dubin, A.E.; Evans, M.J.; Marr, F.; Schultz, P.G.; Cravatt, B.F.; Patapoutian, A. Noxious compounds activate TRPA1 ion channels through covalent modification of cysteines. *Nature* **2007**, *445*, 541–545. [CrossRef] [PubMed]
49. Hinman, A.; Chuang, H.H.; Bautista, D.M.; Julius, D. TRP channel activation by reversible covalent modification. *Proc. Natl. Acad. Sci. USA* **2006**, *103*, 19564–19568. [CrossRef]
50. Ibarra, Y.; Blair, N.T. Benzoquinone reveals a cysteine-dependent desensitization mechanism of TRPA1. *Mol. Pharmacol.* **2013**, *83*, 1120–1132. [CrossRef]
51. Xu, Y.; Jia, J.; Xie, C.; Wu, Y.; Tu, W. Transient Receptor Potential Ankyrin 1 and Substance P Mediate the Development of Gastric Mucosal Lesions in a Water Immersion Restraint Stress Rat Model. *Digestion* **2018**, *97*, 228–239. [CrossRef]
52. Dömötör, A.; Kereskay, L.; Szekeres, G.; Hunyady, B.; Szolcsányi, J.; Mózsik, G. Participation of capsaicin-sensitive afferent nerves in the gastric mucosa of patients with Helicobacter pylori-positive or-negative chronic gastritis. *Dig. Dis. Sci.* **2007**, *52*, 411–417. [CrossRef]
53. Fernandes, E.S.; Fernandes, M.A.; Keeble, J.E. The functions of TRPA1 and TRPV1: Moving away from sensory nerves. *Br. J. Pharmacol.* **2012**, *166*, 510–521. [CrossRef]
54. Ruparel, N.B.; Patwardhan, A.M.; Akopian, A.N.; Hargeaves, K.M. Homologous and Heterologous Desensitization of Capsaicin and Mustard Oil Responses Utilize Different Cellular Pathways in Nociceptors. *Pain* **2008**, *135*, 271–279. [CrossRef] [PubMed]

55. Bielefeldt, K.; Ozaki, N.; Gebhart, G.F. Mild gastritis alters voltage-sensitive sodium currents in gastric sensory neurons in rats. *Gastroenterology* **2002**, *122*, 752–761. [CrossRef] [PubMed]
56. Piqueras, L.; Corpa, J.M.; Martínez, J.; Martínez, V. Gastric hypersecretion associated to iodoacetamide-induced mild gastritis in mice. *Naunyn Schmiedeberg's Arch. Pharmacol.* **2003**, *367*, 140–150. [CrossRef] [PubMed]
57. Holzer, P.; Wultsch, T.; Edelsbrunner, M.; Mitrovic, M.; Shahbazian, A.; Painsipp, E.; Bock, E.; Pabst, M.A. Increase in gastric acid-induced afferent input to the brainstem in mice with gastritis. *Neuroscience* **2007**, *145*, 1108–1119. [CrossRef]
58. Wultsch, T.; Painsipp, E.; Shahbazian, A.; Mitrovic, M.; Edelsbrunner, M.; Waldmann, R.; Lazdunski, M.; Holzer, P. Deletion of the acid-sensing ion channel ASIC3 prevents gastritis-induced acid hyperresponsiveness of the stomach-brainstem axis. *Pain* **2015**, *134*, 245–253. [CrossRef]
59. Painsipp, E.; Wultsch, T.; Shahbazian, A.; Edelsbrunner, M.; Kreissl, C.; Schirbel, A.; Bock, E.; Pabst, M.A.; Thoeringer, C.K.; Huber, H.P.; et al. Experimental gastritis in mice enhances anxiety in a gender- related manner. *Neuroscience* **2007**, *150*, 522–536. [CrossRef]
60. Chen, Z.; Du, S.; Kong, C.; Zhang, Z.; Mokhtar, A. Intrathecal administration of TRPA1 antagonists attenuate cyclophosphamide-induced cystitis in rats with hyper-reflexia micturition. *BMC Urol.* **2016**, *16*. [CrossRef]
61. Price, T.J.; Louria, M.D.; Candelario-Soto, D.; Dussor, G.O.; Jeske, N.A.; Patwardhan, A.M.; Diogenes, A.; Trott, A.A.; Hargreaves, K.M.; Flores, C.M. Treatment of trigeminal ganglion neurons in vitro with NGF, GDNF or BDNF: Effects on neuronal survival, neurochemical properties and TRPV1-mediated neuropeptide secretion. *BMC Neurosci.* **2005**, *6*, 1–15. [CrossRef]
62. Kemény, Á.; Kodji, X.; Horváth, S.; Komlódi, R.; Szőke, É.; Sándor, Z.; Perkecz, A.; Gyömörei, C.; Sétáló, G.; Kelemen, B.; et al. TRPA1 acts in a protective manner in imiquimod-induced psoriasiform dermatitis in mice. *J. Investig. Dermatol.* **2018**, *138*, 1774–1784. [CrossRef]
63. Bohonyi, N.; Pohóczky, K.; Szalontai, B.; Perkecz, A.; Kovács, K.; Kajtár, B.; Orbán, L.; Varga, T.; Szegedi, S.; Bódis, J.; et al. Local upregulation of transient receptor potential ankyrin I and transient receptor potential vanilloid I ion channels in rectosigmoid deep infiltrating endometriosis. *Mol. Pain* **2017**, *13*, 1–13. [CrossRef]
64. Kun, J.; Helyes, Z.; Perkecz, A.; Bán, Á.; Polgár, B.; Szolcsányi, J.; Pintér, E. Effect of Surgical and Chemical Sensory Denervation on Non-neural Expression of the Transient Receptor Potential Vanilloid 1 (TRPV1) Receptors in the Rat. *J. Mol. Neurosci.* **2012**, *48*, 795–803. [CrossRef] [PubMed]
65. Potolicchio, I.; Santambrogio, L.; Strominger, J.L. Molecular interaction and enzymatic activity of macrophage migration inhibitory factor with immunorelevant peptides. *J. Biol. Chem.* **2003**, *278*, 30889–30895. [CrossRef] [PubMed]
66. Neuschwander-Teri, B.A.; Roll, F.J. Glutathione measurement by HPLC separation and fluorometric detection of the glutathione Orthophthalaldehyde adduct. *Anal. Biochem.* **1989**, *179*, 236–241. [CrossRef]
67. Parmentier, C.; Leroy, P.; Wellman, M.; Nicolas, A. Determination of cellular thiols and glutathione-related enzyme activities: Versatility of high-performance liquid chromatography-spectrofluorimetric detection. *J. Chromatogr. B* **1998**, *719*, 37–46. [CrossRef]
68. Bollenbach, A.; Tsikas, D. Measurement of the tripeptides glutathione and ophthalmic acid by gas chromatography-mass spectrometry. *Anal. Biochem.* **2020**. [CrossRef]

Supplementary Material

International Journal of Molecular Sciences

Upregulation of the TRPA1 receptor in the gastric mucosa after iodoacetamide-induced gastritis in rats: a potential new therapeutic target

Kata Csekő, Dániel Pécsi, Béla Kajtár, Ivett Hegedűs, Dimitrios Tsikas, Imre László Szabó, Sándor Szabó*, Zsuzsanna Helyes*

*The authors contributed equally to the present paper.

Methods

GSH measurements

GSH was measured in gastric mucosa specimens by a specific HPLC method after pre-column derivatization with *ortho*-phthaldehyde (OPA) as described previously for erythrocytic GSH [1]. The procedure for gastric mucosa GSH is described below in detail. With the exception of the HPLC analyses, which were all performed at room temperature on an Agilent 1100 Series system equipped with a UV detection and an autosampler Gerstel MPS-3, all other experimental procedures, including homogenization and ultrafiltration, were performed under cooling in ice bath to protect GSH from oxidation.

Wet specimens weighing 122 to 241 mg were homogenized in 1-mL aliquots of ice-cooled phosphate buffered saline (PBS, 0.1 M, pH 7.2) in precellys tubes (Bertin-Instruments, USA) four times each for 20 s at 5500 rpm. The homogenates were immediately centrifuged (5 min, 3345 xg, 4°C), and the supernatants (500 µL) were ultrafiltered by centrifugation using Vivaspin 500 cartridges (15,000 xg, 20 min, 4 °C; Sartorius, Germany). The ultrafiltrate samples (25 – 40 µL aliquots) were frozen immediately and kept stored at -20 °C until subsequent analysis. After thawing, 20-µL aliquots of the ultrafiltrates were diluted with 180 µL of ice-cooled PBS. Aliquots (50 µL) of the dilutions were treated with 900 µL borate buffer (0.4 M, pH 8.5) and 50 µL of the OPA reagent [1]. HPLC analysis with UV absorbance detection (338 nm) was performed 2 min after derivatization by injecting 20-µL aliquots of the derivatized samples.

The 5-µm RP 18 NUCLEOSHELL HPLC columns (guard column, 4 x 3 mm; analytical column, 250 x 4 mm) were from Macherey-Nagel (Düren, Germany) and were thermostated at 20 °C. Isocratic elution was performed with 10 vol% methanol-90 vol% sodium acetate (150 mM, pH 7.5) at a flow rate of 1 mL/min [1]. The GSH-OPA derivative eluted from the column at 3.924±0.027 min (coefficient of variation, 0.7%). The concentration of GSH in the samples was calculated by using a calibration curve generated in the range 0-1000 µM upon sample dilution as performed for the

ultrafiltrate samples. Plotting of the peak area of the GSH-OPA peak (*y*, mAU/min) versus the GSH concentration (*x*, µg/mL) resulted in a line (r^2=0.9987) with the regression equation *y*=1.38+0.31*x*. The calibration curve samples were re-analyzed next day by HPLC and resulted in the regression equation *y*=0.53+0.33*x* (r^2=0.9997), indicating the high inter-assay precision of the method. This HPLC method can also analyze γ-glutamyl-cysteine (GluCys), but not cysteine and other cysteine-containing species [1]. In some samples we observed a peak eluting in front of GSH-OPA peak (retention time, 2.964±0.156 min) and is likely to be the GluCys-OPA derivative [2,3]. HPLC analysis of the GSH calibration curve samples did not reveal presence of GluCys in the GSH preparation. Incubation of biological samples including human erythrocytes with *N*-acetylcysteine ethyl ester (NACET) allows for the measurement of total GSH (tGSH) [1] and total GluCys (tGluCys) [2]. tGluCys includes free GluCys and GluCys released by NACET from symmetric and asymmetric disulfides (R-GluCys). Analogous, tGSH includes free GSH and GSH released by NACET from the symmetric GSH disulfide (i.e., GSSG) and from asymmetric disulfides (R-GSH). The GSH concentration in the homogenate samples was corrected by the protein concentration in the homogenates as measured by the BCA method and is reported as nmol GSH per mg wet protein. Due to the lack of a GluCys reference compound, the concentration of GluCys in the samples was not measured. Yet, it is assumed that GSH and GluCys, at a molar basis, yield closely similar peak areas.

We confirmed the GSH levels obtained by HPLC analysis also with the help of gas chromatography mass spectrometry (GC-MS). We analysed GSH in the gastric mucosa of untreated and treated rats after its in situ conversion to pyroglutamate (pGlu, 5-oxo-proline), as described earlier (Bollenbach, A.; Tsikas, D. 2020). 10-µL aliquots of ultrafiltrates (cut off, 10 kDa) of rat gastric mucosa homogenate samples prepared in ice-cold 67 mM phosphate buffered saline (pH 7.4) were used. The samples were first derivatized with 2 M HCl/CH3OH (60 min, 80 °C), then spiked with the internal standard hexadeutero-GSH and then acylated by pentafluoropropionic anhydride (30 min, 65 °C).

GSH results measured by GC-MS

There were no differences between the three rat groups with respect to pGlu, Glu/Glu-Cys or their molar ratio (see Suppl. Figure 1).

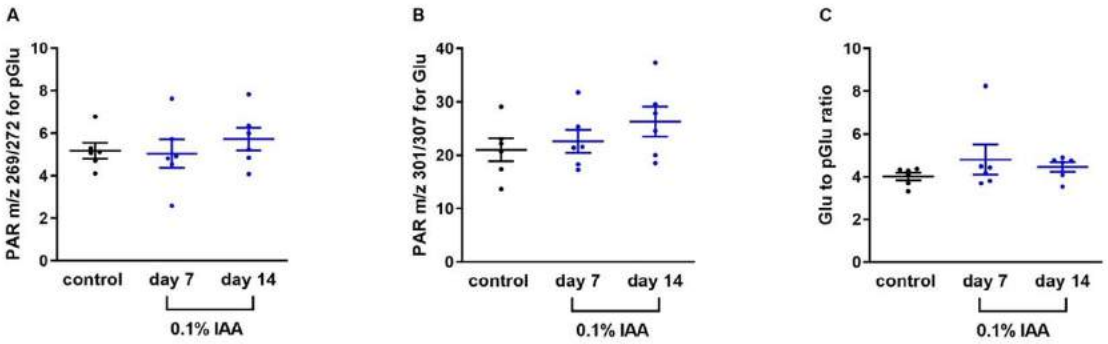

Suppl. Figure 1. Peak area ratio (PAR) of m/z 269/272 for pyroglutamate (pGlu) (A), of m/z 301/307 for glutamate (Glu) (B) and Glu-to-pGlu ratio (C) measured by GC-MS in intact and 0.1% IAA-treated stomach samples. Data are shown as mean ± SEM; n=6/group (ordinary one-way ANOVA; *p < 0.05).

References

1. Michaelsen, J.T.; Dehnert, S.; Giustarini, D.; Beckmann, B.; Tsikas, D. HPLC analysis of human erythrocytic glutathione forms using OPA and N-acetyl-cysteine ethyl ester: Evidence for nitrite-induced GSH oxidation to GSSG. *J. Chromatogr. B* **2009**, *877*, 3405–3417, doi:10.1016/j.jchromb.2009.06.043.
2. Neuschwander-Teri, B.A.; Roll, F.J. Glutathione measurement by HPLC separation and fluorometric detection of the glutathione Orthophthalaldehyde adduct. *Anal. Biochem.* **1989**, *179*, 236–241.
3. Parmentier, C.; Leroy, P.; Wellman, M.; Nicolas, A. Determination of cellular thiols and glutathione-related enzyme activities: Versatility of high-performance liquid chromatography-spectrofluorimetric detection. *J. Chromatogr. B* **1998**, *719*, 37–46, doi:10.1016/S0378-4347(98)00414-9.